frontiers | Research Topics

Self-assembly biomaterials as theragnostic for injury and disease

Edited by
Jin Yan, Sen Hou and Long Wu

Published in
Frontiers in Bioengineering and Biotechnology
Frontiers in Oncology

ISSN 1664-8714
ISBN 978-2-8325-2915-7
DOI 10.3389/978-2-8325-2915-7

About Frontiers

Frontiers is more than just an open access publisher of scholarly articles: it is a pioneering approach to the world of academia, radically improving the way scholarly research is managed. The grand vision of Frontiers is a world where all people have an equal opportunity to seek, share and generate knowledge. Frontiers provides immediate and permanent online open access to all its publications, but this alone is not enough to realize our grand goals.

Frontiers journal series

The Frontiers journal series is a multi-tier and interdisciplinary set of open-access, online journals, promising a paradigm shift from the current review, selection and dissemination processes in academic publishing. All Frontiers journals are driven by researchers for researchers; therefore, they constitute a service to the scholarly community. At the same time, the *Frontiers journal series* operates on a revolutionary invention, the tiered publishing system, initially addressing specific communities of scholars, and gradually climbing up to broader public understanding, thus serving the interests of the lay society, too.

Dedication to quality

Each Frontiers article is a landmark of the highest quality, thanks to genuinely collaborative interactions between authors and review editors, who include some of the world's best academicians. Research must be certified by peers before entering a stream of knowledge that may eventually reach the public - and shape society; therefore, Frontiers only applies the most rigorous and unbiased reviews. Frontiers revolutionizes research publishing by freely delivering the most outstanding research, evaluated with no bias from both the academic and social point of view. By applying the most advanced information technologies, Frontiers is catapulting scholarly publishing into a new generation.

What are Frontiers Research Topics?

Frontiers Research Topics are very popular trademarks of the *Frontiers journals series*: they are collections of at least ten articles, all centered on a particular subject. With their unique mix of varied contributions from Original Research to Review Articles, Frontiers Research Topics unify the most influential researchers, the latest key findings and historical advances in a hot research area.

Find out more on how to host your own Frontiers Research Topic or contribute to one as an author by contacting the Frontiers editorial office: frontiersin.org/about/contact

Self-assembly biomaterials as theragnostic for injury and disease

Topic editors

Jin Yan — Xi'an Jiaotong University, China

Sen Hou — Beihang University, China

Long Wu — University of Maryland, United States

Citation

Yan, J., Hou, S., Wu, L., eds. (2023). *Self-assembly biomaterials as theragnostic for injury and disease*. Lausanne: Frontiers Media SA. doi: 10.3389/978-2-8325-2915-7

Table of contents

frontiers | Frontiers in Bioengineering and Biotechnology

ORIGINAL RESEARCH
published: 17 June 2022
doi: 10.3389/fbioe.2022.928169

Reforming the Chimeric Antigen Receptor by Peptide Towards Optimized CAR T Cells With Enhanced Anti-Cancer Potency and Safety

Cuijuan Liu[1,2], Lin Li[2], Fan Gao[1,2], Jundong Zhou[3], Yingzhou Qin[1,2], Xin Yuan[1,2], Guang Yang[4] and Yimin Zhu[2]**

[1]School of Nano Technology and Nano Bionics, University of Science and Technology of China, Hefei, China, [2]CAS Key Laboratory of Nano-Bio Interface, Suzhou Institute of Nano-Tech and Nano-Bionics, Chinese Academy of Sciences, Suzhou, China, [3]Nanjing Medical University, Affiliated Suzhou Hospital, Department Radio Oncology, Suzhou, China, [4]Department of Oncology, Suzhou BenQ Medical Center, The Affiliated BenQ Hospital of Nanjing Medical University, Suzhou, China

OPEN ACCESS

Edited by:
Jin Yan,
Xi'an Jiaotong University, China

Reviewed by:
Long Wu,
University of Maryland, United States
Jing Geng,
Xi'an Jiaotong University, China
Jiaojiao Xu,
Johns Hopkins Medicine, United States

***Correspondence:**
Guang Yang
yangguang9002@163.com
Yimin Zhu
ymzhu2008@sinano.ac.cn

Specialty section:
This article was submitted to Biomaterials, a section of the journal Frontiers in Bioengineering and Biotechnology

Received: 25 April 2022
Accepted: 25 May 2022
Published: 17 June 2022

Citation:
Liu C, Li L, Gao F, Zhou J, Qin Y, Yuan X, Yang G and Zhu Y (2022) Reforming the Chimeric Antigen Receptor by Peptide Towards Optimized CAR T Cells With Enhanced Anti-Cancer Potency and Safety. Front. Bioeng. Biotechnol. 10:928169. doi: 10.3389/fbioe.2022.928169

The emerging chimeric antigen receptor (CAR) T cell revolutionized the clinic treatment of hematological cancers, but meet its Waterloo in solid tumor therapy. Although there exist many reasons for this limitation, one of the largest challenges is the scarcity of recognition for tumor cells, resulting in the undesirable side effects and the subsequent ineffectiveness. To overcome it, a lung-cancer-cell-targeting peptide termed A1 was used in this work to reform the scFv domain of CAR by genetic manipulation. As a result, this modified ^{A1}CAR T exhibited the optimized cancer-cell targeting and cytotoxicity *in vitro* and *in vivo*. More importantly, by tuning the sensitivity of CAR to antigen, peptide-based ^{A1}CAR T cells could distinguish tumors from normal tissue, thereby eliminating the off-tumor toxicity in healthy organs. Collectively, we herein constructed a genetic peptide-engineered CAR T cells by inserting A1 peptide into the scFv domain. Profitted from the optimized recognition pattern and sensitivity, ^{A1}CAR T cells showed the ascendancy in solid tumor treatment. Our findings demonstrate that peptide-based CAR T holds great potential in solid tumor therapy due to an excellent targeting ability towards tumor cells.

Keywords: chimeric antigen receptor, off-tumor effect, peptide, anti-cancer therapy, affinity

INTRODUCTION

In 2020, 10 million of the 19.3 million people diagnosed with cancer have died of cancer. (Sung et al., 2021). The high fatality rate highlights the urgent requirement to develop effective anti-cancer treatments. Towards this end, Immunotherapy is a rapidly growing area that utilizes the immune system's potential to eliminate tumors, and chimeric antigen receptor T cells (CARs) have powerful anticancer efficacy. (Grupp et al., 2013; Gun et al., 2019). CAR is a fusion protein composed of an antigen recognition moiety (e.g., antibody single chain variable fragments, scFv) and T cell self-activation signaling moiety (Maher et al., 2002; Sadelain et al., 2013; 2016). The FDA has approved five CARs products to treat hematologic malignancies. (Schuster et al., 2017; DiNofia and Maude, 2019). Selecting tumor specific antigen (TSA) as targets provides a way forward to significantly reform the security of CARs (Sadelain et al., 2013; Huang et al., 2020). Nonetheless, cancers barely show unique antigenic markers (Yong et al., 2017; Qu et al., 2021; Xiao et al., 2021; Chen et al., 2022). Most antigens are expressed in possibly vital organ tissues, which are called tumor associated

antigens (TAA), such as MUC1 (mucoprotein 1), EGFR (epidermal growth factor receptor), ErbB2 (HER2, CD340), GD2 (disialoganglioside), and PSMA (prostate-specific membrane antigen) (MacKay et al., 2020). The specific targeting of these antigens by CARs is limited by normal tissue toxicity (Parkhurst et al., 2011; Brudno and Kochenderfer, 2019). To be sure, ErbB2-based designated CARs therapy intended to treating malignant colon cancer were demonstrated deadly to patient, largely because expression of TAA on lung epithelial cells (Morgan et al., 2010). The basical expression levels of EGFR in skin tissue prompts dose-limiting skin harmfulness (Lamers et al., 2013). Therefore, CARs targeting to TAA would induce the on-target, off-tumor toxicity to human organs (Chmielewski et al., 2004; Morgan et al., 2010; Corse et al., 2011; Parkhurst et al., 2011; Hudecek et al., 2013; Lamers et al., 2013; Brudno and Kochenderfer, 2019). Targeting molecules with low affinity to TAA may provide a way forward for design of CARs in treating malignant solid tumors.

The decision of single chain spacer (Milone et al., 2009), extracellular and costimulatory domains in the design of CAR plasmid significantly affect CARs capacity and performance. Be that as it may, little is had some significant awareness of the impact of CAR binding affinity. It has been reported that increasing affinity between receptor and antigen beyond a certain point may adversely affect T cell responses (Schmid et al., 2010; Tan et al., 2015; Richman et al., 2018). T cell's activation may require the accumulated stimulation from a few high-affinity or large number of low-affinity TCRs (Thomas et al., 2011; Tran et al., 2013; Brudno and Kochenderfer, 2019). Previous work from Chmielewski *etc.* (Thomas et al., 2011; Tran et al., 2013; Brudno and Kochenderfer, 2019; Ghorashian et al., 2019) proposed that high-affinity CARs showed less separation between target cells with high or low antigen expression levels. By increasing the KD (reduced affinity) 2- to 3-log of scFv used in CARs, a significant enhancement was accomplished within the restorative list for ErbB2 and EGFR CARs (Caruso et al., 2015; Liu et al., 2015). Additionally, Pameijer, C. R. J. *et al.* discovered that the scFv could be substituted with peptide ligand in CARs therapy (Pameijer et al., 2007; Whilding et al., 2017; Wang et al., 2020). With the lower affinity antigen receptor than scFv, peptide-based CARs would be activated only when they were docked with overexpressed TAA on tumor cells but not with low, baseline TAA expression on normal cells (Arcangeli et al., 2017; Drent et al., 2017; Walker et al., 2017; Drent et al., 2019; Di Roberto et al., 2020).

The CAR's scFv can be substituted with a peptide ligand that interacts with tumor-overexpressed receptors. Chimeric NKG2D receptors (Zhang et al., 2006; Deng et al., 2019; Frazao et al., 2019), IL-13-cytokine CARs for IL-13R2-expressing tumor cells (Kahlon et al., 2004; Sengupta et al., 2014; Brown et al., 2016), integrin v6-binding peptides (Pameijer et al., 2007; Whilding et al., 2017), and heregulin-chimaeras are all presently in preclinical and early clinical trials. Such peptide-based chimeric antigen receptors are proved less immunogenic than traditional scFvs, since they are human protein and are hence liable to be perceived as self-proteins. Peptides with good binding ability have low molecular weights and it is feasible to link peptides in tandem repeats in one molecule. To evaluate performance of peptides in a CAR format, we designed a peptide-based CAR using peptide A1 (WFCSWYGGDTCVQ). Peptide A1 was discovered and identified to specifically bind to the human lung carcinoma A549 cells (Dong et al., 2013). We integrated the peptide in CAR designs and surveyed the antitumor capacity of CARs. *In vitro* and *in vivo,* we demonstrated that the peptide CARs did not compromise the anti-tumor efficacy and improved their immunotherapeutic potential.

MATERIALS AND METHODS

Peptide-CAR Lentiviral Design and Construction

The CAR constructs are contained in a Lentiviral vector under control of hEF1-α promoter, the Lentiviral vector, which was a gift from the Icartab Biomed of Suzhou. Cloning was done in Stbl 3 *E. coli* cells. To produce virus, HEK 293T cells (the human embryo kidney cells) are dealt with PEI (sigma) with the second generation Lentiviral CAR vector, a pSPAX2 and a pMD 2.0 G packaging vector.

The sequence of A1-CAR is as follows: A1 peptide (WFCSWYGGDTCVQ), linker (GGSGGQ), c-Myc tag (CAE84874, aa 1–11), CD8 (transmembrane and cytosolic, NP_001759, aa 167–235), 4-1BB costimulatory signal (AAA53133, aa 214–255) and CD3-ζ (cytosolic, NP_932170.1, aa 52–164). Scramble-CAR sequence is identical to A1-CAR, with the exception of the scramble peptide (DCQYFWSCGGWVT). Cetux-CAR sequence: the cetuximab light chain (PDB:1YY9_C, aa 1–213), Whitlow linker (AAE377080.1, aa 1–18), and cetuximab heavy chain (PDB:1YY9_D, aa 1–221).

Reagents and Cell Culture

Human recombinant protein IL-2 (cat. #11848-HNAY1) were purchased from BD Biosciences. Human T cell-activated CD3/CD28 beads (cat. #11130D) and FITC-labeled human EGFR protein (cat. No. EGR-HF2H5) were purchased from ACRO Biosystems. FBS (cat. #SV30087.02), RPMI1640 medium (cat. #SN30809.06), and penicillin-streptomycin solution (cat. #RF67729.18) were obtained from HyClone. Anti-IFN-γ (cat. #BS9841) was purchased from BOSTER. Human Interleukin-13 ELISA Kit (EK1162) were purchased from sabbiotech. Anti-GZMB (granzyme B) (cat. #24699-2-SO) was purchased from Proteintech. Antihuman CD3 (cat. #17-9930-60) was purchased from eBioscience. D-Luciferin potassium salt (cat. #M8873) was bought from AbMole. Anti-CD31 (cat. #ab37167-050) and IFN-γ ELISA Kit (cat. #70-EK1802) was obtained from Multisciences. $CD3^{-}CD28$ Dynabeads were purchased from Life Technologies.

The human renal carcinoma cell line ACHN, 786-o and the non-small human lung cancer cell A549 cell line, and MCF-7 cell line were purchased from the Chinese Academy of Sciences cell bank, which were verified by short pair rehash composing strategy. The MDB-MB-231 and HEK-293T was a gift from

Prof. Guangli Suo (Chinese Academy of Sciences). All tumor cells are growing in5% CO2 at 37°C in the Thermo CO_2 incubator.

T Cell Isolation, Activation and CAR Transduction and Generation

1.5×10^{7} peripheral blood mononuclear cells (PBMC) were segregated from the human blood according to the producer's guidelines. To generate CARs, T cells were segregated from PBMC by flow cytometry (BD Aria II)following anti-CD3 labeled. Lymphocytes were transduced with lentivirus relating to different second generation CARs develops. Briefly, the human T cells were enacted on day 0 with against human CD3/CD28 Dynabeads and cultured in T cell culture medium with 10% FBS and 20 IU ml^{-1} recombinant protein human IL-2. The activated human T cells were transduced using the Lentivirus generated from 293 T cells with the Lentiviral CAR vector, a pSPAX2 and a pMD 2.0 G packaging vector with PEI (1 mg/ml) on day 3. The activated human T cells were spined at 2000 g with the Lentivirus and polybrene (7.5 ng/ml) mixture. After two spin-fections, cells were allowed to grow until day 10 and along these lines moved to capacity in fluid nitrogen before functional assays. For every practical examine, all kinds of CARs were obtained from the one human. They were all under the same conditions to expansion. In specific analyses CARs were sorted on BD FACS Aria to acquire a pure population of transduced, c-Myc positive T cells on day 10. The number of CARs was calculated using absolute counter tube by flow cytometry based on beads.

Characterization of Peptide Surface Display and Binding Assays

The positive rate of the CARs was portrayed utilizing a flow cytometry based assay. For most CARs, the positive rate was stained with c-Myc antibody to evaluate binding to effectively transduced cells. Briefly, this experiment was carried out at 4°C and cells were prepared in PBS buffer. The CARs was incubated with c-Myc antibody at 4°C for 15 min. Then the binding capacity of CARs was estimated with anti-c-Myc antibody.

In Vitro Cytotoxicity and Activation Assays

CARs's cytotoxicity was appeared utilizing different CARs with target cells co-culture measures. For cytotoxicity, cocultured the CARs with A549-luc cells overnight and supernatants were gathered and utilized for IL-2 and IFN-γ ELISA estimations. The A549-luc cells (human lung cancer cells with stable luciferase express) expressed EGFR naturally. A549-luc cells were cultured with RPMI 1640, and A1-CARs were included with the A549-luc cells for 18 h hatching. Then add D-Luciferin potassium (15 mg/ml) into the supernatants and the number of lived A549 cells were measured with Cytation 3. Results were analyzed based on luciferase activity: % killing = [RLU (relative light units) of control group - RLU of test group]/(RLU of control group) × 100. Supernatants of verious group were gathered to be utilized of IFN-γ estimations (Multisciences). For proliferation assays, PBMCs and CARs were expanded and then sorted on c-Myc-positive CARs.

In Vivo Studies

Female nude mice (Cavens) aged 5 weeks were raised in good environmental conditions, which is specific pathogen-free (SPF) conditions. The ethical approval number for all animal experiments is SINANO/EC/2019–013 approved by the local Ethical Committee for Animal Experiments.

The A549 cells were screened by adding with puromycin (1 mg/ml) and sorted by flow cytometry after transfect with the plvx-puro/luciferase lentiviral vector.

For xenograft tumor studies, nude mice were given s. c. injection with A549 cells (1×10^{6}) suspended in PBS. For CARs treatment, mice were given i. p. injection with 200 mg/kg cyclophosphamide for depleting circulating lymphocytes on the fourth day (Li et al., 2017). After 6 days, 5×10^{6} of scFv-T cells or peptide-based CARs were given i. v. injection on days 10 and 17.

The size of the tumor volume was measured through the bioluminescence by photoing with the IVIS Lumina II system (PerkinElmer). A total of five measurements over a 51-day period, one every 6 days. Before all the mice were sacrificed on day 51, collecting various organs and all tumor tissues. The dimensions of tumor were measured with calipers, and the volume of tumor was figured: $V = 1/2\ ab^2$, where a and b represented the tumor length and width, respectively.

Immunohistochemistry

The articulation human IFN-γ and GZMB in cancer tissues of each not set in stone by IHC with comparing antibodies. Advanced images were taken by a Zeiss Scope A1, and the stained region of immuno-positive level was surveyed by the computerized picture breaking down programming ImageJ.

Statistical Analysis

All the data were expressed as means ± SD. Histograms and line charts were generated by GraphPad Prism 5.0. T tests were utilized to decide the p values. $^{*}p < 0.05$, $^{**}p < 0.01$, $^{***}p < 0.001$, $^{****}p < 0.0001$.

RESULTS

Design and Characteristics of Peptide-Based CARs

In this study, peptide-based CARs were developed following the main design of single-chain antibody CARs, in which the peptide replaced the scFv as the recognition module. Peptides are much shorter than scFvs and it is feasible to link peptides in tandem repeats in one molecule. For the construction of these CARs, we employed the A1 peptide (WFCSWYGGDTCVQ) specific for A549 cells (Dong et al., 2013; Liu et al., 2019). For most experiments, a scramble peptide (DCQYFWSCGGWVT) was designed and served as the negative (nonspecific) control (Li et al., 2018), and Cetuximab scFv was chosen as the positive control. We named them A1-CAR, scramble-CAR and scFv-CAR, respectively. (**Figure 1A**). We tested the recognition ability of the peptide CAR by developing CAR-Jurkat (**Figure 1B**). Before developed CARs with Lentivirus, T cells sorted from human PBMC were activated with CD3/CD28 Dynabeads for

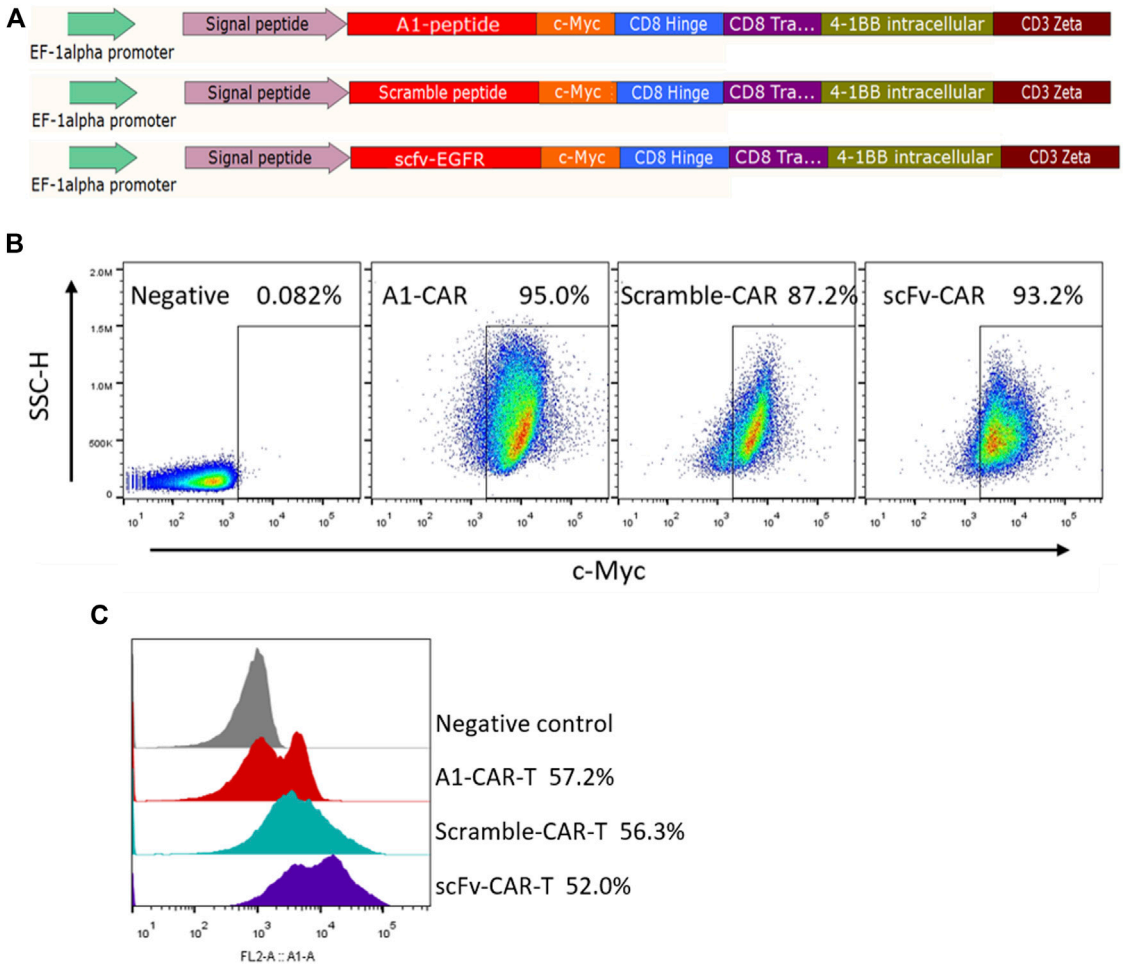

FIGURE 1 | Design and characteristics of peptide-based CARs. **(A)** Lentiviral constructs of peptide-based A1-CAR, Scramble-CAR and EGFR-scFv-CAR. **(B)** Surface expression of the CAR on Jurkat cells at the end of the primary expansion on day 3 detected by binding to c-Myc antibody. Representative of three donors. **(C)** Surface expression of the CAR on the human T cells at the end of the primary expansion on day 3 detected by binding to c-Myc antibody. Representative of three donors.

3 days. T cells were successfully transduced, and the positive rate of peptide-based CARs was almost comparable to or lightly higher than scFv-CARs (c-Myc-positive, typically 40–80% transduced) (**Figure 1C**). As can be seen from a FACS-based assay, the A1-peptide CAR successfully transduced into T cells. These results reveal that peptide is easily displayed as CAR recognition modules on human T cells.

Peptide Based CARs Could be Effectively Activated and Showed Killing Effect on A549 Tumor Cells in Vitro

We firstly assessed the function of A1 peptide on the CARs. As higher expression of CAR is known to upgrade the proliferation and lysis target cell properties of CARs (Sadelain et al., 2013; 2016), the absolute number of cell divisions was evaluated. Multiple rounds stimulation by co-culturing with mitomycin-C-treated A549 cells, induced persistent cellular expansion of A1-CARs. The number was slightly higher for peptide-based CARs compared to traditional scFv-CARs (**Figure 2A**). Having appeared the authoritative specificity of peptide CARs, we decided to investigated functional properties of peptide-based CARs, such as targeting killing effect and the function of cytokine release. To investigate if A1-CARs targeting A549 cells could specifically recognize and lyse A549 cancer cells, a bioluminescence-based cytolytic assay was settled using the human lung carcinoma A549-luc cells. As demonstrated in **Figure 2B**, The L1-CARs lysed the A549-luc cells in a dose-dependent way. No noteworthy differences in cytotoxicity were observed between peptide-based CARs and scFv-CARs (**Figure 2C**). Meanwhile, the function of cytokine release of A1-CARs following co-cultured with A549 lung cancer cell was assessed. Upon incubation of A1-CARs with A549 cells, there were great increases in IFN-γ, GM-CSF and IL-3 in the culture supernatants of A549 cells-specific CARs compared to negative (nonspecific) control (**Figures 2D–F**). These results reveal that the kill ability of the A1 peptide-CARs to A549 tumor cells was specific. Specific cytotoxicity appeared in a dose-dependent way.

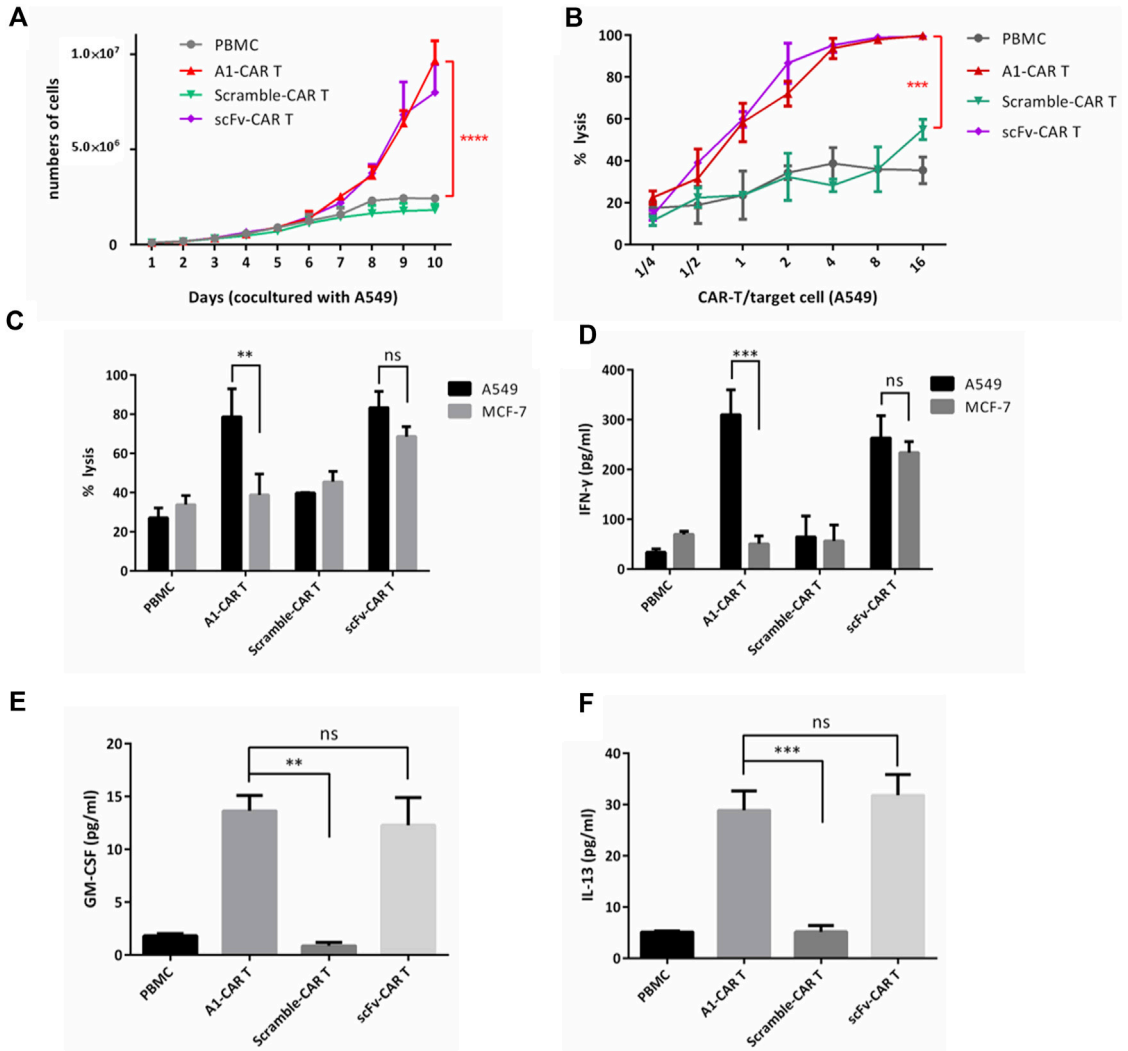

FIGURE 2 | Peptide based CARs could be effectively activated and showed killing effect on A549 tumor cells *in vitro*. **(A)** On different days 1:1 cocultured with mitomycin-C-treated A549 cells, the numbers of PBMC, A1-CARs, scFv-CARs, and Scramble-CARs were examined (n = 3). T tests were utilized to decide the *p* values. **(B)** Cytotoxicity assay using A549-luc cells as targets. Data represent the mean ± SD of quadruplicate wells. T tests were utilized to decide the *p* values. **(C)** CARs were blended with target cells (A549-luc) at the effector/target (E/T = 4:1) ratios. 24 h later, Cytation three was used to detect bioluminescence to evaluate the percentage of lysis. CARs generated from six individual human donors. T tests were utilized to decide the *p* values. **(D–F)** CARs were blended with target cells (A549-luc) at the effector/target (E/T = 4:1) ratios. Supernatants were obtained 24 h after coculture. The amount of IFN-γ, GM-CSF and IL-13 was analyzed by fluorescence-based ELISA Kit (*n* = 4). Data represent the mean ± SD. *T* tests were utilized to decide the *p* values.

That came to the conclusion that the peptide-based CARs have great specific cytotoxicity to tumor cells.

A1-CARs Are More Effective in Inhibiting the Growth of Xenograft Tumors

The superior killing ability of our A1-CARs target A549 cells prompted us to further investigate its tumor-killing properties *in vivo*. The antitumor activities of A1-CARs *in vivo* were assessed in the xenograft mouse model.

A549-luc is a lung cancer cell line with stable luciferase express. We s. c. inoculated nude mice with A549-luc the human lung carcinoma cells on day 0. Mice were burdened with tumors were treated with 100 μL PBS or 100 μL, 200 mg/kg cyclophosphamide (CTX) on day 4. For CARs treatment in part of cyclophosphamide group, mice were not only injected i. p. with CTX to deplete host lymphocyte compartments on day 4. For CARs treatment, mice were given i. p. injection with 200 mg/kg cyclophosphamide for depleting circulating lymphocytes on the fourth day. After 6 days, 5×10^6 of scFv-T cells or peptide-based CARs were given i. v. injection on days 10 and 17. (**Figure 3A**). For PBS group and CTX group, mice were injected i. v. with 100 μL PBS or CTX. The scramble-CARs was used as negative control. The positive rate of all group CARs was greater than 38% (**Figure 1C**). Representative bioluminescence images of tumor-burdened mice in each group are shown in **Figure 3B**. The total brightness (P/s) of each group

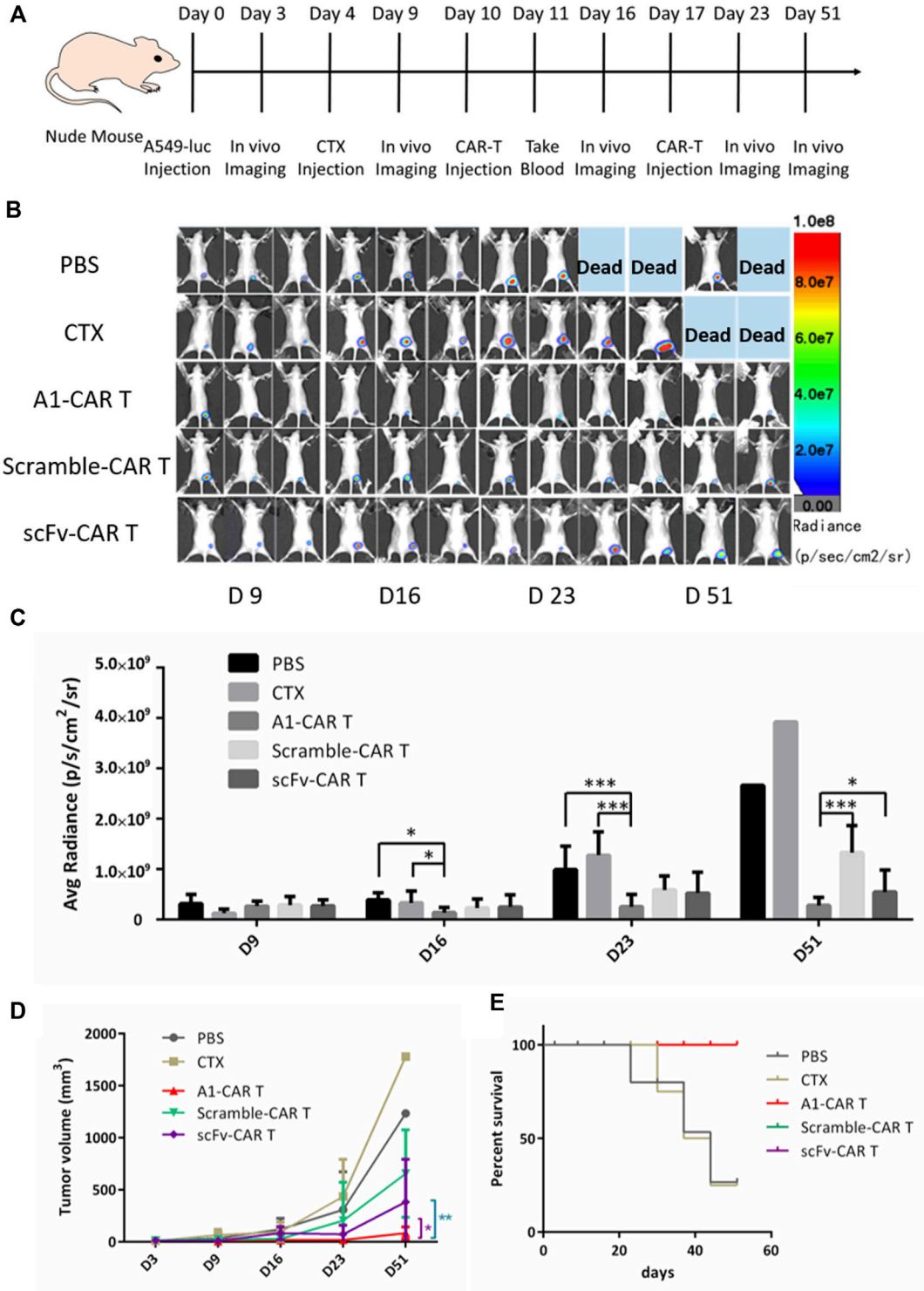

FIGURE 3 | Bispecific CARs are more effective in inhibiting the growth of xenograft tumors. **(A)** The injection process of CARs to the mice with tumor xenografts. **(B)** A1-CARs demonstrated potent antitumor activity indicated by bioluminescent imaging with the IVIS Lumina II system (PerkinElmer) every week for a total of five times **(C)** The bioluminescence intensities in mice were measured. $n = 4$ mice. Values represent mean ± SD. $p = 0.023$ (D16, PBS vs. CTX + A1-CARs); $p = 0.016$ (D16, CTX vs. CTX + A1-CARs); $p = 3.5 \times 10^{-4}$ (D23, PBS vs. CTX + A1-CARs); $p = 7.2 \times 10^{-4}$ (D23, CTX only vs. CTX + A1-CARs); $p = 1.7 \times 10^{-4}$ (D51, CTX + A1-CARs vs. CTX + Scramble-CARs); $p = 0.03$ (CTX + A1-CARs vs. CTX + scFv-CARs). Calculated p values from two-sided Student's t test. n = 4 mice/group. **(D)** The tumor volume average measurements and values of mice are measured. $^{*}p = 0.019$, $^{**}p = 0.009$. $n = 4$ mice/group. T tests were utilized to decide the p values. **(E)** Survival of the mice are shown.

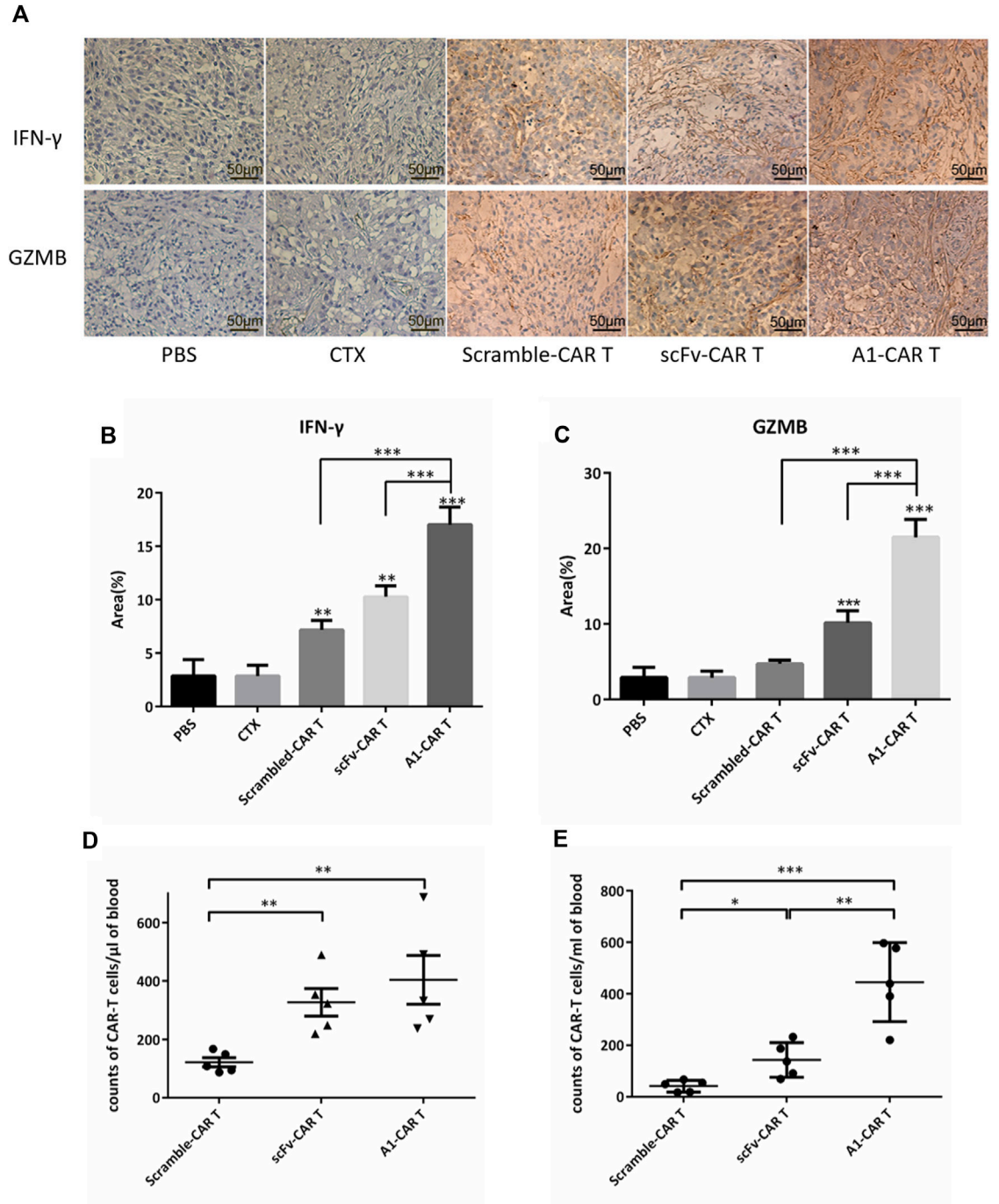

FIGURE 4 | Peptide-based CARs had robust expansion ability and long-term functional persistence *in vivo*. (A) IFN-γ and GZMB immune staining images of tumor tissues from various groups. **(B,C)** Immunohistochemical quantitative analysis of IFN-γ and GZMB. Data were given as mean ± SD from five independent experiments. ***$p < 0.001$. *T* tests were utilized to decide the *p* values. **(D,E)** After 1 day and 21 days following infusion of CARs, CARs in peripheral blood were quantified by flow cytometry. $n = 5$ mice. Data is shown with mean ± SD. *$p < 0.05$, **$p < 0.01$, ***$p < 0.001$. *T* tests were utilized to decide the *p* values.

(**Figure 3C**) and tumor volume (**Figure 3D**) were recorded. The ability of inhibit tumor growth of A1-CARs was consistent with what we observed *in vitro*. There are clear differences between these groups. In xenograft mouse models, two doses of A1-CARs inhibited tumor growth. Notably, one of four (25%) of the mice cells were tumor-free after two dosages in group A1-CARs on days 51, but neither in group scFv-CARs group nor in scramble-CARs group. The tumor growth rate in A1-CARs group or scFv-CARs group treated mice was 82.65% or 32.73% lower than that in control scramble-CARs group, respectively (**Figure 3C**). Mice were

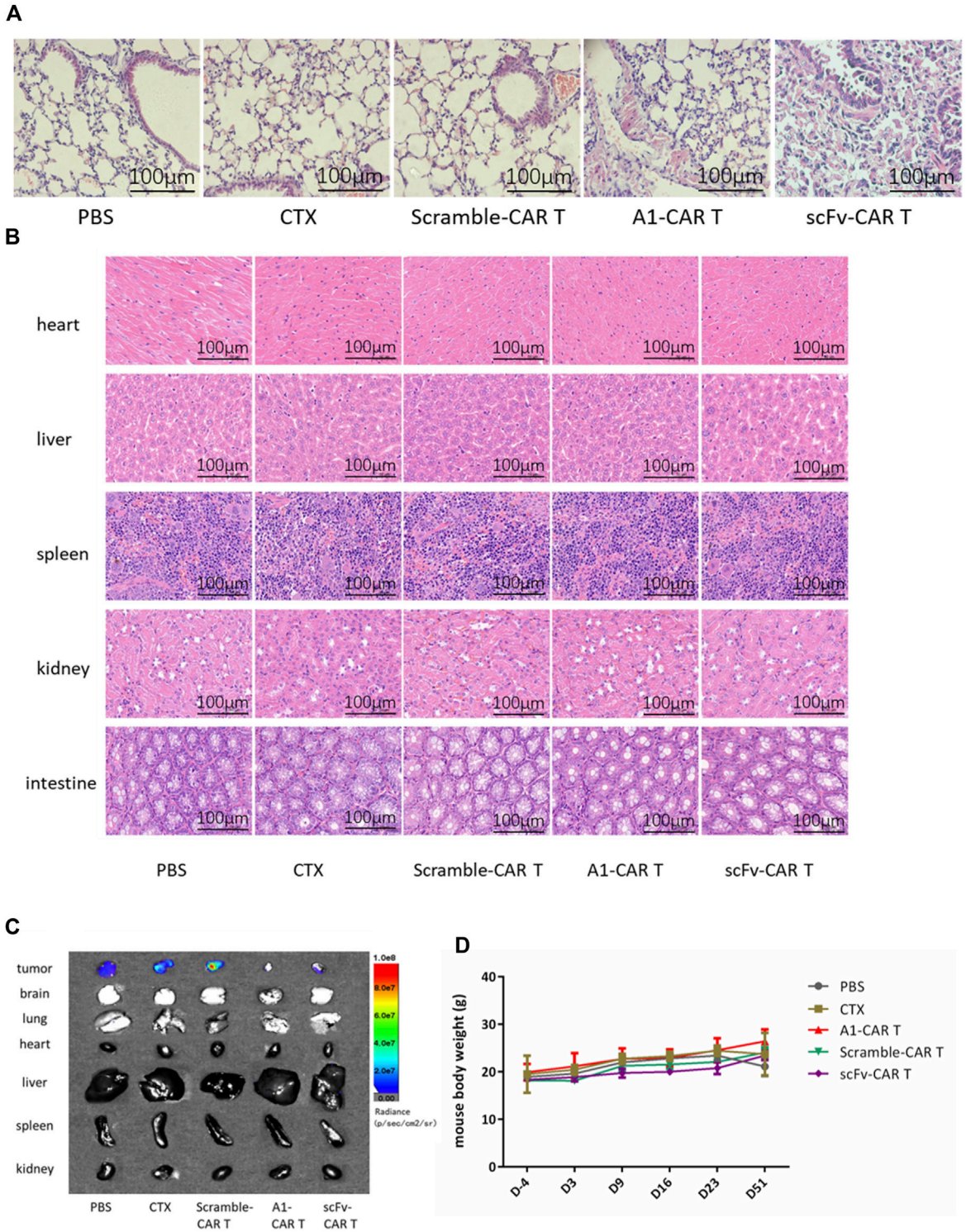

FIGURE 5 | Treatment with A1-CARs reduced on-target, off-tumor toxicity. On day 51, mice were sacrificed after 5 minutes. **(A)** Lung tissue was stained with H&E. **(B)** Heart, liver, spleen, kidney and intestine tissue was stained with H&E. **(C)**On day 51, mice were injected i. p. with D-Luciferin potassium salt and were sacrificed after 5 minutes. Tumor tissues and organs (lung, heart, liver, spleen, kidney, brain and intestine)were resected from the mice, and measured the bioluminescence by the IVIS Lumina II system (PerkinElmer). **(D)** The mice body weight was calculated. n = 4 mice. Values represent mean ± SD.

euthanized once the tumor size reached 2000 mm^3. The survival curve also shows the differences in survival for all CARs groups contrast with the PBS and CTX group were statistically significant ($p < 0.01$). And A1-CARs more significantly decreased the tumor growth contrast with Scramble-CARs or scFv-CARs (**Figure 3E**).

These results confirm that A1-CARs are very effective in suppressing tumor growth.

Peptide-Based CARs Show Better Cytokine Release and Persistence in Vivo

On day 51, tumor masses were detached, fixed for IHC. And then, Tumor masses were stained by IFN-γ and GZMB. IHC results revealed that the secretion level of IFN-γ and GZMB of A1-CARs group was significantly higher compared to the scramble-CARs group (**Figures 3A–C**). The area of IFN-γ was 63.6% more in A1-CARs treated tumors more than scFv-CARs treated, 6 times more than the untreated tumors (**Figure 5B**). As shown in **Figure 5C**, the area of GZMB was 110.5% more in A1-CARs treated tumors more than scFv-CARs treated, 7 times more than the untreated tumors.

To trigger elimination of large tumors, CARs may require robust expansion ability and long-term functional persistence *in vivo*. We evaluated the durability of peptide-based CARs in mice burden malignancies to further verify mechanisms of A1-CARs treatment on tumor progression. Blood was obtained 1 day and 21 days following the first CARs injection. Then, we measured the amount of $CD3^+$ T cells. Substantial differences were observed in different groups mice bearing tumor. A1-CARs showed greater persistence at day 31 than scramble-CARs or scFv-CARs. (**Figures 4D,E**), indicating that small peptide is beneficial for survival of CARs contrast with scFv.

Treatment With A1-CARs Reduced On-Target, Off-Tumor Toxicity

We further investigated the cytotoxicity against normal organs and tissues. As observed in H&E stained tissues, no visible side effects were observed upon repeated administration. The lung tissue of mice in the scFv-CARs group showed obvious fibrosis, with fewer alveoli and denser cells, showing obvious tissue lesions. Unlike the scFv-CARs group, immunogenicity or on-target-off-tumor effect did not adversely affect the lung tissue in A1-CARs group (**Figure 5A**).

In order to verify whether the second-generation CARs have toxic side effects on other normal organs and tissues, H&E staining was performed and photographed under an upright microscope. As results shown in **Figure 5B**, the heart, liver, spleen, kidney and intestine of mice showed normal, with no group differences and no evidence of damaged lesions.

Under instant detection by bioluminescence microscopy, the various organs (lung, heart, liver, spleen, kidney, brain and intestine) of the mice showed no tumor metastasis and no significant size differences (**Figure 5C**). As shown in **Figure 5D**, the body weights of each group mice were non significantly changing by CARs.

We conclude that peptide was beneficial for generating CARs that are effective and safe in suppressing tumor growth in xenograft mouse model.

DISCUSSION

Our findings settle one of the governing challenges of CARs therapy for treating solid tumors: the expression of TAA on some organ tissues. In the results, we certified the ability of peptides-based CARs to target the tumor cells *in vitro* assays and be delivered to the interior of solid tumors *in vivo* assays, which indicated that peptide-based CAR would be an alternative treatment for relapsed and refractory solid tumor.

Compared with the great progress of CARs in the treatment of hematological tumors, many innovations are needed for CARs to defeat solid tumors. One of the major difficulties is the lack of unique antigens. Most antigens recommended as CARs focuses to treat solid tumors are selective to particular disease types, and restricted data on antigens for most of solid tumors put numerous cancers far off for CARs treatment (Dotti et al., 2014). To some extent, the effect of CARs depended on the differential articulation of the objective antigen in tumor and normal tissue. Existing information showed that CARs with known serious on track, off-cancer poison can be reengineered by partiality tuning, holding effect *in vivo* while lessening or diminishing poisonousness. Specifically, the 4D5 CAR in view of trastuzumab had deadly poisonousness (Morgan et al., 2010), because of acknowledgment of physiologic degrees of ErbB2 communicated in cardiopulmonary tissues (Gross and Eshhar, 2016). Past work from Chmielewski and Xiaojun Liu (Thomas et al., 2011; Tran et al., 2013; Brudno and Kochenderfer, 2019; Ghorashian et al., 2019) proposed that the high partiality CARs displayed less segregation between target cells with high or low objective articulation levels. Through lessening the KD of scFv utilized in CARs by 2-to 3-log, a significant improvement in the helpful record for ErbB2 and EGFR CARs. Here, compared to the high liking scFv, we exhibited that CARs with peptides showed similarly powerful effect against target cancers.

Despite the target A549 cell was used to confirm this of-idea, this approach maybe apply in the other targets, such as antigen Her-2, FAP and ErbB2 and so on (MacKay et al., 2020). Maybe they can further enhance the activity of antitumor, in spite of that those targets have serious side effects in CARs with single-chain antibodies.

As with therapies combining different checkpoint-blocked inhibitors, combining CARs with other methods is the best choice for solid tumors, such as antibodies, radiation, or small-molecule drugs. The results of the EGFR-targeted and fibrin-fibronectins-targeted CARs demonstrate that the way of peptide-based CAR can be used in a variety of tumors. When peptides with appropriate specificity are recognized, without any modification, they can express by inserting into the backbone of the CAR. The scope of syngeneic tumors that can be targeted by CARs in mouse xenograft model is broadened by building a platform for the production of peptide-based CARs. Due to peptides are easy to express, as antigen recognition domains for CARs, they are attractive (Pameijer et al., 2007; Whilding et al., 2017; Wang et al., 2020).

CARs therapy are remarkable potential to treat cancers (Larson and Maus, 2021). Keishi Adachi's et al. reported that, in addition to serving as direct antitumor effector cells, CARs can also serve as cellular carriers to transfer immunomodulatory molecules into the tumor microenvironment (Adachi and Tamada, 2018). For improvement of the CARs therapy effect, they developed CARs producing CCL19 and IL-7 to simulate the CARs. This strategy could recruit DCs and T cells to tumor environment, strengthening the treatment effects of CARs toward solid tumors. The combination of immune-regulatory factors with CAR improved the anti-tumor effects of CARs. In our work, the peptide-based CARs were produced and optimized, and their functionalities (cytotoxicity, tumor growth inhibition, *etc*) were verified *in vitro* and *in vivo*. Peptide-based A1-CARs recognizing A549 cells showed ligand specific cytotoxicity, which were efficacious in mouse xenograft model. We plan to further modify these peptides CARs for expression of checkpoint pathway inhibitors, chemokines, and cytokines to enhance the CARs trafficking to tumor tissues and evaluate their anti-tumor functions.

Mouse xenograft models still remain universal for the CARs study (Wilkie et al., 2008; Craddock et al., 2010; Johnson et al., 2015). Although these models enable human tumor and CARs studies, several disadvantages are still encountered. For instance, these models lack intact innate as well as adaptive immunity, and are not capable of depicting the clinical immune potential. Compared with xenograft models, immunocompetent or PDX (patient-derived xenografts) models represent a better option for the evaluation of safety during treatment. Therapeutic strategies without immune depletion are in demand, and endogenous anti-tumor immunity profile is significant in tumor surveillance (Fong et al., 2009). Researchers should pay more attention on combination therapies (e.g. cytokine therapies and checkpoint blockade)for improved treatment effect of solid tumors.

Given that the human lung carcinoma is the most common tumor type, we will determine whether peptide-based CARs therapy could exert influence to diverse other tumor models. Our results endow considerable importance to the clinic. On one hand, this strategy shows capacity to enhance the safety and clinical potential of CARs for validated targets. On the other hand, the applicability of our design can be extended to targets that are not druggable previously with CARs due to on-target toxicity. Beyond doubt, CAR peptides with higher safety profile and efficacy can be designed for various common carcinomas.

Taken together, a safe and effective peptides CAR design is proposed here, and *in vitro* and *in vivo*, T cells treated by peptides CAR lentivirus leads to specific and potent inhibition of the human lung carcinoma A549 cells. These results demonstrate that peptide-based CARs therapeutics might represent an intriguing strategy for the treatment of solid tumors. We propose that the peptide-based CARs might be clinically translated for more solid tumor types.

DATA AVAILABILITY STATEMENT

The original contributions presented in the study are included in the article/**Supplementary Material**, further inquiries can be directed to the corresponding authors.

ETHICS STATEMENT

The animal study was reviewed and approved by the Ethics Committee of Suzhou Institute of Nanotechnology and Nanobionics, Chinese Academy of Sciences.

AUTHOR CONTRIBUTIONS

Conception and design: CL and YZ Development of methodology: CL, LL, and YZ Acquisition of data (provided animals, acquired and managed patients, provided facilities, etc.): CL, FG, YQ, and XY Analysis and interpretation of data (e.g., statistical analysis, biostatistics, computational analysis): CL and YZ Writing, review, and/or revision of the manuscript: CL, LL, GY, and YZ Administrative, technical, or material support (i.e., reporting or organizing data, constructing databases): CL, LL, FG, and YZ Study supervision: CL, GY, YZ, and JZ.

FUNDING

This work was supported by the Science and Technology Bureau of Suzhou (No. SS2019013), the National Natural Science Foundation of China (81972825), the Suzhou medical key disciplines (SZXK202133).

SUPPLEMENTARY MATERIAL

The Supplementary Material for this article can be found online at: https://www.frontiersin.org/articles/10.3389/fbioe.2022.928169/full#supplementary-material

REFERENCES

Adachi, K., and Tamada, K. (2018). Microbial Biomarkers for Immune Checkpoint Blockade Therapy Against Cancer. *J. Gastroenterol.* 53 (9), 999–1005. doi:10.1007/s00535-018-1492-9

Arcangeli, S., Rotiroti, M. C., Bardelli, M., Simonelli, L., Magnani, C. F., Biondi, A., et al. (2017). Balance of Anti-CD123 Chimeric Antigen Receptor Binding Affinity and Density for the Targeting of Acute Myeloid Leukemia. *Mol. Ther.* 25 (8), 1933–1945. doi:10.1016/j.ymthe.2017.04.017

Brown, C. E., Alizadeh, D., Starr, R., Weng, L., Wagner, J. R., Naranjo, A., et al. (2016). Regression of Glioblastoma after Chimeric Antigen Receptor T-Cell Therapy. *N. Engl. J. Med.* 375 (26), 2561–2569. doi:10.1056/NEJMoa1610497

Brudno, J. N., and Kochenderfer, J. N. (2019). Recent Advances in CAR T-Cell Toxicity: Mechanisms, Manifestations and Management. *Blood Rev.* 34, 45–55. doi:10.1016/j.blre.2018.11.002

Caruso, H. G., Hurton, L. V., Najjar, A., Rushworth, D., Ang, S., Olivares, S., et al. (2015). Tuning Sensitivity of CAR to EGFR Density Limits Recognition of Normal Tissue while Maintaining Potent Antitumor Activity. *Cancer Res.* 75 (17), 3505–3518. doi:10.1158/0008-5472.CAN-15-0139

Chen, L., Chen, F., Li, J., Pu, Y., Yang, C., Wang, Y., et al. (2022). CAR-T Cell Therapy for Lung Cancer: Potential and Perspective. *Thorac. Cancer* 13 (7), 889–899. doi:10.1111/1759-7714.14375

Chimeric Antigen Receptor-Modified T Cells in Chronic Lymphoid Leukemia (2016). Chimeric Antigen Receptor-Modified T Cells in Chronic Lymphoid Leukemia Chimeric Antigen Receptor-Modified T Cells for Acute Lymphoid Leukemia; Chimeric Antigen Receptor T Cells for Sustained Remissions Leukemia. *N. Engl. J. Med.* 374 (10), 998. doi:10.1056/NEJMx160005

Chmielewski, M., Hombach, A., Heuser, C., Adams, G. P., and Abken, H. (2004). T Cell Activation by Antibody-Like Immunoreceptors: Increase in Affinity of the Single-Chain Fragment Domain above Threshold Does Not Increase T Cell Activation Against Antigen-Positive Target Cells but Decreases Selectivity. *J. Immunol.* 173 (12), 7647–7653. doi:10.4049/jimmunol.173.12.7647

Corse, E., Gottschalk, R. A., and Allison, J. P. (2011). Strength of TCR-Peptide/MHC Interactions and *In Vivo* T Cell Responses. *J. Immunol* 186 (9), 5039–5045. doi:10.4049/jimmunol.1003650

Craddock, J. A., Lu, A., Bear, A., Pule, M., Brenner, M. K., Rooney, C. M., et al. (2010). Enhanced Tumor Trafficking of GD2 Chimeric Antigen Receptor T Cells by Expression of the Chemokine Receptor CCR2b. *J. Immunother.* 33 (8), 780–788. doi:10.1097/CJI.0b013e3181ee6675

Deng, X., Gao, F., Li, N., Li, Q., Zhou, Y., Yang, T., et al. (2019). Antitumor Activity of NKG2D CAR-T Cells against Human Colorectal Cancer Cells *In Vitro* and *In Vivo*. *Am. J. Cancer Res.* 9 (5), 945–958.

Di Roberto, R. B., Castellanos-Rueda, R., Frey, S., Egli, D., Vazquez-Lombardi, R., Kapetanovic, E., et al. (2020). A Functional Screening Strategy for Engineering Chimeric Antigen Receptors with Reduced On-Target, Off-Tumor Activation. *Mol. Ther.* 28 (12), 2564–2576. doi:10.1016/j.ymthe.2020.08.003

DiNofia, A. M., and Maude, S. L. (2019). Chimeric Antigen Receptor T-Cell Therapy Clinical Results in Pediatric and Young Adult B-ALL. *Hemasphere* 3 (4), e279. doi:10.1097/HS9.0000000000000279

Dong, B., Wang, A., Yuan, L., Chen, L., Pu, K., Duan, W., et al. (2013). Peptide-fluorescent Bacteria Complex as Luminescent Reagents for Cancer Diagnosis. *Plos One* 8 (1), e54467. doi:10.1371/journal.pone.0054467

Dotti, G., Gottschalk, S., Savoldo, B., and Brenner, M. K. (2014). Design and Development of Therapies Using Chimeric Antigen Receptor-Expressing T Cells. *Immunol. Rev.* 257 (1), 107–126. doi:10.1111/imr.12131

Drent, E., Poels, R., Ruiter, R., van de Donk, N. W. C. J., Zweegman, S., Yuan, H., et al. (2019). Combined CD28 and 4-1BB Costimulation Potentiates Affinity-Tuned Chimeric Antigen Receptor-Engineered T Cells. *Clin. Cancer Res.* 25 (13), 4014–4025. doi:10.1158/1078-0432.CCR-18-2559

Drent, E., Themeli, M., Poels, R., de Jong-Korlaar, R., Yuan, H., de Bruijn, J., et al. (2017). A Rational Strategy for Reducing On-Target Off-Tumor Effects of CD38-Chimeric Antigen Receptors by Affinity Optimization. *Mol. Ther.* 25 (8), 1946–1958. doi:10.1016/j.ymthe.2017.04.024

Fong, L., Kwek, S. S., O'Brien, S., Kavanagh, B., McNeel, D. G., Weinberg, V., et al. (2009). Potentiating Endogenous Antitumor Immunity to Prostate Cancer through Combination Immunotherapy with CTLA4 Blockade and GM-CSF. *Cancer Res.* 69 (2), 609–615. doi:10.1158/0008-5472.CAN-08-3529

Frazao, A., Rethacker, L., Messaoudene, M., Avril, M.-F., Toubert, A., Dulphy, N., et al. (2019). NKG2D/NKG2-Ligand Pathway Offers New Opportunities in Cancer Treatment. *Front. Immunol.* 10, 661. doi:10.3389/fimmu.2019.00661

Ghorashian, S., Kramer, A. M., Onuoha, S., Wright, G., Bartram, J., Richardson, R., et al. (2019). Enhanced CAR T Cell Expansion and Prolonged Persistence in Pediatric Patients with ALL Treated with a Low-Affinity CD19 CAR. *Nat. Med.* 25 (9), 1408–1414. doi:10.1038/s41591-019-0549-5

Gross, G., and Eshhar, Z. (2016). Therapeutic Potential of T Cell Chimeric Antigen Receptors (CARs) in Cancer Treatment: Counteracting Off-Tumor Toxicities for Safe CAR T Cell Therapy. *Annu. Rev. Pharmacol. Toxicol.* 56, 59–83. doi:10.1146/annurev-pharmtox-010814-124844

Grupp, S. A., Kalos, M., Barrett, D., Aplenc, R., Porter, D. L., Rheingold, S. R., et al. (2013). Chimeric Antigen Receptor-Modified T Cells for Acute Lymphoid Leukemia. *N. Engl. J. Med.* 368 (16), 1509–1518. doi:10.1056/NEJMoa1215134

Gun, S. Y., Lee, S. W. L., Sieow, J. L., and Wong, S. C. (2019). Targeting Immune Cells for Cancer Therapy. *Redox Biol.* 25, 101174. doi:10.1016/j.redox.2019.101174

Huang, R., Li, X., He, Y., Zhu, W., Gao, L., Liu, Y., et al. (2020). Recent Advances in CAR-T Cell Engineering. *J. Hematol. Oncol.* 13 (1), 86. doi:10.1186/s13045-020-00910-5

Hudecek, M., Lupo-Stanghellini, M.-T., Kosasih, P. L., Sommermeyer, D., Jensen, M. C., Rader, C., et al. (2013). Receptor Affinity and Extracellular Domain Modifications Affect Tumor Recognition by ROR1-specific Chimeric Antigen Receptor T Cells. *Clin. Cancer Res.* 19 (12), 3153–3164. doi:10.1158/1078-0432.CCR-13-0330

Johnson, L. A., Scholler, J., Ohkuri, T., Kosaka, A., Patel, P. R., McGettigan, S. E., et al. (2015). Rational Development and Characterization of Humanized Anti-EGFR Variant III Chimeric Antigen Receptor T Cells for Glioblastoma. *Sci. Transl. Med.* 7 (275). 275ra222. doi:10.1126/scitranslmed.aaa4963

Kahlon, K. S., Brown, C., Cooper, L. J. N., Raubitschek, A., Forman, S. J., and Jensen, M. C. (2004). Specific Recognition and Killing of Glioblastoma Multiforme by Interleukin 13-Zetakine Redirected Cytolytic T Cells. *Cancer Res.* 64 (24), 9160–9166. doi:10.1158/0008-5472.CAN-04-0454

Lamers, C. H., Sleijfer, S., van Steenbergen, S., van Elzakker, P., van Krimpen, B., Groot, C., et al. (2013). Treatment of Metastatic Renal Cell Carcinoma with CAIX CAR-Engineered T Cells: Clinical Evaluation and Management of On-Target Toxicity. *Mol. Ther.* 21 (4), 904–912. doi:10.1038/mt.2013.17

Larson, R. C., and Maus, M. V. (2021). Recent Advances and Discoveries in the Mechanisms and Functions of CAR T Cells. *Nat. Rev. Cancer* 21 (3), 145–161. doi:10.1038/s41568-020-00323-z

Li, C., Zhang, N., Zhou, J., Ding, C., Jin, Y., Cui, X., et al. (2018). Peptide Blocking of PD-1/pd-L1 Interaction for Cancer Immunotherapy. *Cancer Immunol. Res.* 6 (2), 178–188. doi:10.1158/2326-6066.CIR-17-0035

Li, N., Fu, H., Hewitt, S. M., Dimitrov, D. S., and Ho, M. (2017). Therapeutically Targeting Glypican-2 via Single-Domain Antibody-Based Chimeric Antigen Receptors and Immunotoxins in Neuroblastoma. *Proc. Natl. Acad. Sci. U.S.A.* 114 (32), E6623–E6631. doi:10.1073/pnas.1706055114

Liu, C., Cui, X., Zhou, D., Li, C., Zhao, M., Jin, Y., et al. (2019). Cytokine-Induced Killer Cells Co-Cultured with Non-Cell Derived Targeting Peptide-Loaded Dendritic Cells Induce a Specific Antitumor Response. *Cancer Biol. Ther.* 20 (5), 720–728. doi:10.1080/15384047.2018.1564561

Liu, X., Jiang, S., Fang, C., Yang, S., Olalere, D., Pequignot, E. C., et al. (2015). Affinity-Tuned ErbB2 or EGFR Chimeric Antigen Receptor T Cells Exhibit an Increased Therapeutic Index against Tumors in Mice. *Cancer Res.* 75 (17), 3596–3607. doi:10.1158/0008-5472.CAN-15-0159

MacKay, M., Afshinnekoo, E., Rub, J., Hassan, C., Khunte, M., Baskaran, N., et al. (2020). The Therapeutic Landscape for Cells Engineered with Chimeric Antigen Receptors. *Nat. Biotechnol.* 38 (2), 233–244. doi:10.1038/s41587-019-0329-2

Maher, J., Brentjens, R. J., Gunset, G., Rivière, I., and Sadelain, M. (2002). Human T-Lymphocyte Cytotoxicity and Proliferation Directed by a Single Chimeric TCRζ/CD28 Receptor. *Nat. Biotechnol.* 20 (1), 70–75. doi:10.1038/nbt0102-70

Milone, M. C., Fish, J. D., Carpenito, C., Carroll, R. G., Binder, G. K., Teachey, D., et al. (2009). Chimeric Receptors Containing CD137 Signal Transduction Domains Mediate Enhanced Survival of T Cells and Increased Antileukemic Efficacy *In Vivo*. *Mol. Ther.* 17 (8), 1453–1464. doi:10.1038/mt.2009.83

Morgan, R. A., Yang, J. C., Kitano, M., Dudley, M. E., Laurencot, C. M., and Rosenberg, S. A. (2010). Case Report of a Serious Adverse Event Following the Administration of T Cells Transduced with a Chimeric Antigen Receptor Recognizing ERBB2. *Mol. Ther.* 18 (4), 843–851. doi:10.1038/mt.2010.24

Pameijer, C. R. J., Navanjo, A., Meechoovet, B., Wagner, J. R., Aguilar, B., Wright, C. L., et al. (2007). Conversion of a Tumor-Binding Peptide Identified by Phage Display to a Functional Chimeric T Cell Antigen Receptor. *Cancer Gene Ther.* 14 (1), 91–97. doi:10.1038/sj.cgt.7700993

Parkhurst, M. R., Yang, J. C., Langan, R. C., Dudley, M. E., Nathan, D.-A. N., Feldman, S. A., et al. (2011). T Cells Targeting Carcinoembryonic Antigen Can Mediate Regression of Metastatic Colorectal Cancer but Induce Severe Transient Colitis. *Mol. Ther.* 19 (3), 620–626. doi:10.1038/mt.2010.272

Qu, J., Mei, Q., Chen, L., and Zhou, J. (2021). Chimeric Antigen Receptor (CAR)-T-Cell Therapy in Non-Small-Cell Lung Cancer (NSCLC): Current Status and Future Perspectives. *Cancer Immunol. Immunother.* 70 (3), 619–631. doi:10.1007/s00262-020-02735-0

Richman, S. A., Nunez-Cruz, S., Moghimi, B., Li, L. Z., Gershenson, Z. T., Mourelatos, Z., et al. (2018). High-Affinity GD2-specific CAR T Cells Induce Fatal Encephalitis in a Preclinical Neuroblastoma Model. *Cancer Immunol. Res.* 6 (1), 36–46. doi:10.1158/2326-6066.CIR-17-0211

Sadelain, M., Brentjens, R., and Rivière, I. (2013). The Basic Principles of Chimeric Antigen Receptor Design. *Cancer Discov.* 3 (4), 388–398. doi:10.1158/2159-8290.CD-12-0548

Schmid, D. A., Irving, M. B., Posevitz, V., Hebeisen, M., Posevitz-Fejfar, A., Sarria, J.-C. F., et al. (2010). Evidence for a TCR Affinity Threshold Delimiting Maximal CD8 T Cell Function. *J. Immunol.* 184 (9), 4936–4946. doi:10.4049/jimmunol.1000173

Schuster, S. J., Svoboda, J., Chong, E. A., Nasta, S. D., Mato, A. R., Anak, Ö., et al. (2017). Chimeric Antigen Receptor T Cells in Refractory B-Cell Lymphomas. *N. Engl. J. Med.* 377 (26), 2545–2554. doi:10.1056/NEJMoa1708566

Sengupta, S., Thaci, B., Crawford, A. C., and Sampath, P. (2014). Interleukin-13 Receptor Alpha 2-targeted Glioblastoma Immunotherapy. *BioMed Res. Int.* 2014, 1–8. doi:10.1155/2014/952128

Sung, H., Ferlay, J., Siegel, R. L., Laversanne, M., Soerjomataram, I., Jemal, A., et al. (2021). Global Cancer Statistics 2020: GLOBOCAN Estimates of Incidence and Mortality Worldwide for 36 Cancers in 185 Countries. *CA A Cancer J. Clin.* 71 (3), 209–249. doi:10.3322/caac.21660

Tan, M. P., Gerry, A. B., Brewer, J. E., Melchiori, L., Bridgeman, J. S., Bennett, A. D., et al. (2015). T Cell Receptor Binding Affinity Governs the Functional Profile of Cancer-specific CD8+ T Cells. *Clin. Exp. Immunol.* 180 (2), 255–270. doi:10.1111/cei.12570

Thomas, S., Xue, S.-A., Bangham, C. R. M., Jakobsen, B. K., Morris, E. C., and Stauss, H. J. (2011). Human T Cells Expressing Affinity-Matured TCR Display Accelerated Responses but Fail to Recognize Low Density of MHC-Peptide Antigen. *Blood* 118 (2), 319–329. doi:10.1182/blood-2010-12-326736

Tran, E., Chinnasamy, D., Yu, Z., Morgan, R. A., Lee, C.-C. R., Restifo, N. P., et al. (2013). Immune Targeting of Fibroblast Activation Protein Triggers Recognition of Multipotent Bone Marrow Stromal Cells and Cachexia. *J. Exp. Med.* 210 (6), 1125–1135. doi:10.1084/jem.20130110

Walker, A. J., Majzner, R. G., Zhang, L., Wanhainen, K., Long, A. H., Nguyen, S. M., et al. (2017). Tumor Antigen and Receptor Densities Regulate Efficacy of a Chimeric Antigen Receptor Targeting Anaplastic Lymphoma Kinase. *Mol. Ther.* 25 (9), 2189–2201. doi:10.1016/j.ymthe.2017.06.008

Wang, D., Starr, R., Chang, W.-C., Aguilar, B., Alizadeh, D., Wright, S. L., et al. (2020). Chlorotoxin-directed CAR T Cells for Specific and Effective Targeting of Glioblastoma. *Sci. Transl. Med.* 12 (533), eaaw2672. doi:10.1126/scitranslmed.aaw2672

Whilding, L. M., Parente-Pereira, A. C., Zabinski, T., Davies, D. M., Petrovic, R. M. G., Kao, Y. V., et al. (2017). Targeting of Aberrant αvβ6 Integrin Expression in Solid Tumors Using Chimeric Antigen Receptor-Engineered T Cells. *Mol. Ther.* 25 (10), 2427. doi:10.1016/j.ymthe.2017.09.018

Wilkie, S., Picco, G., Foster, J., Davies, D. M., Julien, S., Cooper, L., et al. (2008). Retargeting of Human T Cells to Tumor-Associated MUC1: the Evolution of a Chimeric Antigen Receptor. *J. Immunol.* 180 (7), 4901–4909. doi:10.4049/jimmunol.180.7.4901

Xiao, B.-F., Zhang, J.-T., Zhu, Y.-G., Cui, X.-R., Lu, Z.-M., Yu, B.-T., et al. (2021). Chimeric Antigen Receptor T-Cell Therapy in Lung Cancer: Potential and Challenges. *Front. Immunol.* 12, 782775. doi:10.3389/fimmu.2021.782775

Yong, C. S. M., Dardalhon, V., Devaud, C., Taylor, N., Darcy, P. K., and Kershaw, M. H. (2017). CAR T-Cell Therapy of Solid Tumors. *Immunol. Cell Biol.* 95 (4), 356–363. doi:10.1038/icb.2016.128

Zhang, T., Barber, A., and Sentman, C. L. (2006). Generation of Antitumor Responses by Genetic Modification of Primary Human T Cells with a Chimeric NKG2D Receptor. *Cancer Res.* 66 (11), 5927–5933. doi:10.1158/0008-5472.CAN-06-0130

Conflict of Interest: The authors declare that the research was conducted in the absence of any commercial or financial relationships that could be construed as a potential conflict of interest.

Publisher's Note: All claims expressed in this article are solely those of the authors and do not necessarily represent those of their affiliated organizations, or those of the publisher, the editors and the reviewers. Any product that may be evaluated in this article, or claim that may be made by its manufacturer, is not guaranteed or endorsed by the publisher.

frontiers | Frontiers in Bioengineering and Biotechnology

ORIGINAL RESEARCH
published: 28 June 2022
doi: 10.3389/fbioe.2022.929536

Assembling p53 Activating Peptide With CeO_2 Nanoparticle to Construct a Metallo-Organic Supermolecule Toward the Synergistic Ferroptosis of Tumor

Jingmei Wang[1†], *Wenguang Yang*[2,3†], *Xinyuan He*[4], *Zhang Zhang*[5*] *and Xiaoqiang Zheng*[1,2*]

[1]*Institute for Stem Cell & Regenerative Medicine, The Second Affiliated Hospital of Xi'an Jiaotong University, Xi'an, China,* [2]*Department of Medical Oncology, The First Affiliated Hospital of Xi'an Jiaotong University, Xi'an, China,* [3]*Department of Talent Highland, The First Affiliated Hospital of Xi'an Jiao Tong University, Xi'an, China,* [4]*Department of Infectious Diseases, The Second Affiliated Hospital of Xi'an Jiaotong University, Xi'an, China,* [5]*General Surgery Department, Tang Du Hospital, The Fourth Military Medical University, Xi'an, China*

OPEN ACCESS

Edited by:
Jin Yan,
Xi'an Jiaotong University, China

Reviewed by:
Yumeng Xue,
Northwestern Polytechnical University, China
Li Chen,
First Affiliated Hospital of Chongqing Medical University, China
Jiao Wu,
Fourth Military Medical University, China

***Correspondence:**
Zhang Zhang
pwzhangz@fmmu.edu.cn
Xiaoqiang Zheng
zhengxiaoqiang@xjtu.edu.cn

[†]*These authors have contributed equally to this work*

Specialty section:
This article was submitted to Biomaterials, a section of the journal Frontiers in Bioengineering and Biotechnology

Received: *27 April 2022*
Accepted: *17 May 2022*
Published: *28 June 2022*

Citation:
Wang J, Yang W, He X, Zhang Z and Zheng X (2022) Assembling p53 Activating Peptide With CeO_2 Nanoparticle to Construct a Metallo-Organic Supermolecule Toward the Synergistic Ferroptosis of Tumor. Front. Bioeng. Biotechnol. 10:929536. doi: 10.3389/fbioe.2022.929536

Inducing lipid peroxidation and subsequent ferroptosis in cancer cells provides a potential approach for anticancer therapy. However, the clinical translation of such therapeutic agents is often hampered by ferroptosis resistance and acquired drug tolerance in host cells. Emerging nanoplatform-based cascade engineering and ferroptosis sensitization by p53 provides a viable rescue strategy. Herein, a metallo-organic supramolecular (Nano-PMI@CeO_2) toward p53 restoration and subsequent synergistic ferroptosis is constructed, in which the radical generating module-CeO_2 nanoparticles act as the core, and p53-activator peptide (PMI)-gold precursor polymer is *in situ* reduced and assembled on the CeO_2 surface as the shell. As expected, Nano-PMI@CeO_2 effectively reactivated the p53 signaling pathway *in vitro* and *in vivo*, thereby downregulating its downstream gene GPX4. As a result, Nano-PMI@CeO_2 significantly inhibited tumor progression in the lung cancer allograft model through p53 restoration and sensitized ferroptosis, while maintaining favorable biosafety. Collectively, this work develops a tumor therapeutic with dual functions of inducing ferroptosis and activating p53, demonstrating a potentially viable therapeutic paradigm for sensitizing ferroptosis *via* p53 activation. It also suggests that metallo-organic supramolecule holds great promise in transforming nanomedicine and treating human diseases.

Keywords: peptide, p53, supramolecular, protein–protein interactions, anticancer therapy

1 INTRODUCTION

Lung cancer is the largest contributor to tumor-related death around the world. According to statistics, in 2020, the probable number of new cases was 2,206,771, while mortality was 1,796,144 from 185 countries or territories across the world (Bade and Dela Cruz, 2020; Siegel et al., 2021; Sung et al., 2021). Currently, clinical tumor therapeutic options are unsatisfactory. Conventional pharmacotherapies by chemotherapies and/or targeted drugs are often accompanied by cancer recurrence and poor prognosis due to their inherent limitations and complex heterogeneity of cancer. While the emerging immunotherapy revolutionized the medication of lung cancer, it suffers

from its intrinsic weakness including a narrow anticancer spectrum, low response rate, and potential toxicity triggered by self-immunity (Crunkhorn, 2020; Kennedy and Salama, 2020). Therefore, innovative precision medicine solutions are urgently needed. To induce other forms of non-apoptotic cell death, such as ferroptosis, overcoming drug resistance points a new direction for cancer therapy.

Ferroptosis, a style of cell death with iron-reliance caused by intracellular lipid peroxidation, has different death characteristics compared to apoptosis, pyroptosis, and autophagy (Jiang et al., 2021). Modulating cellular energy metabolism can significantly affect cellular sensitivity to ferroptosis, given that it is dependent on lipid metabolism and oxidative stress (Conrad and Pratt, 2019). Fortunately, metabolic reprogramming also inevitably occurs during carcinogenesis (Chae et al., 2016), making cancer cells highly sensitive to ferroptosis-inducing therapies (Hu et al., 2020). More importantly, induction of the ferroptosis pathway by depleting Xc or GPX4 has been shown effective in killing drug-resistant cancer cells (Chae et al., 2016). The new study also demonstrates the emerging role of ferroptosis in the crosstalk between tumor cells and immune cells (Hu et al., 2020). It indicates that targeting ferroptosis is of great significance for anticancer therapy. However, cancer cells tend to weaken ferroptosis by increasing the expression of antioxidant enzymes (Li et al., 2022a) or upregulating prominin2 (Brown et al., 2021) to promote iron transport. Abundant ferroptosis targets and regulatory networks provide an available resource for ferroptosis sensitization (Luo et al., 2021a). Among them, p53 as a tumor suppressor can enhance the cell sensitivity to ferroptosis in a direct (transcription-dependent inhibition of SLC7A11 expression) and indirect manner (by regulating amino acid metabolism, iron transport, PUFA metabolism, and antioxidant defense) (Ji et al., 2022).

p53 protein, one of the most important tumor suppressor proteins (Levine, 2020; Liu and Gu, 2021), is often abnormally expressed in most human tumors. In wild-type TP53 tumor types, the expression level and transcriptional function of p53 protein are often negatively regulated by MDM2 and the homolog MDMX, resulting in inhibition of its tumor suppressor function (Ivanov et al., 2013; Wade et al., 2013; Meek, 2015; He et al., 2020). Therefore, the p53-MDM2/MDMX protein interaction is a reasonable and broad therapeutic target in TP53 wild-type tumors. Although a large number of small-molecule drugs that activate p53 have been discovered, such as nutlins and imidazole WK23 (Liu et al., 2019), due to the poor targeting and specificity of small molecules, administration of high concentrations and subsequent biological toxicity is inevitable. Peptide drugs with natural advantages such as high affinity and good biosafety are becoming powerful competitive drugs for protein–protein interaction (PPI) modulators (Yan et al., 2022). At present, there have been many explorations and modifications of p53-activator peptides, and considerable therapeutic effects have been achieved at the animal level (Zheng et al., 2021; Yan et al., 2021). However, searching for higher-affinity peptide segments and overcoming their pharmacological barriers (Giribaldi et al., 2021; Gonzalez-Valdivieso et al., 2021) to promote their clinical translation still have a long way to go.

Supramolecular polymers, different from traditional chemistry molecules, are based on non-covalent interactions between molecules, such as metal coordination and hydrogen bonding, and are attracting increasing attention as nano-drugs (Aida et al., 2012; Zhou et al., 2021). However, general supramolecules are often limited by single functional components, inherent limitations, and complex biological environments, resulting in unsatisfactory therapeutic effects. Nano-platform-based cascade engineering has been ingeniously introduced to optimize this cancer therapy (Chen et al., 2020), in which metallo-organic supramolecules have proven to be an effective and thriving strategy (She et al., 2020; Jin et al., 2021; Liu et al., 2022). It relies on metallo-organic coordination interactions, based on rich geometric structures and connections between ligands and nodes (Chong et al., 2020; Ni et al., 2020). Various metal materials such as gold (Bian et al., 2018; He et al., 2019a; Yan et al., 2020a; He et al., 2020; Zheng et al., 2021; Yan et al., 2021), silver (Fehaid and Taniguchi, 2018; Mi et al., 2021), iron (Shen et al., 2018; Chen et al., 2021), rare earth elements (Yan et al., 2015; Zhang et al., 2017; Niu et al., 2018; Yan et al., 2018; He et al., 2019b), etc., and organic modules such as peptides (He et al., 2018a; He et al., 2018b; Yan et al., 2020b), nucleic acids (She et al., 2020; Li et al., 2022b), small molecules (Liang et al., 2021), etc., are selected as basic building blocks for the self-assembly of metallo-organic supramolecules. Abundant combinatorial options offer greater possibilities for generating highly effective cancer defense strategies, which can generate more therapeutic species or achieve stronger antitumor effects. Although many successful examples of metallo-organic supramolecules have been reported in tumor imaging (Li et al., 2020; Sung et al., 2021), regulation of protein interactions (He et al., 2019a), immunotherapy (Liang et al., 2021; He et al., 2022), and combination therapy (Jin et al., 2021; Liu et al., 2022), great challenges remain in the efficient and simple synthesis of such complex nanosystems.

Herein, to realize the combination of ferroptosis therapy and p53 activation, p53 activator peptide (PMI) and the free-radical generating nanoparticle CeO_2 were selected to induce ferroptosis in cancer cells (Sugantharaj David et al., 2017). Based on metal-organic coordination and a "one-pot" self-assembly strategy, a bifunctional metal-organic supramolecular (Nano-PMI@CeO_2) was constructed, in which CeO_2 functioned as the inorganic building block of supramolecules, while the peptide-gold precursor polymer formed based on gold–sulfur bond functioned as the inorganic building block. The end product, Nano-PMI@CeO_2 was obtained by the *in situ* reduction and self-assembly based on gold-thiol coordination bonds of peptide-gold precursor on the surface of the CeO_2 core. Due to the coverage of CeO_2 by the peptide gold precursor, Nano-PMI@CeO_2 has good biosafety in normal sites. The reduction of gold–sulfur bonds in the tumor microenvironment triggers the disassembly and release of CeO_2 and peptides at tumor sites, followed by dual antitumor effects of ferroptosis and p53 activation. In conclusion, this combination therapy is promising to

reinvigorate the use of ferroptosis-sensitizing therapy in antitumor therapy.

2 MATERIALS AND METHODS

2.1 General Instructions

The synthetical peptides were all purchased from CS bio Co. LLC. The additional chemical reagents in our research were obtained from Sigma-Aldrich, unless otherwise expressly announced.

2.2 Synthesis of Nano-PMI@CeO_2

Under the HBTU/HOBT agreement, the peptides were compounded with an optimized agreement developed for the Fmoc-SPPS methodology, which was based on appropriate resins by the automatic peptide synthesizer (CS Bio 336X). The nanoparticles were prepared through a "two-step, one-pot" gradual chemical reaction under appropriate conditions. In the first step, 2 mg PMI and 2 mg NH_2-PEG_n-SH were stirred with 4 ml deionized water, and 1 ml of 10 mM chloroauric acid solution was added at 500 rpm stir for 5 min. During the process, a pale-yellow turbid liquid turned into a purple-red transparent solution in the reaction system, accompanied by an obvious Tyndall effect. In step 2, 5 ml HEPES (100 mM) in which were dissolved 1 mM CeO_2 nanoparticles, subsequently, was added to the precursor polymer solution for its mild reduction. In addition, to verify the effects of p53 activation and ferroptosis acting independently, forming a univariate experimental control with Nano-PMI@CeO_2, we substituted PMI-SH with NH_2-PEG_n-SH in step 1 to synthesize corresponding nanoparticles termed Nano-PEG@CeO_2, and Nano-PMI were obtained by replacing CeO_2 with the prefabricated gold seed solution in step 2, and other conditions remained constant. We also prepared empty carrier gold nanoparticles Nano by replacing PMI-SH and CeO_2 with NH_2-PEG-SH and gold seed solution, respectively.

2.3 Cell Culture

The A549 cell lines (human) and the Lewis lung carcinoma cells (LLC, mouse) were bought from the Chinese Academy of Science Cell Bank (Shanghai, China), cultured in a standard incubator with the DMEM medium, and supplemented with FBS (10%), penicillin (100 U/ml), and streptomycin (100 μg/ml).

2.4 Apoptosis Analysis

Generally, A549 cells were cultured in a 6-well culture dish with a suitable density for 24 h prior to treatments. Then, the cells were incubated with the Nano-PMI@CeO_2 (0.02 mg/ml), the Nano-PEG@CeO_2 (0.02 mg/ml), and the Nano for 48 h. Next, all cells were harvested and stained according to the protocol of the FITC PE-7AAD Apoptosis Detection Kit (BD, United States).

2.5 Western Blot Analysis

After the indicated treatments of 48 h, the A549 cells were collected and the total protein was extracted. The proteins were separated by polyacrylamide gels after preprocessing, transferred to the nitrocellulose transfer membrane, and probed using primary and then secondary antibodies. The primary antibodies are listed as follows: anti-p53(sc-126, United States), anti-MDM2(sc-13161, United States), anti-GPX4 (sc-166570, United States), anti-SLC7A11 (ab37185, United States), anti-COX2 (12375-1-AP, United States), and anti-GAPDH (60,004-1-lg, United States). The ECL substrate (Millipore, MA, United States) was used for signal visualization. The protein expression of p53, MDM2, GPX4, COX2, and SLC7A11 was normalized to GAPDH and analyzed by ImageJ.

2.6 Mouse Study

All C57BL/6 mice were obtained from the Laboratory Animal Center of Xi'an Jiaotong University, providing a standard specific pathogen-free condition. The experimental procedures were approved by The Medical Ethics Committee of Xi'an Jiaotong University.

C57BL/6 mice (aged 5–6 weeks) were age-matched for tumor inoculation. The LLC cell line was inoculated subcutaneously for mice (1×10^6 cells/site). When the volume of the tumor reached ~100 mm^3, the mice were selected randomly into the control group, Nano-PMI@CeO_2 (2 mg/kg), Nano-PMI (2 mg/kg), Nano-PEG@CeO_2 (2 mg/kg) groups (six mice per group). Treatment was administered *via* intraperitoneal injection once every other day. The body weight and condition of mice were monitored daily. In addition, tumor volumes were analyzed by the following formula: 1/2× major axis ×width-$diameter^2$. The humane endpoints were determined based on the level of animal discomfort and tumor sizes.

2.7 H&E and Immunohistochemistry

Tissues were stained with hematoxylin–eosin (H&E) referring to regular histopathological techniques. All sections used for histological analysis were 4 μm thick. For immunohistochemistry, primary antibodies were used: anti-p53 (21891-1-AP, United States), anti-COX2 (12375-1-AP, United States), and anti-GPX4 (sc-166570, United States). The slices were scanned with a Scanner, and images were analyzed through ImageJ.

2.8 Statistics

Student's t-test was chosen to test the statistical difference between the experimental results of the two groups of data. ANOVA was used to analyze more intergroup differences, and the Tukey post-analysis or log-rank test was used when necessary ($^*p < 0.05$, $^{**}p < 0.01$, and $^{***}p < 0.001$).

3 RESULTS AND DISCUSSION

3.1 Synthesis and Characterization of Nano-PMI@CeO_2

To construct this bifunctional metal-organic supramolecular Nano-PMI@CeO_2 with ferroptosis induction and p53 activation, the choice of basic functional building blocks is crucial. In previous reports (He et al., 2020; Zheng et al., 2021), PMI showed potent regulation of p53-MDM2/MDMX, accompanied with huge nano-engineering work on it, which

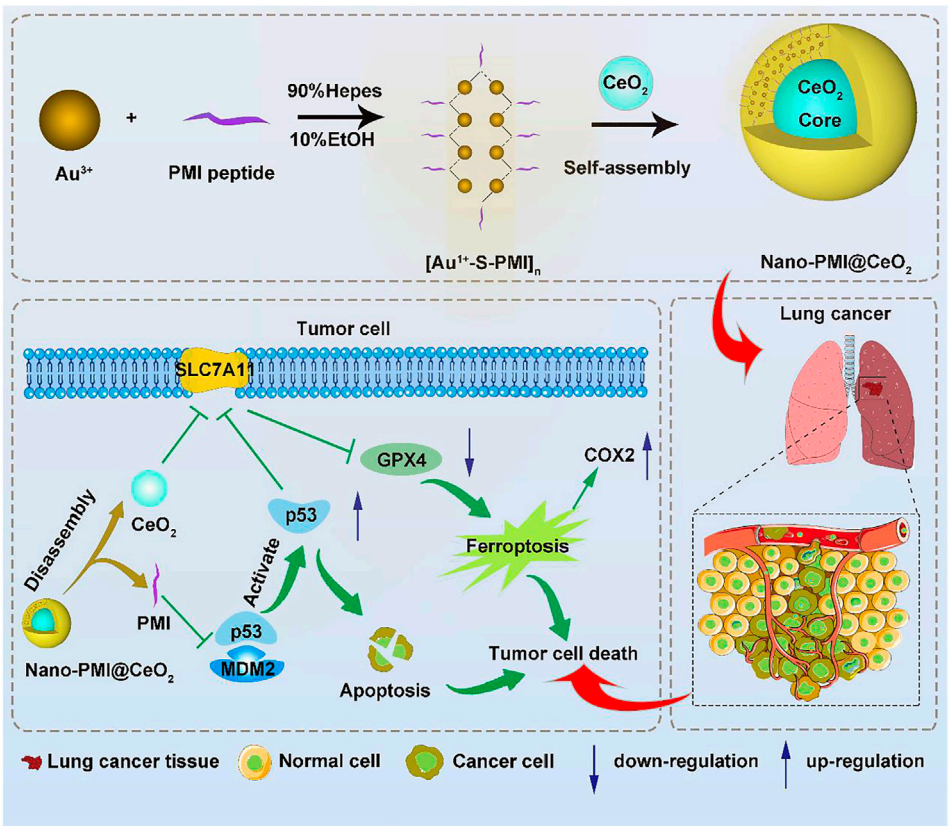

FIGURE 1 | Synthesis and function of Nano-PMI@CeO_2. Schematic depiction for the synthesis procedure of Nano-PMI@CeO_2 and their targeting in the lung cancer site by EPR effect and p53 pathways inducing ferroptosis.

provided us with great convenience. As for the ferroptosis-inducing module, the rare earth element nanoparticle CeO_2 was selected. The fabrication of Nano-PMI@CeO_2 mainly includes two steps: 1) the preparation of PMI peptide-gold precursor polymers [Au^{1+}-S-PMI] n and 2) the reduction and self-assembly of peptide-gold precursors on the surface of nanoparticle CeO_2 (**Figure 1**). In step 1, the peptide-gold precursor was formed by spontaneous coordination between Au^{3+} in chloroauric acid and thiolated PMI peptides. The disappearance of sulfhydryl groups in PMI-SH and the appearance of Au–S in Nano-PMI@CeO_2 were confirmed in the Fourier Transform Infrared (FT-IR) spectrum (**Figure 2A**). PMI could be easily obtained by solid-phase synthesis (SPPS), and the thiolylation of PMI was achieved by introducing a cysteine residue at its C-terminus, which was crucial for the preparation of peptide gold precursor and subsequent self-assembly.

In step 2, 1 mM CeO_2 nanoparticles were dissolved in 5 ml of 100 mM HEPES and added to precursor polymer solution for its mild reduction. The peptide-gold polymer covered the surface of CeO_2 and self-assembles under the aurophilic interactions and van der Waals forces. During the process, the reaction system changed from turbid liquid to a purple transparent solution, accompanied by an obvious Tyndall effect. There was no precipitation after the solution was placed at room temperature for 24 h, which indicated the successful preparation of Nano-PMI@CeO_2 supramolecular colloid. The characteristic absorption peak of the peptide in FT-IR (**Figure 2A**) and the absorption peak in the UV–Vis absorption spectra (**Figure 2B**) confirmed that the peptide was integrated. In addition, we also prepared the empty-cargo counterpart of Nano-PMI@CeO_2, termed Nano-PEG@CeO_2.

Through dynamic light scattering (DLS), we obtained the particle size of the NPs. The average diameter of Nano-PMI@CeO_2 was shown to be 31.74 nm (**Figure 2C**). Under transmission electron microscopy (TEM), both Nano-PMI@CeO_2 and Nano-PEG@CeO_2 exhibited good monodisperse properties and uniform size (**Figure 2D**). The size distribution of Nano-PEG@CeO_2 and Nano-PMI@CeO_2 by TEM was in line with the results of DLS (**Supplementary Figure S1**). Nano-PMI@CeO_2 had a ζ potential of 19.9 mV in PBS solution (pH = 7.4), which suggested that the nanoparticles had good colloidal stability (**Figure 2E**). Moreover, the colloidal stability of Nano-PMI@CeO_2 was proved again by the co-incubation test with 10% FBS, in which Nano-PMI@CeO_2 maintained its hydrodynamic diameter and ζ potential during the 72 h incubation (**Supplementary Figure S2**).

To identify the composition of Nano-PMI@CeO_2, we centrifugally removed the nanoparticle and quantified the residual in the supernatant. First, the nanoparticles were centrifuged at high speed (10,000 g × 10 min), and HPLC was used to detect the

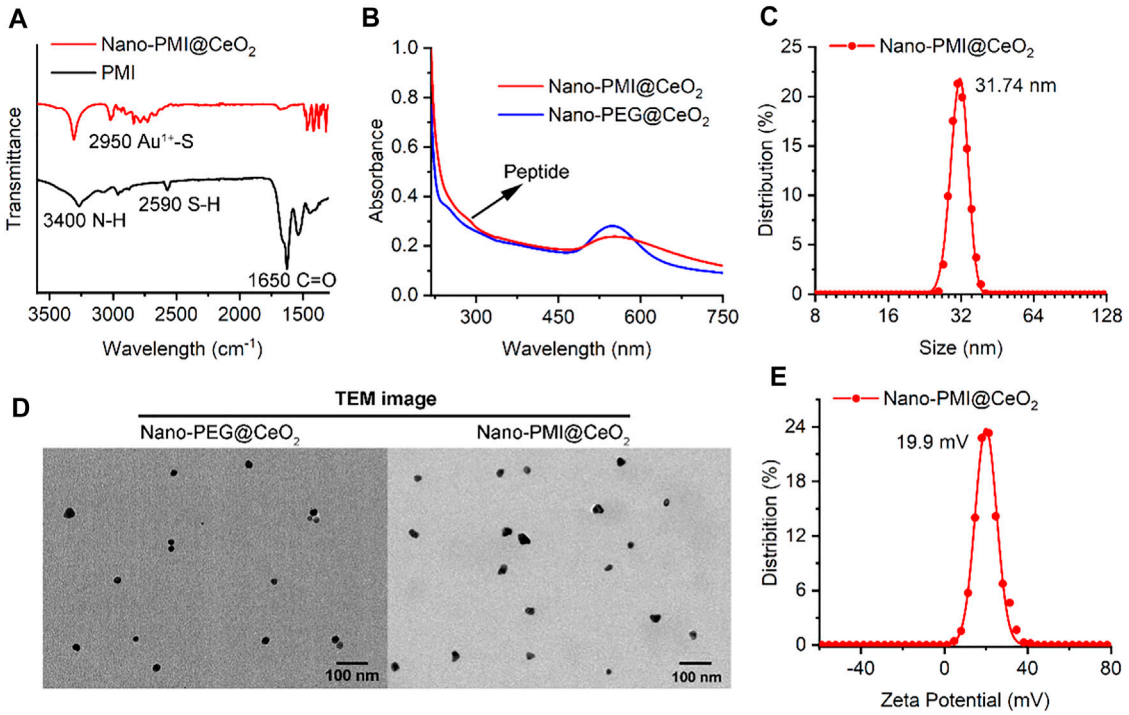

FIGURE 2 | Characterization of Nano-PMI@CeO_2. **(A)** FT-IR spectroscopy of Nano-PMI@CeO_2 and PMI. Two absorption peaks at 3400 cm^{-1} and 1650 cm^{-1} were distributed to the stretching vibration of N-H and C=O of peptides. **(B)** UV–Vis spectra of peptides Nano-PMI@CeO_2 and Nano-PEG@CeO_2. The typical Au nano shell absorption peak was observed closely at 550 nm. **(C)** Surface charge (Zeta potential) of Nano-PMI@CeO_2 was measured in PBS at pH 7.4. **(D)** TEM images of Nano-PEG@CeO_2 and Nano-PMI@CeO_2. **(E)** Hydrodynamic diameter of the Nano-PMI@CeO_2 was measured by dynamic light scattering.

polypeptide content in the supernatant. As shown in **Supplementary Figure S3**, there was almost no residual polypeptide in the supernatant. The nanoparticles were incubated with a high concentration of dithiothreitol (DTT) to disrupt the binding of peptides and gold and passed through the HPLC column again, and the peptide loading in the nanoparticles was calculated to be 91.8%. Furthermore, the Au and Ce elements in the epipelagic liquor were analyzed by inductively coupled plasma mass spectrometry (ICP-MS), and the results (**Supplementary Table S1**) showed that the Au and Ce elements in the supernatant accounted for 2.2% and 0.4% of the reactants, respectively. Calculated from the ratio of the reactants, the elemental concentrations of gold and cerium in the particles were 0.197 mg/ml and 0.04 mg/ml, respectively, which showed that our nanoparticles contain almost all the gold and Ce elements. Thus, the resulting nanoparticle solution had almost no impurities remaining, and purification is unnecessary. To validate the biodistribution of the Nano-PMI@CeO_2 *in vivo*, the ^{197}Au in the blood, the main organs, and the tumor extracted from LLC-bearing C57BL/6 mice were analyzed *via* ICP-MS. The noticeable blood cycle time of Nano-PMI@CeO_2 (**Supplementary Figure S4**) was supported by the metabolic level measured *via* time-based ICP-MS. Nano-PMI@CeO_2 exhibited low normal tissue storage in a period of 4 h ~ 1 week due to the metabolism and elimination, while the cumulation of Nano-PMI@CeO_2 at the tumor focus was high due to the EPR effect. Furthermore, quantitative analysis of Au and Ce elements in the dissociated organs from different time points showed that Nano-PMI@CeO_2 could be cleared from the body by the mononuclear phagocytosis system. In summary, Nano-PMI@CeO_2 was co-self-assembly constructed as a metallo-organic supermolecule based on CeO_2 nanoparticle (metal part) and peptide PMI (organic part), with advantages of stable transport and controlled release for intracellular peptide.

3.2 Nano-PMI@CeO_2 Reactivated p53 Signaling and Augmented Ferroptosis of Lung Cancer *in Vitro*

To explore the potential of Nano-PMI@CeO_2 nanoparticles for suppressing tumor growth *in vitro*, the antitumor mechanism of Nano-PMI@CeO_2 (0.02 mg/ml) was first tested on the lung cancer cells A549 carrying wild-type p53 and overexpression of MDM2/MDMX. After cells were treated with 0.02 mg/ml Nano-PMI@CeO_2, Nano-PEG@CeO_2, and Nano for 48 h, flow cytometric quantification of the increase in the number of PI and Annexin V in different treatment groups was carried out. In contrast to the control group, the apoptotic cell ratio in the Nano-PMI@CeO_2 group significantly increased by more than 70% (**Figures 3A,B**), while the Nano-PEG@CeO_2 group also showed some potent activity in the A549 cells. We designed Nano-PMI@CeO_2 to induce tumor cell death *via* the ferroptosis and apoptosis hybrid pathway, in which ferroptosis played an important position. Although there was only a minor increase in the Nano-PMI@CeO_2 group compared to the Nano-PEG@CeO_2, this evidence still suggested that Nano-PMI@CeO_2 has

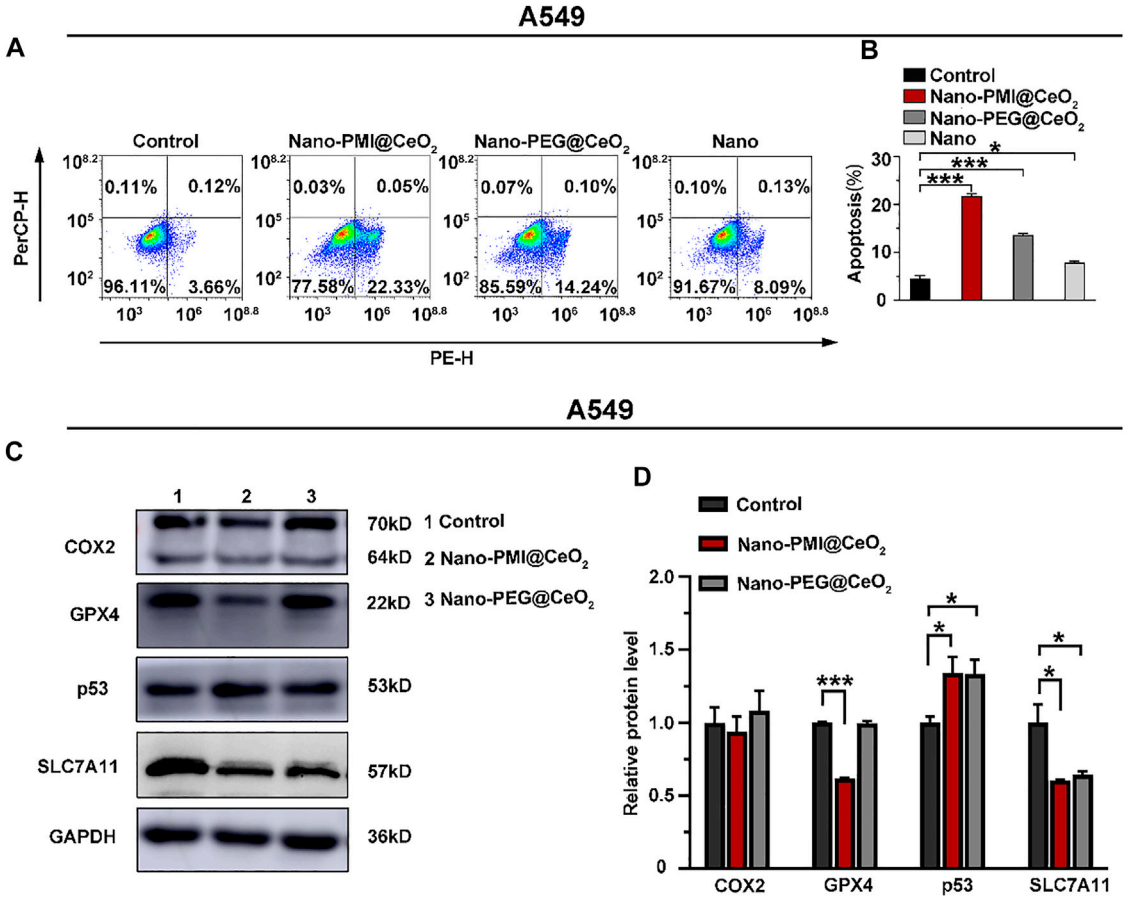

FIGURE 3 | Nano-PMI@CeO_2 potently enhanced tumor apoptosis *in vitro* by targeting p53 pathways and inducing ferroptosis. **(A)** Apoptosis effects of these NPs on the A549 cell line measured by flow cytometric analysis. **(B)** Apoptosis rate was showed as mean ± SE ($n = 3$). p values were calculated by t-test (*, $p < 0.05$; **, $p < 0.01$; ***, $p < 0.001$). **(C)** Protein expression was shown of COX2, GPX4, p53, and SLC7A11 in A549 cell line treatment with 0.02 mg/ml Nano-PMI@CeO_2, 0.02 mg/ml Nano-PEG@CeO_2 using Western blot. **(D)** Relative protein levels of COX2, GPX4, p53, and SLC7A11 were calculated using ImageJ. Experiment results were presented as mean ± SE ($n = 3$) p values were calculated by t-test (*, $p < 0.05$; **, $p < 0.01$; ***, $p < 0.001$).

potentially suppressed the proliferation process in tumor cells by inducing apoptosis.

Next, we also used the $HCT116^{-/-}$ cells, a p53 knockout cell line, and the NCI-H1975 cells, a p53 mutation cell line, to further verify the cytocompatibility of the Nano-PMI@CeO_2. Apoptosis experiments showed that after Nano-PMI@CeO_2 (0.02 mg/ml) treatment for 48 h, there was no significant increase in the apoptosis rate in the p53 knockout cell lines (**Supplementary Figures S5A,B**), and the p53 mutant cell lines showed almost the same content (**Supplementary Figures S5C,D**). This result indicated that Nano-PMI@CeO_2 was dependent on p53 activation to upregulate p53 levels. The apoptosis rate of HUVECs treated with Nano-PMI@CeO_2 (0.02 mg/ml) for 48 h analyzed by flow cytometry was consistent with the control, which reflected the specific killing effect of the nanoparticles on tumor cells (**Supplementary Figures S5E,F**).

After demonstrating the Nano-PMI@CeO_2 exact antitumor effect on the lung cancer cell lines, we further explored the underlying mechanism through Western blotting. Since then, with the treatment indicated with 0.02 mg/ml concentration for 48 h, we harvested the protein of A549 cells. Notably, CeO_2, a well-known oxidative stress inducer, could trigger the production of OH and iron death in tumors (Ha et al., 2018; Das et al., 2013). As displayed in **Figure 3C**, the expression of SLC7A11 in the Nano-PEG@CeO_2 group was significantly downregulated, in comparison with the control group. It was reflected that Nano-PEG@CeO_2 could regulate ferroptosis of tumor cells, as similarly reported before (Hong et al., 2021; Luo et al., 2021b). Furthermore, the expression of p53 with Nano-PMI@CeO_2 treatment was remarkably increased compared with the control group. By contrast, the MDM2 was markedly downregulated in the Nano-PMI@CeO_2 group (**Supplementary Figure S6**). It was demonstrated that Nano-PMI@CeO_2 could achieve p53 accumulation in A549 cells by blocking the p53 and MDM2 interactions (**Figures 3C,D**). In addition, owing to the oxidative stress environment by CeO_2, reactivating p53 could significantly downregulate the intracellular concentrations of SLC7A11 and GPX4 (**Figures 3C,D**). These key protein expression levels reflected that Nano-PMI@CeO_2 was helpful

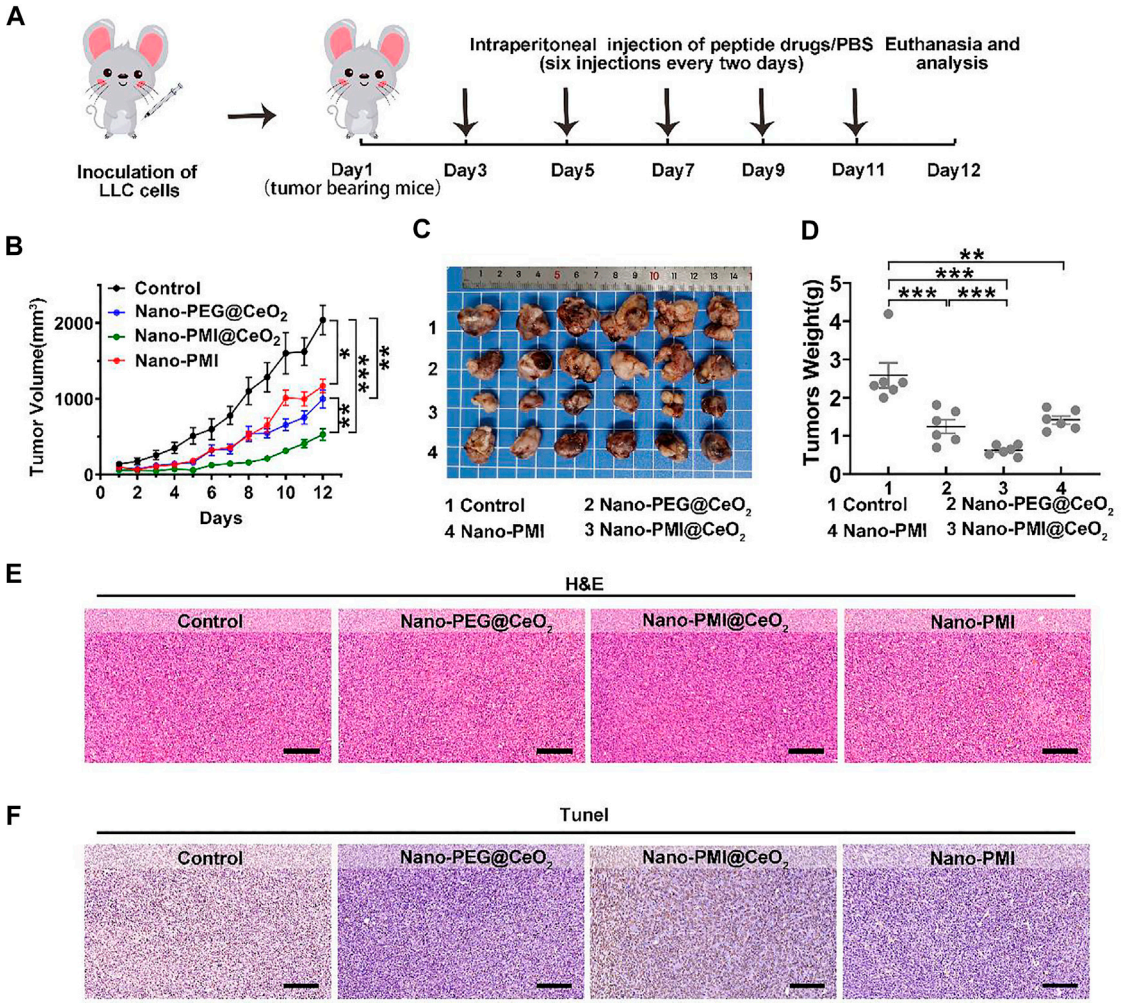

FIGURE 4 | Nano-PMI@CeO_2 *in vivo* antitumor activity. **(A)** Schematic depiction of the subcutaneous allograft lung cancer model and therapeutic process LLC allograft lung cancer model was established by subcutaneous injection LLC cells. Mice were treated with intraperitoneal injection every 2 days six times with nanoparticle drugs (2 mg/kg) or PBS. **(B)** Tumor sizes were measured by a vernier caliper every day. Tumor volume data were shown as mean ± SE (n = 6/group). p values were calculated by t-test (*, $p < 0.05$; **, $p < 0.01$; ***, $p < 0.001$).**(C)** Photographs and **(D)** average weights of tumors were collected at the end of the experiment (n = 6). p values were calculated by t-test (*, $p < 0.05$; **, $p < 0.01$; ***, $p < 0.001$). (E&F) Allograft tumors from mice after the 12 days of treatment staining by H&E **(E)** and TUNEL **(F)**. (Scale bar: 200 μm).

in further augmenting ferroptosis in A549 cells (Jiang et al., 2015; Lei et al., 2021). Taken together, these results demonstrated that Nano-PMI@CeO_2 not only induced tumor cell deaths by promoting the apoptosis pathway but also owed to augment ferroptosis *in vitro* through reactivation of the p53 pathway.

3.3 Nano-PMI@CeO_2 Suppresses Tumor Progression *In Vivo*

In the process of further verification of the *in vivo* therapeutic effect of Nano-PMI@CeO_2, lung cancer allografts were constructed for animal models. In detail, it was achieved by seeding LLC cells (1×10^6/mouse) into the epidermis of C57BL/6, as described in **Figure 4A**. The Nano-PEG@CeO_2 (2 mg/kg), Nano-PMI@CeO_2 (2 mg/kg), and Nano-PMI (2 mg/kg) were injected intraperitoneally every 2 days after the tumor grew to around 100 mm^3. The tumor volume and body weight were recorded every day. Compared with the group treated with PBS, Nano-PEG@CeO_2 inhibited tumor proliferation by 51% at the end of treatment (**Figure 4B**). Also, Nano-PMI@CeO_2 successfully suppressed the tumor growth with a tumor inhibition rate greater than 74% (**Figure 4B**), limiting the tumor volume to <550 mm^3. The comparison of the operated tumors at the end of the 12-day experimental process revealed that tumor growth was noticeably hindered in the Nano-PMI@CeO_2 treatment group (**Figure 4C**). At the same time, the tumor weight (**Figure 4D**) also proved the highest efficiency of Nano-PMI@CeO_2 compared to the other two groups. In addition, in the survival curve experiment (**Supplementary Figure S7**), Nano-PMI@CeO_2 greatly prolonged the median survival time of mice (26 days), significantly surpassing other control groups (19.5 days for Control, 24 days for Nano-PEG@

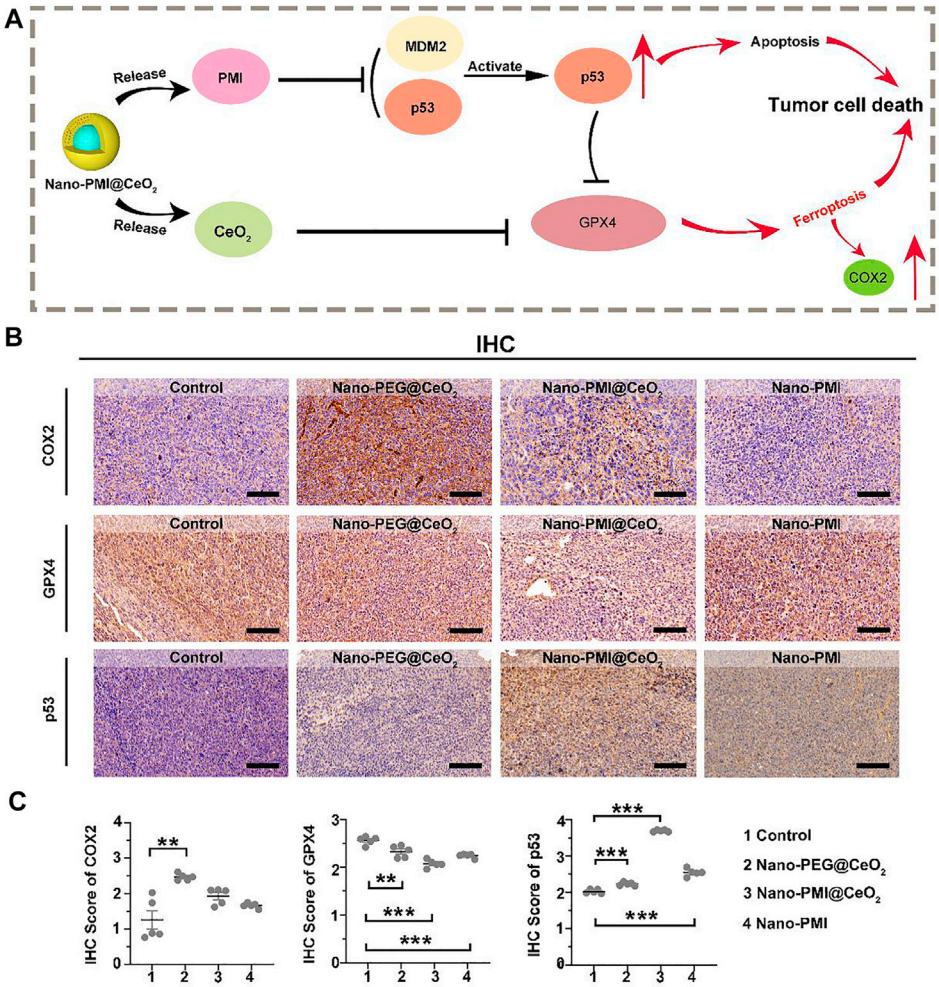

FIGURE 5 | Mechanism of Nano-PMI@CeO_2 *in vivo* induced tumor cell death. **(A)** Schematic diagram for antitumor activity of Nano-PMI@CeO_2 targeting the p53 pathways and inducing ferroptosis. **(B)** Representative IHC staining of COX2, GPX4, and p53 in tumor sections. (Scale bar:100 μm). **(C)** IHC scores analysis presented intratumoral protein levels of p53, GPX4, and COX2. *p* values were calculated by *t*-test (*, $p < 0.05$; **, $p < 0.01$; ***, $p < 0.001$).

CeO_2 and 21 days for Nano-PMI). Collectively, these data demonstrated that Nano-PMI@CeO_2 was a potent antitumor therapy therapeutic agent. In addition, H&E staining assays (**Figure 4E**) and TUNEL staining assays (**Figure 4F**) with the quantitative analysis (**Supplementary Figure S8**) of the tumor tissue further confirmed the superior therapeutic effect of Nano-PMI@CeO_2. In short, this evidence suggested that Nano-PMI@CeO_2, as a novel nano-drug, was strongly efficacious in inducing a cancer-killing effect *in vivo*.

3.4 Nano-PMI@CeO_2 Augmented Ferroptosis Through p53 Accumulation *In Vivo*

Based on the results above, we reckoned that Nano-PMI@CeO_2 could reactivate the p53 pathway by inhibiting the negative regulation of MDM2/MDMX. Under this, the protein levels of SLC7A11 were reduced, and downregulation of GPX4 induced far more ferroptotic cell death when compared to Nano-PEG@CeO_2 *in vivo* (**Figure 5A**). To further reveal the underlying mechanisms of Nano-PMI@CeO_2 on antitumor effect *in vivo*, immunohistochemical staining was used to validate the p53 expression levels and other key proteins relating to ferroptosis. From **Figures 5B,C**, we could observe that the nanoparticles CeO_2 inhibited GPX4 protein expression and triggered COX2 protein. Based on this, we reckoned that the nanoparticles CeO_2 lead to the tumor cell ferroptosis *via* the GPX4 pathway. At the same time, the results showed that the Nano-PMI@CeO_2 could effectively activate the accumulation of p53 protein in tumor cells *in vivo*, while inducing the ferroptosis process with noticeable downregulation of GPX4 (**Figures 5B,C**). As a result, Nano-PMI@CeO_2 earned more active inhibition of tumor proliferation than the Nano-PEG@CeO_2 group in the regimen. Nano-PMI@CeO_2 could not only effectively activate the accumulation of p53 protein in tumor cells *in vivo* but also induce the noticeable downregulation of GPX4 (**Figure 5**). Overall, owing to the

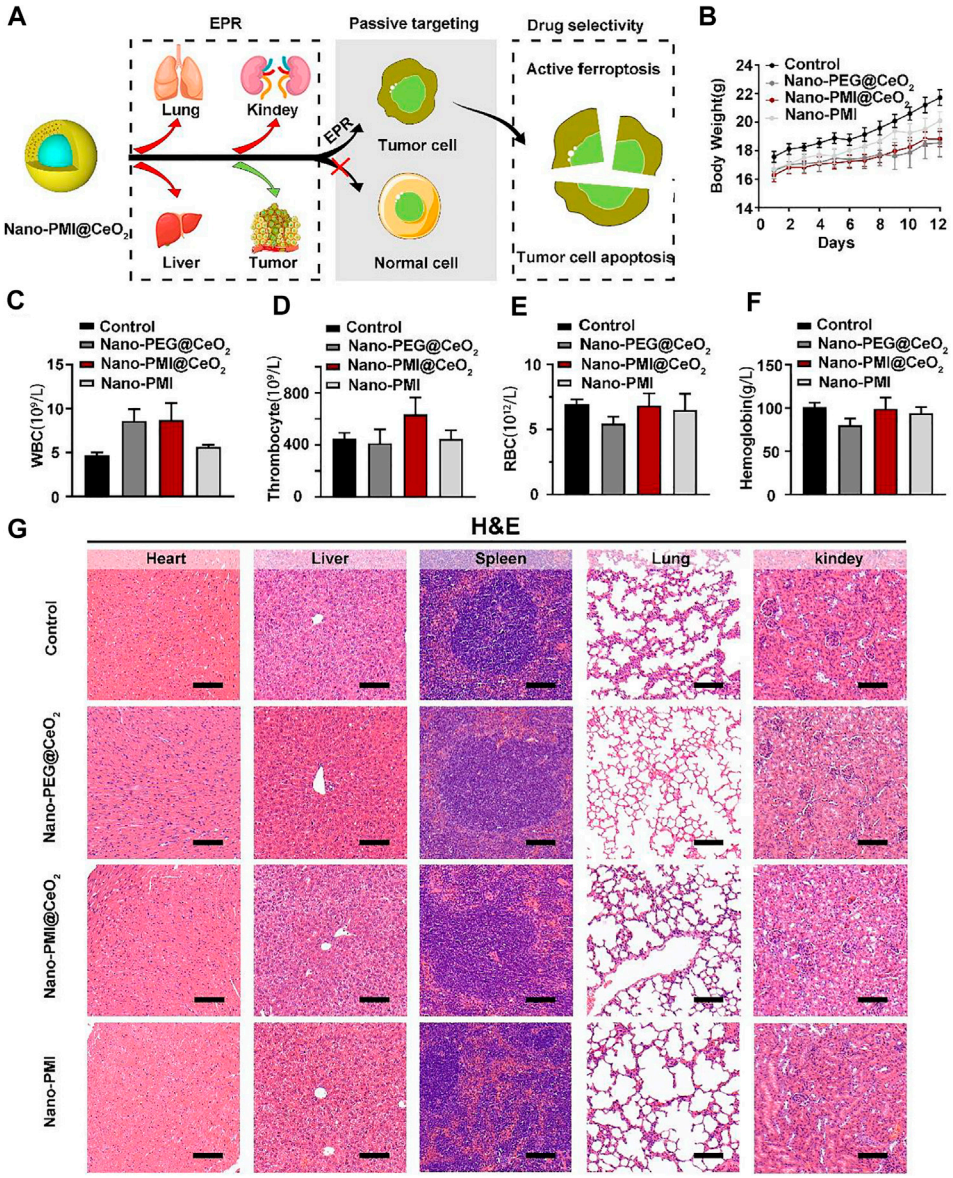

FIGURE 6 | Nano-PMI@CeO_2 safety evaluation *in vivo*. **(A)** Schematic illustration of tumor specificity for Nano-PMI@CeO_2 *via* the EPR effect. **(B)** Body weights were measured every day to evaluate the safety of Nano-PMI@CeO_2, Nano-PEG@CeO_2, and Nano-PMI *in vivo*. **(C–F)** Count of white blood cells (WBCs) **(C)**, thrombocytes **(D)**, red blood cells (RBCs) **(E)**, and hemoglobin **(F)** in C57BL/6 mice with the different treatments. **(G)** Representative histological H&E staining images of the heart, liver, spleen, lung, and kidney in mice with the indicated treatment. (scale bar: 100 μm).

enhanced tumor permeability and retention (EPR) effects, the metallo-organic supramolecule could passively be accumulated in the tumor location *in vivo*, validating their potential for facilitating p53 reactivation, while achieving tumor cell apoptosis and enhanced tumor cell ferroptosis.

3.5 Nano-PMI@CeO_2 Safety Evaluation *In Vivo*

Metallo-organic supramolecules often enhance the therapeutic performance *via* reducing functional molecule concentrations in normal tissues and increasing concentrations in tumors sufficiently under the EPR effect (**Figure 6A**). To evaluate the biosafety with Nano-PMI@CeO_2 treatment *in vivo*, we performed comprehensive toxicity research using C57BL/6 mice. The Nano-PMI@CeO_2 was administered intraperitoneally (2 mg/kg) to the mice on alternate days for 12 days. Then, we recorded the changes in body weight of each group, as shown in **Figure 6B**, and the body weight of mice in the four groups gradually increased. Although the growth rate of body weight in the Nano-PMI@CeO_2 group was slightly lower than that in the control group and Nano-PMI group at the later stage of treatment, there was no

remarkable difference between the groups. Then, as expected, the safety of both Nano-PMI@CeO_2 and Nano-PEG@CeO_2 was further confirmed by analysis of white blood cells (**Figure 6C**), thrombocytes (**Figure 6D**), red blood cells (RBCs) (**Figure 6E**), and hemoglobin (**Figure 6F**) in peripheral blood of mice. The H&E staining for the key organ slice also confirmed the abovementioned results that Nano-PMI@CeO_2 was enough biosecurity as a potential therapeutic effect (**Figure 6G**). The meaning of this research was to verify the antitumor and biosafety of Nano-PMI@CeO_2 for the treatment of lung cancer to identify evidence-based resources that could better facilitate informed consent.

4 CONCLUSION

Ferroptosis, as a novel tumor therapy strategy, has gained a great lot of attention in tumor development and treatment. As the primary hallmark of cancer is a valid escape from conventional modes of cell death, the traditional cancer therapeutic schedules still face enormous challenges, covering drug resistance, off-target effects, and so on (Shan et al., 2020; Luo et al., 2021a). Recently, nanoparticles have provided a new form of opportunity for anticancer therapy because of ferroptosis activation. For example, Zhao et al. developed a micellar delivery nano-drug, called DHM@RSL3, to release RSL3 in the hypoxia environment around the tumor, suppressed GPX4 protein expression with site-selectivity, and induced ferroptosis (Guo et al., 2020). Furthermore, Lin et al. constructed an arginine-capped silicate nano, named AMSNs, which presented huge responsiveness of GSH to activate GPX4-related ferroptosis in tumors (Wang et al., 2018). Beyond that, compared to small molecules, nanomaterials had higher power of clinical application in inducing iron death, taking advancements of longer blood circulation, stronger targeting, more controllable release ability, etc. Therefore, nanoparticle-induced iron death is considered an effective and safe way for various malignant tumor treatments.

Although multiple advances have been tapped out to produce iron death in malignancy tumors, the nano-drug as a single ferroptosis strategy may be unsatisfied with the demands of the complex tumor situation, such as drug resistance (Zhang et al., 2019; Guo et al., 2020). In recent years, several studies have combined iron toxicity measures with other therapeutic approaches to kill tumor cells, that is, introducing other strategies with ferroptosis for more efficient multi-modal carcinoma therapy (Liu et al., 2018; Zheng et al., 2021c). Our results indicated that metallo-organic supramolecular realized ferroptosis sensitization through p53 pathway reactivation and provided a feasible delivery scheme for p53-mediated tumor ferroptosis death. As described above, supramolecular therapeutic agents have been extensively developed in cancer therapy to elevate target specificity and treatment efficacy and, at the same time, reduce the side effects on normal cells.

In conclusion, under the combination of peptide chemistry and nanotechnology, we developed an intracellular-activatable nanoparticle for promoting p53 of the tumor cells and combining ferroptosis and apoptosis. Here, Nano-PMI@CeO_2 showed the enormous potential of metallo-organic supramolecular in restoring the p53 pathway *in vitro* and *in vivo*, primed the tumor cells to cell apoptosis, and augmented GPX4-related ferroptosis. This is an effective attempt to apply metal-organic supramolecules to sensitize tumor iron death. Taken together, this study not only validated sensitizing ferroptosis *via* reactivation p53 as a clinical translational potential but also more importantly provided a practicable pattern to translate metal-organic supramolecules into a candidate drug for tumor-targeted strategy.

DATA AVAILABILITY STATEMENT

The original contributions presented in the study are included in the article/**Supplementary Material**; further inquiries can be directed to the corresponding authors.

ETHICS STATEMENT

The animal study was reviewed and approved by The Medical Ethics Committee of Xi'an Jiaotong University.

AUTHOR CONTRIBUTIONS

Data curation, JW and WY; formal analysis, JW and XH; methodology, JW and WY; funding acquisition, ZZ; writing—review & editing, ZZ; resources: XH; writing—original draft: XZ; supervision: XZ; project administration: XZ. All authors have read and agreed to the published version of the manuscript. JW and WY contributed equally to this study.

FUNDING

This work was supported by the Key Research and Development Program of Shaanxi Province (No. 2020GXLH-Y-020).

ACKNOWLEDGMENTS

We thank the Instrument Analysis Center of Xi'an Jiaotong University for their assistance with TEM, DLS, FT-IR, and XPS analysis.

SUPPLEMENTARY MATERIAL

The Supplementary Material for this article can be found online at: https://www.frontiersin.org/articles/10.3389/fbioe.2022.929536/full#supplementary-material

REFERENCES

Aida, T., Meijer, E. W., and Stupp, S. I. (2012). Functional Supramolecular Polymers. *Science* 335 (6070), 813–817. doi:10.1126/science.1205962

Bade, B. C., and Dela Cruz, C. S. (2020). Lung Cancer 2020. *Clin. chest Med.* 41 (1), 1–24. doi:10.1016/j.ccm.2019.10.001

Bian, Z., Yan, J., Wang, S., Li, Y., Guo, Y., Ma, B., et al. (2018). Awakening P53 *In Vivo* by D-Peptides-Functionalized Ultra-small Nanoparticles: Overcoming Biological Barriers to D-Peptide Drug Delivery. *Theranostics* 8 (19), 5320–5335. doi:10.7150/thno.27165

Brown, C. W., Chhoy, P., Mukhopadhyay, D., Karner, E. R., and Mercurio, A. M. (2021). Targeting Prominin2 Transcription to Overcome Ferroptosis Resistance in Cancer. *EMBO Mol. Med.* 13 (8), e13792. doi:10.15252/emmm.202013792

Chae, Y. C., Vaira, V., Caino, M. C., Tang, H.-Y., Seo, J. H., Kossenkov, A. V., et al. (2016). Mitochondrial Akt Regulation of Hypoxic Tumor Reprogramming. *Cancer Cell* 30 (2), 257–272. doi:10.1016/j.ccell.2016.07.004

Chen, J., Zhu, Y., Wu, C., and Shi, J. (2020). Nanoplatform-based Cascade Engineering for Cancer Therapy. *Chem. Soc. Rev.* 49 (24), 9057–9094. doi:10.1039/d0cs00607f

Chen, J., Wang, X., Zhang, Y., Zhang, S., Liu, H., Zhang, J., et al. (2021). A Redox-Triggered C-Centered Free Radicals Nanogenerator for Self-Enhanced Magnetic Resonance Imaging and Chemodynamic Therapy. *Biomaterials* 266, 120457. doi:10.1016/j.biomaterials.2020.120457

Chong, G., Zang, J., Han, Y., Su, R., Weeranoppanant, N., Dong, H., et al. (2020). Bioengineering of Nano Metal-Organic Frameworks for Cancer Immunotherapy. *Nano Res.* 14 (5), 1–16. doi:10.1007/s12274-020-3179-9

Conrad, M., and Pratt, D. A. (2019). The Chemical Basis of Ferroptosis. *Nat. Chem. Biol.* 15 (12), 1137–1147. doi:10.1038/s41589-019-0408-1

Crunkhorn, S. (2020). Improving Immunotherapy. *Nat. Rev. Drug Discov.* 19 (2), 92. doi:10.1038/d41573-020-00010-6

Das, S., Dowding, J. M., Klump, K. E., McGinnis, J. F., Self, W., and Seal, S. (2013). Cerium Oxide Nanoparticles: Applications and Prospects in Nanomedicine. *Nanomedicine* 8 (9), 1483–1508. doi:10.2217/nnm.13.133

Fehaid, A., and Taniguchi, A. (2018). Silver Nanoparticles Reduce the Apoptosis Induced by Tumor Necrosis Factor-α. *Sci. Technol. Adv. Mater.* 19 (1), 526–534. doi:10.1080/14686996.2018.1487761

Giribaldi, J., Smith, J. J., and Schroeder, C. I. (2021). Recent Developments in Animal Venom Peptide Nanotherapeutics with Improved Selectivity for Cancer Cells. *Biotechnol. Adv.* 50, 107769. doi:10.1016/j.biotechadv.2021.107769

Gonzalez-Valdivieso, J., Girotti, A., Schneider, J., and Arias, F. J. (2021). Advanced Nanomedicine and Cancer: Challenges and Opportunities in Clinical Translation. *Int. J. Pharm.* 599, 120438. doi:10.1016/j.ijpharm.2021.120438

Guo, X., Liu, F., Deng, J., Dai, P., Qin, Y., Li, Z., et al. (2020). Electron-Accepting Micelles Deplete Reduced Nicotinamide Adenine Dinucleotide Phosphate and Impair Two Antioxidant Cascades for Ferroptosis-Induced Tumor Eradication. *ACS Nano* 14 (11), 14715–14730. doi:10.1021/acsnano.0c00764

Ha, H., Yoon, S., An, K., and KimYou, H. Y. (2018). Catalytic CO Oxidation over Au Nanoparticles Supported on CeO2 Nanocrystals: Effect of the Au-CeO2 Interface. *ACS Catal.* 8 (12), 11491–11501. doi:10.1021/acscatal.8b03539

He, W., Yan, J., Sui, F., Wang, S., Su, X., Qu, Y., et al. (2018). Turning a Luffa Protein into a Self-Assembled Biodegradable Nanoplatform for Multitargeted Cancer Therapy. *Acs Nano* 12 (11), 11664–11677. doi:10.1021/acsnano.8b07079

He, W., Yan, J., Jiang, W., Li, S., Qu, Y., Niu, F., et al. (2018). Peptide-Induced Self-Assembly of Therapeutics into a Well-Defined Nanoshell with Tumor-Triggered Shape and Charge Switch. *Chem. Mat.* 30 (20), 7034–7046. doi:10.1021/acs.chemmater.8b02572

He, W., Wang, S., Yan, J., Qu, Y., Jin, L., Sui, F., et al. (2019). Self-Assembly of Therapeutic Peptide into Stimuli-Responsive Clustered Nanohybrids for Cancer-Targeted Therapy. *Adv. Funct. Mater* 29 (10). 1807736. doi:10.1002/adfm.201807736

He, W., Yan, J., Wang, L., Lei, B., Hou, P., Lu, W., et al. (2019). A Lanthanide-Peptide-Derived Bacterium-like Nanotheranostic with High Tumor-Targeting, -imaging and -killing Properties. *Biomaterials* 206, 13–24. doi:10.1016/j.biomaterials.2019.03.026

He, W., Yan, J., Li, Y., Yan, S., Wang, S., Hou, P., et al. (2020). Resurrecting a P53 Peptide Activator - an Enabling Nanoengineering Strategy for Peptide Therapeutics. *J. Control. Release* 325, 293–303. doi:10.1016/j.jconrel.2020.06.041

He, W., Zhang, Z., Yang, W., Zheng, X., You, W., Yao, Y., et al. (2022). Turing Milk into Pro-apoptotic Oral Nanotherapeutic: De Novo Bionic Chiral-Peptide Supramolecule for Cancer Targeted and Immunological Therapy. *Theranostics* 12 (5), 2322–2334. doi:10.7150/thno.70568

Hong, T., Lei, G., Chen, X., Li, H., Zhang, X., Wu, N., et al. (2021). PARP Inhibition Promotes Ferroptosis via Repressing SLC7A11 and Synergizes with Ferroptosis Inducers in BRCA-Proficient Ovarian Cancer. *Redox Biol.* 42, 101928. doi:10.1016/j.redox.2021.101928

Hu, K., Li, K., Lv, J., Feng, J., Chen, J., Wu, H., et al. (2020). Suppression of the SLC7A11/glutathione axis Causes Synthetic Lethality in KRAS-Mutant Lung Adenocarcinoma. *J. Clin. investigation* 130 (4), 1752–1766. doi:10.1172/jci124049

Ivanov, A. A., Khuri, F. R., and Fu, H. (2013). Targeting Protein-Protein Interactions as an Anticancer Strategy. *Trends Pharmacol. Sci.* 34 (7), 393–400. doi:10.1016/j.tips.2013.04.007

Ji, H., Wang, W., Li, X., Han, X., Zhang, X., Wang, J., et al. (2022). p53: A Double-Edged Sword in Tumor Ferroptosis. *Pharmacol. Res.* 177, 106013. doi:10.1016/j.phrs.2021.106013

Jiang, L., Kon, N., Li, T., Wang, S.-J., Su, T., Hibshoosh, H., et al. (2015). Ferroptosis as a P53-Mediated Activity during Tumour Suppression. *Nature* 520 (7545), 57–62. doi:10.1038/nature14344

Jiang, X., Stockwell, B. R., and Conrad, M. (2021). Ferroptosis: Mechanisms, Biology and Role in Disease. *Nat. Rev. Mol. Cell Biol.* 22 (4), 266–282. doi:10.1038/s41580-020-00324-8

Jin, Y., He, W., Xiao, L., You, W., Liu, X., Lin, S., et al. (2021). Carnosic Acid-Induced Co-self-assembly of Metal-Peptide Complexes into a Nanocluster-Based Framework with Tumor-specific Accumulation for Augmented Immunotherapy. *Chem. Eng. J.* 416, 129141. doi:10.1016/j.cej.2021.129141

Kennedy, L. B., and Salama, A. K. S. (2020). A Review of Cancer Immunotherapy Toxicity. *CA A Cancer J. Clin.* 70 (2), 86–104. doi:10.3322/caac.21596

Lei, G., Zhang, Y., Hong, T., Zhang, X., Liu, X., Mao, C., et al. (2021). Ferroptosis as a Mechanism to Mediate P53 Function in Tumor Radiosensitivity. *Oncogene* 40 (20), 3533–3547. doi:10.1038/s41388-021-01790-w

Levine, A. J. (8002). p53: 800 Million Years of Evolution and 40 Years of Discovery. *Nat. Rev. Cancer* 20 (8), 471–480. doi:10.1038/s41568-020-0262-1

Li, K., Liu, C.-J., and Zhang, X.-Z. (2020). Multifunctional Peptides for Tumor Therapy. *Adv. Drug Deliv. Rev.* 160, 36–51. doi:10.1016/j.addr.2020.10.009

Li, M., Jin, S., Zhang, Z., Ma, H., and Yang, X. (2022). Interleukin-6 Facilitates Tumor Progression by Inducing Ferroptosis Resistance in Head and Neck Squamous Cell Carcinoma. *Cancer Lett.* 527, 28–40. doi:10.1016/j.canlet.2021.12.011

Li, L., He, W., You, W., Yan, J., and Liu, W. (2022). Turing miRNA into Infinite Coordination Supermolecule: a General and Enabling Nanoengineering Strategy for Resurrecting Nuclear Acid Therapeutics. *J. Nanobiotechnol* 20 (1), 10. doi:10.1186/s12951-021-01212-9

Liang, M., Chen, M., Zhong, Y., Singh, S., and Singh, S. (2021). Construction of a Prognostic Model in Lung Adenocarcinoma Based on Ferroptosis-Related Genes. *Front. Genet.* 12, 739520. doi:10.3389/fgene.2021.739520

Liu, Y., and Gu, W. (2021). The Complexity of P53-Mediated Metabolic Regulation in Tumor Suppression. *Semin. Cancer Biol.* [online ahead of print] (21) 00060-2. doi:10.1016/j.semcancer.2021.03.010

Liu, Y., Zhen, W., Jin, L., Zhang, S., Sun, G., Zhang, T., et al. (2018). All-in-One Theranostic Nanoagent with Enhanced Reactive Oxygen Species Generation and Modulating Tumor Microenvironment Ability for Effective Tumor Eradication. *ACS Nano* 12 (5), 4886–4893. doi:10.1021/acsnano.8b01893

Liu, Y., Wang, X., Wang, G., Yang, Y., Yuan, Y., and Ouyang, L. (2019). The Past, Present and Future of Potential Small-Molecule Drugs Targeting P53-MDM2/MDMX for Cancer Therapy. *Eur. J. Med. Chem.* 176, 92–104. doi:10.1016/j.ejmech.2019.05.018

Liu, T., Jin, Y., He, C., You, W., Fang, M., Chang, Z., et al. (2022). A Tumor-Targeting Metal-Organic Nanoparticle Constructed by Dynamic Combinatorial Chemistry toward Accurately Redressing Carcinogenic Wnt Cascade. *Small* 18 (3):2104849. doi:10.1002/smll.202104849

Luo, L., Wang, H., Tian, W., Li, X., Zhu, Z., Huang, R., et al. (2021). Targeting Ferroptosis-Based Cancer Therapy Using Nanomaterials: Strategies and Applications. *Theranostics* 11 (20), 9937–9952. doi:10.7150/thno.65480

Luo, Y., Gao, X., Zou, L., Lei, M., Feng, J., and Hu, Z. (2021). Bavachin Induces Ferroptosis through the STAT3/P53/SLC7A11 Axis in Osteosarcoma Cells. *Oxid. Med. Cell Longev.* 2021, 1783485. doi:10.1155/2021/1783485

Meek, D. W. (2015). Regulation of the P53 Response and its Relationship to Cancer. *Biochem. J.* 469 (3), 325–346. doi:10.1042/bj20150517

Mi, Z., Guo, L., Liu, P., Qi, Y., Feng, Z., Liu, J., et al. (2021). "Trojan Horse" Salmonella Enabling Tumor Homing of Silver Nanoparticles via Neutrophil Infiltration for Synergistic Tumor Therapy and Enhanced Biosafety. *Nano Lett.* 21 (1), 414–423. doi:10.1021/acs.nanolett.0c03811

Ni, K., Lan, G., and Lin, W. (2020). Nanoscale Metal-Organic Frameworks Generate Reactive Oxygen Species for Cancer Therapy. *ACS Cent. Sci.* 6 (6), 861–868. doi:10.1021/acscentsci.0c00397

Niu, F., Yan, J., Ma, B., Li, S., Shao, Y., He, P., et al. (2018). Lanthanide-doped Nanoparticles Conjugated with an Anti-CD33 Antibody and a P53-Activating Peptide for Acute Myeloid Leukemia Therapy. *Biomaterials* 167, 132–142. doi:10.1016/j.biomaterials.2018.03.025

Shan, X., Li, S., Sun, B., Chen, Q., Sun, J., He, Z., et al. (2020). Ferroptosis-driven Nanotherapeutics for Cancer Treatment. *J. Control. Release* 319, 322–332. doi:10.1016/j.jconrel.2020.01.008

She, J., Li, Y., Yan, S., Yan, Y., Liu, D., Li, S., et al. (2020). De Novo supraparticle Construction by a Self-Assembled Janus Cyclopeptide to Tame Hydrophilic microRNA and Hydrophobic Molecule for Anti-tumor Cocktail Therapy and Augmented Immunity. *Chem. Eng. J.* 401, 126080. doi:10.1016/j.cej.2020.126080

Shen, Z., Song, J., Yung, B. C., Zhou, Z., Wu, A., and Chen, X. (2018). Emerging Strategies of Cancer Therapy Based on Ferroptosis. *Adv. Mater* 30 (12), e1704007. doi:10.1002/adma.201704007

Siegel, R. L., Miller, K. D., Fuchs, H. E., and JemalCancer Statistics, A. (2021). Cancer Statistics, 2021. *CA A Cancer J. Clin.* 71 (1), 7–33. doi:10.3322/caac.21654

Sugantharaj David, E. M. D., Madurantakam Royam, M., Rajamani Sekar, S. K., Manivannan, B., Jalaja Soman, S., Mukherjee, A., et al. (2017). Toxicity, Uptake, and Accumulation of Nano and Bulk Cerium Oxide Particles in *Artemia salina*. *Environ. Sci. Pollut. Res.* 24 (31), 24187–24200. doi:10.1007/s11356-017-9975-4

Sung, H., Ferlay, J., Siegel, R. L., Laversanne, M., Soerjomataram, I., Jemal, A., et al. (2021). Global Cancer Statistics 2020: GLOBOCAN Estimates of Incidence and Mortality Worldwide for 36 Cancers in 185 Countries. *CA A Cancer J. Clin.* 71 (3), 209–249. doi:10.3322/caac.21660

Wade, M., Li, Y.-C., and WahlMDM2, G. M. (2013). MDM2, MDMX and P53 in Oncogenesis and Cancer Therapy. *Nat. Rev. Cancer* 13 (2), 83–96. doi:10.1038/nrc3430

Wang, S., Li, F., Qiao, R., Hu, X., Liao, H., Chen, L., et al. (2018). Arginine-Rich Manganese Silicate Nanobubbles as a Ferroptosis-Inducing Agent for Tumor-Targeted Theranostics. *ACS Nano* 12 (12), 12380–12392. doi:10.1021/acsnano.8b06399

Yan, J., He, W., Li, N., Yu, M., Du, Y., Lei, B., et al. (2015). Simultaneously Targeted Imaging Cytoplasm and Nucleus in Living Cell by Biomolecules Capped Ultra-small GdOF Nanocrystals. *Biomaterials* 59, 21–29. doi:10.1016/j.biomaterials.2015.04.041

Yan, J., He, W., Yan, S., Niu, F., Liu, T., Ma, B., et al. (2018). Self-Assembled Peptide-Lanthanide Nanoclusters for Safe Tumor Therapy: Overcoming and Utilizing Biological Barriers to Peptide Drug Delivery. *ACS Nano* 12 (2), 2017–2026. doi:10.1021/acsnano.8b00081

Yan, J., Ji, F., Yan, S., You, W., Ma, F., Li, F., et al. (2020). A General-Purpose Nanohybrid Fabricated by Polymeric Au(I)-peptide Precursor to Wake the Function of Peptide Therapeutics. *Theranostics* 10 (19), 8513–8527. doi:10.7150/thno.47243

Yan, J., Yao, Y., Yan, S., Gao, R., Lu, W., and He, W. (2020). Chiral Protein Supraparticles for Tumor Suppression and Synergistic Immunotherapy: An Enabling Strategy for Bioactive Supramolecular Chirality Construction. *Nano Lett.* 20 (8), 5844–5852. doi:10.1021/acs.nanolett.0c01757

Yan, S., YanLiu, J. D., Liu, D., Li, X., Kang, Q., You, W., et al. (2021). A Nano-Predator of Pathological MDMX Construct by Clearable Supramolecular Gold(I)-thiol-peptide Complexes Achieves Safe and Potent Anti-tumor Activity. *Theranostics* 11 (14), 6833–6846. doi:10.7150/thno.59020

Yan, J., Zheng, X., You, W., He, W., and Xu, G. K. (2022). A Bionic-Homodimerization Strategy for Optimizing Modulators of Protein-Protein Interactions: From Statistical Mechanics Theory to Potential Clinical Translation. *Adv. Sci. (Weinh)*, 9(11):2105179. doi:10.1002/advs.202105179

Zhang, J., YanYang, J. Q., Yang, Q., Yan, Y., Li, S., Wang, L., et al. (2017). Arginine-modified Dual Emission Photoluminescent Nanocrystals for Bioimaging at Subcellular Resolution. *J. Biomater. Appl.* 32 (4), 533–542. doi:10.1177/0885328217725203

Zhang, F., Li, F., Lu, G.-H., Nie, W., Zhang, L., Lv, Y., et al. (2019). Engineering Magnetosomes for Ferroptosis/Immunomodulation Synergism in Cancer. *ACS Nano* 13 (5), 5662–5673. doi:10.1021/acsnano.9b00892

Zheng, X., Yan, J., You, W., Li, F., Diao, J., He, W., et al. (2021). De Novo Nano-Erythrocyte Structurally Braced by Biomimetic Au(I)-peptide Skeleton for MDM2/MDMX Predation toward Augmented Pulmonary Adenocarcinoma Immunotherapy. *Small (Weinheim der Bergstrasse, Ger.* 17 (20), e2100394. doi:10.1002/smll.202100394

Zheng, H., Jiang, J., Xu, S., Liu, W., Xie, Q., Cai, X., et al. (2021). Nanoparticle-induced Ferroptosis: Detection Methods, Mechanisms and Applications. *Nanoscale* 13 (4), 2266–2285. doi:10.1039/d0nr08478f

Zhou, J., Rao, L., Yu, G., Cook, T. R., Chen, X., and Huang, F. (2021). Supramolecular Cancer Nanotheranostics. *Chem. Soc. Rev.* 50 (4), 2839–2891. doi:10.1039/d0cs00011f

Conflict of Interest: The authors declare that the research was conducted in the absence of any commercial or financial relationships that could be construed as a potential conflict of interest.

The handling editor, JY, declared a shared parent affiliation with the authors JW, WY, XH, and XZ at the time of review.

Publisher's Note: All claims expressed in this article are solely those of the authors and do not necessarily represent those of their affiliated organizations, or those of the publisher, the editors, and the reviewers. Any product that may be evaluated in this article, or claim that may be made by its manufacturer, is not guaranteed or endorsed by the publisher.

frontiers | Frontiers in Bioengineering and Biotechnology

REVIEW
published: 05 August 2022
doi: 10.3389/fbioe.2022.943906

Nanomedicines Targeting Metabolism in the Tumor Microenvironment

Mengdi Ren[1], Xiaoqiang Zheng[2], Huan Gao[1], Aimin Jiang[1], Yu Yao[1] and Wangxiao He[3]**

[1]Department of Oncology, The First Affiliated Hospital of Xi'an Jiaotong University, Xi'an, China, [2]Institute for Stem Cell and Regenerative Medicine, The Second Affiliated Hospital of Xi'an Jiaotong University, Xi'an, China, [3]Department of Talent Highland, The First Affiliated Hospital of Xi'an Jiaotong University, Xi'an, China

Cancer cells reprogram their metabolism to meet their growing demand for bioenergy and biosynthesis. The metabolic profile of cancer cells usually includes dysregulation of main nutritional metabolic pathways and the production of metabolites, which leads to a tumor microenvironment (TME) having the characteristics of acidity, hypoxic, and/or nutrient depletion. Therapies targeting metabolism have become an active and revolutionary research topic for anti-cancer drug development. The differential metabolic vulnerabilities between tumor cells and other cells within TME provide nanotechnology a therapeutic window of anti-cancer. In this review, we present the metabolic characteristics of intrinsic cancer cells and TME and summarize representative strategies of nanoparticles in metabolism-regulating anti-cancer therapy. Then, we put forward the challenges and opportunities of using nanoparticles in this emerging field.

Keywords: metabolic reprograming, tumor microenvironment, nanomedicine, metabolism, cancer treatment

OPEN ACCESS

Edited by:
Long Wu,
University of Maryland, United States

Reviewed by:
Jiaojiao Xu,
Johns Hopkins Medicine, United States
Li Pan,
University of Maryland, United States

****Correspondence:***
Yu Yao
13572101611@163.com
Wangxiao He
hewangxiao5366@xjtu.edu.cn

Specialty section:
This article was submitted to Biomaterials, a section of the journal Frontiers in Bioengineering and Biotechnology

Received: *14 May 2022*
Accepted: *01 June 2022*
Published: *05 August 2022*

Citation:
Ren M, Zheng X, Gao H, Jiang A, Yao Y and He W (2022) Nanomedicines Targeting Metabolism in the Tumor Microenvironment. Front. Bioeng. Biotechnol. 10:943906. doi: 10.3389/fbioe.2022.943906

INTRODUCTION

Metabolic reprogramming, a hallmark of cancer, is considered to be one of their driving forces. It endows cancer cells with the potential for initiation and proliferation in the nutrient-deficient tumor microenvironment (TME) (Yoshida, 2015; Martínez-Reyes and Chandel, 2021). Cancer cells usually abandon the efficient metabolic pathway used by most normal cells and switch to alternative pathways that produce less energy and more materials to meet the needs of biosynthesis and bioenergy synthesis (Vander Heiden et al., 2009). The metabolic reprogramming is regulated by an oncogene and influenced by an external TME. For example, the metabolic composition of the TME can affect the metabolic phenotype of cancer cells (Seth Nanda et al., 2020). Other cells within TME, including stromal and immune cells, form a metabolic network and crosstalk to regulate tumor growth and anti-cancer immunity (Guo et al., 2019; Pacella and Piconese, 2019; Vettore et al., 2020). Changes in the cellular metabolism of these cells also involve nutrient limitation and immunosuppressive functions (Yin et al., 2019). Moreover, various metabolites within TME play an important role in cancer cell behavior and cellular communication (Sola-Penna et al., 2020). Thus, the metabolism of various cells and metabolites in TME plays pivotal roles in tumor progression and maintenance.

As metabolism is the basic determinant of the viability and function of cancer and noncancer cells in TME (10), targeting metabolic pathways opens up a new way to thwart tumor growth (Elia and Haigis, 2021). However, therapeutic progress in disrupting cancer metabolism is limited (Stine et al., 2022). A part of the reason is that cellular metabolism is huge and complex networks of enzymes and compounds acting together. The technical limitations also make all elements still not fully understood. Another part is that strategies for targeting the intrinsic metabolism of cancer cells usually do not consider the metabolism and crosstalk of noncancer cells within TME (Stine et al.,

TABLE 1 | Representative nanoparticles targeting cancer metabolism.

Metabolism Pathway	Nanoparticle	Nanocarrier Material	Size	Cargo	Targets	Mechanism	Indication	Advantages	References
Aerobic glycolysis	Nanoenabled Energy Interrupter	ZIF-8; hydrophilic shell	117 nm	GLUT1 mRNA-cleaving DNAzyme	GLUT1 mRNA	GLUT1 specific depletion	glycolysis Inhibition therapy	HAase-responsive and pH-sensitive; cut off glucose supply	Wu et al. (2022)
	GNR/HA-DC	plasmonic gold nanorods	768 nm	HA-targeting moiety and DC	GLUT1	inhibiting glucose uptake and glycolysis	improved PTT	HAase-responsive; overcoming the heat endurance of tumor cells	Chen et al. (2017a)
	l-Arg-HMON-GOx	hollow mesoporous organosilica nanoparticle	pore size of 3.7 nm	Gox and l-Arg	endogenous glucose	cutting off the energy supply and generating toxic H2O2	synergistic cancer starving-like/gas therapy	Glucose-Responsive; without the need for external excitation	Fan et al. (2017)
	Lip-(2DG + Dox)	liposomes	<200 nm	Dox and 2DG	hexokinase	inhibit glycolysis; promote mitochondrial depolarization and apoptosis	tumor-specific chemotherapy	mitigates the harmful side effect of chemotherapy	Yang et al. (2020b)
	2DG-PLGA-NPs	poly (lactic-co-glycolic acid) nanoparticles	120 nm	2DG	hexokinase	induce antitumor immunity	overcome the immune-resistance	decreasing lactate production and increasing T cells in tumors	Sasaki et al. (2021)
	GSH-responsive nanoprodrug	pluronic F126	100 nm	LND and NLG919	HK II and IDO-1	restrained glycolysis and reduce the kynurenine	alleviate immunosuppression	GSH-Responsive; destructed the immunosuppressive microenvironment	Liu et al. (2021)
	RBCm@Ag-MOFs/PFK15 (A-RAMP)	metal–organic frameworks; red blood cell membrane shell	20 nm	PFK15	PFK-2/FBPase-2/ PFKFB	inhibit glycolysis	targeted B-cell lymphoma	CD20 aptamer-targeting	Zhao et al. (2020a)
Mitochondrial respiration	Copper-depleting nanoparticle (CDN)	semiconducting polymer nanoparticle	86.6/ 81 nm	CDM and SPN	mitochondrial ETC	shifts metabolism pattern	treat TNBC	specific accumulation to be less toxic	Cui et al. (2021)
	polymersome nanoparticle	amphiphilic grafted-polyphosphazene nanovesicle	135.9 nm	VES and DOX·HCl	mitochondrial ETC	inducing mitochondrial malfunction and apoptosis	overcome multidrug resistance	result in mitochondria dysfunctions	Liang et al. (2021)
	IR780@Pt NPs	β-CD and adamantyl group	150 nm	Pt-CD and IR780	mitochondrial	mitochondrial dysfunction	chemotherapy synergetic treatments	track tumor accumulation; guide the NIR laser irradiation	Zhang et al. (2021b)
	UCNPs- MSN-MnO2 (UNMM)	the mesoporous silicon middle layer; MnO2 gatekeeper layer	36 nm	MnO2, Ce6, and ATO	mitochondrial ETC	inhibit respiration metabolism and generate O2	enhanced PDT	inhibiting oxygen metabolism and generating oxygen	Wang et al. (2020a)
	VSeM-N=CH-PEG	acidity-cleavable PEG	~100 nm	VES and MTX	mitochondrial ETC	interfere ETC	synergistic oxidation-chemotherapy	self-targeting activation and ROS regeneration	Li et al. (2020a)
	ACSN	carrier-free	193.5 nm	ATO and Ce6	mitochondrial ETC	interrupt ETC, relieve the hypoxia microenvironment	improving PDT	self-delivery; reverse the tumor hypoxia	Zhao et al. (2020b)
Glycolysis and mitochondrial metabolism	LMGC	liquid metal nanoparticles	250 nm	Gox	endogenous glucose	inhibit glycolysis; increased H2O2 level	synergetic PTT	acidity-responsive; reduce heat resistance	Ding et al. (2022)
	Pt-Pd@DON		97 nm	DON		glutamine analog			

(Continued on following page)

TABLE 1 | (*Continued*) Representative nanoparticles targeting cancer metabolism.

Metabolism Pathway	Nanoparticle	Nanocarrier Material	Size	Cargo	Targets	Mechanism	Indication	Advantages	References
Glutamine metabolism		porous Pt–Pd nanoflowers			binds covalently to multiple enzymes that use glutamine		electrodynamic synergetic treatments	motivate the protective immune response	Chen et al. (2022)
	ABFP NPs	BSA-based NPs	140 nm	purpurin	GDH1	inhibiting the decomposition of mitochondrial Gln	synergetic chemodynamic treatments	real-time tracking of the Fenton reaction	Xu et al. (2021)
GSH depelition	AM-L@NBS	DSPE-PEG2k-Maleimide; CD44-specific polypeptide (A6) modified liposome	60–80 nm	maleimide	GSH	exhaust intracellular GSH; upregulate ROS levels	amplify PDT	CD44-specific targeting; good specificity and biocompatibility	Shi et al. (2021)
	CuO2@mPDA/DOX-HA (CPPDH)	copper peroxide	106 nm	HA; PA; DOX	GSH	Cu + catalyzed H2O2 to produce •OH	synergetic PDT/CDT	HA-targeting and acidic-triggering	Xiao et al. (2021)

NPs, nanoparticles; HA, hyaluronic acid; DC, diclofenac; GOx, glucose oxidase; 2DG, 2-Deoxy-d-glucose; PLGA, poly (lactic-co-glycolic acid); LND, lonidamine; HK II, hexokinase II; IDO-1, 2,3-dioxygenase 1; A-RAMP, RBCm@Ag-MOFs/PFK15; PFK15, 1-(4-pyridyl)-3-(2-quinolinyl)-2-propyl-1-one; PFKFB3, 6-phosphofructo-2-kinase/fructose-2, 6-bisphosphatase 3; CDN, Copper-depleting nanoparticle; CDM, copper-depleting moiety; SPN, semiconducting polymer; ETC, electron transport chain; VES, vitamin E succinate; DOX·HCl, Doxorubicin hydrochloride; β-CD, β-cyclodextrin; CDDP, cisplatin; UNMM, UCNPs- MSN- MnO2 nanocomposites; Ce6, chlorine 6; ATO, atovaquone; MTX, methotrexate; PDT, photodynamic therapy; PTT, photothermal therapy; DON, 6-diazo-5-oxo-l-norleucine; GDH1, Glutamate dehydrogenase 1; CDT, chemodynamic therapy; CPPDH, CuO2@mPDA/DOX-HA; PA, photoacoustic; and DOX, doxorubicin.

2021). This means that blocking only one metabolic pathway may be counterproductive because many pathways of cancer cells are also important for immune cells.

Over the past few decades, nanotechnology has made brilliant achievements in diagnosis, imaging, and cancer treatment *in vivo* (Liu et al., 2019; Yang et al., 2020a; Irvine and Dane, 2020). Because of various unique advantages of nanomedicine, such as good biocompatibility, biological degradation, high targetability, and therapeutic efficacy, the development of nanotechnology is leading anti-cancer therapy into a new era for multimode treatment (Yan et al., 2019; Yan et al., 2020a; Li et al., 2021a; Yan et al., 2022), including targeting metabolism in tumors. The strategy of using nanomedicines to modulate metabolic pathways offers a promising opportunity to fight against tumors. Nanomedicine can specifically target cancer cells by regulating their physicochemical properties, thereby controlling the pharmacokinetics and biodistribution of compounds (Wicki et al., 2015; Li et al., 2021b; Liu et al., 2022). Nanomedicine can also be used as carriers carrying multiple therapeutic cargos capable of metabolic modulation or acting with metabolites in TME to improve immunosuppressive TME [(Cao et al., 2021); (Yan et al., 2021a)], which results in more effective and less toxic effects (Yang et al., 2019; She et al., 2020; Zheng et al., 2021).

In this review, we will briefly summarize the representative work of nanoparticles contributing to the metabolic modulation in the context of cancer (**Table 1**) and TME (**Table 2**). In addition, we will discuss and analyze some possible reasons limiting the applications and prospect new insights into this field.

CANCER CELL METABOLISM AND TARGETS

To meet the demands of unrestrained proliferation, cancer cells undergo specialized alterations in various metabolic pathways (DeBerardinis and Chandel, 2016). In general, the characteristics of cancer cells metabolically reprogramming mainly involves the abnormality of the main nutritional metabolic pathways (glucose, amino acid, and lipids) (Guo et al., 2019).

In both normal and cancerous cells, glucose is the source of energy via glycolysis in the cytoplasm and oxidative phosphorylation (OXPHOS) in the mitochondrion. The pentose phosphate pathway (PPP), a vital branch of glycolysis, makes an important contribution to helping cancerous cells meet the needs of anabolism and anti-oxidative stress (Patra and Hay, 2014). Glucose breakdown generates pyruvic acid providing acetyl-CoA for the tricarboxylic acid (TCA) cycle, which is a hub of bioenergy synthesis and precursor for biosynthesis (Eniafe and Jiang, 2021). The uptake and upregulated *de novo* synthesis of amino acids is also abnormally upregulated, which has diverse and important roles in tumors (Lukey et al., 2017). The enhancement of glutamine metabolism is the main feature that promotes tumor progression by facilitating energic synthesis and biosynthesis (Yoo et al., 2020). Amino acid metabolism also includes pathways of one-carbon metabolism, TCA cycle, and reduced glutathione synthesis (Wei et al., 2020). In addition, cancer cells show an increase in exogenous lipids uptake and

TABLE 2 | Representative nanoparticles targeting TME metabolism.

Metabolism pathway	Name	Nanocarrier material	Size	Cargo	Targets	Mechanism	Indication	Advantages	References
Lactic acid	PMLR	mRBC-camouflaged hollow MnO2 catalytic nanosystem	65 nm	3PO and LOX	lactic acid oxidation and glycolysis	catalyze the oxidation reaction of lactic acid and inhibit glycolysis	synergistic metabolic therapy and immunotherapy	remove lactic acid; lead to an immunocompetent TME	Gao et al. (2019b)
Lactic acid	PFOB@TA-Fe (III)-LOX, PTFL	TA-Fe (III) coordination complexes-coated PFOB	182 ± 13 nm	LOX	lactic acid oxidation	dual-depletion of lactate and ATP with hydroxyl • OH radicals' generation	cascade metabolic-CDT	provide imaging guidance	Tian et al. (2021)
Kynurenine	1-MT@i-aCMP nanosheets	aCMP nanosheets	200 ± 18 nm	IDO inhibitors	IDO-1	IDO inhibition; evokes ICD by generating ROS and hyperthermia under NIR irradiation	reversing Immunosuppression in hypoxic and immune-cold tumors	reshaped cold tumors into hot ones	Jiang et al. (2021)
Kynurenine	AIM NPs	CaCO3	174.2 nm	4PI	IDO-1	suppress Kyn accumulation	reinforces radiotherapy by reprogramming the immunosuppressive metabolic microenvironment	pH-responsive; suppress the distant tumors; result in immune memory responses	Wang et al. (2022b)
Prostaglandin E2 (PGE2)	Cele-BMS-NPs	human serum albumin	43.5 ± 4.0 nm	BMS-202; GSH-activatable prodrug of celecoxib	COX-2	inactivating COX-2	regulate immunosuppressive pivot	pH-sensitive; resolve the different pharmacokinetic profiles and the spatial obstacles	Feng et al. (2022)
Hypoxia and kynurenine	PF-PEG@Ce6@NLG919 NPs	fluorinated polymeric	94.6 nm	Ce6 and NLG919	IDO-1; Hypoxia	the combined action of hypoxia alleviation-induced PDT and IDO inhibitor	hypoxia alleviation-triggered enhanced photodynamic therapy	hypoxia alleviation-triggered	Xing et al. (2019)
Lipid metabolism	aCD3/F/AN	F/Ans	~150 nm	fenofibrate	activate T cells	activate fatty acid metabolism; restore mitochondrial functions	immunometabolism therapy	enhances the production of various cytokines in tumor tissues	Kim et al. (2021)
Lipid metabolism	T-Tre/BCN-Lipo-Ava	liposomes	91.5 nm	Ava	increase the concentration of cholesterol in the T cell membrane	induced rapid T cell receptor clustering and sustained T cell activation	cell-surface anchor-engineered T cells	safe cell-surface anchor-engineered T cells	Hao et al. (2020)

RBC, red blood cell membrane; 3PO, 3-(3-pyridinyl)-1-(4-pyridinyl)-2-propen-1-one; LOX, lactate oxidase; CDT, chemodynamic therapy; IDO-1, 2,3-dioxygenase 1; AIM NPs, acidity-IDO1-modulation nanoparticles; CaCO3, carbonate; 4PI, 4-phenylimidazole; Kyn, kynurenine; PGE2, Prostaglandin E2; GSH, glutathione; COX-2, cyclooxygenase-2; Ce6, Chlorin e6; F/Ans, amphiphilic poly (γ-glutamic acid)-based nanoparticles; and Ava, Avasimibe.

hyperactivating lipogenesis pathway to produce key lipid cell structures, such as cell membranes. Fatty acids (FAs) and cholesterol are synthesized from glucose-derived cytoplasmic acetyl-CoA. Long-chain fatty acids split into acetyl-CoA via fatty acid β oxidation (FAO) to drive the TCA cycle in order to produce adenosine triphosphate (ATP) and biosynthesis, which is also important for proliferation, drug resistance, and metastatic progression in cancer (Ma et al., 2018). In this section, we briefly present the fundamental targets of metabolism in cancer cells and mainly focus on recent nanoparticle efforts to target cancer metabolism (**Figure 1**).

Aerobic Glycolysis and Mitochondrial Aerobic Respiration

Glucose is the main source of energy available to all cells. The utilization of glucose starts from the uptake by cells and conversion to glucose 6-phosphate, which could enter into glycolysis to yield pyruvate, glycogen synthesis, and the PPP. The breakdown of energy sources includes glycolysis, the TCA cycle, and oxidative phosphorylation OXPHOS (36). Under aerobic conditions, normal cells mainly produce energy through the OXPHOS pathway, and glycolysis is inhibited, while tumor cells, even under aerobic conditions, mainly produce ATP through glycolysis, which is called aerobic glycolysis, namely, the Warburg effect (Warburg, 1925; Kuntz et al., 2017; Courtney et al., 2018). Metabolic targeting therapy of tumor glucose metabolism is the most common anti-cancer nanoparticle strategy, which mainly focuses on glycolysis and mitochondrial OXPHOS.

Glucose is an object that can be controlled directly. Extracellular glucose is transported into the cell through glucose transporters (GLUTs), which makes it a potential therapeutic target for suppressing tumors (Zhang et al., 2021a). A novel paradigm therapy of systematic energy exhaustion is proposed to synergize the glycolysis inhibition and GLUT1 depletion using a "nano-enabled energy interrupter," which enables energy exhaustion via zinc (II) interference for effective tumor therapy (Wu et al., 2022). Chen et al. (2017a) prepared a nanodrug GNR/HA-DC, which contains hyaluronic acid (HA)-targeting part and diclofenac (DC, a GLUT1 inhibitor). Upon specifically targeting CD44, the GNR/HA-DC shows that it can sensitize tumor cells for photothermal therapy (PTT) by inhibiting anaerobic glycolysis. Besides, glucose is catalyzed by glucose oxidase (GOx), which could help convert glucose into gluconic acid and toxic H2O2, thereby inhibiting the process of glycolysis and enhancing tumor therapy (Fan et al., 2017; Ding et al., 2022). A multifunctional liquid metal-based nanoparticle attached with GOx and mineralizing calcium carbonate can inhibit glycolysis and mitochondrial metabolism to improve PTT efficiency (Ding et al., 2022). Another report of nanoparticles, as a biocompatible nanocarrier, is used to deliver GOx, which also yields a significant anti-cancer effect (Fan et al., 2017).

Other candidate approaches include the targeting of metabolites in glycolysis or inhibition of key enzymes. Key enzymes include hexokinase (HK), phosphofructokinase (PFK), and pyruvate kinase (such as M-type isozyme, PKM). (DiTullio and Dell'Angelica, 2019) 2-Deoxy-D-glucose (2DG) is a glucose analog (Ralser et al., 2008), which can inhibit HK and prevent glycolysis. Synthesized a liposome nanoparticle that is co-loaded with doxorubicin (Dox) and 2DG in liposomes could inhibit glycolysis of cancerous cells, which also leads to mitochondrial depolarization and subsequent apoptosis Yang et al. (2020b). Sasaki et al. (2021) also developed 2DG-encapsulated poly (lactic-co-glycolic acid) (PLGA) NPs, which shows antitumor immunity and cytotoxicity in tumors. As an effective inhibitor of glycolysis, Lonidamine (LND) is an effective inhibitor of hexokinase II (HK II), a rate-limiting enzyme for glycolysis pathways. A GSH-responsive nanodrug that is loaded with LND restrains the glycolysis of tumor cells and inhibits tumor growth (Liu et al., 2021). In a similar manner, a nanodrug consists of 1-(4-pyridyl)-3-(2-quinoline)-2-propyl-1-one (PFK15), which is a PFKFB3 inhibitor targeting glycolysis metabolism (Zhao et al., 2020a). This work shows that synchronously molecular-targeting and metabolic-regulating can exert a better anti-tumor effect.

However, cancer cells not only metabolize glucose by glycolysis but also produce ATP via mitochondrial glucose metabolism (Weinberg and Chandel, 2015). This hybrid energetic metabolic pattern makes the traditional single metabolic anti-cancer therapy hardly obtain satisfactory efficacy (Gottschalk et al., 2004). For example, triple-negative breast cancer (TNBC) is insensitive to enzyme inhibitors targeting glucose transport, which makes OXPHOS a more important target for the treatment of TNBC (52). Therefore, Cui developed a mitochondria-targeted, copper-depleting nanoparticle, which is effective against TNBC that depends on oxidative phosphorylation (Koppenol et al., 2011). This nanoplatform has a positive surface charge, which helps accumulation in the mitochondria and local depletion of copper. However, cancer cells will compensate by increasing the other pathway to produce ATP if a single pathway of glucose metabolism is inhibited (Gottschalk et al., 2004). Therefore, many energy-depletion strategies of nanoparticles are designed to block both energy synthesis pathways synergistically (Ding et al., 2022; Dong et al., 2022). A cancer cell membrane camouflaged nanoinhibitor co-encapsulates OXPHOS inhibitor and glycolysis inhibitor for synergistically blocking two pathways that significantly suppress tumor growth (Dong et al., 2022), while some studies have confirmed that the strategy of targeting mitochondria can also reduce the occurrence and metastasis of tumors (Zhang et al., 2021b; Lin et al., 2021). The common scheme is inhibiting mitochondrial complexes of the electron transport chain (ETC). Vitamin E succinate (VES) is a molecule that can bind with the ubiquinone in Complex II to interfere with the mitochondrial respiratory metabolism (Dong et al., 2011). Inducing mitochondrial malfunction through VES loaded in a self-assembly polymersome nanoplatform is an appealing strategy to improve cancer therapy and overcome multidrug resistance (Liang et al., 2021). A pH/ROS cascade-responsive vitamin E nanodrug releases VES interfering with the ETC to aggravate tumor cell killing (Li et al., 2020a). Atovaquone (ATO) is an ETC inhibitor that disturbs the activity of OXPHOS,

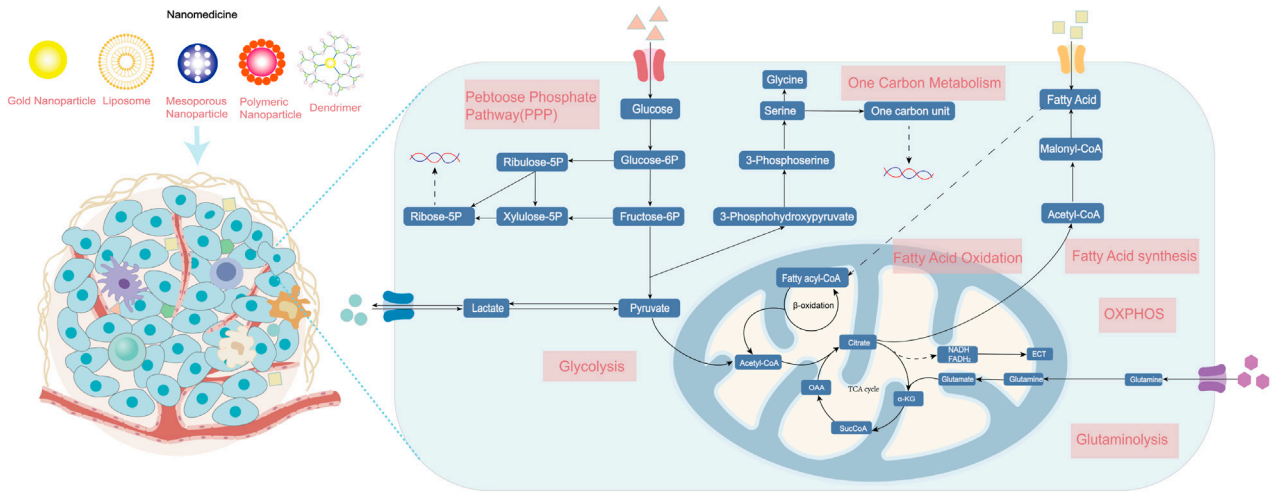

FIGURE 1 | The metabolism of cancer cells. Enhanced aerobic glycolysis, also known as the Warburg effect, enables cancer cells to generate large amounts of biomolecules for biomass production. Glutamine is converted into glutamate and ammonia in the process of glutaminolysis. The upregulation of *de novo* lipid synthesis and fatty acid oxidation is related to bioenergy synthesis and signaling molecules needed for proliferation. Various nanomedicines can target these metabolic vulnerabilities in cancer cells and improve therapeutic effects, including photothermal, gene, chemo-, and immunotherapy. ETC, electron transport chain; OXPHOS, oxidative phosphorylation; and TCA, tricarboxylic acid cycle.

which is another commonly nanoloaded drug (Xia et al., 2019). A carrier-free self-delivery nanomedicine based on photosensitizer (PSs) Ce6 and OXPHOS inhibitors of ATO exhibited marked efficacy and low toxicity (Zhao et al., 2020b). An intelligent multilayer nanostructure was also designed based on ATO (61): the decomposition of outer MnO2 can create O2, which elevates the oxygen content of TME. Then, the released ATO molecules of the middle mesoporous silicon layer could effectively inhibit tumor respiration metabolism.

As glucose metabolism is a crucial regulatory target in tumors, its regulation has attracted increasing attention in recent years. Using nanotechnology to develop medicines based on glucose metabolic regulation has become a promising strategy. Combining the metabolic therapy of glucose with other therapeutic strategies to achieve better therapeutic effects will be an important future research direction.

Glutamine and Glutathione Metabolism

Glutamine (Gln) is a nonessential amino acid and an important metabolic fuel that participates in multiple biological processes, including biosynthesis, signal transduction, and protecting cells from oxidative stress (Matés et al., 2019). Gln is absorbed by cells through alanine–serine–cysteine transporter 2 (ASCT2). Glutamine is further converted into glutamate and α-ketoglutarate (α-KG) in mitochondria by glutaminase enzymes and by glutamate dehydrogenase (GDH) or aminotransferases (Jin et al. 2015), respectively. Thus, it can be seen that Gln is an alternative source of carbon elements to replenish the TCA cycle (Masisi et al., 2020). Under hypoxia or mitochondrial dysfunction, α-KG is carboxylated into citrate by isocitrate dehydrogenase. The citrate is exported to cytosol and further transferred into *de novo* fatty acid synthesis or produces another amino acid. In the cytoplasm, glutamine provides an amide (γ-nitrogen) group, which enables nucleotides to be synthesized from scratch. Glutamate produced during this process is further transformed into reduced glutathione (GSH), which plays a key role in protecting cells from oxidative damage and maintaining redox homeostasis (Forman et al., 2009).

Cancer cells exhibit addiction to Gln (Wang et al., 2018). Targeting Gln has become an attractive anti-cancer strategy using nanoplatform-based drug delivery systems. 6-diazo-5-oxo-l-norleucine (DON) is a reactive diazo glutamine analog that binds to multiple enzymes in glutamine metabolism. DON displays anti-tumor activity as a glutamine antagonist in animal tumor models (Lemberg et al., 2018). A therapeutic platform was designed, which combined porous Pt–Pd nanoflowers (Pt–Pd NFs) with DON (Pt–Pd@DON) and was used to enhance electrodynamic immunotherapy (Chen et al., 2022). Under the promotion of DON, the joint functions of the immunogenic cell death (ICD) effect and $CD8^+$ T cell infiltration stimulate an anti-cancer immune reaction in immunosuppressive tumors and exert a therapeutic effect. Moreover, inhibiting the activity of key enzymes could not only cut the nutrition supply for tumor cells via blocking of glutaminolysis but also disrupt the intracellular redox homeostasis. The overexpressed GDH1 can promote α-KG generation and is a key regulatory target. A group developed a nanoparticle by inhibiting mitochondrial glutaminolysis for preventing the nutrient supply of tumor cells (Xu et al., 2021). This tumor-targeted theranostic nanoplatform was constructed using the bovine serum albumin (BSA), ferrocene, and GDH1 inhibitor purpurin. BSA provides long circulation and well biocompatibility, and the ferrocene-triggered Fenton reaction provides effective chemodynamic therapy (CDT).

The glutamate-derived GSH is the main redox buffer in cancer cells. Therefore, consuming GSH is considered to be an effective

solution for fighting cancer. Numerous nanomedicines, by delivering GSH-depleting agents, have achieved decent therapeutic effects. Chen et al. developed a CD44-specific targeting nanoreactor (AM-L@NBS) that can exhaust the intracellular GSH and cause apoptosis in cancer cells (Shi et al., 2021). The maleimide on the AM-L@NBS interacts with GSH via Michael addition, thereby resulting in the annihilation of GSH and an increase in ROS production, which facilitates the anti-cancer effect. As a reducing substance in cells, GSH can be consumed by reacting with oxidizing agents. General strategies of depleting intracellular GSH mostly are mainly based on the Fenton reaction or Fenton-like reaction. The available GSH-depleting components include various oxidizing agents, such as MnO_2 (Lin et al., 2018), Cu^{2+} (Xiao et al., 2021), Fe^{3+} (Shen et al., 2020), and Ce^{4+} (Dong et al., 2020). For example, Xiao et al. presented a multifunctional intelligent nanoplatform CuO2@mPDA/DOX-HA (CPPDH), which induced the consumption of GSH and the self-supply of H2O2 (72).

Other glutamine metabolism antagonists (such as ASCT2 antagonist) have also shown antitumor activity in preclinical models (Stine et al., 2021). In a theoretical sense, glutamine metabolic drugs can target glutamine-dependent tumor cells, thereby being applied to different types of cancers, which could be exploited as a "metabolic checkpoint" for tumor immunotherapy (Leone et al., 2019). The related nanomedicine may be one of the development directions in this field.

Lipid Metabolism and Nucleotide Metabolism

FAs and cholesterol are necessary for cell membranes and other key structures. In addition, lipid metabolism is also related to bioenergy synthesis and signaling molecules needed for proliferation (Röhrig and Schulze, 2016). Dysregulation of lipid metabolism is a prominent metabolic characteristic of cancer cells (Bian et al., 2021). The alterations of lipid metabolism in tumor cells mainly include abnormal upregulation of *de novo* lipid synthesis and FAO [(Carracedo et al., 2013)]. The main substrate for lipid synthesis is cytoplasmic acetyl-CoA: both FAs and cholesterol are synthesized from acetyl-CoA through a series of reactions. Key enzymes involved in acetyl-CoA production, FAs' biosynthesis, cholesterol biosynthesis, and FAO are key methods targeted to destroy lipid metabolism in cancer treatment (Bian et al., 2021).

Hyperactive acetyl-CoA and FAs production in cancer is mediated by the increase in key enzymes. The main targets commonly used in preclinical and clinical research of drug development include ATP citrate lyase (ACLY), acetyl-CoA carboxylase, and fatty acid synthase (Stine et al., 2022). A study reported that nanomaterials with peroxidase-like activity inhibit tumor growth *in vivo* through an ACLY-dependent rat sarcoma viral oncogene (RAS) signaling mechanism (Wang et al., 2020b). Moreover, the success of therapeutic efficacy of targeting key enzymes supports the potential to deliver counterpart inhibitors through nanoparticles in the future (Wang et al., 2022a). Monoacylglycerol lipase (MGLL), an important enzyme catabolizing lipid that extensively exists in pancreatic cancer cells, plays an important role in triacylglycerol (TG) metabolism. Cao et al. (2022) developed a reduction-responsive poly nanoplatform to deliver MGLL siRNA (siMGLL). This platform can efficiently silence MGLL in cancer cells and lead to the inhibition of free FAs (FFAs) generation and tumor growth. Ferroptosis is a regulatory cell death triggered by lipid peroxidation of membrane unsaturated FAs catalyzed by iron ions (Jiang et al., 2020). It is an attractive target for anti-cancer treatment in nanotechnology (Shan et al., 2020). The design principle of many nanoparticles is based on increasing the lipid peroxidation level of tumor cells by providing exogenous FAs, thereby synergistically inducing iron death (Zhou et al., 2017; Gao et al., 2019a).

The proliferation of tumors depends on *de novo* nucleotide synthesis (pyrimidines and purines). One-carbon (1C) metabolism includes a series of interconnected pathways, providing 1C units (methyl groups) for nucleic acid synthesis (Ducker and Rabinowitz, 2017). Therefore, these pathways contain many promising therapeutic targets for disrupting mRNA synthesis and DNA replication in cancer cells. DNA damage repair pathways are also a common target in clinics for small-molecule inhibitors, chemotherapy, and nanomedicine (Stine et al., 2021). Mut-T homolog 1 (MTH1) is a protein that can inhibit the deoxynucleotide damage in DNA. The effective inhibition of MTH1 of a self-delivery photodynamic synergists nanoparticle could augment DNA damage and promote tumor cell apoptosis (Li et al., 2021c). Many nanoparticles encapsulate inhibitors of DNA damage repair that have been used clinically. For example, the therapeutic effect of BRCA-deficient breast cancer can be improved by encapsulating tarazolpani in bilayer nanoliposomes (Zhang et al., 2019a). In a similar manner, Wang et al. (2020c) designed an amphiphilic peptide nanoparticle encapsulating olaparib and JQ1 to treat non-BRCA mutant pancreatic cancer by inhibiting DNA damage repair pathways. The same idea could be seen in other nanoparticles loaded with doxorubicin to interfere with DNA/RNA synthesis. (Chen et al., 2020; Yang et al., 2021).

TUMOR MICROENVIRONMENT METABOLISM AND TARGETS

The TME is composed of diverse cell populations in a complex matrix, which includes tumor cells, extracellular matrix, immune cells (myeloid and lymphoid lineage), supporting cells (fibroblasts, stromal cells, and endothelial cells), and various other components (Quail and Joyce, 2013; Quail and Joyce, 2017; Hinshaw and Shevde, 2019; Li et al., 2021a). Tumor cells, fibroblasts, or inflammatory cells secret various pro-tumorigenic proteases, cytokines, and growth factors, thereby supporting growth, angiogenesis, and invasion of tumor cells (Quail and Joyce, 2013). Meanwhile, under the attraction of chemokines, immune cells enter and locally proliferate, differentiate, and function in the TME, which includes innate immune cells (macrophages, neutrophils, dendritic cells, innate lymphoid cells, myeloid-derived suppressor cells, and natural

killer cells) and adaptive immune cells (T and B cells) (Hinshaw and Shevde, 2019).

For decades, an important limiting factor in the clinical transformation of nanomedicine has been the heterogeneity of tumors. To circumvent this tumor cell heterogeneity, the academic community has shifted attention to leveraging immune cells (Zhang et al., 2020), which are less heterogeneous than tumor cells in the TME [(Trinh and Polyak, 2019)]. On the one hand, immune cells play vital roles in anti-tumor immunity, thereby making targeted immune cell metabolism a promising therapeutic strategy. On the other hand, the behavior of cancer is also regulated by the inherent metabolism of cancer cells and metabolites in local TME [(Augustin et al., 2020)]. Metabolic changes in cancer cells have reshaped the TME and promoted the progression of tumor: glucose, amino acid, and oxygen compete with immune cells, and lactate secretion promotes the formation of immunosuppressive TME (8). For example, tumor cell exerts immunosuppressive functions by inhibiting the infiltration of effector T cells, promoting the regulatory T cell (Tregs) differentiation, and accumulating lactic acid and carbon dioxide (Kouidhi et al., 2017). Meanwhile, the complicated metabolic patterns of noncancer cells within TME also affect the differentiation of its own subsets and increase the immunogenicity of the tumor (Xia et al., 2021). That implies that an essential consideration should be given to the possible beneficial or adverse effects on TME in the future design of metabolic nanodrugs. DRP-104, a glutamine antagonist example that can increase the immune cell response, is a small-molecule metabolic inhibitor undergoing clinical trials (NCT04471415).

Recent research on cancer metabolism has explosively increased but mainly focused on tumor cells. Research on the metabolism of TME is an important direction in the future. The metabolic components and pathways of noncancer cells within TME have also undergone reprogramming and contributed to tumor progression. In this section, we will summarize the alterations of noncancer cells within TME (**Figure 2**) and metabolic regulation nanoparticles that act on the metabolites of the TME and the surrounding immune or stromal cells (**Table 2**).

Metabolites Within Tumor Microenvironment

The competition and crosstalk of metabolites between different cell types of TME are important determinants of cancer. Tumor vascular abnormalities restrict oxygen exchange and create regions of hypoxia (Fukumura et al., 2018). Metabolic reprogramming of hypoxic cells and disordered blood vessels increases the production and accumulation of immunosuppressive metabolites: lactate, kynurenine, prostaglandin E2 (PGE2), etc. (Chen et al., 2015; Pérez-Tomás and Pérez-Guillén, 2020). Targeting these metabolic features and metabolites, such as hypoxia and low pH, has been a promising strategy in different types of cancer (Bader et al., 2020; DePeaux and Delgoffe, 2021).

Among them, lactate acidifies the TME (pH 6.5–6.8) (Webb et al., 2011) and plays multifaceted roles in local TME, including impairing the immune responses and involving intracellular metabolic crosstalk (Lyssiotis and Kimmelman, 2017; Certo et al., 2021). In detail, accumulation of lactate is deleterious for T cell effector function and anti-tumor response (Fischer et al., 2007). The lactic acid in TME is an active checkpoint for the function of regulatory T cells by promoting PD-1 expression (Kumagai et al., 2022). Lactate also has a critical function in tumor-associated macrophages (TAMs) and myeloid-derived suppressor cells (MDSCs) polarization (Chen et al., 2017b; Zhao et al., 2022). Moreover, cancer cells of normoxia regions consume lactate generated by the hypoxic cancer cells and cancer cancer-associated fibroblasts (CAFs) to fuel the TCA cycle (Lyssiotis and Kimmelman, 2017). One strategy for nanomedicines is to encapsulate lactate oxidase (LOX) and consume lactic acid in the TME by catalyzing its oxidation. A cascade catalytic nanosystem delivers LOX and glycolysis inhibitor with hollow MnO2 (HMnO2) nanoparticles to realize lactic acid exhaustion, which is used for synergistic metabolic therapy of tumors (Gao et al., 2019b). A tannic acid (TA)-Fe (III) coordination complexes-coated perfluorooctyl bromide (PFOB) nanodroplets also load with LOX (PFOB@TA-Fe (III)-LOX, PTFL), which is used for the simultaneous consumption of lactic acid and ATP, and simultaneously generates hydroxyl OH radicals (Tian et al., 2021).

Kynurenine can accumulate in IDO-positive cancers, which is related to the inactivation of effector T cells and promotes immunosuppressive cells (Bader et al., 2020). The kynurenine pathway is controlled by the rate-limiting enzyme indoleamine-2,3-dioxygenase (IDO1) (Platten et al., 2019). IDO1-modulation nanoparticles are always used as an immunometabolism drug to block kynurenine metabolic pathways (Jiang et al., 2021; Liu et al., 2021; Wang et al., 2022b). A work utilizes aza-fused conjugated microporous polymer (aCMP) nanosheets inducing dual-type of ICD and the interference of the IDO pathway in hypoxic tumors (Jiang et al., 2021). Furthermore, cancer cells secret PGE2, thereby directly inactivating T cells. It has been proved that the elimination of PGE2 by inactivation of cyclooxygenase -2 (COX-2) based on nanoparticles could inhibit the growth of tumors (Feng et al., 2022). The group solved the challenge of pharmacokinetic differences and the spatial barrier that PD-1/PD-L1 interaction occurred outside the cell while COX-2 was located intracellularly: this intelligent nanoparticle could release celecoxib (COX-2 inhibitor) in cells in response to the elevated GSH concentration inside tumor cells.

Acidic/hypoxia TME has a close relationship with immune suppression, and it is important for nanodrug development (Watson et al., 2021). These physiological characteristics of TME make it convenient to design the programmed release nanoparticles. Furthermore, taking advantage of the metabolic characteristics of TME, nanomedicines have a better immune response and therapeutic improvement (Huang et al., 2019; Xing et al., 2019; Wang et al., 2022b). For example, a carbonate (CaCO3) nanoparticle was developed to encapsulate 4-phenylimidazole (4PI), thereby inhibiting IDO1 from constructing an acidic pH-activatable nanomedicine, which reinforces the immunity and treatment outcome of radiotherapy (Huang et al., 2019). A multifunctional nanoplatform was constructed using fluorinated polymer

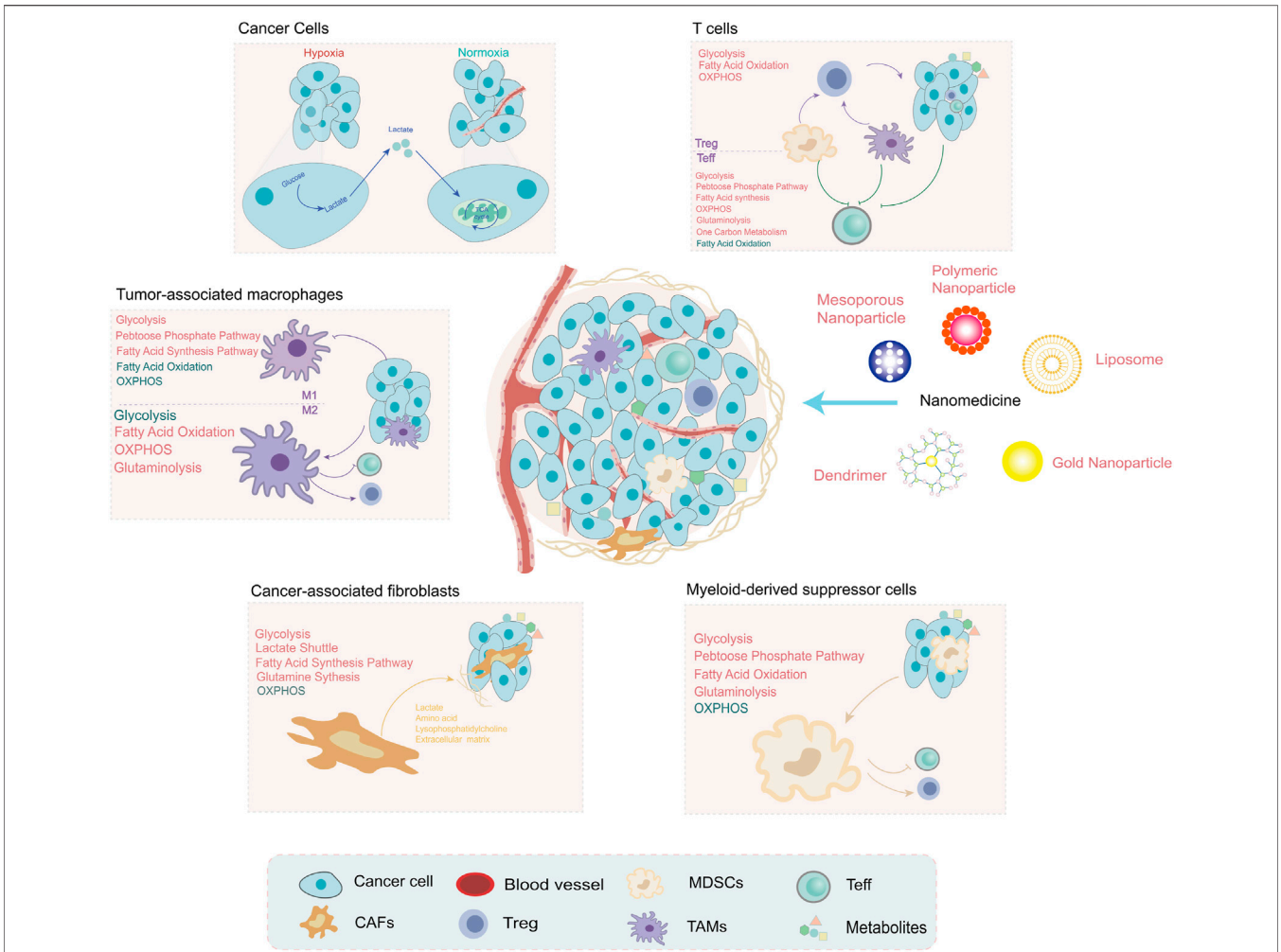

FIGURE 2 | The metabolites are shaped by noncancer cells within the tumor microenvironment (TME), which have unique metabolic profiles and vulnerabilities. Under hypoxia conditions, the metabolites produced by tumor cells are regulators of noncancer cell function, such as lactate and PGE2. The metabolic pathway alterations of noncancer cells within TME are depicted in different colors (red: upregulation and green: downregulation). These alterations provide a promising direction for the development of nanomedicine: targeting metabolism to improve the TME for cancer treatment.

nanoparticles and encapsulated with IDO1 inhibitor (NLG919) for pH-responsive metabolic therapy (Xing et al., 2019). This nanoparticle alleviated the hypoxia situation of the TME and improved the therapeutic efficiency.

Cancer cells can also produce various other immunosuppressant metabolites (Stine et al., 2022), such as adenosine and 2-hydroxyglutarateand methylthioadenosine, which offer developers more choice in this field. It can be seen as an optimization direction of nanomedicines that can specifically be activated by simultaneously targeting metabolites and reinvigorating the antitumor immune response.

T Cell Metabolism in the Tumor Microenvironment

The heterogeneity of antitumor immunity depends, to a great extent, on the diversity and composition of T cells in TME [(Woolaver et al., 2021)]. Existing cognition has identified that metabolism is an important regulatory factor for T cell biological behavior and function (Klein Geltink et al., 2018). Extensive efforts have been made to explore metabolic changes in effector T cells and Treg cells in the TME, which have important therapeutic significance for the development of nanomedicines.

Unlike quiescence status, effector T cells (Teff) activation generally adopts an anabolic metabolism phenotype, which mainly depends on glycolysis and glutaminolysis to rapidly increase the energy supply to achieve proliferation and effector functions (Sharabi and Tsokos, 2020). Activated T cells also upregulate the lipid synthesis, PPP, and one-carbon metabolism pathways, which play important roles in membrane synthesis, nucleotide biosynthesis, and cellular redox balance (Wei et al., 2021). The biochemical intermediates of metabolic reprogramming are essential for the biosynthesis process (nucleotides, amino acids, and lipids) (MacIver et al., 2013). Competitive consumption of glucose by tumor cells restricts the cytotoxicity of Teff (Chang et al., 2015).

Therefore, metabolic reprogramming of Teff cells may be a feasible strategy. Nanotechnology has already made some achievements in this field. For instance, it has been reported that promoting fatty acid metabolism could activate T cells and fight against tumor cells (Zhang et al., 2017). A study (Kim et al., 2021) designed a T cell-targeting nanoparticle (aCD3/F/AN) encapsulating the lipid metabolism-activating drug, fenofibrate, which can further activate fatty acid metabolism and restore mitochondrial functions. aCD3/F/AN can specifically target T cells by modifying the surface of nanoparticles with an anti-CD3e f (ab′)2 fragment and exerting an effector-killing effect against tumor cells. Another example is that the function of T cells is affected by the metabolism of cholesterol. Avasimibe (Ava), an inhibitor of the cholesterol-esterification enzyme acetyl-CoA acetyltransferase 1 (ACAT1), potentiates the antitumor response of CD8 (+) T cells by regulating cholesterol metabolism (Yang et al., 2016). Nanomaterials can also be attached to T cells in a strategy known as "backpacking" to carry liposomal Ava in order to enhance solid tumor immunotherapy (Hao et al., 2020). In addition to specific targets within T cells, the metabolism regulation of tumor cells can improve T cell-associated immunity. The knockdown of lactate dehydrogenase A (LDHA) in tumor cells by RNAi nanoparticles, pyruvate metabolism, is reprogrammed to increase $CD8^+$ T and NK cells infiltration (Zhang et al., 2019b).

In contrast, regulatory T cells (Treg) cells are essential for tumoral immunosuppression and mainly rely on OXPHOS and FAO for survival (Yu et al., 2018). The specific metabolic mechanisms involving differentiation and maintenance remain unclear. Recent advances in Treg metabolism shed new light on further understanding of the balance of metabolism in TME. For instance, increased uptake of lactic acid can induce Treg cells to express PD-1, and MCT1 is an important metabolic checkpoint in this process (Kumagai et al., 2022). In addition, it is reported that lipid modifications mediated by bidirectional metabolic signaling are important for differentiation and maintenance, which provides a potential target for Treg cell regulation (Su et al., 2020). Some developed drugs are also found to be involved in the metabolic process of Treg cells. Imatinib, a BCR-ABL kinase inhibitor, induces apoptosis of Treg by downregulating the expression of IDO [(Beckermann et al., 2017)]. A hybrid nanoparticle enhances the effect of imatinib in downregulating Treg cell suppression for targeting and modulating Treg cell function in the TME (Ou et al., 2018).

Other Adjacent Cells' Metabolism in the Tumor Microenvironment

Besides T cells, there are many kinds of cells in TME, such as dendritic cells (DCs), CAFs, TAMs, and MDSCs (Hinshaw and Shevde, 2019). Among them, CAFs account for the largest proportion of stroma. The function of TAMs and MDSCs is to act as an inhibitor for anti-cancer immunity and to promote tumor progression and metastasis (Gabrilovich, 2017). These cells sense the change in TME and respond by reprogramming the metabolic pathways to maintain the function of suppressive and pro-tumorigenic. Recent progress in these adjacent cells based on metabolic features not only deepens our insight into their metabolic phenotype but also brings nanotargeting therapies onto the agenda.

The promoting functions that CAFs exert on cancer development make them tempting therapeutic targets. Some progress in nanomedicine has been made in this field. For example, it has been reported that the activation of CAFs enhances the delivery of doxorubicin in graphene-based nanosheets (Kim et al., 2017). CAFs were recently reported to undergo upregulated pathways of glycolysis and glutamine and FAs synthesis (Yan et al., 2018a; Becker et al., 2020; Gong et al., 2020). As opposed to tumor cells, CAFs exhibit a catabolism phenotype, which is characterized by the shift in glucose metabolism, referred to as the reverse "Warburg effect" [(Martinez-Outschoorn et al., 2011)]. The self-metabolic reprogramming of CAFs provides fuel (lactate, fatty acid, and amino acids) for biosynthesis in cancer cells (Li et al., 2021d).

TAMs and their influence on the metabolic profile of the TME constitute promising targets for the development of novel anti-cancer nanoagents. Glucose metabolism is vital for the polarization and anti/pro-tumoral function of TAM (Leone and Powell, 2020; O'Neill and Artyomov, 2019). Different macrophages get energy in different ways: M1 macrophages get energy through glycolysis with a fast energy supply and M2 macrophages obtained by OXPHOS (143) and account for the main subgroup in TME. Contrary to the M1 subtype, M2-TAMs exhibit elevated OXPHOS, glutamine, and fatty acid consumption (Vitale et al., 2019). While M1-TAM has a high glycolytic rate, fatty acid synthesis, and increased PPP (Rabold et al., 2017).

The metabolic environment change can affect the polarization and function of TAM subsets. For instance, a CaCO3-based nanoparticle scavenging of H+ provides a simple approach to promoting M1-like macrophage polarization (Chen et al., 2019). Besides, in the model of atherosclerosis (van Leent et al., 2021), nanobiologics that inhibit the genes involved in the energy metabolism of macrophages suggest that the metabolic reprogramming shaped by nanotechnology can phenotypically and functionally affect TAM's behavior.

The immunosuppressive functions of MDSCs are characterized by the increased accumulation of lipids and FAO. In their differentiation and activation, MDSCs exhibit an increase in glycolysis, glutaminolysis, and the PPP during a decrease in OXPHOS [(Veglia et al., 2021)]. Inhibiting the proliferation of MDSCs may be a safe and effective strategy for cancer intervention. A previous study has reported that the nanosized pseudoneutrophil cytokine sponges (pCSs) can disrupt the expansion and trafficking of MDSCs to improve the cancer immunotherapy effect (Li et al., 2020b).

CHALLENGE AND OUTLOOK

The development of the understanding of tumor metabolism provides a perspective; that is, metabolic molecules that determine the fate of single cells can be used to determine the life and death of an individual (Cassidy et al., 2019). Since the

milestone of the cancer metabolism that the FDA approved inhibitors of mutant enzymes for AML [(Pirozzi and Yan, 2021)], metabolic anti-cancer therapy has aroused extensive interest for its potential for cancer treatment. This blossoming field has made some significant progress, but there are still some obstacles to realizing the therapeutic potential of nanomedicines in the clinic.

Metabolic Nanomedicine Superiority

The traditional strategy of metabolic-targeting drugs has some limitations, such as insufficient drug distribution specificity and systemic toxicity (Yan et al., 2018b; He et al., 2020). However, nanotechnology has greatly broken through these limitations because of its selective targeting, increased drug payload and controlled release, and good biocompatibility (Kim et al., 2010; Niu et al., 2018; He et al., 2019). The application of nanocarriers in metabolic treatment strategy can enhance the accumulation of cargo drugs in local TME, increase the tolerated dose, and promote the curative effect.

Benefiting from elaborate nanotechnology, various metabolic-targeting drugs/molecules encapsulated with nanoparticles show remarkable targeting and anti-cancer abilities (He et al., 2018a; Yan et al., 2020b; Yan et al., 2021b). This superiority is partly due to the well-known enhanced permeability and retention (EPR) (Maeda et al., 2000) and partly because of the elaborate design of nanoparticles to realize better-targeting tropism (He et al., 2022; Li et al., 2022; Ma et al., 2022). Examples of the above research show that nanoparticles can load specific therapeutic molecules (Liang et al., 2021), and change their physical properties (Cui et al., 2021) to achieve precise delivery or specific response. The reasonable design of nanocarriers makes combined medications achieve the optimal synergistic effect (He et al., 2018b; Bian et al., 2018; Ma et al., 2019), which can realize not only dual-pathway targeting but also avoid systemic toxicity.

Heterogeneity of Metabolism

The heterogeneity of tumors limits the clinical transformation of anti-tumor nanomedicines. The composition of TME is different among the different cancer types. The phenotype of the TME is constantly changing: stromal cells, the composition of growth factors, blood vessels, and immune cells are all in a dynamic state of change (Junttila and de Sauvage, 2013). Corresponding to the phenotype, solid tumors also showed the characterization of significant metabolic heterogeneity (Li and Simon, 2020). Tumor cells from different sources have different characteristics of metabolic gene expression (Xiao et al., 2019). The metabolism in different subtypes of the same tumor is different (Parida et al., 2022). Different regions of the same tumor also exhibit distinct metabolic profiles (Li and Simon, 2020). The metabolic properties and preferences also change during cancer progression (Schug et al., 2016). Above all, tumor cells will adapt to different metabolic modes according to the concentration of external nutrients and different stress conditions (Xia et al., 2021). In other words, cells in different situations and stages will employ different signaling pathways involved in metabolic processes to meet different demands for biological energy and biosynthesis. Therefore, a key consideration is drug specificity. One of the main challenges for active sites is the ubiquity of hydrophobic pockets of metabolizing enzymes (Stine et al., 2022). It is also notable that metabolic plasticity will also result in the impairment of precision-targeted effect (Martínez-Reyes and Chandel, 2021). Many nanoparticle-based drug delivery systems have become suitable carriers to overcome the targeting limitations of traditional drug preparations (Peer et al., 2007; Lim et al., 2019). However, considering the established controversial EPR effect (Ojha et al., 2017) and the limited therapeutic ability of nanomedicines in clinical trials (Wilhelm et al., 2016), tailoring the properties of nanomedicines to increase the target efficiency is still a challenging future direction. Synergistic metabolic therapy that acts on two or more metabolic pathways simultaneously is a way of solving metabolic plasticity (Gao et al., 2019b; Liu et al., 2021). At the same time, dividing patients into different molecular and metabolic subtypes is a clinical method suitable for future personalized treatments.

As the heterogeneity of cancer increases the difficulty of anti-cancer treatment, cancer stem cells (CSCs) provide a possible way to solve this problem (Chen et al., 2021). CSCs-targeting nanomedicine has already become an important research direction and therapeutic target in the development of tumor drugs (Hassani Najafabadi et al., 2020; Zhu et al., 2022). At the metabolic level, CSCs have highly elevated methionine cycle activity and transmethylation rate, which may provide a potential strategy for targeting CSCs (Wang et al., 2019).

Biosafety and Therapeutic Efficacy

The biological safety of nanoparticles is the premise for clinical application. Targeting metabolism is expected to act on the same enzyme in cancer cells, which may cause toxicity to normal cells (Stine et al., 2022). In particular, current metabolic nanomedicines are effective and safe in animal models, but it is still unknown whether the real effects can be manifested clinically. Therefore, in the long run, the safety profiles of metabolic nanomedicines should be systemically explored, especially in combination with immunotherapy and other agents. In addition, the plasticity and complexity of metabolic networks may result in drug resistance: inhibition of a single metabolic step may cause the replenishment of other pathways (Schug et al., 2016). Compared with the single drug targeting metabolism, the current nanomedicine metabolic strategy mostly adopts combination therapy or blocks multiple pathways (**Table 1**). The ideal future direction of nanoparticle development is killing cancer cells and synchronously enhancing other strategies, especially those beneficial to immunotherapy. The development of nanotechnology has provided a multifunctional platform for carrying two or more drugs, which provides a broad prospect for the combination treatment of cancer.

In the future, efforts should be made to optimize the characteristics of nanodrugs, such as the material composition, structure, and physical and chemical parameters, to achieve ideal targeted drug delivery, best curative effect, and minimum toxicity.

Perspective and Conclusion

Metabolism is an active and revolutionary field in oncology, which may be a new checkpoint for anti-cancer treatment (Oh et al., 2021). However, there are still many undetermined issues needing further exploration: 1) distinct cell types have divergent metabolism, but we cannot determine whether the metabolite signals detected are coming from the cancer cells or other cells present within the TME and 2) the metabolic phenotype of many cell types within the TME still needs further investigation. For example, the upregulated aerobic glycolysis is the main pattern of the glucose metabolism of antitumor Teff (Leone and Powell, 2020). That raises the question of whether the activity of Teff will be impaired when we inhibit glucose metabolism in malignant cells. Further, how the metabolism of other cells will be affected when we target a specific metabolic pathway in a specific cell. It is essential to further evaluate the nutritional competition and metabolic interference between neighboring cells and malignant cells. For example, it has long been believed that there is competition between cancer cells and immune cells for metabolic nutrients, such as glucose. But a recent study (Reinfeld et al., 2021) shows that the main culprit of intratumoral glucose consumption by tumors is not cancer cells but immune cells, such as myeloid cells in TME. A recent study reported that the increase in obesity is related to tumor growth and mortality (Turbitt et al., 2019), thereby implying that systemic metabolism is critical for treatment (Lien and Vander Heiden, 2019). Future research needs to determine the mechanism of linking the systemic metabolic state with anti-tumor immunity and use these insights to improve cancer treatment with nanodrugs. Besides, other systemic metabolic factors also play a key role in an anti-cancer immune response. It is worth mentioning that gut microbiota has shown the ability to improve immunotherapy in various preclinical or clinical trials of various cancers (Chaput et al., 2017; Matson et al., 2018; Routy et al., 2018). In addition, some studies have confirmed that antibiotics have negative effects on immunotherapy, thereby indicating that intestinal factors may indirectly affect systemic immune function and anti-tumor immune reaction (Derosa et al., 2018). The underlying mechanism of this connection is attributed to intestinal microbial metabolites (mainly short-chain FAs) (Li et al., 2017). Such systemic metabolism should also be taken into account in the development of nanomedicines.

This review summarizes the latest research progress on nanomedicines in cancer metabolism. This progress includes targeting the metabolic programs of cancer cells and the metabolism of TME. Targeting metabolic pathways is a new field that brings brand-new inspiration for developing anti-cancer nanomedicine. However, it will be a new challenge for the development of nanomedicine to improve anti-cancer immunity while destroying the metabolism of tumor cells.

AUTHOR CONTRIBUTIONS

MR wrote the manuscript. WH reviewed and edited the manuscript. All authors contributed to the article and approved the submitted version.

FUNDING

This work was financially supported by the Key Research and development program of Shaanxi Province (No. 2020GXLH-Y-020, for YY), the National Natural Science Foundation of China (No. 82141126) and The Innovation Capability Program of Shaanxi (No. 2021TD-44).

REFERENCES

Augustin, R. C., Delgoffe, G. M., and Najjar, Y. G. (2020). Characteristics of the Tumor Microenvironment That Influence Immune Cell Functions: Hypoxia, Oxidative Stress, Metabolic Alterations. *Cancers (Basel)* 12 (12), 3802. doi:10.3390/cancers12123802

Bader, J. E., Voss, K., and Rathmell, J. C. (2020). Targeting Metabolism to Improve the Tumor Microenvironment for Cancer Immunotherapy. *Mol. Cell* 78 (6), 1019–1033. doi:10.1016/j.molcel.2020.05.034

Becker, L. M., O'Connell, J. T., Vo, A. P., Cain, M. P., Tampe, D., Bizarro, L., et al. (2020). Epigenetic Reprogramming of Cancer-Associated Fibroblasts Deregulates Glucose Metabolism and Facilitates Progression of Breast Cancer. *Cell Rep.* 31 (9), 107701. doi:10.1016/j.celrep.2020.107701

Beckermann, K. E., Dudzinski, S. O., and Rathmell, J. C. (2017). Dysfunctional T Cell Metabolism in the Tumor Microenvironment. *Cytokine & growth factor Rev.* 35, 7–14. doi:10.1016/j.cytogfr.2017.04.003

Bian, X., Liu, R., Meng, Y., Xing, D., Xu, D., and Lu, Z. (2021). Lipid Metabolism and Cancer. *J. Exp. Med.* 218 (1), e20201606. doi:10.1084/jem.20201606

Bian, Z., Yan, J., Wang, S., Li, Y., Guo, Y., Ma, B., et al. (2018). Awakening P53 *In Vivo* by D-Peptides-Functionalized Ultra-small Nanoparticles: Overcoming Biological Barriers to D-Peptide Drug Delivery. *Theranostics* 8 (19), 5320–5335. doi:10.7150/thno.27165

Cao, S., Lin, C., Li, X., Liang, Y., and Saw, P. E. (2021). TME-Responsive Multistage Nanoplatform for siRNA Delivery and Effective Cancer Therapy. *Int. J. nanomedicine.* 16, 5909–5921. doi:10.2147/ijn.s322901

Cao, S., Saw, P. E., Shen, Q., Li, R., Liu, Y., and Xu, X. (2022). Reduction-responsive RNAi Nanoplatform to Reprogram Tumor Lipid Metabolism and Repolarize Macrophage for Combination Pancreatic Cancer Therapy. *Biomaterials* 280, 121264. doi:10.1016/j.biomaterials.2021.121264

Carracedo, A., Cantley, L. C., and Pandolfi, P. P. (2013). Cancer Metabolism: Fatty Acid Oxidation in the Limelight. *Nat. Rev. Cancer* 13 (4), 227–232. doi:10.1038/nrc3483

Cassidy, J. J., Bernasek, S. M., Bakker, R., Giri, R., Peláez, N., Eder, B., et al. (2019). Repressive Gene Regulation Synchronizes Development with Cellular Metabolism. *Cell* 178 (4), 980–992. e17. doi:10.1016/j.cell.2019.06.023

Certo, M., Tsai, C.-H., Pucino, V., Ho, P.-C., and Mauro, C. (2021). Lactate Modulation of Immune Responses in Inflammatory versus Tumour Microenvironments. *Nat. Rev. Immunol.* 21 (3), 151–161. doi:10.1038/s41577-020-0406-2

Chang, C.-H., Qiu, J., O'Sullivan, D., Buck, M. D., Noguchi, T., Curtis, J. D., et al. (2015). Metabolic Competition in the Tumor Microenvironment Is a Driver of Cancer Progression. *Cell* 162 (6), 1229–1241. doi:10.1016/j.cell.2015.08.016

Chaput, N., Lepage, P., Coutzac, C., Soularue, E., Le Roux, K., Monot, C., et al. (2017). Baseline Gut Microbiota Predicts Clinical Response and Colitis in Metastatic Melanoma Patients Treated with Ipilimumab. *Ann. Oncol.* 28 (6), 1368–1379. doi:10.1093/annonc/mdx108

Chen, E., Chen, B.-M., Su, Y.-C., Chang, Y.-C., Cheng, T.-L., Barenholz, Y., et al. (2020). Premature Drug Release from Polyethylene Glycol (PEG)-Coated Liposomal Doxorubicin via Formation of the Membrane Attack Complex. *ACS Nano* 14 (7), 7808–7822. doi:10.1021/acsnano.9b07218

Chen, G., Xu, Q., Feng, Z., Xu, Q., Zhang, X., Yang, Y., et al. (2022). Glutamine Antagonist Synergizes with Electrodynamic Therapy to Induce Tumor Regression and Systemic Antitumor Immunity. *ACS Nano* 16, 951–962. doi:10.1021/acsnano.1c08544

Chen, K., Zhang, C., Ling, S., Wei, R., Wang, J., and Xu, X. (2021). The Metabolic Flexibility of Quiescent CSC: Implications for Chemotherapy Resistance. *Cell Death Dis.* 12 (9), 835. doi:10.1038/s41419-021-04116-6

Chen, P., Zuo, H., Xiong, H., Kolar, M. J., Chu, Q., Saghatelian, A., et al. (2017). Gpr132 Sensing of Lactate Mediates Tumor-Macrophage Interplay to Promote Breast Cancer Metastasis. *Proc. Natl. Acad. Sci. U.S.A.* 114 (3), 580–585. doi:10.1073/pnas.1614035114

Chen, Q., Liu, X., Chen, J., Zeng, J., Cheng, Z., and Liu, Z. (2015). A Self-Assembled Albumin-Based Nanoprobe for *In Vivo* Ratiometric Photoacoustic pH Imaging. *Adv. Mat.* 27 (43), 6820–6827. doi:10.1002/adma.201503194

Chen, Q., Wang, C., Zhang, X., Chen, G., Hu, Q., Li, H., et al. (2019). *In Situ* sprayed Bioresponsive Immunotherapeutic Gel for Post-surgical Cancer Treatment. *Nat. Nanotech* 14 (1), 89–97. doi:10.1038/s41565-018-0319-4

Chen, W.-H., Luo, G.-F., Lei, Q., Hong, S., Qiu, W.-X., Liu, L.-H., et al. (2017). Overcoming the Heat Endurance of Tumor Cells by Interfering with the Anaerobic Glycolysis Metabolism for Improved Photothermal Therapy. *ACS Nano* 11 (2), 1419–1431. doi:10.1021/acsnano.6b06658

Courtney, K. D., Bezwada, D., Mashimo, T., Pichumani, K., Vemireddy, V., Funk, A. M., et al. (2018). Isotope Tracing of Human Clear Cell Renal Cell Carcinomas Demonstrates Suppressed Glucose Oxidation *In Vivo*. *Cell metab.* 28 (5), 793–800. doi:10.1016/j.cmet.2018.07.020

Cui, L., Gouw, A. M., LaGory, E. L., Guo, S., Attarwala, N., Tang, Y., et al. (2021). Mitochondrial Copper Depletion Suppresses Triple-Negative Breast Cancer in Mice. *Nat. Biotechnol.* 39 (3), 357–367. doi:10.1038/s41587-020-0707-9

DeBerardinis, R. J., and Chandel, N. S. (2016). Fundamentals of Cancer Metabolism. *Sci. Adv.* 2 (5), e1600200. doi:10.1126/sciadv.1600200

DePeaux, K., and Delgoffe, G. M. (2021). Metabolic Barriers to Cancer Immunotherapy. *Nat. Rev. Immunol.* 21 (12), 785–797. doi:10.1038/s41577-021-00541-y

Derosa, L., Hellmann, M. D., Spaziano, M., Halpenny, D., Fidelle, M., Rizvi, H., et al. (2018). Negative Association of Antibiotics on Clinical Activity of Immune Checkpoint Inhibitors in Patients with Advanced Renal Cell and Non-small-cell Lung Cancer. *Ann. Oncol.* 29 (6), 1437–1444. doi:10.1093/annonc/mdy103

Ding, X.-L., Liu, M.-D., Cheng, Q., Guo, W.-H., Niu, M.-T., Huang, Q.-X., et al. (2022). Multifunctional Liquid Metal-Based Nanoparticles with Glycolysis and Mitochondrial Metabolism Inhibition for Tumor Photothermal Therapy. *Biomaterials* 281, 121369. doi:10.1016/j.biomaterials.2022.121369

DiTullio, D., and Dell'Angelica, E. C. (2019). *Glucose Metabolism. Fundamentals of Biochemistry: Medical Course & Step 1 Review*. New York, NY: McGraw-Hill Education.

Dong, F., Jiang, Q., Li, L., Liu, T., Zuo, S., Gao, L., et al. (2022). Synergetic Lethal Energy Depletion Initiated by Cancer Cell Membrane Camouflaged Nano-Inhibitor for Cancer Therapy. *Nano Res.* 15, 3422–3433. doi:10.1007/s12274-021-3948-0

Dong, L.-F., Jameson, V. J. A., Tilly, D., Cerny, J., Mahdavian, E., Marín-Hernández, A., et al. (2011). Mitochondrial Targeting of Vitamin E Succinate Enhances its Pro-apoptotic and Anti-cancer Activity via Mitochondrial Complex II. *J. Biol. Chem.* 286 (5), 3717–3728. doi:10.1074/jbc.m110.186643

Dong, S., Dong, Y., Jia, T., Liu, S., Liu, J., Yang, D., et al. (2020). GSH-Depleted Nanozymes with Hyperthermia-Enhanced Dual Enzyme-Mimic Activities for Tumor Nanocatalytic Therapy. *Adv. Mater* 32 (42), e2002439. doi:10.1002/adma.202002439

Ducker, G. S., and Rabinowitz, J. D. (2017). One-Carbon Metabolism in Health and Disease. *Cell metab.* 25 (1), 27–42. doi:10.1016/j.cmet.2016.08.009

Elia, I., and Haigis, M. C. (2021). Metabolites and the Tumour Microenvironment: from Cellular Mechanisms to Systemic Metabolism. *Nat. Metab.* 3 (1), 21–32. doi:10.1038/s42255-020-00317-z

Eniafe, J., and Jiang, S. (2021). The Functional Roles of TCA Cycle Metabolites in Cancer. *Oncogene* 40 (19), 3351–3363. doi:10.1038/s41388-020-01639-8

Fan, W., Lu, N., Huang, P., Liu, Y., Yang, Z., Wang, S., et al. (2017). Glucose-Responsive Sequential Generation of Hydrogen Peroxide and Nitric Oxide for Synergistic Cancer Starving-Like/Gas Therapy. *Angew. Chem. Int. Ed.* 56 (5), 1229–1233. doi:10.1002/anie.201610682

Feng, L., Yang, L., Li, L., Xiao, J., Bie, N., Xu, C., et al. (2022). Programmed Albumin Nanoparticles Regulate Immunosuppressive Pivot to Potentiate Checkpoint Blockade Cancer Immunotherapy. *Nano Res.* 15 (1), 593–602. doi:10.1007/s12274-021-3525-6

Fischer, K., Hoffmann, P., Voelkl, S., Meidenbauer, N., Ammer, J., Edinger, M., et al. (2007). Inhibitory Effect of Tumor Cell-Derived Lactic Acid on Human T Cells. *Blood* 109 (9), 3812–3819. doi:10.1182/blood-2006-07-035972

Forman, H. J., Zhang, H., and Rinna, A. (2009). Glutathione: Overview of its Protective Roles, Measurement, and Biosynthesis. *Mol. Asp. Med.* 30 (1-2), 1–12. doi:10.1016/j.mam.2008.08.006

Fukumura, D., Kloepper, J., Amoozgar, Z., Duda, D. G., and Jain, R. K. (2018). Enhancing Cancer Immunotherapy Using Antiangiogenics: Opportunities and Challenges. *Nat. Rev. Clin. Oncol.* 15 (5), 325–340. doi:10.1038/nrclinonc.2018.29

Gabrilovich, D. I. (2017). Myeloid-Derived Suppressor Cells. *Cancer Immunol. Res.* 5 (1), 3–8. doi:10.1158/2326-6066.cir-16-0297

Gao, F., Tang, Y., Liu, W. L., Zou, M. Z., Huang, C., Liu, C. J., et al. (2019). Intra/Extracellular Lactic Acid Exhaustion for Synergistic Metabolic Therapy and Immunotherapy of Tumors. *Adv. Mater* 31 (51), e1904639. doi:10.1002/adma.201904639

Gao, M., Deng, J., Liu, F., Fan, A., Wang, Y., Wu, H., et al. (2019). Triggered Ferroptotic Polymer Micelles for Reversing Multidrug Resistance to Chemotherapy. *Biomaterials* 223, 119486. doi:10.1016/j.biomaterials.2019.119486

Gong, J., Lin, Y., Zhang, H., Liu, C., Cheng, Z., Yang, X., et al. (2020). Reprogramming of Lipid Metabolism in Cancer-Associated Fibroblasts Potentiates Migration of Colorectal Cancer Cells. *Cell Death Dis.* 11 (4), 267. doi:10.1038/s41419-020-2434-z

Gottschalk, S., Anderson, N., Hainz, C., Eckhardt, S. G., and Serkova, N. J. (2004). Imatinib (STI571)-Mediated Changes in Glucose Metabolism in Human Leukemia BCR-ABL-Positive Cells. *Clin. Cancer Res.* 10 (19), 6661–6668. doi:10.1158/1078-0432.ccr-04-0039

Guo, C., Chen, S., Liu, W., Ma, Y., Li, J., Fisher, P. B., et al. (2019). Immunometabolism: A New Target for Improving Cancer Immunotherapy. *Adv. cancer Res.* 143, 195–253. doi:10.1016/bs.acr.2019.03.004

Hao, M., Hou, S., Li, W., Li, K., Xue, L., Hu, Q., et al. (2020). Combination of Metabolic Intervention and T Cell Therapy Enhances Solid Tumor Immunotherapy. *Sci. Transl. Med.* 12 (571), eaaz6667. doi:10.1126/scitranslmed.aaz6667

Hassani Najafabadi, A., Zhang, J., Aikins, M. E., Najaf Abadi, Z. I., Liao, F., Qin, Y., et al. (2020). Cancer Immunotherapy via Targeting Cancer Stem Cells Using Vaccine Nanodiscs. *Nano Lett.* 20 (10), 7783–7792. doi:10.1021/acs.nanolett.0c03414

He, W., Wang, S., Yan, J., Qu, Y., Jin, L., Sui, F., et al. (2019). Self-Assembly of Therapeutic Peptide into Stimuli-Responsive Clustered Nanohybrids for Cancer-Targeted Therapy. *Adv. Funct. Mater* 29 (10), 1807736. doi:10.1002/adfm.201807736

He, W., Yan, J., Jiang, W., Li, S., Qu, Y., Niu, F., et al. (2018). Peptide-Induced Self-Assembly of Therapeutics into a Well-Defined Nanoshell with Tumor-Triggered Shape and Charge Switch. *Chem. Mat.* 30 (20), 7034–7046. a publication of the American Chemical Society. doi:10.1021/acs.chemmater.8b02572

He, W., Yan, J., Li, Y., Yan, S., Wang, S., Hou, P., et al. (2020). Resurrecting a P53 Peptide Activator - An Enabling Nanoengineering Strategy for Peptide Therapeutics. *J. Control. Release* 325, 293–303. doi:10.1016/j.jconrel.2020.06.041

He, W., Yan, J., Sui, F., Wang, S., Su, X., Qu, Y., et al. (2018). Turning a Luffa Protein into a Self-Assembled Biodegradable Nanoplatform for Multitargeted Cancer Therapy. *ACS Nano* 12 (11), 11664–11677. doi:10.1021/acsnano.8b07079

He, W., Zhang, Z., Yang, W., Zheng, X., You, W., Yao, Y., et al. (2022). Turing Milk into Pro-apoptotic Oral Nanotherapeutic: De Novo Bionic Chiral-Peptide Supramolecule for Cancer Targeted and Immunological Therapy. *Theranostics* 12 (5), 2322–2334. doi:10.7150/thno.70568

Hinshaw, D. C., and Shevde, L. A. (2019). The Tumor Microenvironment Innately Modulates Cancer Progression. *Cancer Res.* 79 (18), 4557–4566. doi:10.1158/0008-5472.can-18-3962

Huang, H., Jiang, C.-T., Shen, S., Liu, A., Gan, Y.-J., Tong, Q.-S., et al. (2019). Nanoenabled Reversal of Ido1-Mediated Immunosuppression Synergizes with Immunogenic Chemotherapy for Improved Cancer Therapy. *Nano Lett.* 19 (8), 5356–5365. doi:10.1021/acs.nanolett.9b01807

Irvine, D. J., and Dane, E. L. (2020). Enhancing Cancer Immunotherapy with Nanomedicine. *Nat. Rev. Immunol.* 20 (5), 321–334. doi:10.1038/s41577-019-0269-6

Jiang, M., Qiao, M., Zhao, C., Deng, J., Li, X., and Zhou, C. (2020). Targeting Ferroptosis for Cancer Therapy: Exploring Novel Strategies from its Mechanisms and Role in Cancers. *Transl. Lung Cancer Res.* 9 (4), 1569–1584. doi:10.21037/tlcr-20-341

Jiang, W., Wang, L., Wang, Q., Zhou, H., Ma, Y., Dong, W., et al. (2021). Reversing Immunosuppression in Hypoxic and Immune-Cold Tumors with Ultrathin Oxygen Self-Supplementing Polymer Nanosheets under Near Infrared Light Irradiation. *Adv. Funct. Mat.* 31 (20), 2100354. doi:10.1002/adfm.202100354

Jin, L., Li, D., Alesi, G. N., Fan, J., Kang, H.-B., Lu, Z., et al. (2015). Glutamate Dehydrogenase 1 Signals through Antioxidant Glutathione Peroxidase 1 to Regulate Redox Homeostasis and Tumor Growth. *Cancer Cell* 27 (2), 257–270. doi:10.1016/j.ccell.2014.12.006

Junttila, M. R., and de Sauvage, F. J. (2013). Influence of Tumour Microenvironment Heterogeneity on Therapeutic Response. *Nature* 501 (7467), 346–354. doi:10.1038/nature12626

Kim, B. Y. S., Rutka, J. T., and Chan, W. C. W. (2010). Nanomedicine. *N. Engl. J. Med.* 363 (25), 2434–2443. doi:10.1056/nejmra0912273

Kim, D., Wu, Y., Li, Q., and Oh, Y.-K. (2021). Nanoparticle-Mediated Lipid Metabolic Reprogramming of T Cells in Tumor Microenvironments for Immunometabolic Therapy. *Nano-Micro Lett.* 13 (1), 31. doi:10.1007/s40820-020-00555-6

Kim, M. G., Shon, Y., Kim, J., and Oh, Y. K. (2017). Selective Activation of Anticancer Chemotherapy by Cancer-Associated Fibroblasts in the Tumor Microenvironment. *J. Natl. Cancer Inst.* 109 (1), djw186. doi:10.1093/jnci/djw186

Klein Geltink, R. I., Kyle, R. L., and Pearce, E. L. (2018). Unraveling the Complex Interplay Between T Cell Metabolism and Function. *Annu. Rev. Immunol.* 36, 461–488. doi:10.1146/annurev-immunol-042617-053019

Koppenol, W. H., Bounds, P. L., and Dang, C. V. (2011). Otto Warburg's Contributions to Current Concepts of Cancer Metabolism. *Nat. Rev. Cancer* 11 (5), 325–337. doi:10.1038/nrc3038

Kouidhi, S., Elgaaied, A. B., and Chouaib, S. (2017). Impact of Metabolism in on T-Cell Differentiation and Function and Cross Talk with Tumor Microenvironment. *Front. Immunol.* 8, 270. doi:10.3389/fimmu.2017.00270

Kumagai, S., Koyama, S., Itahashi, K., Tanegashima, T., Lin, Y.-t., Togashi, Y., et al. (2022). Lactic Acid Promotes PD-1 Expression in Regulatory T Cells in Highly Glycolytic Tumor Microenvironments. *Cancer Cell* 40 (2), 201–218. e9. doi:10.1016/j.ccell.2022.01.001

Kuntz, E. M., Baquero, P., Michie, A. M., Dunn, K., Tardito, S., Holyoake, T. L., et al. (2017). Targeting Mitochondrial Oxidative Phosphorylation Eradicates Therapy-Resistant Chronic Myeloid Leukemia Stem Cells. *Nat. Med.* 23 (10), 1234–1240. doi:10.1038/nm.4399

Lemberg, K. M., Vornov, J. J., Rais, R., and Slusher, B. S. (2018). We're Not "DON" Yet: Optimal Dosing and Prodrug Delivery of 6-Diazo-5-Oxo-L-Norleucine. *Mol. Cancer Ther.* 17 (9), 1824–1832. doi:10.1158/1535-7163.mct-17-1148

Leone, R. D., and Powell, J. D. (2020). Metabolism of Immune Cells in Cancer. *Nat. Rev. Cancer* 20 (9), 516–531. doi:10.1038/s41568-020-0273-y

Leone, R. D., Zhao, L., Englert, J. M., Sun, I.-M., Oh, M.-H., Sun, I.-H., et al. (2019). Glutamine Blockade Induces Divergent Metabolic Programs to Overcome Tumor Immune Evasion. *Science* 366 (6468), 1013–1021. doi:10.1126/science.aav2588

Li, F., and Simon, M. C. (2020). Cancer Cells Don't Live Alone: Metabolic Communication within Tumor Microenvironments. *Dev. Cell* 54 (2), 183–195. doi:10.1016/j.devcel.2020.06.018

Li, L., He, W., You, W., Yan, J., and Liu, W. (2022). Turing miRNA into Infinite Coordination Supermolecule: a General and Enabling Nanoengineering Strategy for Resurrecting Nuclear Acid Therapeutics. *J. Nanobiotechnol* 20 (1), 10. doi:10.1186/s12951-021-01212-9

Li, S., Xu, S., Liang, X., Xue, Y., Mei, J., Ma, Y., et al. (2021). Nanotechnology: Breaking the Current Treatment Limits of Lung Cancer. *Adv. Healthc. Mater.* 10 (12), e2100078. doi:10.1002/adhm.202100078

Li, S., Wang, Q., Shen, Y., Hassan, M., Shen, J., Jiang, W., et al. (2020). Pseudoneutrophil Cytokine Sponges Disrupt Myeloid Expansion and Tumor Trafficking to Improve Cancer Immunotherapy. *Nano Lett.* 20 (1), 242–251. doi:10.1021/acs.nanolett.9b03753

Li, X., Gohain, N., Chen, S., Li, Y., Zhao, X., Li, B., et al. (2021). Design of Ultrahigh-Affinity and Dual-Specificity Peptide Antagonists of MDM2 and MDMX for P53 Activation and Tumor Suppression. *Acta Pharm. Sin. B* 11 (9), 2655–2669. doi:10.1016/j.apsb.2021.06.010

Li, X. Y., Deng, F. A., Zheng, R. R., Liu, L. S., Liu, Y. B., Kong, R. J., et al. (2021). Carrier Free Photodynamic Synergists for Oxidative Damage Amplified Tumor Therapy. *Small (Weinheim der Bergstrasse, Ger.* 17 (40), e2102470. doi:10.1002/smll.202102470

Li, X., Yao, W., Yuan, Y., Chen, P., Li, B., Li, J., et al. (2017). Targeting of Tumour-Infiltrating Macrophages via CCL2/CCR2 Signalling as a Therapeutic Strategy against Hepatocellular Carcinoma. *Gut* 66 (1), 157–167. doi:10.1136/gutjnl-2015-310514

Li, Y., Lin, J., Wang, P., Luo, Q., Zhu, F., Zhang, Y., et al. (2020). Tumor Microenvironment Cascade-Responsive Nanodrug with Self-Targeting Activation and ROS Regeneration for Synergistic Oxidation-Chemotherapy. *Nano-Micro Lett.* 12 (1), 182. doi:10.1007/s40820-020-00492-4

Li, Z., Sun, C., and Qin, Z. (2021). Metabolic Reprogramming of Cancer-Associated Fibroblasts and its Effect on Cancer Cell Reprogramming. *Theranostics* 11 (17), 8322–8336. doi:10.7150/thno.62378

Liang, L., Peng, Y., and Qiu, L. (2021). Mitochondria-targeted Vitamin E Succinate Delivery for Reversal of Multidrug Resistance. *J. Control. Release* 337, 117–131. doi:10.1016/j.jconrel.2021.07.023

Lien, E. C., and Vander Heiden, M. G. (2019). A Framework for Examining How Diet Impacts Tumour Metabolism. *Nat. Rev. Cancer* 19 (11), 651–661. doi:10.1038/s41568-019-0198-5

Lim, S., Park, J., Shim, M. K., Um, W., Yoon, H. Y., Ryu, J. H., et al. (2019). Recent Advances and Challenges of Repurposing Nanoparticle-Based Drug Delivery Systems to Enhance Cancer Immunotherapy. *Theranostics* 9 (25), 7906–7923. doi:10.7150/thno.38425

Lin, L.-S., Song, J., Song, L., Ke, K., Liu, Y., Zhou, Z., et al. (2018). Simultaneous Fenton-like Ion Delivery and Glutathione Depletion by MnO_2 -Based Nanoagent to Enhance Chemodynamic Therapy. *Angew. Chem. Int. Ed.* 57 (18), 4902–4906. doi:10.1002/anie.201712027

Lin, X., Li, L., Li, S., Li, Q., Xie, D., Zhou, M., et al. (2021). Targeting the Opening of Mitochondrial Permeability Transition Pores Potentiates Nanoparticle Drug Delivery and Mitigates Cancer Metastasis. *Adv. Sci.* 8 (4), 2002834. doi:10.1002/advs.202002834

Liu, J., Yan, J., Yan, S., Wang, Y., Zhang, R., Hou, P., et al. (2019). Biomimetic and Self-Assembled Nanoclusters Targeting β-Catenin for Potent Anticancer Therapy and Enhanced Immunotherapy. *Nano Lett.* 19 (12), 8708–8715. doi:10.1021/acs.nanolett.9b03414

Liu, T., Yan, J., He, C., You, W., Ma, F., Chang, Z., et al. (2022). A Tumor-Targeting Metal-Organic Nanoparticle Constructed by Dynamic Combinatorial Chemistry toward Accurately Redressing Carcinogenic Wnt Cascade. *Small (Weinheim der Bergstrasse, Ger.* 18 (3), e2104849. doi:10.1002/smll.202104849

Liu, X., Li, Y., Wang, K., Chen, Y., Shi, M., Zhang, X., et al. (2021). GSH-Responsive Nanoprodrug to Inhibit Glycolysis and Alleviate Immunosuppression for Cancer Therapy. *Nano Lett.* 21 (18), 7862–7869. doi:10.1021/acs.nanolett.1c03089

Lukey, M. J., Katt, W. P., and Cerione, R. A. (2017). Targeting Amino Acid Metabolism for Cancer Therapy. *Drug Discov. today* 22 (5), 796–804. doi:10.1016/j.drudis.2016.12.003

Lyssiotis, C. A., and Kimmelman, A. C. (2017). Metabolic Interactions in the Tumor Microenvironment. *Trends Cell Biol.* 27 (11), 863–875. doi:10.1016/j.tcb.2017.06.003

Ma, B., Niu, F., Qu, X., He, W., Feng, C., Wang, S., et al. (2019). A Tetrameric Protein Scaffold as a Nano-Carrier of Antitumor Peptides for Cancer Therapy. *Biomaterials* 204, 1–12. doi:10.1016/j.biomaterials.2019.03.004

Ma, F., Liu, T., Yang, W., You, W., He, W., Yan, J., et al. (2022). Turning Fluvastatin into a Supramolecular Immuno-Sensitizer towards Augmented Tumor Immunotherapy. *Chem. Eng. J.* 437, 135310. doi:10.1016/j.cej.2022.135310

Ma, Y., Temkin, S. M., Hawkridge, A. M., Guo, C., Wang, W., Wang, X.-Y., et al. (2018). Fatty Acid Oxidation: An Emerging Facet of Metabolic Transformation in Cancer. *Cancer Lett.* 435, 92–100. doi:10.1016/j.canlet.2018.08.006

MacIver, N. J., Michalek, R. D., and Rathmell, J. C. (2013). Metabolic Regulation of T Lymphocytes. *Annu. Rev. Immunol.* 31, 259–283. doi:10.1146/annurev-immunol-032712-095956

Maeda, H., Wu, J., Sawa, T., Matsumura, Y., and Hori, K. (2000). Tumor Vascular Permeability and the EPR Effect in Macromolecular Therapeutics: a Review. *J. Control Release* 65 (1-2), 271–284. doi:10.1016/s0168-3659(99)00248-5

Martinez-Outschoorn, U. E., Lin, Z., Trimmer, C., Flomenberg, N., Wang, C., Pavlides, S., et al. (2011). Cancer Cells Metabolically "fertilize" the Tumor Microenvironment with Hydrogen Peroxide, Driving the Warburg Effect: Implications for PET Imaging of Human Tumors. *Cell Cycle* 10 (15), 2504–2520. doi:10.4161/cc.10.15.16585

Martínez-Reyes, I., and Chandel, N. S. (2021). Cancer Metabolism: Looking Forward. *Nat. Rev. Cancer* 21 (10), 669–680. doi:10.1038/s41568-021-00378-6

Masisi, B. K., El Ansari, R., Alfarsi, L., Rakha, E. A., Green, A. R., and Craze, M. L. (2020). The Role of Glutaminase in Cancer. *Histopathology* 76 (4), 498–508. doi:10.1111/his.14014

Matés, J. M., Campos-Sandoval, J. A., Santos-Jiménez, J. L., and Márquez, J. (2019). Dysregulation of Glutaminase and Glutamine Synthetase in Cancer. *Cancer Lett.* 467, 29–39. doi:10.1016/j.canlet.2019.09.011

Matson, V., Fessler, J., Bao, R., Chongsuwat, T., Zha, Y., Alegre, M.-L., et al. (2018). The Commensal Microbiome Is Associated with Anti-PD-1 Efficacy in Metastatic Melanoma Patients. *Science* 359 (6371), 104–108. doi:10.1126/science.aao3290

Niu, F., Yan, J., Ma, B., Li, S., Shao, Y., He, P., et al. (2018). Lanthanide-doped Nanoparticles Conjugated with an Anti-CD33 Antibody and a P53-Activating Peptide for Acute Myeloid Leukemia Therapy. *Biomaterials* 167, 132–142. doi:10.1016/j.biomaterials.2018.03.025

O'Neill, L. A. J., and Artyomov, M. N. (2019). Itaconate: the Poster Child of Metabolic Reprogramming in Macrophage Function. *Nat. Rev. Immunol.* 19 (5), 273–281. doi:10.1038/s41577-019-0128-5

Oh, D. Y., Fong, L., Newell, E. W., Turk, M. J., Chi, H., Chang, H. Y., et al. (2021). Toward a Better Understanding of T Cells in Cancer. *Cancer Cell* 39 (12), 1549–1552. doi:10.1016/j.ccell.2021.11.010

Ojha, T., Pathak, V., Shi, Y., Hennink, W. E., Moonen, C. T. W., Storm, G., et al. (2017). Pharmacological and Physical Vessel Modulation Strategies to Improve EPR-Mediated Drug Targeting to Tumors. *Adv. drug Deliv. Rev.* 119, 44–60. doi:10.1016/j.addr.2017.07.007

Ou, W., Thapa, R. K., Jiang, L., Soe, Z. C., Gautam, M., Chang, J.-H., et al. (2018). Regulatory T Cell-Targeted Hybrid Nanoparticles Combined with Immuno-Checkpoint Blockage for Cancer Immunotherapy. *J. Control. Release* 281, 84–96. doi:10.1016/j.jconrel.2018.05.018

Pacella, I., and Piconese, S. (2019). Immunometabolic Checkpoints of Treg Dynamics: Adaptation to Microenvironmental Opportunities and Challenges. *Front. Immunol.* 10, 1889. doi:10.3389/fimmu.2019.01889

Parida, P. K., Marquez-Palencia, M., Nair, V., Kaushik, A. K., Kim, K., Sudderth, J., et al. (2022). Metabolic Diversity within Breast Cancer Brain-Tropic Cells Determines Metastatic Fitness. *Cell metab.* 34 (1), 90–105. e7. doi:10.1016/j.cmet.2021.12.001

Patra, K. C., and Hay, N. (2014). The Pentose Phosphate Pathway and Cancer. *Trends Biochem. Sci.* 39 (8), 347–354. doi:10.1016/j.tibs.2014.06.005

Peer, D., Karp, J. M., Hong, S., Farokhzad, O. C., Margalit, R., and Langer, R. (2007). Nanocarriers as an Emerging Platform for Cancer Therapy. *Nat. Nanotech* 2 (12), 751–760. doi:10.1038/nnano.2007.387

Pérez-Tomás, R., and Pérez-Guillén, I. (2020). Lactate in the Tumor Microenvironment: An Essential Molecule in Cancer Progression and Treatment. *Cancers* 12 (11), 3244. doi:10.3390/cancers12113244

Pirozzi, C. J., and Yan, H. (2021). The Implications of IDH Mutations for Cancer Development and Therapy. *Nat. Rev. Clin. Oncol.* 18 (10), 645–661. doi:10.1038/s41571-021-00521-0

Platten, M., Nollen, E. A. A., Röhrig, U. F., Fallarino, F., and Opitz, C. A. (2019). Tryptophan Metabolism as a Common Therapeutic Target in Cancer, Neurodegeneration and beyond. *Nat. Rev. Drug Discov.* 18 (5), 379–401. doi:10.1038/s41573-019-0016-5

Quail, D. F., and Joyce, J. A. (2013). Microenvironmental Regulation of Tumor Progression and Metastasis. *Nat. Med.* 19 (11), 1423–1437. doi:10.1038/nm.3394

Quail, D. F., and Joyce, J. A. (2017). The Microenvironmental Landscape of Brain Tumors. *Cancer Cell* 31 (3), 326–341. doi:10.1016/j.ccell.2017.02.009

Rabold, K., Netea, M. G., Adema, G. J., and Netea-Maier, R. T. (2017). Cellular Metabolism of Tumor-Associated Macrophages - Functional Impact and Consequences. *FEBS Lett.* 591 (19), 3022–3041. doi:10.1002/1873-3468.12771

Ralser, M., Wamelink, M. M., Struys, E. A., Joppich, C., Krobitsch, S., Jakobs, C., et al. (2008). A Catabolic Block Does Not Sufficiently Explain How 2-deoxy- D -glucose Inhibits Cell Growth. *Proc. Natl. Acad. Sci. U.S.A.* 105 (46), 17807–17811. doi:10.1073/pnas.0803090105

Reinfeld, B. I., Madden, M. Z., Wolf, M. M., Chytil, A., Bader, J. E., Patterson, A. R., et al. (2021). Cell-programmed Nutrient Partitioning in the Tumour Microenvironment. *Nature* 593 (7858), 282–288. doi:10.1038/s41586-021-03442-1

Röhrig, F., and Schulze, A. (2016). The Multifaceted Roles of Fatty Acid Synthesis in Cancer. *Nat. Rev. Cancer* 16 (11), 732–749. doi:10.1038/nrc.2016.89

Routy, B., Le Chatelier, E., Derosa, L., Duong, C. P. M., Alou, M. T., Daillère, R., et al. (2018). Gut Microbiome Influences Efficacy of PD-1-Based Immunotherapy against Epithelial Tumors. *Science* 359 (6371), 91–97. doi:10.1126/science.aan3706

Sasaki, K., Nishina, S., Yamauchi, A., Fukuda, K., Hara, Y., Yamamura, M., et al. (2021). Nanoparticle-Mediated Delivery of 2-Deoxy-D-Glucose Induces Antitumor Immunity and Cytotoxicity in Liver Tumors in Mice. *Cell. Mol. gastroenterology hepatology* 11 (3), 739–762. doi:10.1016/j.jcmgh.2020.10.010

Schug, Z. T., Vande Voorde, J., and Gottlieb, E. (2016). The Metabolic Fate of Acetate in Cancer. *Nat. Rev. Cancer* 16 (11), 708–717. doi:10.1038/nrc.2016.87

Seth Nanda, C., Venkateswaran, S. V., Patani, N., and Yuneva, M. (2020). Defining a Metabolic Landscape of Tumours: Genome Meets Metabolism. *Br. J. Cancer* 122 (2), 136–149. doi:10.1038/s41416-019-0663-7

Shan, X., Li, S., Sun, B., Chen, Q., Sun, J., He, Z., et al. (2020). Ferroptosis-driven Nanotherapeutics for Cancer Treatment. *J. Control. Release* 319, 322–332. doi:10.1016/j.jconrel.2020.01.008

Sharabi, A., and Tsokos, G. C. (2020). T Cell Metabolism: New Insights in Systemic Lupus Erythematosus Pathogenesis and Therapy. *Nat. Rev. Rheumatol.* 16 (2), 100–112. doi:10.1038/s41584-019-0356-x

She, J., Li, Y., Yan, S., Yan, Y., Liu, D., Li, S., et al. (2020). De Novo supraparticle Construction by a Self-Assembled Janus Cyclopeptide to Tame Hydrophilic microRNA and Hydrophobic Molecule for Anti-tumor Cocktail Therapy and Augmented Immunity. *Chem. Eng. J.* 401, 126080. doi:10.1016/j.cej.2020.126080

Shen, J., Rees, T. W., Zhou, Z., Yang, S., Ji, L., and Chao, H. (2020). A Mitochondria-Targeting Magnetothermogenic Nanozyme for Magnet-Induced Synergistic Cancer Therapy. *Biomaterials* 251, 120079. doi:10.1016/j.biomaterials.2020.120079

Shi, C., Zhou, X., Zhao, Q., Zhang, Z., Ma, H., Lu, Y., et al. (2021). CD44-Specific Targeting Nanoreactors with Glutathione Depletion for Magnifying Photodynamic Tumor Eradication. *CCS Chem.* doi:10.31635/ccschem.021.202101222

Sola-Penna, M., Paixão, L. P., Branco, J. R., Ochioni, A. C., Albanese, J. M., Mundim, D. M., et al. (2020). Serotonin Activates Glycolysis and Mitochondria Biogenesis in Human Breast Cancer Cells through Activation of the Jak1/STAT3/ERK1/2 and Adenylate cyclase/PKA, Respectively. *Br. J. Cancer* 122 (2), 194–208. doi:10.1038/s41416-019-0640-1

Stine, Z. E., Schug, Z. T., Salvino, J. M., and Dang, C. V. (2021). Targeting Cancer Metabolism in the Era of Precision Oncology. *Nat. Rev. Drug Discov.* 21, 141–162. doi:10.1038/s41573-021-00339-6

Stine, Z. E., Schug, Z. T., Salvino, J. M., and Dang, C. V. (2022). Targeting Cancer Metabolism in the Era of Precision Oncology. *Nat. Rev. Drug Discov.* 21 (2), 141–162. doi:10.1038/s41573-021-00339-6

Su, W., Chapman, N. M., Wei, J., Zeng, H., Dhungana, Y., Shi, H., et al. (2020). Protein Prenylation Drives Discrete Signaling Programs for the Differentiation and Maintenance of Effector T_{reg} Cells. *Cell metab.* 32 (6), 996–1011. doi:10.1016/j.cmet.2020.10.022

Tian, F., Wang, S., Shi, K., Zhong, X., Gu, Y., Fan, Y., et al. (2021). Dual-Depletion of Intratumoral Lactate and ATP with Radicals Generation for Cascade Metabolic-Chemodynamic Therapy. *Adv. Sci. (Weinheim, Baden-Wurttemberg, Ger.* 8 (24), e2102595. doi:10.1002/advs.202102595

Trinh, A., and Polyak, K. (2019). Tumor Neoantigens: When Too Much of a Good Thing Is Bad. *Cancer Cell* 36 (5), 466–467. doi:10.1016/j.ccell.2019.10.009

Turbitt, W. J., Collins, S. D., Meng, H., and Rogers, C. J. (2019). Increased Adiposity Enhances the Accumulation of MDSCs in the Tumor Microenvironment and Adipose Tissue of Pancreatic Tumor-Bearing Mice and in Immune Organs of Tumor-Free Hosts. *Nutrients* 11 (12), 3012. doi:10.3390/nu11123012

van Leent, M. M. T., Beldman, T. J., Toner, Y. C., Lameijer, M. A., Rother, N., Bekkering, S., et al. (2021). Prosaposin Mediates Inflammation in Atherosclerosis. *Sci. Transl. Med.* 13 (584), eabe1433. doi:10.1126/scitranslmed.abe1433

Vander Heiden, M. G., Cantley, L. C., and Thompson, C. B. (2009). Understanding the Warburg Effect: the Metabolic Requirements of Cell Proliferation. *Science* 324 (5930), 1029–1033. doi:10.1126/science.1160809

Veglia, F., Sanseviero, E., and Gabrilovich, D. I. (2021). Myeloid-derived Suppressor Cells in the Era of Increasing Myeloid Cell Diversity. *Nat. Rev. Immunol.* 21 (8), 485–498. doi:10.1038/s41577-020-00490-y

Vettore, L., Westbrook, R. L., and Tennant, D. A. (2020). New Aspects of Amino Acid Metabolism in Cancer. *Br. J. Cancer* 122 (2), 150–156. doi:10.1038/s41416-019-0620-5

Vitale, I., Manic, G., Coussens, L. M., Kroemer, G., and Galluzzi, L. (2019). Macrophages and Metabolism in the Tumor Microenvironment. *Cell metab.* 30 (1), 36–50. doi:10.1016/j.cmet.2019.06.001

Wang, C., Dong, Z., Hao, Y., Zhu, Y., Ni, J., Li, Q., et al. (2022). Coordination Polymer-Coated CaCO(3) Reinforces Radiotherapy by Reprogramming the Immunosuppressive Metabolic Microenvironment. *Adv. Mater. Deerf. Beach, Fla)* 34 (3), e2106520. doi:10.1002/adma.202106520

Wang, C., Wu, J., Wang, Z., Yang, Z., Li, Z., Deng, H., et al. (2018). Glutamine Addiction Activates Polyglutamine-Based Nanocarriers Delivering Therapeutic siRNAs to Orthotopic Lung Tumor Mediated by Glutamine Transporter SLC1A5. *Biomaterials* 183, 77–92. doi:10.1016/j.biomaterials.2018.08.035

Wang, D., Xue, B., Ohulchanskyy, T. Y., Liu, Y., Yakovliev, A., Ziniuk, R., et al. (2020). Inhibiting Tumor Oxygen Metabolism and Simultaneously Generating Oxygen by Intelligent Upconversion Nanotherapeutics for Enhanced Photodynamic Therapy. *Biomaterials* 251, 120088. doi:10.1016/j.biomaterials.2020.120088

Wang, H., Zhou, Y., Xu, H., Wang, X., Zhang, Y., Shang, R., et al. (2022). *Therapeutic Efficacy of FASN Inhibition in Preclinical Models of HCC*. Baltimore, Md: Hepatology.

Wang, P., Liu, S., Hu, M., Zhang, H., Duan, D., He, J., et al. (2020). Peroxidase-Like Nanozymes Induce a Novel Form of Cell Death and Inhibit Tumor Growth *In Vivo*. *Adv. Funct. Mat.* 30 (21), 2000647. doi:10.1002/adfm.202000647

Wang, Y., Du, C., Zhao, Y., Nie, G., and Yang, Y. (2020). Trap and Kill Strategy for Non-BRCA Mutant Pancreatic Cancer by Co-delivery of Olaparib and JQ1 with Plectin-1 Targeting Peptide Nanoparticles. *Nano Today* 33, 100877. doi:10.1016/j.nantod.2020.100877

Wang, Z., Yip, L. Y., Lee, J. H. J., Wu, Z., Chew, H. Y., Chong, P. K. W., et al. (2019). Methionine Is a Metabolic Dependency of Tumor-Initiating Cells. *Nat. Med.* 25 (5), 825–837. doi:10.1038/s41591-019-0423-5

Warburg, O. (1925). The Metabolism of Carcinoma Cells. *Am. Assoc. Cancer Res.* 9, 148. doi:10.1158/jcr.1925.148

Watson, M. J., Vignali, P. D. A., Mullett, S. J., Overacre-Delgoffe, A. E., Peralta, R. M., Grebinoski, S., et al. (2021). Metabolic Support of Tumour-Infiltrating Regulatory T Cells by Lactic Acid. *Nature* 591 (7851), 645–651. doi:10.1038/s41586-020-03045-2

Webb, B. A., Chimenti, M., Jacobson, M. P., and Barber, D. L. (2011). Dysregulated pH: a Perfect Storm for Cancer Progression. *Nat. Rev. Cancer* 11 (9), 671–677. doi:10.1038/nrc3110

Wei, J., Zheng, W., Chapman, N. M., Geiger, T. L., and Chi, H. (2021). T Cell Metabolism in Homeostasis and Cancer Immunity. *Curr. Opin. Biotechnol.* 68, 240–250. doi:10.1016/j.copbio.2021.02.003

Wei, Z., Liu, X., Cheng, C., Yu, W., and Yi, P. (2020). Metabolism of Amino Acids in Cancer. *Front. Cell Dev. Biol.* 8, 603837. doi:10.3389/fcell.2020.603837

Weinberg, S. E., and Chandel, N. S. (2015). Targeting Mitochondria Metabolism for Cancer Therapy. *Nat. Chem. Biol.* 11 (1), 9–15. doi:10.1038/nchembio.1712

Wicki, A., Witzigmann, D., Balasubramanian, V., and Huwyler, J. (2015). Nanomedicine in Cancer Therapy: Challenges, Opportunities, and Clinical Applications. *J. Control. Release* 200, 138–157. doi:10.1016/j.jconrel.2014.12.030

Wilhelm, S., Tavares, A. J., Dai, Q., Ohta, S., Audet, J., Dvorak, H. F., et al. (2016). Analysis of Nanoparticle Delivery to Tumours. *Nat. Rev. Mater.* 1, 1–12. doi:10.1038/natrevmats.2016.14

Woolaver, R. A., Wang, X., Krinsky, A. L., Waschke, B. C., Chen, S. M. Y., Popolizio, V., et al. (2021). Differences in TCR Repertoire and T Cell Activation Underlie the Divergent Outcomes of Antitumor Immune Responses in Tumor-Eradicating versus Tumor-Progressing Hosts. *J. Immunother. Cancer* 9 (1), e001615. doi:10.1136/jitc-2020-001615

Wu, S., Zhang, K., Liang, Y., Wei, Y., An, J., Wang, Y., et al. (2022). Nano-enabled Tumor Systematic Energy Exhaustion via Zinc (II) Interference Mediated Glycolysis Inhibition and Specific GLUT1 Depletion. *Adv. Sci. (Weinheim, Baden-Wurttemberg, Ger.* 9 (7), e2103534. doi:10.1002/advs.202103534

Xia, D., Xu, P., Luo, X., Zhu, J., Gu, H., Huo, D., et al. (2019). Overcoming Hypoxia by Multistage Nanoparticle Delivery System to Inhibit Mitochondrial Respiration for Photodynamic Therapy. *Adv. Funct. Mat.* 29 (13), 1807294. doi:10.1002/adfm.201807294

Xia, L., Oyang, L., Lin, J., Tan, S., Han, Y., Wu, N., et al. (2021). The Cancer Metabolic Reprogramming and Immune Response. *Mol. Cancer* 20 (1), 28. doi:10.1186/s12943-021-01316-8

Xiao, Z., Dai, Z., and Locasale, J. W. (2019). Metabolic Landscape of the Tumor Microenvironment at Single Cell Resolution. *Nat. Commun.* 10 (1), 3763. doi:10.1038/s41467-019-11738-0

Xiao, Z., Zuo, W., Chen, L., Wu, L., Liu, N., Liu, J., et al. (2021). H2O2 Self-Supplying and GSH-Depleting Nanoplatform for Chemodynamic Therapy Synergetic Photothermal/Chemotherapy. *ACS Appl. Mat. Interfaces* 13 (37), 43925–43936. doi:10.1021/acsami.1c10341

Xing, L., Gong, J.-H., Wang, Y., Zhu, Y., Huang, Z.-J., Zhao, J., et al. (2019). Hypoxia Alleviation-Triggered Enhanced Photodynamic Therapy in Combination with Ido Inhibitor for Preferable Cancer Therapy. *Biomaterials* 206, 170–182. doi:10.1016/j.biomaterials.2019.03.027

Xu, L., Xu, R., Saw, P. E., Wu, J., Cheng, S.-X., and Xu, X. (2021). Nanoparticle-Mediated Inhibition of Mitochondrial Glutaminolysis to Amplify Oxidative Stress for Combination Cancer Therapy. *Nano Lett.* 21 (18), 7569–7578. doi:10.1021/acs.nanolett.1c02073

Yan, J., Zheng, X., You, W., He, W., and Xu, G. K. (2022). A Bionic-Homodimerization Strategy for Optimizing Modulators of Protein-Protein Interactions: From Statistical Mechanics Theory to Potential Clinical Translation. *Adv. Sci. (Weinheim, Baden-Wurttemberg, Ger.* 9 (11), e2105179. doi:10.1002/advs.202105179

Yan, J., He, W., Li, X., You, W., Liu, X., Lin, S., et al. (2021). Carnosic Acid-Induced Co-self-assembly of Metal-Peptide Complexes into a Nanocluster-Based Framework with Tumor-specific Accumulation for Augmented Immunotherapy. *Chem. Eng. J.* 416, 129141. doi:10.1016/j.cej.2021.129141

Yan, J., He, W., Yan, S., Niu, F., Liu, T., Ma, B., et al. (2018). Self-Assembled Peptide-Lanthanide Nanoclusters for Safe Tumor Therapy: Overcoming and Utilizing Biological Barriers to Peptide Drug Delivery. *ACS Nano* 12 (2), 2017–2026. doi:10.1021/acsnano.8b00081

Yan, J., Ji, F., Yan, S., You, W., Ma, F., Li, F., et al. (2020). A General-Purpose Nanohybrid Fabricated by Polymeric Au(I)-peptide Precursor to Wake the Function of Peptide Therapeutics. *Theranostics* 10 (19), 8513–8527. doi:10.7150/thno.47243

Yan, J., Yan, S., Hou, P., Lu, W., Ma, P. X., He, W., et al. (2019). A Hierarchical Peptide-Lanthanide Framework To Accurately Redress Intracellular Carcinogenic Protein-Protein Interaction. *Nano Lett.* 19 (11), 7918–7926. doi:10.1021/acs.nanolett.9b03028

Yan, J., Yao, Y., Yan, S., Gao, R., Lu, W., and He, W. (2020). Chiral Protein Supraparticles for Tumor Suppression and Synergistic Immunotherapy: An Enabling Strategy for Bioactive Supramolecular Chirality Construction. *Nano Lett.* 20 (8), 5844–5852. doi:10.1021/acs.nanolett.0c01757

Yan, S., Yan, J., Liu, D., Li, X., Kang, Q., You, W., et al. (2021). A Nano-Predator of Pathological MDMX Construct by Clearable Supramolecular Gold(I)-thiol-peptide Complexes Achieves Safe and Potent Anti-tumor Activity. *Theranostics* 11 (14), 6833–6846. doi:10.7150/thno.59020

Yan, W., Wu, X., Zhou, W., Fong, M. Y., Cao, M., Liu, J., et al. (2018). Cancer-cell-secreted Exosomal miR-105 Promotes Tumour Growth through the MYC-dependent Metabolic Reprogramming of Stromal Cells. *Nat. Cell Biol.* 20 (5), 597–609. doi:10.1038/s41556-018-0083-6

Yang, B., Chen, Y., and Shi, J. (2020). Tumor-Specific Chemotherapy by Nanomedicine-Enabled Differential Stress Sensitization. *Angew. Chem. Int. Ed.* 59 (24), 9693–9701. doi:10.1002/anie.202002306

Yang, G., Zhang, J., Yan, J., You, W., Hou, P., He, W., et al. (2019). Modulating Protein-Protein Interactions *In Vivo* via Peptide-Lanthanide-Derived Nanoparticles for Hazard-Free Cancer Therapy. *J. Biomed. Nanotechnol.* 15 (9), 1937–1947. doi:10.1166/jbn.2019.2820

Yang, G., Zhang, J., You, W., Zhao, X., Hou, P., He, W., et al. (2020). Targeted Disruption of the BCL9/β-Catenin Interaction by Endosomal-Escapable Nanoparticles Functionalized with an E-Cadherin-Derived Peptide. *Nanotechnology* 31 (11), 115102. doi:10.1088/1361-6528/ab5a03

Yang, L., He, X., Zeng, Z., Tang, J., Qi, D., Ma, H., et al. (2021). Clickable Amino Acid Tuned Self-Assembly of a Nucleus-Selective Multi-Component Nanoplatform for Synergistic Cancer Therapy. *Chem. Sci.* 12 (24), 8394–8400. doi:10.1039/d1sc01073e

Yang, W., Bai, Y., Xiong, Y., Zhang, J., Chen, S., Zheng, X., et al. (2016). Potentiating the Antitumour Response of $CD8^+$ T Cells by Modulating Cholesterol Metabolism. *Nature* 531 (7596), 651–655. doi:10.1038/nature17412

Yin, Z., Bai, L., Li, W., Zeng, T., Tian, H., and Cui, J. (2019). Targeting T Cell Metabolism in the Tumor Microenvironment: an Anti-cancer Therapeutic Strategy. *J. Exp. Clin. Cancer Res.* 38 (1), 403. doi:10.1186/s13046-019-1409-3

Yoo, H. C., Yu, Y. C., Sung, Y., and Han, J. M. (2020). Glutamine Reliance in Cell Metabolism. *Exp. Mol. Med.* 52 (9), 1496–1516. doi:10.1038/s12276-020-00504-8

Yoshida, G. J. (2015). Metabolic Reprogramming: the Emerging Concept and Associated Therapeutic Strategies. *J. Exp. Clin. Cancer Res.* 34, 111. doi:10.1186/s13046-015-0221-y

Yu, X., Teng, X.-L., Wang, F., Zheng, Y., Qu, G., Zhou, Y., et al. (2018). Metabolic Control of Regulatory T Cell Stability and Function by TRAF3IP3 at the Lysosome. *J. Exp. Med.* 215 (9), 2463–2476. doi:10.1084/jem.20180397

Zhang, D., Baldwin, P., Leal, A. S., Carapellucci, S., Sridhar, S., and Liby, K. T. (2019). A Nano-Liposome Formulation of the PARP Inhibitor Talazoparib Enhances Treatment Efficacy and Modulates Immune Cell Populations in Mammary Tumors of BRCA-Deficient Mice. *Theranostics* 9 (21), 6224–6238. doi:10.7150/thno.36281

Zhang, N., Liu, S., Shi, S., Chen, Y., Xu, F., Wei, X., et al. (2020). Solubilization and Delivery of Ursolic-Acid for Modulating Tumor Microenvironment and Regulatory T Cell Activities in Cancer Immunotherapy. *J. Control. Release* 320, 168–178. doi:10.1016/j.jconrel.2020.01.015

Zhang, W., Du, X. F., Liu, B., Li, C., Long, J., Zhao, M. X., et al. (2021). Engineering Supramolecular Nanomedicine for Targeted Near Infrared-Triggered Mitochondrial Dysfunction to Potentiate Cisplatin for Efficient Chemophototherapy. *ACS Nano* 16, 1421–1435. doi:10.1021/acsnano.1c09555

Zhang, Y.-X., Zhao, Y.-Y., Shen, J., Sun, X., Liu, Y., Liu, H., et al. (2019). Nanoenabled Modulation of Acidic Tumor Microenvironment Reverses Anergy of Infiltrating T Cells and Potentiates Anti-PD-1 Therapy. *Nano Lett.* 19 (5), 2774–2783. doi:10.1021/acs.nanolett.8b04296

Zhang, Y., Kurupati, R., Liu, L., Zhou, X. Y., Zhang, G., Hudaihed, A., et al. (2017). Enhancing $CD8^+$ T Cell Fatty Acid Catabolism within a Metabolically Challenging Tumor Microenvironment Increases the Efficacy of Melanoma Immunotherapy. *Cancer Cell* 32 (3), 377–391. doi:10.1016/j.ccell.2017.08.004

Zhang, Z., Li, X., Yang, F., Chen, C., Liu, P., Ren, Y., et al. (2021). DHHC9-mediated GLUT1 S-Palmitoylation Promotes Glioblastoma Glycolysis and Tumorigenesis. *Nat. Commun.* 12 (1), 5872. doi:10.1038/s41467-021-26180-4

Zhao, J.-L., Ye, Y.-C., Gao, C.-C., Wang, L., Ren, K.-X., Jiang, R., et al. (2022). Notch-mediated Lactate Metabolism Regulates MDSC Development through the Hes1/MCT2/c-Jun axis. *Cell Rep.* 38 (10), 110451. doi:10.1016/j.celrep.2022.110451

Zhao, L.-P., Zheng, R.-R., Chen, H.-Q., Liu, L.-S., Zhao, X.-Y., Liu, H.-H., et al. (2020). Self-Delivery Nanomedicine for O_2-Economized Photodynamic Tumor Therapy. *Nano Lett.* 20 (3), 2062–2071. doi:10.1021/acs.nanolett.0c00047

Zhao, Q., Li, J., Wu, B., Shang, Y., Huang, X., Dong, H., et al. (2020). Smart Biomimetic Nanocomposites Mediate Mitochondrial Outcome through Aerobic Glycolysis Reprogramming: A Promising Treatment for Lymphoma. *ACS Appl. Mat. Interfaces* 12 (20), 22687–22701. doi:10.1021/acsami.0c05763

Zheng, X., Yan, J., You, W., Li, F., Diao, J., He, W., et al. (2021). De Novo Nano-Erythrocyte Structurally Braced by Biomimetic Au(I)-peptide Skeleton for MDM2/MDMX Predation toward Augmented Pulmonary Adenocarcinoma Immunotherapy. *Small (Weinheim der Bergstrasse, Ger.* 17 (20), e2100394. doi:10.1002/smll.202100394

Zhou, Z., Song, J., Tian, R., Yang, Z., Yu, G., Lin, L., et al. (2017). Activatable Singlet Oxygen Generation from Lipid Hydroperoxide Nanoparticles for Cancer Therapy. *Angew. Chem. Int. Ed.* 56 (23), 6492–6496. doi:10.1002/anie.201701181

Zhu, X., Li, L., Tang, J., Yang, C., Yu, H., Liu, K., et al. (2022). Cascade-responsive Nano-Assembly for Efficient Photothermal-Chemo Synergistic Inhibition of Tumor Metastasis by Targeting Cancer Stem Cells. *Biomaterials* 280, 121305. doi:10.1016/j.biomaterials.2021.121305

Conflict of Interest: The authors declare that the research was conducted in the absence of any commercial or financial relationships that could be construed as a potential conflict of interest.

Publisher's Note: All claims expressed in this article are solely those of the authors and do not necessarily represent those of their affiliated organizations or those of the publisher, the editors, and the reviewers. Any product that may be evaluated in this article or claim that may be made by its manufacturer is not guaranteed or endorsed by the publisher.

frontiers | Frontiers in Bioengineering and Biotechnology

TYPE Original Research
PUBLISHED 26 August 2022
DOI 10.3389/fbioe.2022.949724

OPEN ACCESS

EDITED BY
Jin Yan,
Xi'an Jiaotong University, China

REVIEWED BY
Yong Zhao,
Institute of Zoology (CAS), China
Ming Guan,
Zhejiang University, China

*CORRESPONDENCE
Cailing Tong,
674637912@qq.com
Zhongquan Qi,
yxyyz@gxu.edu.cn

SPECIALTY SECTION
This article was submitted to Biomaterials, a section of the journal Frontiers in Bioengineering and Biotechnology

RECEIVED 21 May 2022
ACCEPTED 27 July 2022
PUBLISHED 26 August 2022

CITATION
Gu Z, Yin Z, Song P, Wu Y, He Y, Zhu M, Wu Z, Zhao S, Huang H, Wang H, Tong C and Qi Z (2022), Safety and biodistribution of exosomes derived from human induced pluripotent stem cells.
Front. Bioeng. Biotechnol. 10:949724.
doi: 10.3389/fbioe.2022.949724

Safety and biodistribution of exosomes derived from human induced pluripotent stem cells

Zhewei Gu[1], Zhiyu Yin[1], Pengbo Song[1], Ying Wu[1], Ying He[1], Maoshu Zhu[1], Zhengxin Wu[1], Sicheng Zhao[1], Hongri Huang[3], Huihuang Wang[3], Cailing Tong[2]* and Zhongquan Qi[1]*

[1]Medical College, Guangxi University, Nanning, China, [2]Biotechcomer Co., Ltd., Xiamen, China, [3]GuangXi TaiMeiRenSheng Biotechnology Co., LTD., Nanning, China

As a new cell-free therapy, exosomes have provided new ideas for the treatment of various diseases. Human induced pluripotent stem cells (hiPSCs) cannot be used in clinical trials because of tumorigenicity, but the exosomes derived from hiPSCs may combine the advantages of iPSC pluripotency and the nanoscale size of exosomes while avoiding tumorigenicity. Currently, the safety and biodistribution of hiPSC-exosomes *in vivo* are unclear. Here, we investigated the effects of hiPSC-exosomes on hemolysis, DNA damage, and cytotoxicity through cell experiments. We also explored the safety of vein injection of hiPSC-exosomes in rabbits and rats. Differences in organ distribution after nasal administration were compared in normal and Parkinson's disease model mice. This study may provide support for clinical therapy and research of intravenous and nasal administration of hiPSC-exosomes.

KEYWORDS

exosomes, HiPSCs, safety, biodistribution, nasal administration, Parkinson's disease

Introduction

When induced pluripotent stem cells (iPSCs) were first established (Takahashi and Yamanaka, 2006), they were a promising cell treatment method in regenerative medicine because of their pluripotency and therapeutic potential for various human diseases. iPSC therapy is currently one of the best options to slow or even stop the progression of Parkinson's disease (Doi et al., 2020; Schweitzer et al., 2020; Song et al., 2020) because iPSCs selectively differentiate into dopaminergic neurons and have a reduced risk of immune rejection (Deuse et al., 2019; Stoddard-Bennett and Reijo Pera, 2019). Organoids and models derived from iPSCs have provided new ideas for disease treatments and drug screening, and a culture protocol capable of efficiently generating small human brain organoids was optimized to establish subcortical projections in the mouse brain (Dong et al., 2021). The property of differentiation into the three germ layers allows engineering functional tissues (Rao et al., 2018). However, their tumorigenicity is a great challenge in clinical research (Blum and Benvenisty, 2009; Itakura et al., 2017; Liu et al., 2021).

Exosomes can be used as a novel cell-free therapy to resolve issues in cell therapy. The nanoscale particle size of exosomes gives them the ability to cross the blood-brain barrier. Exosomes derived from mesenchymal stem cells pass through the blood-brain barrier and migrate to an injured spinal cord area when administered intranasally (Guo et al., 2019). The combined pluripotency of iPSCs and advantages of exosomes may facilitate development of disease therapies. Adamiak et al. (2018) reported that, among 282 miRNAs detected in iPSCs, 199 miRNAs were also present in iPSC-extracellular vesicles (EVs), indicating that these regulatory transcripts were efficiently transferred from iPSCs to EVs. As a subset of EVs (Kalluri and LeBleu, 2020), iPSC-exosomes may inherit features that exert therapeutic effects on some diseases. To date, there has been no successful strategy that can repair a brain or neural injury and exosomes derived from human induced pluripotent stem cells may be a promising approach (Ghosh et al., 2020).

iPSC-exosomes have specific therapeutic effects on cardiovascular, skin, and eye diseases. Exosomes derived from iPSCs deliver cytoprotective signals to cardiomyocytes to efficiently rescue ischemic cardiomyocytes under conditions such as myocardial ischemia/reperfusion (Wang et al., 2015). iPSC-exosomes may promote the migration of fibroblasts *in vitro* and *in vivo*, and provide a possible treatment for diabetic ulcers (Kobayashi et al., 2018). A corneal epithelial defect model showed that both iPSC- and MSC-exosomes accelerate healing of corneal epithelial defects and the effect of iPSC-exosomes is much stronger than that of MSC-exosomes (Wang et al., 2020). For a promising treatment method, it is crucial to establish the relevant safety evaluation system to facilitate clinical research advances. To accomplish such evaluation, we examined hemolysis, DNA damage, and cytotoxicity of hiPSC-exosomes at the cellular level, their effects on tissues, organs, immunity, and the blood system at the animal level, and their biodistribution.

Materials and methods

Statement of ethics and animal treatment

This study was approved by the Animal Studies Committee of Guangxi University (Nanning, China). Animal experiments were carried out in accordance with the committee guidelines. New Zealand rabbits, Sprague-Dawley (SD) rats, and C57 mice purchased from Changsha Tianqing Biotechnology Co., Ltd. (Changsha, China) were fed ad libitum for 1 week for acclimation. Animals were kept in a clean room under stable temperature (22–26°C), humidity (50%–70%), and illumination (12-h light/dark cycle) with water and food freely available.

Cell culture

hiPSCs purchased from iCell Bioscience Inc., (Shanghai, China) were maintained in mTeSR1 (STEMCELL, #85850) serum-free maintenance medium on Matrigel (Corning, 354277)-coated culture flasks. The medium was replaced with fresh maintenance medium in accordance with cell growth. The culture supernatant was collected for exosome extraction. Mouse macrophage-like cell line RAW264.7 purchased from Biotechcomer Co., Ltd. (Xiamen, China) was maintained in Dulbecco's modified Eagle's medium (Gibco, 11965092) containing 10% fetal bovine serum.

hiPSC identification

Human Embryonic Stem Cell Marker Panel (Hicks et al., 2020; Roth et al., 2020; Bomba et al., 2021; Osnato et al., 2021) (Abcam, ab238602) was used to analyze pluripotency protein markers by immunofluorescence. A Trilineage Differentiation Kit (Ward et al., 2017) (STEMCELL, #05230) was used to induce differentiation into the three germ layers. Human three Germ Layer 3-Color Immunocytochemistry Kit (Han et al., 2020) (R&D, SC022) was used to identify specific protein markers of the three germ layers. A Giemsa Stain solution (Solarbio, G1015) was used to analyze the karyotype. Fluorescence images were obtained under an LSM900 laser scanning confocal microscope (Zeiss, Germany).

Purification of hiPSC-exosomes

Culture supernatants were stored at 4°C, filtered through a 0.45-μm membrane filter (Millipore, United States), and then concentrated with a 100-kDa molecular weight cutoff hollowfiber membrane. After centrifuging at 2,000 × *g* for 20 min to remove dead cells, the supernatant was centrifuged at 10,000 × *g* for 30 min to remove cell debris. The supernatant was filtered through a 0.22-μm membrane filter (Millipore) and the final supernatant was subjected to ultracentrifugation (Beckman, United States) at 100,000 × *g* for 90 min. All centrifugation steps were at 4°C. The exosome precipitate was resuspended in cold PBS or physiological saline. Exosomes in PBS or physiological saline were filtered again through a 0.22-μm membrane filter. Purified exosomes were stored at −80°C for long-term use or 4°C for short-term use (Cheng et al., 2019; Wu et al., 2021).

Characterization of hiPSC-exosomes

The protein concentration of hiPSC-exosomes was determined using a BCA protein quantitation kit (Zoman

Biotechnology, ZD301). An HT7700 transmission electron microscope (Hitachi, Japan) was used to determine the morphology and size of hiPSC-exosomes. The particle size distribution of hiPSC-exosomes was measured by nanoparticle tracking analysis (Particle Metrix zataview, Germany). Marker proteins of hiPSC-exosomes were detected by western blotting using anti-CD9 (Yang et al., 2022) (Affinity, DF6565), anti-TSG101 (Qi et al., 2022) (Proteintech, 67381-1-Ig), and negative protein marker anti-Calnexin (Sun et al., 2021a) (Proteintech, 66903-1-Ig) antibodies. hiPSC-exosome-specific protein markers CD63 (BD, 556019) and CD81 (BD, 551108) were detected by a Flow NanoAnalyzer (Nanofcm, China).

Labeling hiPSC-exosomes with PKH26 dye

A PKH26 stock solution (Merck, MINI26) was prepared at 20 μM and mixed at an equal volume with an exosome solution for a final concentration of 10 μM PKH26. After incubation for 1 h at room temperature. the mixture was ultracentrifuged at 100,000 × *g* for 70 min at 4°C to remove excess dye. The precipitate was resuspended in cold PBS(Franzen et al., 2014; Pužar Dominkuš et al., 2018).

Hemolysis

Twenty milliliters of blood was collected from a New Zealand rabbit, gently stirred to remove fibrin, and then thoroughly mixed with 100 ml physiological saline. After centrifugation at 500 × *g* for 15 min, the supernatant was discarded. The precipitated red blood cells were washed three times with physiological saline until the supernatant was clear. The red blood cell samples were diluted with physiological saline to prepare a 2% suspension and divided into three groups as follows. Negative control group:100 μl suspension with 100 μl physiological saline; Exosome group: 100 μl suspension with 20 μg hiPSC-exosomes in 100 μl physiological saline (final concentration: 100 μg/ml); Positive group: 100 μl suspension with 100 μl distilled water. All experiments were conducted in a 96-well plate. Samples were incubated at 37°C for 3 h and then absorbance was measured at 540 nm in a microplate reader (Tecan, Switzerland).

DNA damage assay

Leukocytes were isolated from blood using lymphocyte separation medium (Solarbio, P8900) and incubated in a 6-well plate at 37°C for 24 h. Camptothecin (Aladdin, C111281-20mg; 50 μM) was used as a positive control, PBS as a negative control, and 200 μg hiPSC-exosomes (final concentration: 100 μg/ml) as the experimental group. Treated cells were collected and an OxiSelect™ Comet Assay kit (Cell Biolabs STA-350) was used to perform the alkaline comet assay (Singh et al., 1988). The condition for single cell electrophoresis was 1 V/cm (width of electrophoresis tank), electrophoresis time was 20 min, and 300 mA lateral flow electrophoresis was adjusted. Vista Green DNA Dye was used to detect comet its entirety under a fluorescence microscope (Mshot, China). Comet length was analyzed by open comet software (Gyori et al., 2014).

Cellular uptake and cytotoxicity assays

RAW264.7 cells were seeded in a 6-well plate to prepare for hiPSC-exosome uptake. After washing with PBS, cells were treated with PKH26-labeled hiPSC-exosomes at 37°C for 3 h in serum-free medium (Somiya et al., 2018; Guan et al., 2022). Then, the cells were washed with cold PBS twice and fixed with 4% paraformaldehyde. After mounting on coverslips with anti-fluorescence quenching mounting medium containing DAPI (Solarbio, S2110), the sample was observed under a laser scanning confocal microscope (Olympus, Japan). RAW264.7 cells were seeded in a 96-well plate (2×10^4 cells/well) and treated with up to 200 μg/ml hiPSC-exosomes at 37°C for 24 h. Cell viability was then measured by Cell Counting Kit-8 (Solarbio, CA1210) in accordance with the manufacturer's instructions.

Muscle stimulation

Eight healthy New Zealand rabbits weighing approximately 2 kg were selected (equal number of males and females). Negative control group: 200 μl PBS; Exosome groups: 100 and 200 μg hiPSC-exosomes diluted with 200 μl PBS (final concentrations: 500 and 1,000 μg/ml, respectively). Left and right legs were used as experimental and negative control groups, respectively. Animals were acclimated for 1 week before injection. For injection, the needle was inserted vertically into the quadricep muscle in the front of the thigh halfway between the knee and hip joint.

At 48 h after injection, we observed whether the injection site had changed (Sun et al., 2016). After sacrifice by an air injection, two pieces of tissue parallel and perpendicular to the quadricep muscle were collected to perform pathological analysis.

Vascular stimulation

Eight healthy New Zealand rabbits weighing approximately 2 kg were selected for the experiment (equal number of males and females). Marginal ear vein administration was performed after 1 week of acclimation. Then, 100 and 200 μg hiPSC-exosomes

diluted with 200 μl PBS (final concentrations: 500 and 1,000 μg/ml, respectively) were applied to the experimental group, and the negative control received 200 μl PBS. hiPSC-exosomes were injected *via* the left ear marginal vein, and the right ear was injected with the same amount of PBS as the control. Rabbits were injected at the same time for three consecutive days and the location of each injection point was continuously close to the proximal end of the ear. We observed whether blood vessels and surrounding tissues had changed and recorded rectal temperature. Animals were sacrificed at 48 h after the last injection. Surrounding tissues were collected, fixed with 10% formaldehyde solution, and the degree of vascular irritation was evaluated by visual observation and pathological sections.

Hematology assay

SD rats weighing 250–350 g were selected (15 males and 15 females). A total of 30 rats were divided into five groups with an equal number of males and females in each group. Group 1 rats were subjected to tail vein injection of 200 μl PBS as the negative control for the tail vein group. Group 2 rats were subjected to tail vein injection of 100 μg hiPSC-exosomes diluted with 200 μl PBS (final concentration: 500 μg/ml). Group 3 rats were subjected to tail vein injection of 200 μg hiPSC-exosomes diluted with 200 μl PBS (final concentration: 1,000 μg/ml). Group 4 rats were subjected to nasal administration of 20 μl PBS in left and right nostrils as the negative control for the nasal administration group. Group 5 rats were subjected to nasal administration of 3×10^9 hiPSC-exosomes diluted with 20 μl PBS in left and right nostrils. At days 1, 6, 13, and 20 after administration, 1 ml blood was collected for routine blood examinations using an automatic blood cell analyzer (Mindray, China) and blood biochemistry using an automatic blood biochemical analyzer (Urit, China). Changes in cellular and humoral immunities were analyzed by an Acoustic Focusing Flow Cytometer (Invitrogen, United States) and microplate reader (Tecan). The antibodies used for flow cytometry were anti-CD3 (Invitrogen, 11-0030-82) (Steines et al., 2021), anti-CD4 (Invitrogen, 17-0040-80), anti-CD8 (Invitrogen, 12-0084-82) (Aiello et al., 2017). ELISA kits (Elabscience, IgA E-EL-R3015, IgM E-EL-R3016, and IgG E-EL-R0518c) (He et al., 2019) were used to detect immunoglobulins.

Parkinson's disease model

Twelve-week-old C57 male mice were selected for model establishment. Mice were anesthetized with a 2,2,2-tribromoethanol solution before injection with 6-hydroxydopamine (3.3 μg/μl) using a stereotaxic apparatus. Injections were performed at the following two coordinates: anteroposterior (AP), 0.3 mm; mediolateral (ML), −2.2 mm; dorsoventral (DV), −3 mm; AP, 1.1 mm; ML, −1.7 mm; DV, −2.9 mm. The 6-hydroxydopamine solution (2 μl) was injected at each point and the needle was left in place for 5 min to promote drug absorption and prevent reflux. Then, 20,000 IU penicillin was injected for the first 3 days after the operation to prevent surgical infection. One week after surgery, mice received an i.p. injection of apomorphine (0.5 mg/kg). After 5 min of acclimatization, rotational data were continuously recorded for 30 min and the number of revolutions of more than seven circles per minute was considered to be successful model establishment (Pan et al., 2015; Niu et al., 2018; Chen et al., 2020). Additionally, western blotting (Tyrosine Hydroxylase, Abcam, ab75875) (Henriques et al., 2020), HE staining, immunohistochemistry (Tyrosine Hydroxylase, Abcam, ab137869) (Sun et al., 2021b), and Nissl staining were used to verify the reliability of the model.

Biodistribution of hiPSC-exosomes

Nasal administration of hiPSC-exosomes labeled with PKH26 (excitation: 551 nm; emission: 567 nm) was performed for mouse organ imaging (PerkinElmer, United States; IVIS Lumina LT Series III). The Parkinson's mouse model established by 6-hydroxydopamine was used as the experimental group and normal mice were the control group. The dose administered to mice was about one-tenth of the number of particles administered to rats in accordance with body weight. A total of 3×10^8 hiPSC-exosomes in 20 μl was administered nasally to each mouse. Mice were deprived of water and food for 12 h before imaging and sacrificed at specific time points for organ fluorescence intensity imaging (Yi et al., 2020). Fluorescence values of each organ were used for analysis.

Statistical analysis

Statistical analysis was performed using GraphPad Prism v.8.3 for Windows. Intergroup differences were analyzed by the *t*-test for two groups or one-way ANOVA for more than two groups. Data are presented as the mean ± SEM.

Results

Typical features of hiPSCs

To determine whether the cell line had the features of hiPSCs, we assessed the morphological appearance, karyotype, pluripotency markers, and differentiation of the three germ layers. The cells showed colony formation in serum-free medium under trophoblast-free growth

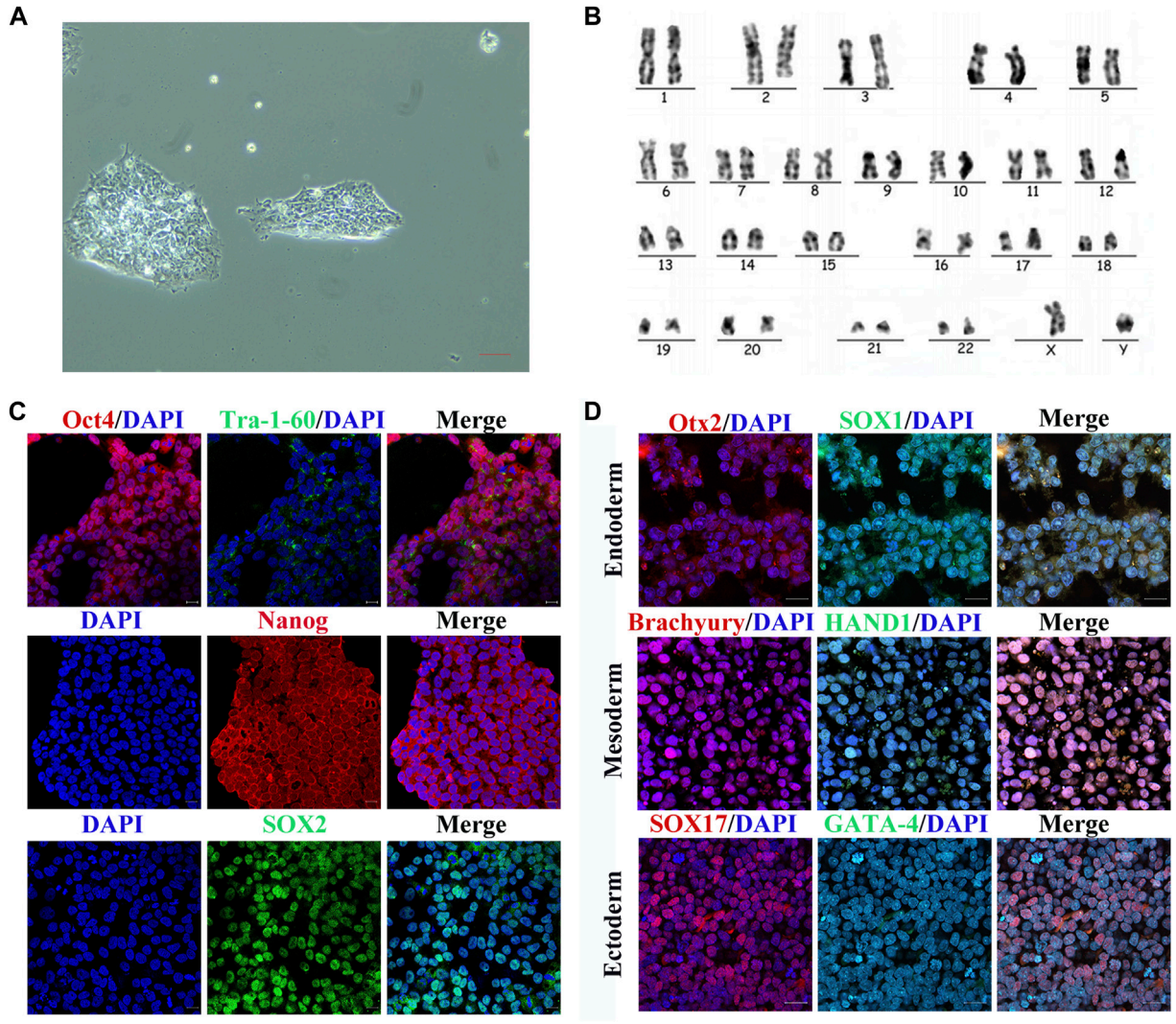

FIGURE 1
Characterization of hiPSCs. **(A)** Normal monoclonal morphology of hiPSCs in serum-free medium assessed by optical microscopy. Scale bar represents 20 μm. **(B)** Normal chromosomes revealed by karyotype analysis of hiPSCs. **(C)** Immunofluorescence images of pluripotency markers (Oct4, Tra-1-60, Nanog, and SOX2) in hiPSCs. Scale bar represents 50 μm. **(D)** Immunofluorescence images of germ layer markers after hiPSC differentiation. Scale bar represents 50 μm.

conditions (Figure 1A). There were 22 pairs of autosomes and one pair of XY sex chromosomes, which demonstrated a normal karyotype (Figure 1B). Immunofluorescence demonstrated that the cells expressed pluripotency markers Oct4, Tra-1-60, Nanog, and Sox2 (Figure 1C). They had the ability to differentiate into the three germs layers, including endoderm, mesoderm, and ectoderm, as evidenced by expressing Otx2 and Sox1 in endoderm, Brachyury and Hand1 in mesoderm, and Sox17 and Gata-4 in ectoderm (Figure 1D). These findings indicated that the cell line had the characteristics of hiPSCs and could be used in subsequent experiments.

Characterization of hiPSC-exosomes

To evaluate the characteristics, exosomes was isolated from serum-free medium of hiPSCs though ultracentrifugation. Exosomes derived from hiPSCs were cup-shaped under a transmission electron microscope (Figure 2A). The mean diameter of 143.5 nm was observed by nanoparticle tracking analysis (Figure 2B). Typical protein markers CD9 and TSG101 were detected, whereas Calnexin was not detected by western blotting (Figure 2C). Other specific protein markers were detected by a Flow NanoAnalyzer, a novel detection method for hiPSC-exosomes (Figure 2D). These results confirmed the

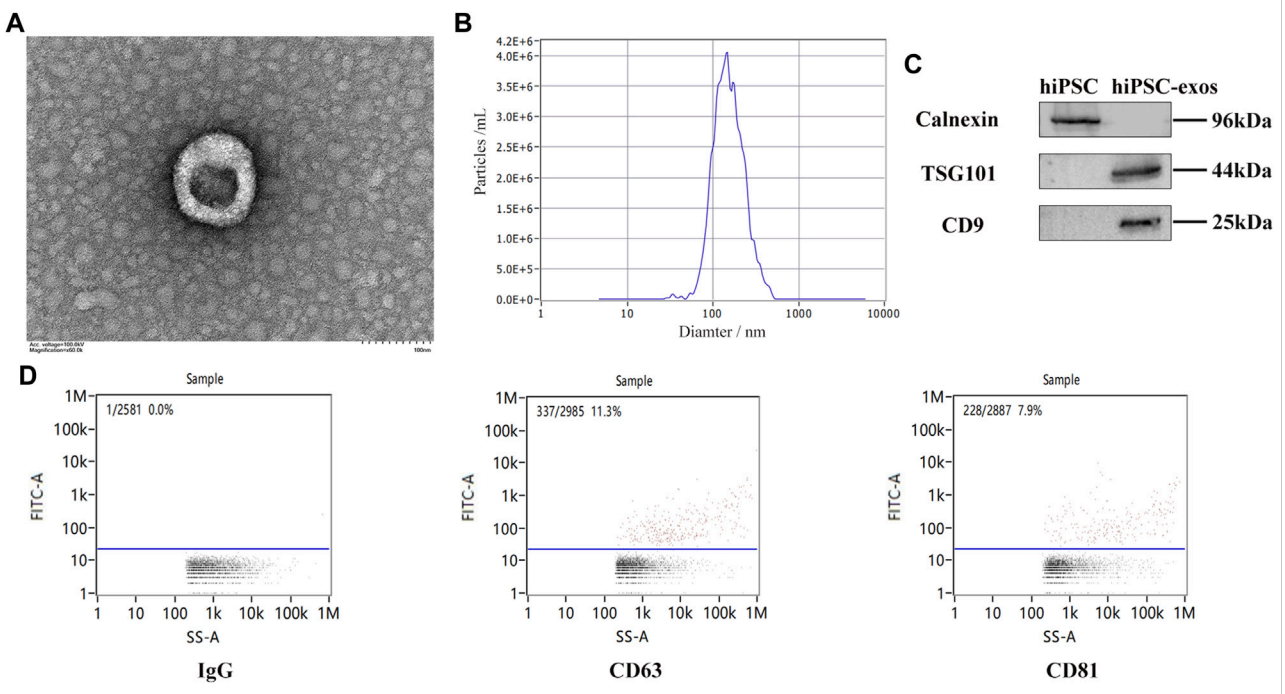

FIGURE 2
Characterization of exosomes derived from hiPSCs. **(A)** Cup-shaped structure of hiPSC-exosomes under a transmission electron microscope. **(B)** Particle size distribution map of hiPSC-exosomes generated by nanoparticle tracking analysis. **(C)** Specific protein markers (CD9 and TSG101) and negative protein marker (Calnexin) in hiPSC-exosomes detected by western blotting. **(D)** Isotype control IgG and specific markers (CD63, and CD81) in hiPSC-exosomes detected by a Flow NanoAnalyzer.

characteristics of hiPSC-exosomes, indicating that the exosomes had been successfully purified and could be used for subsequent cell and animal experiments.

Hemolytic effect of hiPSC-exosomes

Because hemoglobin released by hemolysis can affect blood vessels and body systems, we first evaluated the safety of hiPSC-exosomes at the cell membrane. The influence of hiPSC-exosomes on the cell membrane was determined by a red blood cell hemolysis assay. After 3 h of incubation with hiPSC-exosomes, no hemolysis was observed in a red blood cell suspension (Figure 3A). The absorbance of the hiPSC-exosome group was similar to that of the control and showed significant difference from the positive group. Taken together, these finding indicated that hiPSC-exosomes had no effect on hemolysis.

Assessment of DNA damage caused by hiPSC-exosomes

Next, we performed a comet assay to evaluate the effect of hiPSC-exosomes on DNA. The degree of DNA damage was determined by the length of the comet tail. White blood cells were treated with PBS, hiPSC-exosomes, and CPT and then subjected to single cell electrophoresis. A DNA dye was used to detect the whole comet. Compared with the positive group, PBS and hiPSC-exosome groups did not clearly display the comet tail. Thus, there was no significant effect of hiPSC-exosomes in causing DNA damage (Figures 3B,C).

Cellular uptake and cytotoxicity of hiPSC-exosomes

We assessed cellular uptake and cytotoxicity to determine the effects of hiPSC-exosomes on cells. Macrophages have ability to phagocytose exosomes (Parada et al., 2021). Mouse macrophage-like cell line RAW264.7 was treated with PKH26-labeled hiPSC-exosomes. Confocal microscopy showed that PKH26-labeled hiPSC-exosomes were phagocytized by RAW264.7 cells (Figure 3D).

RAW264.7 cells were treated with various protein concentrations of hiPSC-exosomes for 24 h. Cell Counting Kit-8 was then used to evaluate cytotoxicity. The cell viability curve showed that the growth status of macrophages was unchanged by hiPSC-exosomes at all concentrations

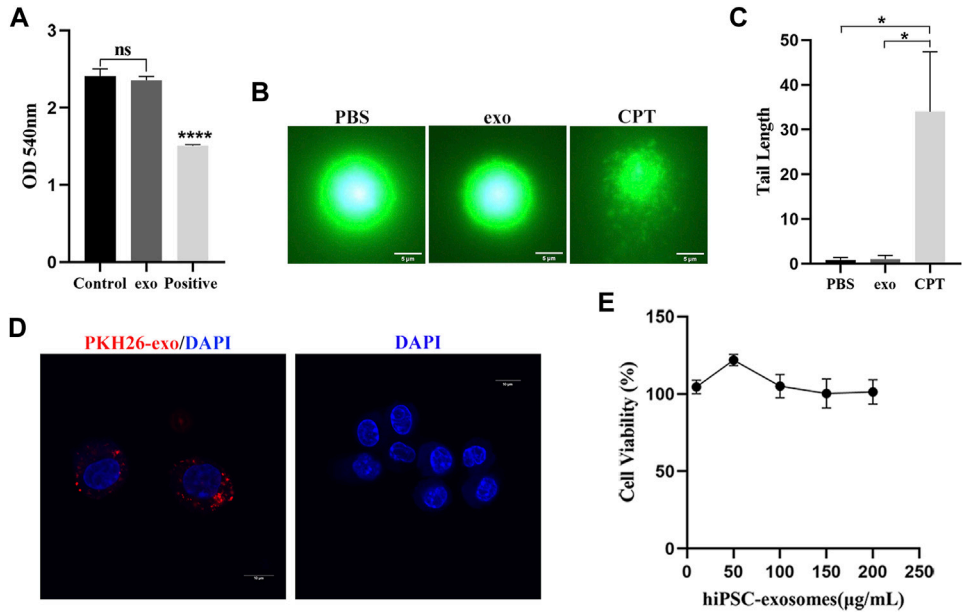

FIGURE 3
Safety evaluation of hiPSC-exosomes at the cellular level. **(A)** Absorbance values of various groups of erythrocyte suspensions at 540 nm. *N* = 4 per group (ns, no statistical difference; ****$p < 0.0001$). **(B)** Fluorescence image of DNA after alkaline comet electrophoresis of leukocytes in PBS, hiPSC-exosomes, and the 50 μM camptothecin group. **(C)** Tail length analysis of comets in the three groups. *N* = 5 per group (*$p < 0.05$). **(D)** PKH26-labeled hiPSC-exosome uptake by RAW264.7 cells under laser scanning confocal microscopy. **(E)** Viability of RAW264.7 cells treated with up to 200 μg/ml hiPSC-exosomes. *N* = 4 per group. Data are expressed as the mean ± SEM.

(Figure 3E). The viability of RAW264.7 cells remained at near 100%, even with the highest concentration of 200 μg/ml. These data suggested that the hiPSC-exosomes had no cytotoxicity *in vitro*.

The evaluation of hiPSC-exosomes at the cellular level indicated that the hiPSC-exosomes had no adverse effects on cell membranes, DNA, or cell proliferation.

Muscle stimulation

To further investigate the safety of hiPSC-exosomes at the animal level, we explored three injection methods to evaluate the influence on various tissues, organs, and systems. We first evaluated the effect of hiPSC-exosomes on muscle tissues by intramuscular injection. Intramuscular injection into quadriceps was performed after the rabbits were acclimated for 1 week. After injection, there was no edema or congestion at the injection sites in hiPSC-exosome and control groups. Samples were collected from the quadricep femoris after sacrificing the rabbits.

By visual observation and analysis of pathological sections, muscle tissues showed well-defined muscle fiber bundles with a normal form. Muscle cells in the cut surface of muscle tissue were slender and cylindrical multinucleated with different lengths. The nucleus was located near the sarcolemma around the cell, the nucleus was oval, and the nucleolus was obvious. The muscle fibers in the muscle bundles were closely arranged and most of them had an angular appearance without degeneration, necrosis, or inflammatory cell infiltration in hiPSC-exosome groups and showed no significant differences comparing with the control. Taken together, these results showed that i.m. injection of hiPSC-exosomes was safe and hiPSC-exosomes did not stimulate muscle tissues (Figure 4B).

Vascular stimulation

To determine the effect of hiPSC-exosomes on blood vessels, we performed ear vein injections in New Zealand rabbits. During the administration, ear veins of the rabbits were clear and there was no vascular hemorrhage, congestion, edema, inflammation, tissue necrosis, or other phenomena. At 48 h after the last administration, vascular tissue was collected for sectioning.

H&E staining showed that the morphology of subcutaneous tissue was normal in control and hiPSC-exosome groups. Vascular endothelial cells of the ear vein were arranged normally, skin tissue of the auricle showed slight hyperkeratosis of the epidermis, and no obvious abnormality

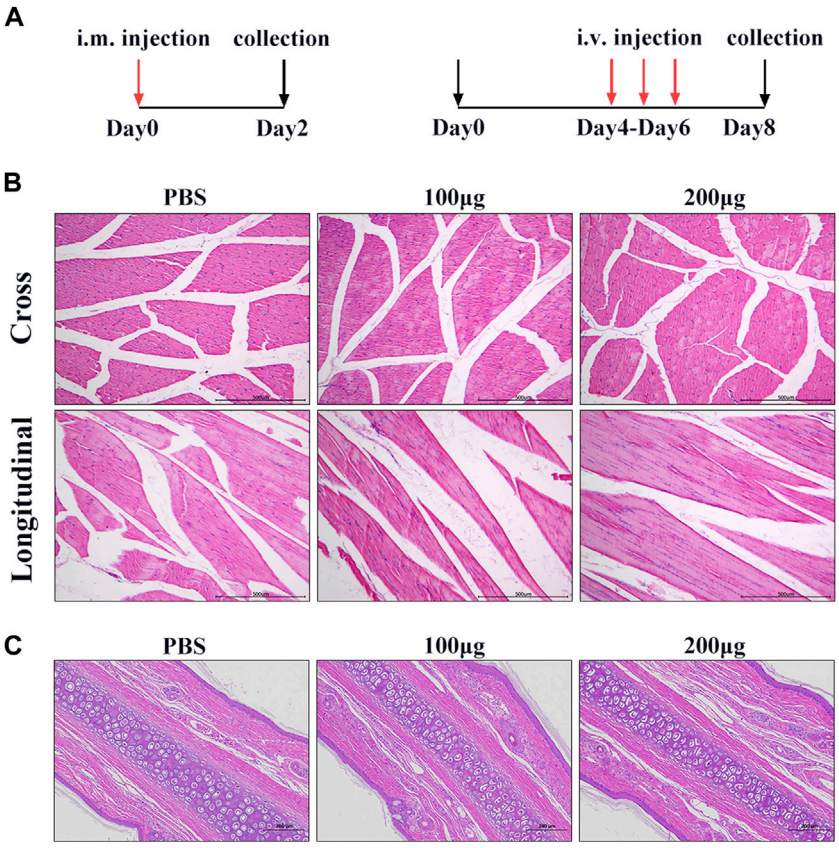

FIGURE 4
Muscle and vascular stimulation by hiPSC-exosomes. **(A)** Experimental design for injection of hiPSC-exosomes into muscle and vascular stimulation. **(B)** HE staining of muscle in cross-sections and longitudinal sections from control and experimental groups. *N* = 4 per group. **(C)** HE-stained sections of marginal ear veins in control and experimental groups. *N* = 4 per group.

was observed in the dermis. There was no inflammatory cell infiltration in blood vessels, thickening of the blood vessel wall, or obvious necrosis, degeneration, and inflammation around the wall change (Figure 4C). Similarly, there was no significant difference in the rectal temperature of the rabbits over time in hiPSC-exosome groups compared with the control group (Supplementary Table S1). These results suggested that the injections of hiPSC-exosomes did not affect body temperature and had no stimulatory or adverse effects on vessels. Therefore, we further evaluated other safety through intravenous injection.

Safety evaluation of hiPSC-exosomes in terms of hemocyte parameters

To confirm whether blood and immunity were influenced by hiPSC-exosomes, we performed hiPSC-exosome administration in rats. Administration of hiPSC-exosomes was divided into three groups including tail vein injection of two protein concentrations and nasal administration (n.a.). The two control groups were administered PBS *via* the tail vein (C1) or nasal cavity (C2). At various days after administrations, blood was collected for analysis.

The blood was collected from rats for assessment by a hematology analyzer. On day 1 (Figure 5), there was a statistically significant difference in HCT and PLT between C2 and nasal administration groups. On day 6, there was a statistically significant difference in Gran between C2 and nasal administration groups as well as HGB on day 20 (Supplementary Figure S1). RBC showed no significant differences between the groups at the four time points. The number of WBCs and Lymph showed some differences among the groups, but there was no significant difference. There were no significant differences in Lymph% or MPV at each time point. Gran%, Mon, and Mon% showed no significant different at each time. The trend at other times was similar with no significant difference (Supplementary Figure S1). Changes in routine blood indexes were all within the reference ranges of healthy rat indexes.

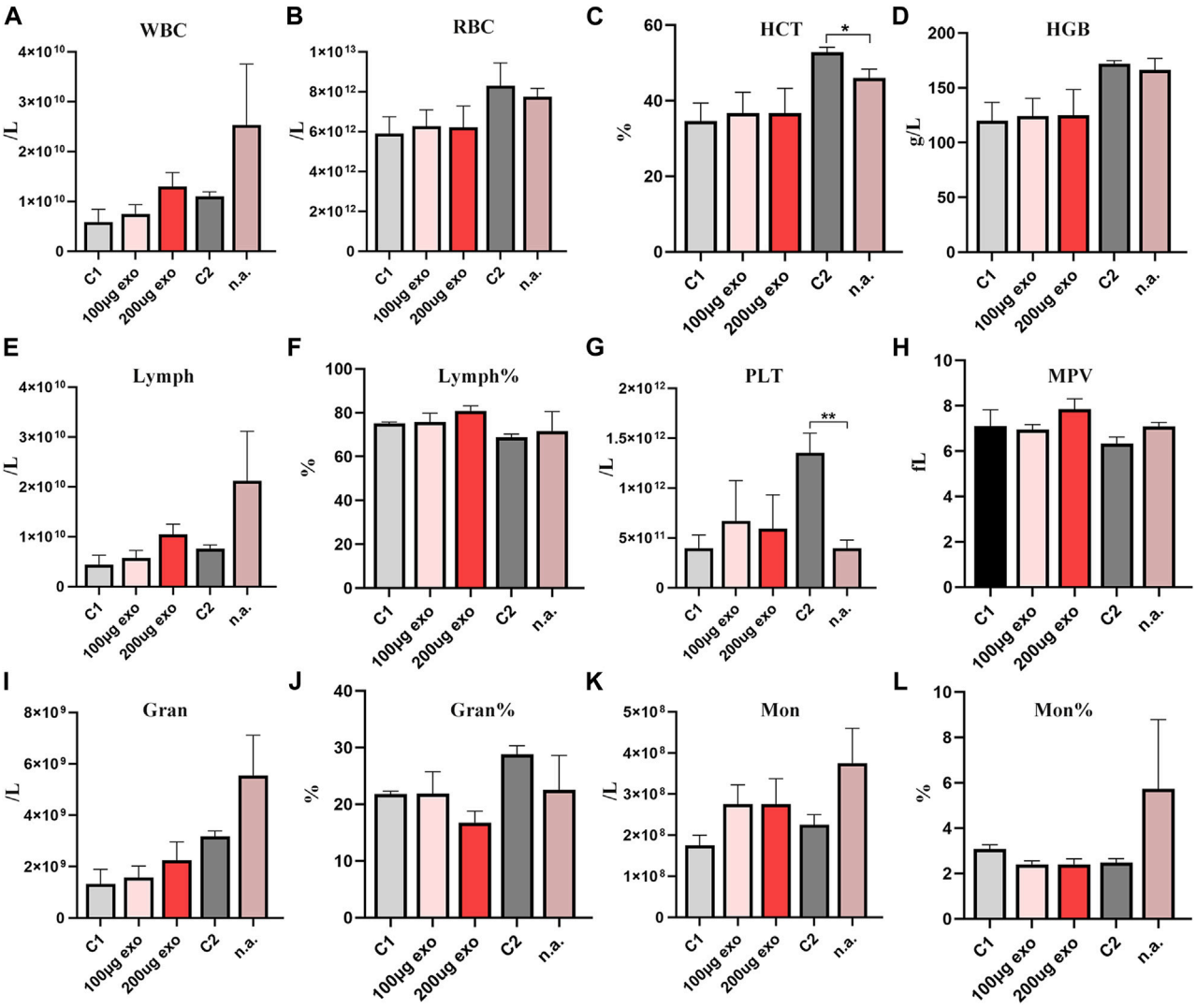

FIGURE 5
Routine blood analyses of SD rats on day 1. **(A)** White blood cell count. **(B)** Red blood cell count. **(C)** Hematocrit (*$p < 0.05$). **(D)** Hemoglobin. **(E)** Lymphocyte count. **(F)** % Lymphocytes. **(G)** Platelet count (**$p < 0.01$). **(H)** Mean platelet volume. **(I)** Neutrophil count. **(J)** % Neutrophils. **(K)** Monocyte count. **(L)** % Monocytes. $N = 4$ per group. Data are expressed the mean ± SEM. (C1, Control 1; C2, Control 2). Reference ranges: WBCs. 2.9–15.3 × 10^9/L; RBCs, 5.60–7.89 × 10^{12}/L; HCT 36%–46%; HGB, 120–150 g/L; Lymph, 2.6–13.5 × 10^9/L; Lymph%, 63.7%–90.1%; PLT, 100–1,610 × 10^9/L; MPV, 3.8–6.2 fL; Gran. 0.4–3.2 × 10^9/L; Gran% 7.3%–30.1%; Mon, 0–0.5 × 10^9/L; Mon%, 1.5%–4.5%.

Thus, we considered that different injection routes may influence some routine blood indexes, but all of them were within the reference range, indicating that tail vein injection and nasal administration of hiPSC-exosomes have no effect on blood cells.

Safety evaluation of hiPSC-exosomes in the rat liver and kidneys

Next, rat serum was collected to evaluate liver and kidney functions by blood biochemical indexes. Liver and kidney function indicators showed changes in all groups at each time point (Figures 6A–F). ALT content showed significant difference on days 13 and 20 between C2 and n.a. groups. The urea content showed a significant difference on day 1 between C2 and n.a. groups and on day 6 between 200 μg and C1, 100 μg, n.a. groups. ALB and TP contents showed significant differences between C2 and n.a. groups on day 1. There were no significant differences in AST and CHOL. All values evaluated were within the reference ranges. These results suggested that hiPSC-exosomes had no negative effect on the liver and kidney functions of rats.

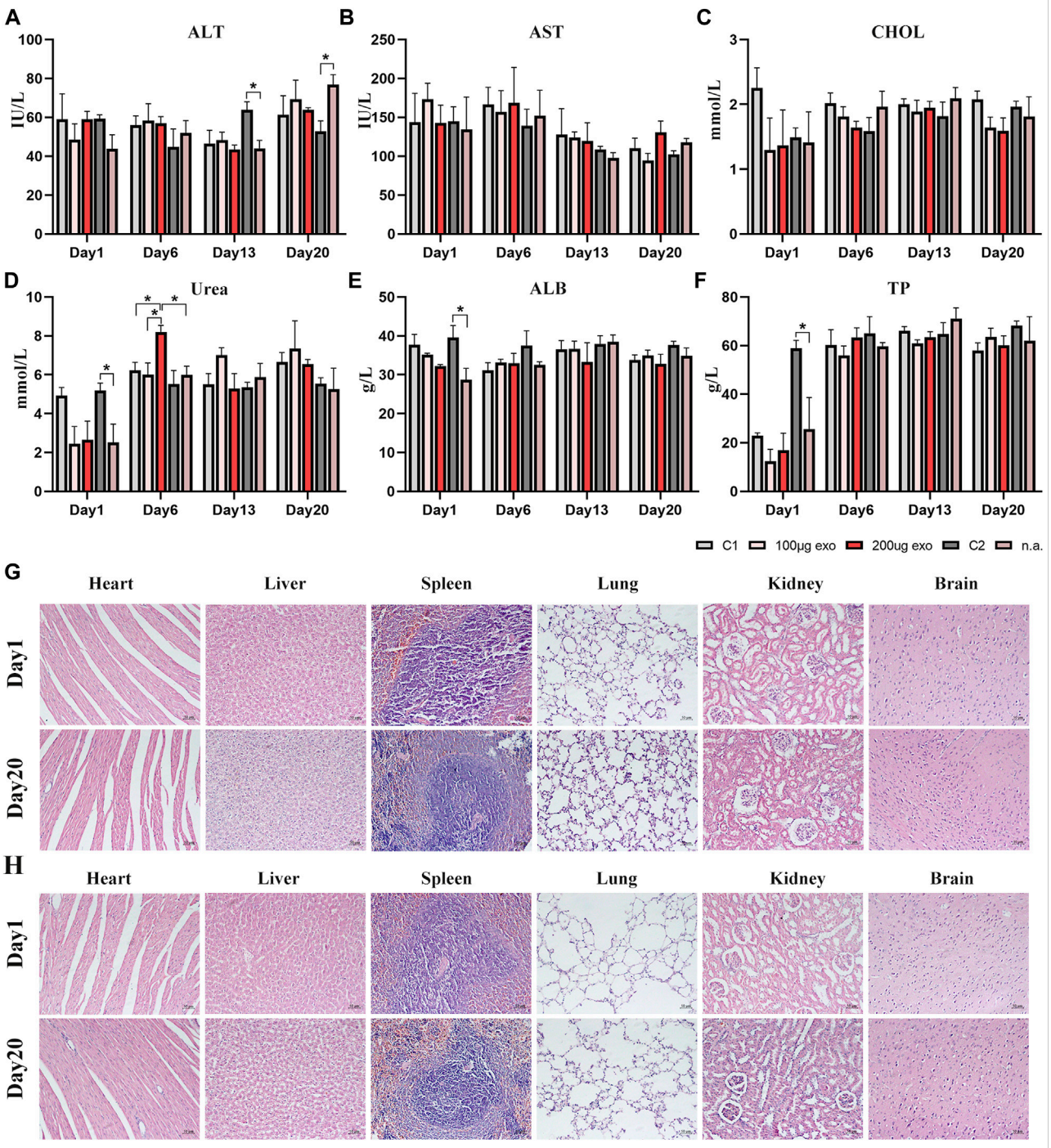

FIGURE 6
Blood biochemical indexes and pathological changes in rat organs. **(A)** Alanine aminotransferase (*$p < 0.05$). **(B)** Aspartate aminotransferase. **(C)** Total cholesterol. **(D)** Urea (*$p < 0.05$). **(E)** Albumin (*$p < 0.05$). **(F)** Total protein (*$p < 0.05$). $N = 4$ per group. Data are expressed the mean ± SEM. (C1, Control 1; C2, Control 2). Reference ranges: ALT, 38.84–85.56 IU/L; AST, 75.79–237.34 IU/L; CHOL, 1.05–2.61 mmol/L; Urea, 2.15–8.31 mmol/L; ALB, 30.89–45.08 g/L; TP, 52.41–85.53 g/L. **(G)** HE-stained pathological sections of major organs in the Control 1 group on days 1 and 20. **(H)** HE-stained pathological sections of major organs in the 200 μg hiPSC-exosome group on days 1 and 20.

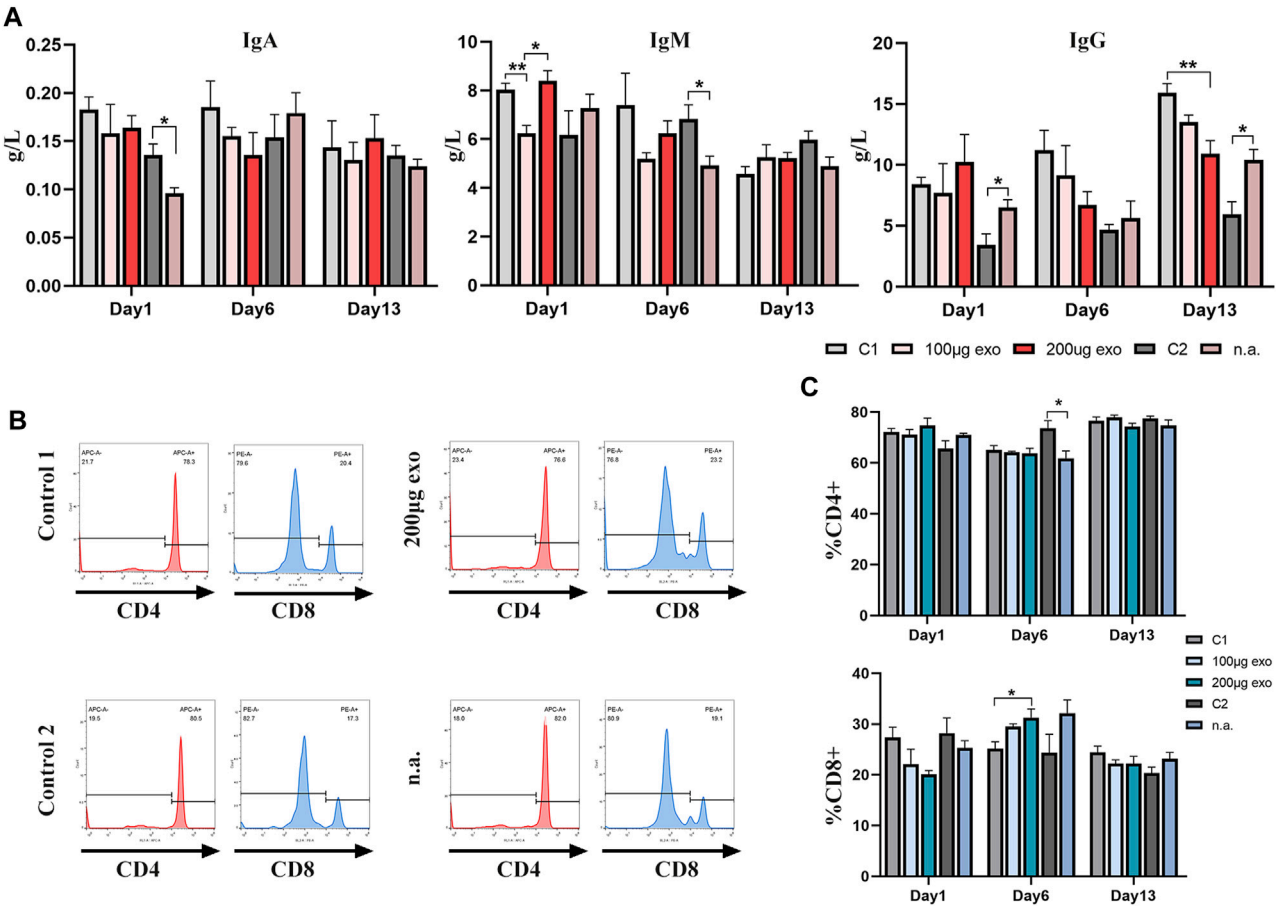

FIGURE 7
Effects of hiPSC-exosomes on humoral and cellular immunities. **(A)** Changes of IgA, IgM, and IgG contents in the four groups of rats on days 1, 6, and 13. $N = 4$ per group (*$p < 0.05$; **$p < 0.01$). **(B)** Representative histograms of tail vein and nasal administration of hiPSC-exosome groups and their control groups in flow cytometry. **(C)** Analysis of changes in the ratios of $CD4^+$ and $CD8^+$ T-cells on days 1, 6, and 13. $N = 4$ per group (*$p < 0.05$). Data are expressed as the mean ± SEM.

Pathological observation of hiPSC-exosomes in various rat organs

Next, we prepared HE-stained pathological sections from rats on days 1 and 20 to investigate whether rat organs had been influenced by the injections (Figures 6G,H). Visual observation and pathological analysis demonstrated no pathological abnormalities or inflammatory cells infiltrates in sections of the heart, liver, spleen, lungs, kidneys, or brain.

Safety evaluation of hiPSC-exosomes in terms of humoral and cellular immunities in rats

Effects on humoral and cellular immunities in rats were investigated by ELISAs and flow cytometry. On day 1, IgA contents were different between C2 and nasal administration groups. IgM showed significant differences on day 1 between 100 μg, 200 μg, and C1 groups as well as C2 and n.a. groups on day 6. IgG content showed more obvious differences on days 1 and 13 (Figure 7A).

Flow cytometry was used to measure the ratios of T-cell subsets (Figures 7B,C). The ratio of $CD4^+$ T-cells showed a difference on day 6 between C1 and n.a. groups. The ratio of $CD8^+$ T-cells between C1 and 200 μg groups showed a difference on day 6.

These data suggested that the influence of hiPSC-exosomes on humoral and cellular immunities reflected by immunoglobulins and T-cell subsets was slight and no obvious trend of negative effects was observed.

Taken together, these findings provided evidence that both administration routes of hiPSC-exosomes were safe in terms of blood components, liver and kidney functions, and organs, and had no adverse trend in humoral and cellular immunities of rats.

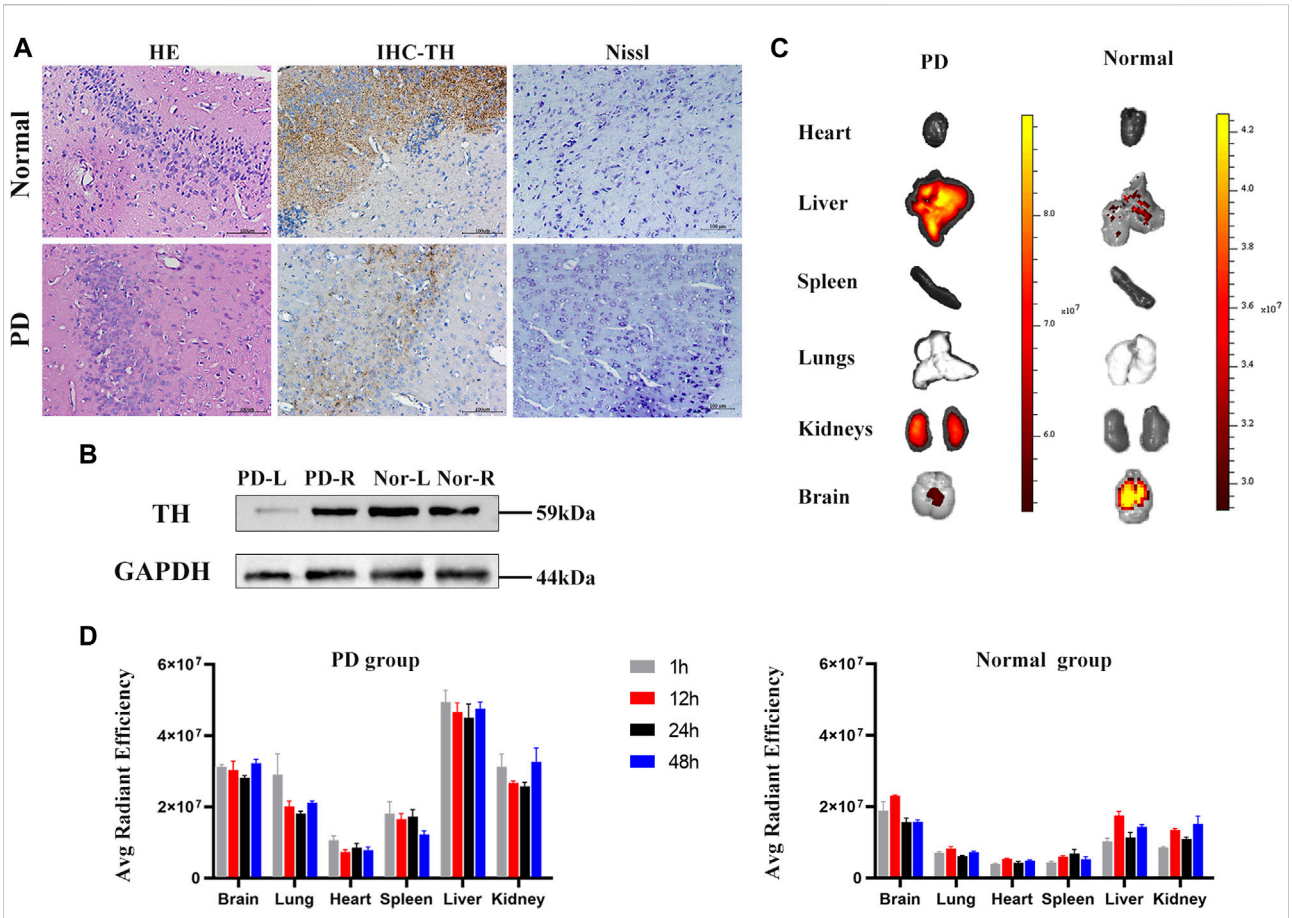

FIGURE 8
Parkinson's mouse model test and *in vivo* organ imaging. **(A)** HE staining, IHC of tyrosine hydroxylase, and Nissl-stained sections of control and PD groups. **(B)** Contents of tyrosine hydroxylase in left and right brain hemispheres of PD and control mice measured by western blotting. **(C)** Representative fluorescence images of organs in control and PD groups. **(D)** Fluorescent intensity of major organs at 1, 12, 24, and 48 h. $N = 3$ per group. Data are expressed as the mean ± SEM.

Biodistribution of hiPSC-exosomes in a mouse model of Parkinson's disease

Next, we evaluated the biodistribution of hiPSC-exosomes in a Parkinson's disease model in mice. Parkinson's disease model mice dosed after apomorphine verified for successful model establishment.

HE pathological sections, immunohistochemistry, and Nissl staining also demonstrated the reliability of the model (Figure 8A). There were differences in the contents of tyrosine hydroxylase in left and right brain hemispheres of control and Parkinson's disease model mice (Figure 8B). Immediately after sacrificing the mice, organs were harvested for fluorescence imaging.

Fluorescence images showed that labeled hiPSC-exosomes were mainly in the liver, kidneys, brain, and lungs (Figures 8C,D). The tendency of the exosome distribution was essentially consistent with a previous study (Wiklander et al., 2015). The differences between control and Parkinson's disease model mice were mostly in the brain and liver. Control mice had the highest average fluorescence in the brain, whereas the Parkinson's disease model mice had the highest average fluorescence in the liver. The average florescence of the PD group was mainly higher than that of the control group. The exosome residence time in both groups was >48 h. Therefore, the labeled hiPSC-exosomes had a different organ biodistribution between control and Parkinson's disease model mice.

Discussion

As a new regenerative medicine and drug delivery system, exosomes have received much attention in recent years. hiPSC-exosomes from pluripotent stem cells may inherit their advantages, which may enable more treatment

approaches for diseases (Jung et al., 2017; Wang, 2021; Zhou et al., 2021). Exosomes derived from hiPSCs have the potential to treat skin and eye diseases, and especially cardiovascular diseases (Germena and Hinkel, 2021). With the wide applications of hiPSC-exosomes, the establishment of a safety evaluation system is urgent and important to boost the progress of research and clinical trials.

To this end, we evaluated hiPSC-exosomes at the cell level by their influence on the cell membrane, DNA, and cell proliferation as well as the animal leave by their influence on muscle, vessels, the blood system, and humoral and cellular immunities.

First, we identified the characteristics of hiPSCs and their exosomes to ensure the accuracy of experiments. Because exosomes have the same topology as cells (Kalluri and LeBleu, 2020), exosomes pass through the cell membrane by exocytosis and not through channels. Accordingly, the interaction occurs first at the cell membrane. We used red blood cell suspension from rabbits to determine whether exosomes rupture the cell membrane and cause hemolysis. Our results indicated that hiPSC-exosomes did not affect the cell membrane. These results are consistent with a previous study on the hemolytic effect of exosomes derived from mesenchymal stem cells (Sun et al., 2016), which indicated they have the same safety profile in terms of hemolytic effects.

Exosomes enriched with miRNA, RNA, and DNA enter cells and interact with intracellular RNA and DNA (Pegtel and Gould, 2019). To investigate the influence of hiPSC-exosomes on DNA in cells, we performed an alkaline comet experiment. The findings showed that hiPSC-exosomes did not cause DNA damage in cells. A previous study found that EVs from various sources have different effects of DNA (Maji et al., 2017). Our results demonstrated the safety of hiPSC-exosomes in terms of DNA integrity.

Additionally, we assessed their influence on cell proliferation, one of the most important functions of a cell. We first confirmed that the mouse macrophage-like cell line had ability to phagocytose exosomes and the results were consistent with a related study (Xie et al., 2018). Then, we analyzed cell proliferation using Cell Counting Kit-8. The results showed that hiPSC-exosomes slightly promoted cell proliferation. This result is similar to previous findings of EVs (Somiya et al., 2018) which proved their safety in terms of normal cell proliferation. Taken together, we established relevant safety evaluations at the cell level and confirmed that hiPSC-exosomes had no adverse cellular effects.

Exosomes also have close contact with tissues, organs, and systems. For proper evaluation, appropriate methods should be chosen to deliver exosomes *in vivo*. Unlike i.p. injection, i.m. and i.v. injections better describe the effect around the injection site. We chose the quadriceps and ear veins to identify the feasibility of injection methods and effects on the surrounding tissue. The results indicated that both injection approaches were safe and did not cause lesions or inflammatory cell infiltration. Therefore, intramuscular and intravenous injections of hiPSC-exosomes are appropriate for research.

Because the blood system, organs, and humoral and cellular immunities are potential targets of exosomes, we carried out routine blood examinations, blood biochemistry, ELISAs, and flow cytometry for evaluation. Our results demonstrated that i.v. injection and nasal administration did not have adverse effect on blood components, liver and kidney functions, or organs. Some routine blood examinations and blood biochemical indicators showed significant differences at some time points, but all were within the reference ranges of a healthy rat. There were some differences in the relevant indexes of humoral and cellular immunities for both administration routes. We considered that, as a product of human cells, hiPSC-exosomes may be taken up by rat immune cells (Wan et al., 2020) and induce a response by immune cells, which influenced the immune status.

Nasal administration is a novel route of administration, especially for nanoscale particles that may avoid first-pass metabolism and gastrointestinal degradation (Cunha et al., 2017). Our results showed that nasal administration was feasible in most situations with little differences that may cause an immune cell response. A previous study reported that nasal administration might cause an immunoglobulin response (Prado et al., 2008; Jiang et al., 2022), and we also found that nasal administration of hiPSC-exosomes caused a slight immunoglobulin response.

Furthermore, we investigated the distribution characteristics of nasal administration *in vivo*. hiPSC-exosomes had a different biodistribution between control and Parkinson's disease model mice. The average fluorescence of Parkinson's disease model mice was overall higher than that in the control group. The largest difference in distribution was found in the brain and liver. A previous study showed that intranasal administration of exosomes leads to a more widespread biodistribution, and in particular, demonstrated enhanced brain accumulation over a long period (Betzer et al., 2017). Our results are consistent with previous studies with hiPSC-exosomes in the control group showing stronger accumulation in the brain. The difference in organs with the highest fluorescence intensity may be caused by modeling. Our data showed that the residence time of hiPSC-exosomes in the body was >48 h, which may facilitate determining when to perform nasal administration.

In conclusion, the safety of intravenous administration of hiPSC-exosomes has been proven at the cell level. Nasal administration as a novel approach to efficiently accumulate exosomes in the brain may be more easily accepted in the clinic. The suitable administration route needs to be determined in

accordance with the experimental requirements. The distribution, *in vivo* effects, and pharmacokinetics of hiPSC-exosomes still require be further study.

Data availability statement

The original contributions presented in the study are included in the article/Supplementary Material, further inquiries can be directed to the corresponding authors.

Ethics statement

The studies involving human participants were reviewed and approved by the Committee of Guangxi University. The patients/participants provided their written informed consent to participate in this study. The animal study was reviewed and approved by the Animal Studies Committee of Guangxi University.

Author contributions

ZQ and CT conceived the study. ZG, ZY, PS, YW and YH conducted the experiments. MZ, ZW and SZ generated and analyzed the data. ZG drafted the manuscript.

Funding

This study was supported by grants from the National Key Technology R&D Program of China (2018YFA0108304) and the National Natural Science Foundation of China (81771721 and 81971505).

Acknowledgments

We are grateful to Liangcheng Li, Yu Liu, Jianhua Yan, and Yixiang Li for their helpful discussions and technical assistance. We thank Mitchell Arico from Liwen Bianji (Edanz) (https://www.liwenbianji.cn) for editing the language of a draft of this manuscript.

Conflict of interest

Author CT is employed by Biotechcomer Co., Ltd. Author HH and author HW are employed by GuangXi TaiMeiRenSheng Biotechnology Co., LTD.

The remaining authors declare that the research was conducted in the absence of any commercial or financial relationships that could be construed as a potential conflict of interest.

Publisher's note

All claims expressed in this article are solely those of the authors and do not necessarily represent those of their affiliated organizations, or those of the publisher, the editors and the reviewers. Any product that may be evaluated in this article, or claim that may be made by its manufacturer, is not guaranteed or endorsed by the publisher.

Supplementary material

The Supplementary Material for this article can be found online at: https://www.frontiersin.org/articles/10.3389/fbioe.2022.949724/full#supplementary-material

References

Adamiak, M., Cheng, G., Bobis-Wozowicz, S., Zhao, L., Kedracka-Krok, S., Samanta, A., et al. (2018). Induced pluripotent stem cell (iPSC)-Derived extracellular vesicles are safer and more effective for cardiac repair than iPSCs. *Circ. Res.* 122 (2), 296–309. doi:10.1161/circresaha.117.311769

Aiello, S., Rocchetta, F., Longaretti, L., Faravelli, S., Todeschini, M., Cassis, L., et al. (2017). Extracellular vesicles derived from T regulatory cells suppress T cell proliferation and prolong allograft survival. *Sci. Rep.* 7 (1), 11518. doi:10.1038/s41598-017-08617-3

Betzer, O., Perets, N., Angel, A., Motiei, M., Sadan, T., Yadid, G., et al. (2017). *In vivo* neuroimaging of exosomes using gold nanoparticles. *ACS Nano* 11 (11), 10883–10893. doi:10.1021/acsnano.7b04495

Blum, B., and Benvenisty, N. (2009). The tumorigenicity of diploid and aneuploid human pluripotent stem cells. *Cell Cycle* 8 (23), 3822–3830. doi:10.4161/cc.8.23.10067

Bomba, H. N., Sheets, K. T., Valdivia, A., Khagi, S., Ruterbories, L., Mariani, C. L., et al. (2021). Personalized-induced neural stem cell therapy: Generation, transplant, and safety in a large animal model. *Bioeng. Transl. Med.* 6 (1), e10171. doi:10.1002/btm2.10171

Chen, H. X., Liang, F. C., Gu, P., Xu, B. L., Xu, H. J., Wang, W. T., et al. (2020). Exosomes derived from mesenchymal stem cells repair a Parkinson's disease model by inducing autophagy. *Cell Death Dis.* 11 (4), 288. doi:10.1038/s41419-020-2473-5

Cheng, Y., Zeng, Q., Han, Q., and Xia, W. (2019). Effect of pH, temperature and freezing-thawing on quantity changes and cellular uptake of exosomes. *Protein Cell* 10 (4), 295–299. doi:10.1007/s13238-018-0529-4

Cunha, S., Amaral, M. H., Lobo, J. M. S., and Silva, A. C. (2017). Lipid nanoparticles for nasal/intranasal drug delivery. *Crit. Rev. Ther. Drug Carr. Syst.* 34 (3), 257–282. doi:10.1615/CritRevTherDrugCarrierSyst.2017018693

Deuse, T., Hu, X., Gravina, A., Wang, D., Tediashvili, G., De, C., et al. (2019). Hypoimmunogenic derivatives of induced pluripotent stem cells evade immune rejection in fully immunocompetent allogeneic recipients. *Nat. Biotechnol.* 37 (3), 252–258. doi:10.1038/s41587-019-0016-3

Doi, D., Magotani, H., Kikuchi, T., Ikeda, M., Hiramatsu, S., Yoshida, K., et al. (2020). Pre-clinical study of induced pluripotent stem cell-derived dopaminergic progenitor cells for Parkinson's disease. *Nat. Commun.* 11 (1), 3369. doi:10.1038/s41467-020-17165-w

Dong, X., Xu, S. B., Chen, X., Tao, M., Tang, X. Y., Fang, K. H., et al. (2021). Human cerebral organoids establish subcortical projections in the mouse brain after transplantation. *Mol. Psychiatry* 26 (7), 2964–2976. doi:10.1038/s41380-020-00910-4

Franzen, C. A., Simms, P. E., Van Huis, A. F., Foreman, K. E., Kuo, P. C., and Gupta, G. N. (2014). Characterization of uptake and internalization of exosomes by bladder cancer cells. *Biomed. Res. Int.* 2014, 1–11. doi:10.1155/2014/619829

Germena, G., and Hinkel, R. (2021). iPSCs and exosomes: Partners in crime fighting cardiovascular diseases. *J. Pers. Med.* 11 (6), 529. doi:10.3390/jpm11060529

Ghosh, S., Garg, S., and Ghosh, S. (2020). Cell-derived exosome therapy: A novel approach to treat post-traumatic brain injury mediated neural injury. *ACS Chem. Neurosci.* 11 (14), 2045–2047. doi:10.1021/acschemneuro.0c00368

Guan, P., Liu, C., Xie, D., Mao, S., Ji, Y., Lin, Y., et al. (2022). Exosome-loaded extracellular matrix-mimic hydrogel with anti-inflammatory property Facilitates/promotes growth plate injury repair. *Bioact. Mat.* 10, 145–158. doi:10.1016/j.bioactmat.2021.09.010

Guo, S., Perets, N., Betzer, O., Ben-Shaul, S., Sheinin, A., Michaelevski, I., et al. (2019). Intranasal delivery of mesenchymal stem cell derived exosomes loaded with phosphatase and tensin homolog siRNA repairs complete spinal cord injury. *ACS Nano* 13 (9), 10015–10028. doi:10.1021/acsnano.9b01892

Gyori, B. M., Venkatachalam, G., Thiagarajan, P. S., Hsu, D., and Clement, M. V. (2014). OpenComet: An automated tool for comet assay image analysis. *Redox Biol.* 2, 457–465. doi:10.1016/j.redox.2013.12.020

Han, M. J., Annunziata, I., Weesner, J., Campos, Y., Salie, M., O'Reilly, C., et al. (2020). Generation of human induced pluripotent stem cells (hIPSCs) from sialidosis types I and II patients with pathogenic neuraminidase 1 mutations. *Stem Cell Res.* 46, 101836. doi:10.1016/j.scr.2020.101836

He, D., Zhang, J., Wu, W., Yi, N., He, W., Lu, P., et al. (2019). A novel immunodeficient rat model supports human lung cancer xenografts. *FASEB J.* 33 (1), 140–150. doi:10.1096/fj.201800102RR

Henriques, F., Bedard, A. H., Guilherme, A., Kelly, M., Chi, J., Zhang, P., et al. (2020). Single-cell RNA profiling reveals adipocyte to macrophage signaling sufficient to enhance thermogenesis. *Cell Rep.* 32 (5), 107998. doi:10.1016/j.celrep.2020.107998

Hicks, D. A., Jones, A. C., Corbett, N. J., Fisher, K., Pickering-Brown, S. M., Ashe, M. P., et al. (2020). Extracellular vesicles isolated from human induced pluripotent stem cell-derived neurons contain a transcriptional network. *Neurochem. Res.* 45 (7), 1711–1728. doi:10.1007/s11064-020-03019-w

Itakura, G., Kawabata, S., Ando, M., Nishiyama, Y., Sugai, K., Ozaki, M., et al. (2017). Fail-safe system against potential tumorigenicity after transplantation of iPSC derivatives. *Stem Cell Rep.* 8 (3), 673–684. doi:10.1016/j.stemcr.2017.02.003

Jiang, L., Driedonks, T. A. P., Jong, W. S. P., Dhakal, S., Bart van den Berg van Saparoea, H., Sitaras, I., et al. (2022). A bacterial extracellular vesicle-based intranasal vaccine against SARS-CoV-2 protects against disease and elicits neutralizing antibodies to wild-type and Delta variants. *J. Extracell. Vesicles* 11 (3), e12192. doi:10.1002/jev2.12192

Jung, J. H., Fu, X., and Yang, P. C. (2017). Exosomes generated from iPSC-derivatives: New direction for stem cell therapy in human heart diseases. *Circ. Res.* 120 (2), 407–417. doi:10.1161/circresaha.116.309307

Kalluri, R., and LeBleu, V. S. (2020). The biology, function, and biomedical applications of exosomes. *Science* 367 (6478), eaau6977. doi:10.1126/science.aau6977

Kobayashi, H., Ebisawa, K., Kambe, M., Kasai, T., Suga, H., Nakamura, K., et al. (2018). <Editors' Choice> Effects of exosomes derived from the induced pluripotent stem cells on skin wound healing. *Nagoya J. Med. Sci.* 80 (2), 141–153. doi:10.18999/nagjms.80.2.141

Liu, Q. W., Huang, Q. M., Wu, H. Y., Zuo, G. S., Gu, H. C., Deng, K. Y., et al. (2021). Characteristics and therapeutic potential of human amnion-derived stem cells. *Int. J. Mol. Sci.* 22 (2), 970. doi:10.3390/ijms22020970

Maji, S., Yan, I. K., Parasramka, M., Mohankumar, S., Matsuda, A., and Patel, T. (2017). *In vitro* toxicology studies of extracellular vesicles. *J. Appl. Toxicol.* 37 (3), 310–318. doi:10.1002/jat.3362

Niu, J., Xie, J., Guo, K., Zhang, X., Xia, F., Zhao, X., et al. (2018). Efficient treatment of Parkinson's disease using ultrasonography-guided rhFGF20 proteoliposomes. *Drug Deliv. (Lond).* 25 (1), 1560–1569. doi:10.1080/10717544.2018.1482972

Osnato, A., Brown, S., Krueger, C., Andrews, S., Collier, A. J., Nakanoh, S., et al. (2021). TGFβ signalling is required to maintain pluripotency of human naïve pluripotent stem cells. *Elife* 10, e67259. doi:10.7554/eLife.67259

Pan, X., Chen, C., Huang, J., Wei, H., and Fan, Q. (2015). Neuroprotective effect of combined therapy with hyperbaric oxygen and madopar on 6-hydroxydopamine-induced Parkinson's disease in rats. *Neurosci. Lett.* 600, 220–225. doi:10.1016/j.neulet.2015.06.030

Parada, N., Romero-Trujillo, A., Georges, N., and Alcayaga-Miranda, F. (2021). Camouflage strategies for therapeutic exosomes evasion from phagocytosis. *J. Adv. Res.* 31, 61–74. doi:10.1016/j.jare.2021.01.001

Pegtel, D. M., and Gould, S. J. (2019). Exosomes. *Annu. Rev. Biochem.* 88, 487–514. doi:10.1146/annurev-biochem-013118-111902

Prado, N., Marazuela, E. G., Segura, E., Fernández-García, H., Villalba, M., Théry, C., et al. (2008). Exosomes from bronchoalveolar fluid of tolerized mice prevent allergic reaction. *J. Immunol.* 181 (2), 1519–1525. doi:10.4049/jimmunol.181.2.1519

Pužar Dominkuš, P., Stenovec, M., Sitar, S., Lasič, E., Zorec, R., Plemenitaš, A., et al. (2018). PKH26 labeling of extracellular vesicles: Characterization and cellular internalization of contaminating PKH26 nanoparticles. *Biochimica Biophysica Acta - Biomembr.* 1860 (6), 1350–1361. doi:10.1016/j.bbamem.2018.03.013

Qi, D., Deng, W., Chen, X., Fan, S., Peng, J., Tang, X., et al. (2022). Adipose-derived circulating exosomes promote protection of the pulmonary endothelial barrier by inhibiting EndMT and oxidative stress through down-regulation of the TGF-β pathway: A potential explanation for the obesity paradox in ards. *Oxid. Med. Cell. Longev.* 2022, 1–25. doi:10.1155/2022/5475832

Rao, L., Qian, Y., Khodabukus, A., Ribar, T., and Bursac, N. (2018). Engineering human pluripotent stem cells into a functional skeletal muscle tissue. *Nat. Commun.* 9 (1), 126. doi:10.1038/s41467-017-02636-4

Roth, J. G., Muench, K. L., Asokan, A., Mallett, V. M., Gai, H., Verma, Y., et al. (2020). 16p11.2 microdeletion imparts transcriptional alterations in human iPSC-derived models of early neural development. *Elife* 9, e58178. doi:10.7554/eLife.58178

Schweitzer, J. S., Song, B., Herrington, T. M., Park, T. Y., Lee, N., Ko, S., et al. (2020). Personalized iPSC-derived dopamine progenitor cells for Parkinson's disease. *N. Engl. J. Med. Overseas. Ed.* 382 (20), 1926–1932. doi:10.1056/NEJMoa1915872

Singh, N. P., McCoy, M. T., Tice, R. R., and Schneider, E. L. (1988). A simple technique for quantitation of low levels of DNA damage in individual cells. *Exp. Cell Res.* 175 (1), 184–191. doi:10.1016/0014-4827(88)90265-0

Somiya, M., Yoshioka, Y., and Ochiya, T. (2018). Biocompatibility of highly purified bovine milk-derived extracellular vesicles. *J. Extracell. Vesicles* 7 (1), 1440132. doi:10.1080/20013078.2018.1440132

Song, B., Cha, Y., Ko, S., Jeon, J., Lee, N., Seo, H., et al. (2020). Human autologous iPSC-derived dopaminergic progenitors restore motor function in Parkinson's disease models. *J. Clin. Invest.* 130 (2), 904–920. doi:10.1172/jci130767

Steines, L., Poth, H., Schuster, A., Amann, K., Banas, B., and Bergler, T. (2021). Disruption of tfh:B cell interactions prevents antibody-mediated rejection in a kidney transplant model in rats: Impact of calcineurin inhibitor dose. *Front. Immunol.* 12, 657894. doi:10.3389/fimmu.2021.657894

Stoddard-Bennett, T., and Reijo Pera, R. (2019). Treatment of Parkinson's disease through personalized medicine and induced pluripotent stem cells. *Cells* 8 (1), 26. doi:10.3390/cells8010026

Sun, L., Xu, R., Sun, X., Duan, Y., Han, Y., Zhao, Y., et al. (2016). Safety evaluation of exosomes derived from human umbilical cord mesenchymal stromal cell. *Cytotherapy* 18 (3), 413–422. doi:10.1016/j.jcyt.2015.11.018

Sun, N. N., Zhang, Y., Huang, W. H., Zheng, B. J., Jin, S. Y., Li, X., et al. (2021a). Macrophage exosomes transfer angiotensin II type 1 receptor to lung fibroblasts mediating bleomycin-induced pulmonary fibrosis. *Chin. Med. J. Engl.* 134 (18), 2175–2185. doi:10.1097/cm9.0000000000001605

Sun, X., Yu, X., Zhang, L., Zhao, W., Wang, M., Zhang, Y., et al. (2021b). Comparison of the expression and toxicity of AAV2/9 carrying the human A53T α-synuclein gene in presence or absence of WPRE. *Heliyon* 7 (2), e06302. doi:10.1016/j.heliyon.2021.e06302

Takahashi, K., and Yamanaka, S. (2006). Induction of pluripotent stem cells from mouse embryonic and adult fibroblast cultures by defined factors. *Cell* 126 (4), 663–676. doi:10.1016/j.cell.2006.07.024

Wan, Z., Zhao, L., Lu, F., Gao, X., Dong, Y., Zhao, Y., et al. (2020). Mononuclear phagocyte system blockade improves therapeutic exosome delivery to the myocardium. *Theranostics* 10 (1), 218–230. doi:10.7150/thno.38198

Wang, A. Y. L. (2021). Human induced pluripotent stem cell-derived exosomes as a new therapeutic strategy for various diseases. *Int. J. Mol. Sci.* 22 (4), 1769. doi:10.3390/ijms22041769

Wang, S., Hou, Y., Li, X., Song, Z., Sun, B., Li, X., et al. (2020). Comparison of exosomes derived from induced pluripotent stem cells and mesenchymal stem cells

as therapeutic nanoparticles for treatment of corneal epithelial defects. *Aging (Albany NY)* 12 (19), 19546–19562. doi:10.18632/aging.103904

Wang, Y., Zhang, L., Li, Y., Chen, L., Wang, X., Guo, W., et al. (2015). Exosomes/microvesicles from induced pluripotent stem cells deliver cardioprotective miRNAs and prevent cardiomyocyte apoptosis in the ischemic myocardium. *Int. J. Cardiol.* 192, 61–69. doi:10.1016/j.ijcard.2015.05.020

Ward, E., Twaroski, K., and Tolar, J. (2017). Feeder-free derivation of naive human pluripotent stem cells. *Stem Cells Dev.* 26 (15), 1087–1089. doi:10.1089/scd.2017.0067

Wiklander, O. P., Nordin, J. Z., O'Loughlin, A., Gustafsson, Y., Corso, G., Mäger, I., et al. (2015). Extracellular vesicle *in vivo* biodistribution is determined by cell source, route of administration and targeting. *J. Extracell. Vesicles* 4, 26316. doi:10.3402/jev.v4.26316

Wu, J. Y., Li, Y. J., Hu, X. B., Huang, S., and Xiang, D. X. (2021). Preservation of small extracellular vesicles for functional analysis and therapeutic applications: A comparative evaluation of storage conditions. *Drug Deliv. (Lond).* 28 (1), 162–170. doi:10.1080/10717544.2020.1869866

Xie, Z., Wang, X., Liu, X., Du, H., Sun, C., Shao, X., et al. (2018). Adipose-derived exosomes exert proatherogenic effects by regulating macrophage foam cell formation and polarization. *J. Am. Heart Assoc.* 7 (5), e007442. doi:10.1161/jaha.117.007442

Yang, S., Liu, Q., Chen, S., Zhang, F., Li, Y., Fan, W., et al. (2022). Extracellular vesicles delivering nuclear factor I/C for hard tissue engineering: Treatment of apical periodontitis and dentin regeneration. *J. Tissue Eng.* 13, 1. doi:10.1177/20417314221084095

Yi, Y. W., Lee, J. H., Kim, S. Y., Pack, C. G., Ha, D. H., Park, S. R., et al. (2020). Advances in analysis of biodistribution of exosomes by molecular imaging. *Int. J. Mol. Sci.* 21 (2), 665. doi:10.3390/ijms21020665

Zhou, Y., Gao, Y., Zhang, W., Chen, Y., Jin, M., and Yang, Z. (2021). Exosomes derived from induced pluripotent stem cells suppresses M2-type macrophages during pulmonary fibrosis via miR-302a-3p/TET1 axis. *Int. Immunopharmacol.* 99, 108075. doi:10.1016/j.intimp.2021.108075

frontiers | Frontiers in Bioengineering and Biotechnology

TYPE Original Research
PUBLISHED 06 September 2022
DOI 10.3389/fbioe.2022.994628

OPEN ACCESS

EDITED BY
Long Wu,
University of Maryland, Baltimore,
United States

REVIEWED BY
Weinan Guo,
Fourth Military Medical University, China
Dan Lv,
Sichuan University, China

*CORRESPONDENCE
Suxia Han,
shan87@mail.xjtu.edu.cn

SPECIALTY SECTION
This article was submitted to Biomaterials,
a section of the journal
Frontiers in Bioengineering and Biotechnology

RECEIVED 15 July 2022
ACCEPTED 11 August 2022
PUBLISHED 06 September 2022

CITATION
Zhao Q, Luo X, Li H, Bai Y, Chen Q, Yang M, Pei B, Xu C and Han S (2022), Targeting EIF3C to suppress the development and progression of nasopharyngeal carcinoma.
Front. Bioeng. Biotechnol. 10:994628.
doi: 10.3389/fbioe.2022.994628

Targeting EIF3C to suppress the development and progression of nasopharyngeal carcinoma

Qian Zhao[1], Xuehui Luo[2], Honghui Li[1], Yanxia Bai[1], Qian Chen[1], Ming Yang[1], Bei Pei[1], Chongwen Xu[1] and Suxia Han[2]*

[1]Department of Otorhinolaryngology Head and Neck Surgery, The First Affiliated Hospital of Xi'an Jiaotong University, Xi'an, Shaanxi, China, [2]Department of Radiation Oncology, The First Affiliated Hospital of Xi'an Jiaotong University, Xi'an, Shaanxi, China

Nasopharyngeal carcinoma occurs in many parts of the pars nasalis pharyngis, and the pathological type is mainly squamous cell carcinoma. Because of the special position of nasopharynx, breathing, pronunciation and daily life will be seriously affected. At present, the research direction of nasopharyngeal carcinoma is mainly to explore the law of tumor cell proliferation and migration, study the molecular mechanism, master its biological behavior and clinical significance, try to find therapeutic targets, and further improve the level of tumor treatment. However, the pathologic structure and molecular mechanism of nasopharyngeal carcinoma have not been fully elucidated. In this study, the Lentivirus-mediated EIF3C shRNA vector (L.V-shEIF3C) was constructed to down-regulate the expression of EIF3C in human pharyngeal squamous carcinoma cell FaDu and the human nasopharyngeal carcinoma cell 5-8F, it was found that down-regulation of EIF3C could significantly inhibit the cell proliferation, promote cell apoptosis, induce cell cycle arrest, and inhibit the formation and growth of tumors in mouse models. This study provides strong evidence that EIF3C is a key gene driving the development and progression of head and neck cancer, which is of great significance for the diagnosis, prognosis or treatment of tumors, suggesting that EIF3C may become a valuable therapeutic development and intervention target.

KEYWORDS

EIF3C, cancer therapy, head and neck cancer, pharyngeal cancer, nucleic acid drug

Introduction

Head and neck cancer is the sixth most common malignant tumor in the world (Hsieh et al., 2019). According to statistics, there were about 700,000 cases and 350,000 deaths of lip, oral, oropharyngeal, and hypopharyngeal cancers worldwide in 2020 (Sung et al., 2021). Nasopharyngeal carcinoma (NPC) and head and neck squamous cell carcinoma (HNSCC) were broadly defined as head and neck cancer (HNC) (Luo et al., 2018). The pathological types of head and neck tumors were mainly squamous cell carcinoma, which can occur in many parts of head and neck, including larynx, thyroid, nasopharynx, and maxillofacial (Johnson et al., 2020). Although head and neck tumors account for only

about 4% of malignancies in all parts of the body, a wide range of symptoms can occur in this relatively small area (Aupérin, 2020). The head and neck organs were inextricably linked to vital basic physiological functions, including appearance, expression, breathing, nutrition and social interaction (Kristensen et al., 2020). Different sites, tumor size, invasion mode and treatment complications of head and neck tumors may lead to different degrees of structural damage and dysfunction, which can significantly reduce the quality of life of patients (Gavrielatou et al., 2020).

Oral squamous cell carcinoma is the most common and malignant oral-maxillofacial tumor, which etiology has certain relevance with bad habits, and may be associated with excess of alcohol, tobacco, and nutritional factors (Kawakita and Matsuo, 2017). Furthermore, the cancer cells generally have low differentiation, strong invasion and metastasis ability making early detection difficult, which results in the middle and late stage at the time of diagnosis (Saloura et al., 2013). In addition, there are many tissues around the larynx and throat, and lymphatic tissue is unusually rich, leading to lymph node tissue metastasis in the early stage of malignant tumor. Studies have shown that about 50% patients had the surrounding lymph node metastasis, the 5 years survival rate less than 50% (Horton et al., 2019).

Nasopharyngeal carcinoma (NPC) is a malignant tumor originating from the mucosal epithelium of the nasopharynx, and is also a common head and neck tumor (Lam and Chan, 2018). According to the latest classification of WHO, NPC is divided into two histological subtypes: non-keratinocarcinoma (differentiated or undifferentiated) and keratinized squamous cell carcinoma (Chen et al., 2019). Compared with common squamous cell carcinoma of the head and neck, nasopharyngeal carcinoma has characteristic clinical manifestations, which is sensitive to radiotherapy and chemotherapy, and has a better prognosis. With the emphasis on the development of radiotherapy technology and the optimization of chemotherapy regimen, the local regional control rate of Nasopharyngeal carcinoma has been significantly improved, but there are still 3%–27% patients with treatment failure (Liao et al., 2020; Rosenberg, 2020; Huang et al., 2021).

Protein synthesis is a complex, multi-step, precisely regulated process of gene translation, which is divided into three stages: initiation, extension and termination. The initiation stage of translation is the most complex stage in the whole translation process, and its core is the initiation control of translation (Jackson et al., 2010). Eukaryotic translation initiation factors (EIFs) are a series of proteins involved in the initiation of eukaryotic protein translation. EIFs interacts with other EIFs, messenger RNA, transport RNA and ribosomes to form a complex interaction network system to participate the initiation of eukaryotic translation. Currently, there are 12 known EIFs, among which eukaryotic translation initiation factor 3 (EIF3), with a molecular weight of about 650 kDa, is the largest and most complex eukaryotic translation initiation factor, specifically involved in the targeted regulation of cell cycle, differentiation, apoptosis, and other biological processes (Lee et al., 2015; Robichaud et al., 2019). Meanwhile, more and more studies have found that EIFs is closely related to the occurrence and development of human diseases, especially tumors. Among them, the core subunit C of eukaryotic translation initiation factor 3 (EIF3C) has been found to be significantly overexpressed in a variety of tumors, including osteosarcoma, cervical cancer, liver cancer and breast cancer (Li et al., 2017; Zhao et al., 2017; Gao et al., 2019; Hu et al., 2019). However, the specific mechanism of EIF3C in head and neck cancer is still unclear.

In order to clarify the biological function of EIF3C in head and neck cancer, this study constructed EIF3C-shRNA lentvirus and inhibited the expression of EIF3C to study the biological effects of EIF3C on the proliferation, growth and apoptosis of FaDu and 5-8F cells. This study provides a theoretical basis for further understanding the molecular mechanism of EIF3C in the occurrence and development of head and neck cancer, and also provides a potential new target for the treatment of head and neck cancer.

Materials and methods

General remarks

Minimum essential medium (MEM), RPMI-1640 medium, phosphate buffer saline (PBS), fetal bovine serum (FBS), penicillin streptomycin (Pen Strep), and TRIzol™Reagent were purchased from Fisher Scientific Ltd. Other chemicals used in this study were purchased from Sigma-Aldrich unless otherwise specified.

Cell culture

The human pharyngeal squamous carcinoma cell line FaDu and the human nasopharyngeal carcinoma cell line 5-8F were purchased from the national Biomedical Cell Resource (BMCR, China). Fadu cells were cultured in MEM medium supplemented with 10% FBS and 1% Pen Strep, 5-8F cells were cultered in RPMI-1640 medium supplemented with 10% FBS and 1% Pen Strep, the two cells were incubated at 37°C in 5% CO_2.

Lentiviral-mediated shRNA vector and infection

The lentiviral-mediated EIF3C shRNA vector (L.v-shEIF3C), the negative control shRNA vector (L.v-shCtrl) and transfection reagent Polybrene were purchased from GenePharma (Shanghai, China). 1×10^6 FaDu or 5–8F cells were plated into 6-well plates and were infected with L.v-shEIF3C (MOI = 50) or L.v-shCtrl

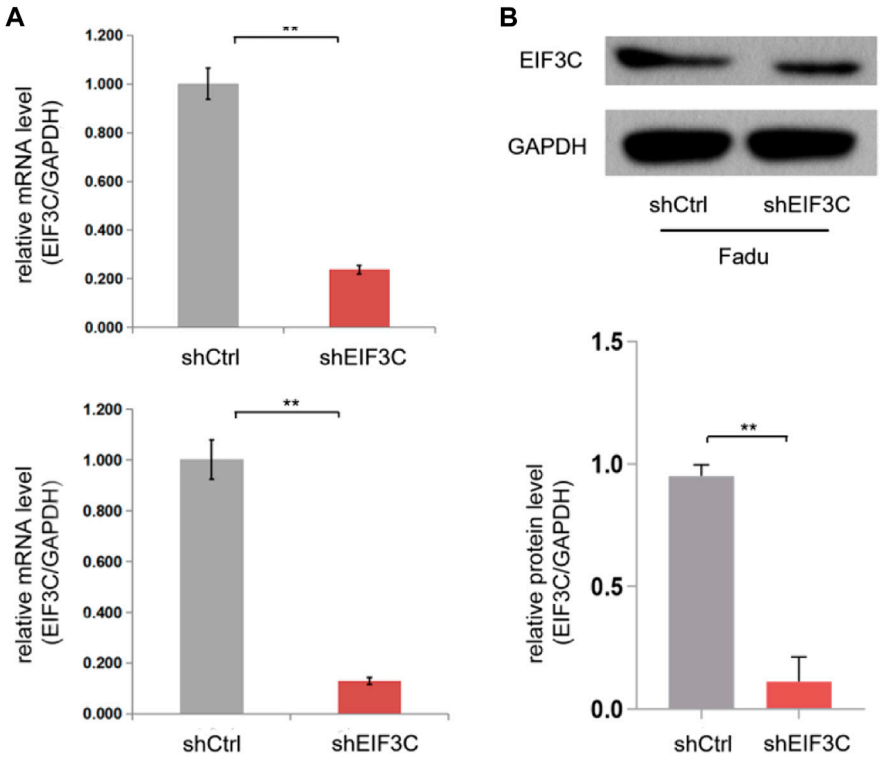

FIGURE 1
The L.v-shEIF3C decreased the expression of EIF3C in FaDu and 5-8F cells. **(A)** qRT-PCR analysis showed that the L.v-shEIF3C significantly decreased the mRNA expression of EIF3C in FaDu and 5-8F cells. **(B)** Western blot showed that the L.v-shEIF3C significantly decreased the protein expression of EIF3C in FaDu cells, the grey scale of the protein bands was analyzed with ImageJ software. The data is the means ± SDs of three independent experiments. The differences were statistically significant. $^{**}p < 0.01$.

(MOI = 50) respectively when the cell density reached 30%–40%, 12 h after infection, the medium was replaced with conventional complete medium, 72 h after infection, the cells can be used to the subsequent experiments when transduction efficiency reached 70% or more. The EIF3C and negative control shRNA sequence was as follows:

L.v-shEIF3C: 5′-CCATCCGTAATGCCATGAA-3′.
L.v-shCtrl: 5′-TTCTCCGAACGTGTCACGT-3′.

RNA extraction and quantitative real-time PCR

The total RNA of cells was isolated by Trizol method, and the concentration and purity of which were detected by ultraviolet spectrophotometer. Then, RNA was converted into complementary DNA (cDNA) first with RevertAid First Strand cDNA Synthesis Kit and DNase I (Thermo Scientific™). QRT-PCR was conducted using TB Green qPCR Master Mix (Takara) with LightCycler® 2.0 Real-time PCR System.

The primer sequences of EIF3C were as follows: 5′-AGATGA GGATGAGGATGAGGAC-3′ (forward) and 5′- GGAATCGGA AGATGTGGAACC-3′ (reverse); the primer sequences of GAPDH were as follows: 5′-TGACTTCAACAGCGACACCCA-3′ (forward) and 5′-CACCCTGTTGCTGTAGCCAAA-3′ (reverse).

Western blot

The total protein of cells was extracted by radio-immune precipitation assay (RIPA) lysis buffer adding protease inhibitors PMSF (Beyotime, China) at a ratio of 100:1 (v/v), the protein concentration was detected by BCA reagent kit (Beyotime). To denature protein, mixing the protein sample with 5× loading buffer at ratio of 4:1 (v/v), boiling the mixed solution at 100°C for 10 min. Then, 30 μg of total protein was loaded into the wells of SDS-PAGE gel to separate, after running time, the gel was transferred to polyvinylidene difluoride (PVDF) membrane and the proteins were detected by different antibodies including antibodies against EIF3C (Abcam, United States) and GAPDH (Proteintech, China). An anti-mouse horseradish peroxidase antibody was used as a secondary antibody. Finally, the PVDF membranes were imaged

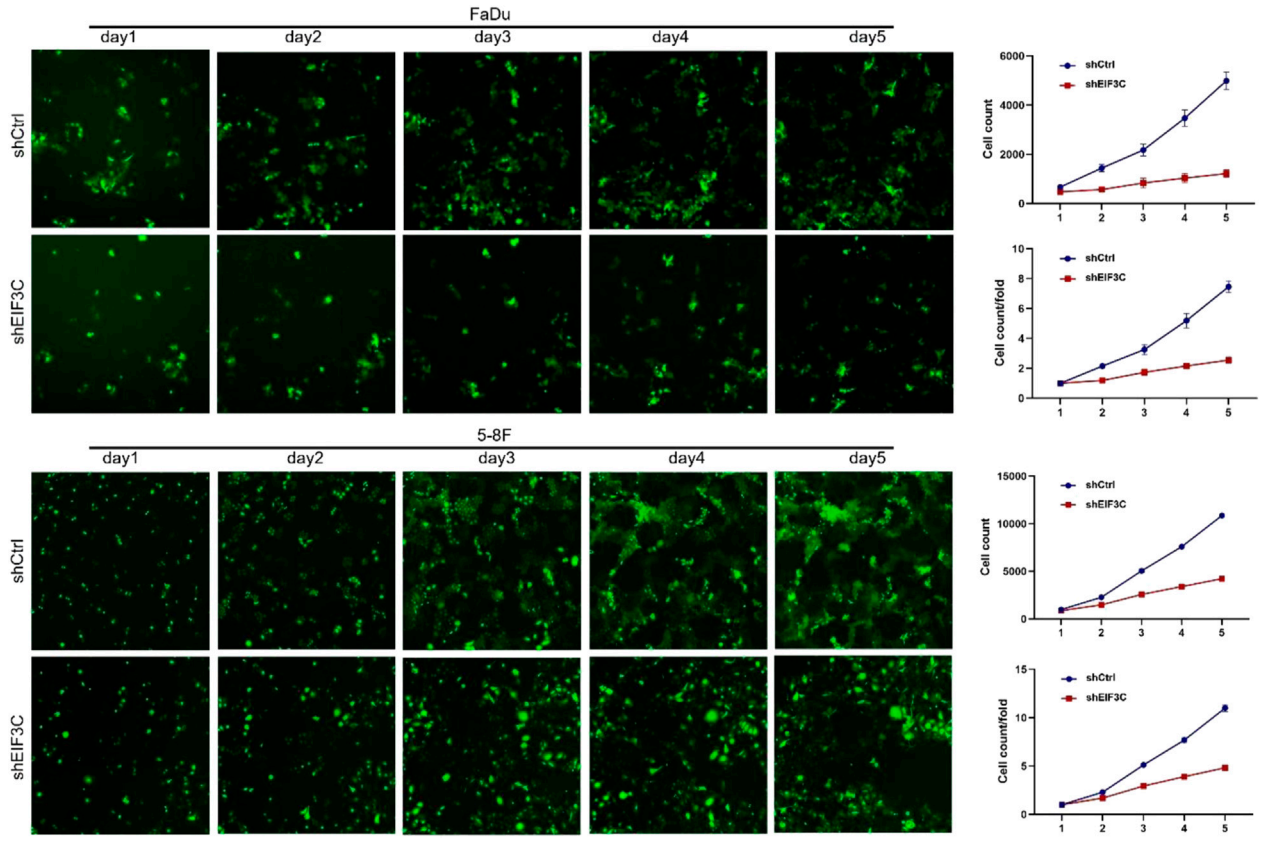

FIGURE 2
The L.v-shEIF3C inhibited the proliferation of FaDu and 5-8F cells in cell growth assay. For five consecutive days, the images and the statistics exhibited that the number of cells with fluorescence in the L.v-shEIF3C group was less than that in the L.v-shCtrl group. The differences were statistically significant.

with the enhanced chemiluminescence reagent (ECL, Millipore) by a chemiluminometer (BioRad, United States).

Cell growth assay

2×10^3 FaDu and 5-8F cells infected with L.v-shEIF3C or L.v-shCtrl were planted in 96-well plate and incubated overnight, each group had three replicates. The plate was read and the cells were photographed by Cellomics (Thermo) for five consecutive days, to accurately calculate the number of cells with green fluorescence in hole plates by adjusting the input parameters of Cellomics ArrayScan, the data were statistically plotted and the 5-days cell proliferation curve was drawn.

Colony formation assay

The FaDu and 5-8F cells infected with L.v-shEIF3C or L.v-shCtrl were counted, and each group 500 cells were plated in six-well plates with three replicates. After 2 weeks of culture, the cell colonies were fixed with methanol for 20 min and were subsequently stained with a 0.5% crystal violet staining solution for 20 min. Finally, the cell colonies were photographed and counted.

BrdU cell proliferation assay

4×10^4 FaDu cells infected with L.v-shEIF3C or L.v-shCtrl were seeded at varying density in serum free medium in a 96-well plate and incubated overnight, then the medium was replaced with complete medium adding 10% serum and the cells were incubated for 24 h. Next, 10 μl bromodeoxyuridine (BrdU, Merck) was added to the plate and cells were incubated for 4 h, after removing labeling medium, cells were fixed by FixDenat 200 μl/well for 30 min, a BrdU mouse mAb was then added to detect the incorporated BrdU, and substrate solution was added to develop color. Finally, the magnitude of the absorbance for the developed color can be detected at 450 nm with a microplate reader (Tecan infinite).

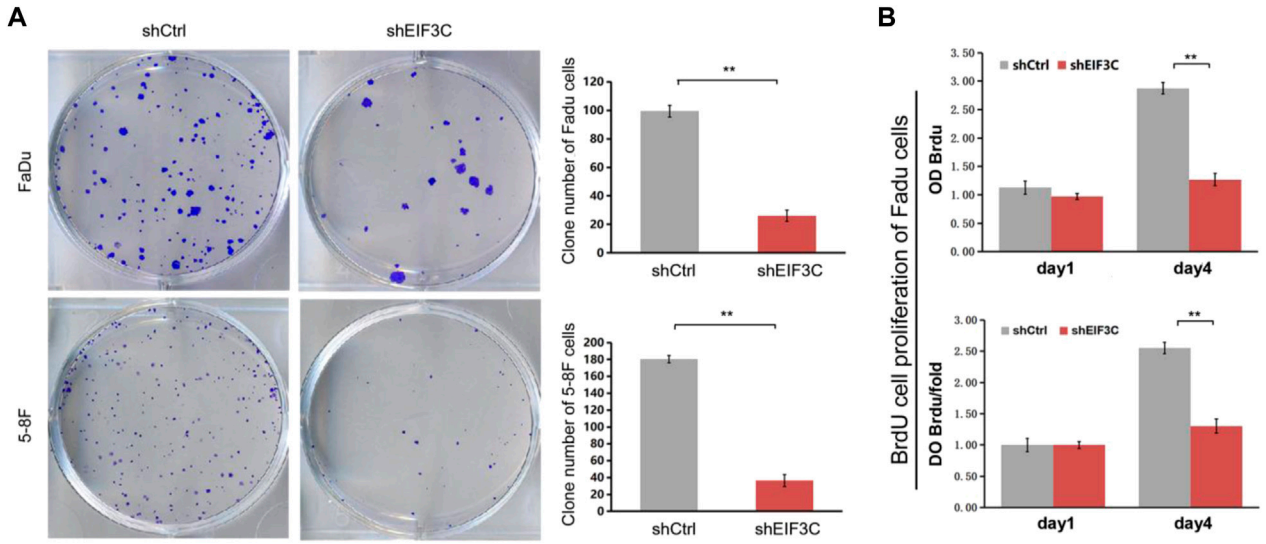

FIGURE 3
The L.v-shEIF3C inhibited the proliferation of FaDu and 5-8F cells in Colony formation assay and BrdU cell proliferation assay. **(A)** The images and the statistics exhibited that the number of clone cells in the L.v-shEIF3C group was less than that in the L.v-shCtrl group. **(B)** The magnitude of the absorbance for the developed color in the L.v-shCtrl group was greater than that in the L.v-shEIF3C group detected at 450 nm. The data is the means ± SDs of three independent experiments. The differences were statistically significant. $^{**}p < 0.01$.

Cell cycle analysis with flow cytometry

2×10^5 FaDu and 5-8F cells infected with L.v-shEIF3C or L.v-shCtrl were planted in 6-well plate and incubated for 48 h, the cells were collected and fixed with 70% ice-cold ethanol overnight, then stained with 0.3 ml PI/RNase Staining Buffer (BD Biosciences) for 15 min and analyzed by flow cytometry.

Apoptosis analysis with flow cytometry

FaDu and 5-8F cells infected with L.v-shEIF3C or L.v-shCtrl were collected and washed twice with cold PBS and then resuspended in 1X Binding Buffer at a concentration of ~1×10^6 cells/ml, then stained with 5 μl Annexin V and 5 μl Vital Dye 7-AAD (BD Biosciences) for 15 min in the dark and analyzed by flow cytometry.

PathScan sandwich ELISA

Using Cell Signaling Technology (CST) PathScan® Antibody Array Kit to detect and compare the changes of key signal molecules in the signal pathway in the samples. FaDu cells infected with L.v-shEIF3C or L.v-shCtrl were collected and lysed by cell lysate plus protease inhibitor, the cell lysate was then added to the prepared test well plate, 70 μl per well at 4 Covernight. After the cell samples were removed on the second day, the plate was washed three times with PBS buffer, and then 1X antibody detection mixture was added for incubating at room temperature, after 1 h, the plate was cleaned again, 1X HRP-linked streptomavidin was subsequently added for incubating for 0.5 h. Finally, chemiluminescence was performed.

FaDu cell line derived tumor xenograft mouse model

Four-week-old female BALB/c nude mice were purchased from Beijing Vital River Laboratory Animal Technology (Beijing, China). The nude mice were randomly divided into two groups, each group had 10 mice. FaDu cells were transfected with L.v-shEIF3C or L.v-shCtrl according to Multiplicity of Infection (MOI) 50:1 for 4 days. Then, the cells were collected and resuspended in PBS at a concentration of 2×10^7 cells/ml, we subcutaneously injected 200 μl cell suspension into the back of the nude mice. After 14 days, we measured the longest and shortest diameters of tumors every 4 days with calipers, which were, respectively, recorded as L and W, and the tumor volumes were calculated as $V = L \times W^2 \times 0.5$. After 32 days, before the mice were sacrificed, we used a small-animal *in vivo* imaging system to detect the fluorescence of tumors in nude mice, and then the mice were photographed, the tumors were taking out and weighted.

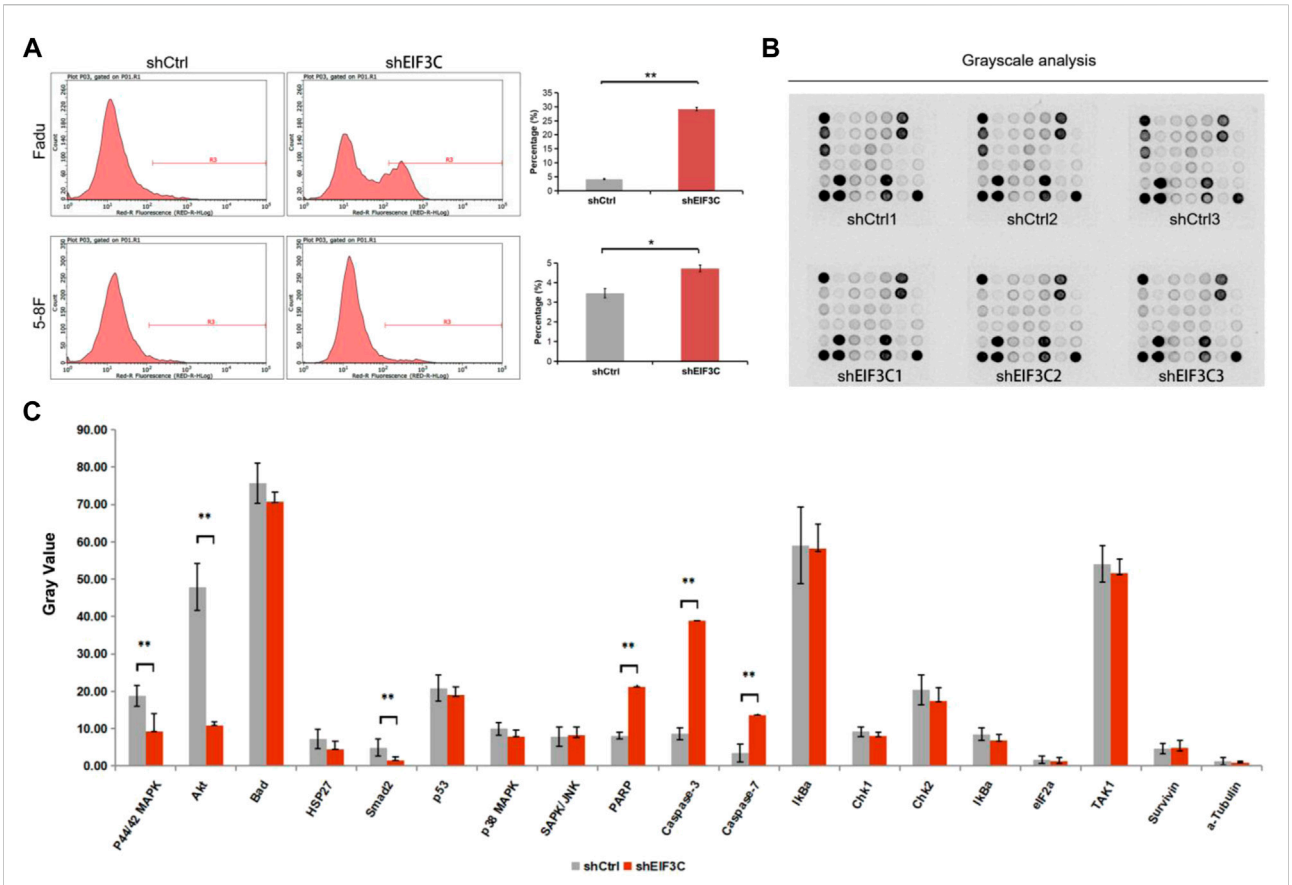

FIGURE 4
The L.v-shEIF3C promoted the apoptosis of FaDu and 5-8F cells. **(A)** The flow cytometry analysis showed that the apoptotic cells in the L.v-shEIF3C group were more than that in the L.v-shCtrl group. **(B)** Images were captured by exposing the slide slightly to standard chemiluminescent film. **(C)** Pathscan sandwich ELISA was used to detect the protein expression of key genes in apoptosis-related signaling pathways, and the results showed that the expression of phospho-P44/P42 MAPK, phospho-Akt and phospho-Smad2 was decreased, the expression of cleaved-PARP, cleaved-Caspase3 and cleaved-Caspase7 was increased by L.v-shEIF3C. The data is the means ± SDs of three independent experiments. The differences were statistically significant. $*p < 0.05$, $**p < 0.01$.

Results

L.v-shEIF3C significantly decreased the expression of EIF3C in FaDu and 5-8F cells

In order to research the role of EIF3C in head and neck carcinoma, the lentiviral-mediated EIF3C shRNA vector (L.v-shEIF3C) and the negative control shRNA vector (L.v-shCtrl) were constructed to infect the human pharyngeal squamous carcinoma cell line FaDu and the human nasopharyngeal carcinoma cell line 5-8F. The RNA (Figure 1A) and protein (Figure 1B) expression of EIF3C in cells were respectively detected by qRT-PCR and western blotting, the results showed that L.v-shEIF3C could significantly down-regulate the expression of EIF3C in FaDu and 5-8F cells. Next, we used this strategy to study the effects of EIF3C on the proliferation, apoptosis and cell cycle of head and neck carcinoma cells.

Down-regulation of EIF3C inhibited the proliferation of FaDu and 5-8F cells

Cellomics was used to analyze the cell growth by taking pictures of cells with green fluorescent protein (GFP) came from L.v-shEIF3C and L.v-shCtrl. Images taken for five consecutive days, as well as the number of cells with fluorescence statistics exhibited that the number of cells infected with L.v-shEIF3C was remarkably less than another group (Figure 2). In the colony formation assay (Figure 3A), the number of clone cells in the two groups was counted, and it was found that the number of clone cells in the L.v-shCtrl group was higher than that in the L.v-shEIF3C group. Likewise, in the BrdU cell proliferation assay (Figure 3B), we found that the magnitude of the absorbance for the developed color in the L.v-shCtrl group was greater than that in the L.v-shEIF3C group detected at 450 nm. These results suggested that down-regulation of EIF3C can inhibit cell proliferation and retard tumor growth.

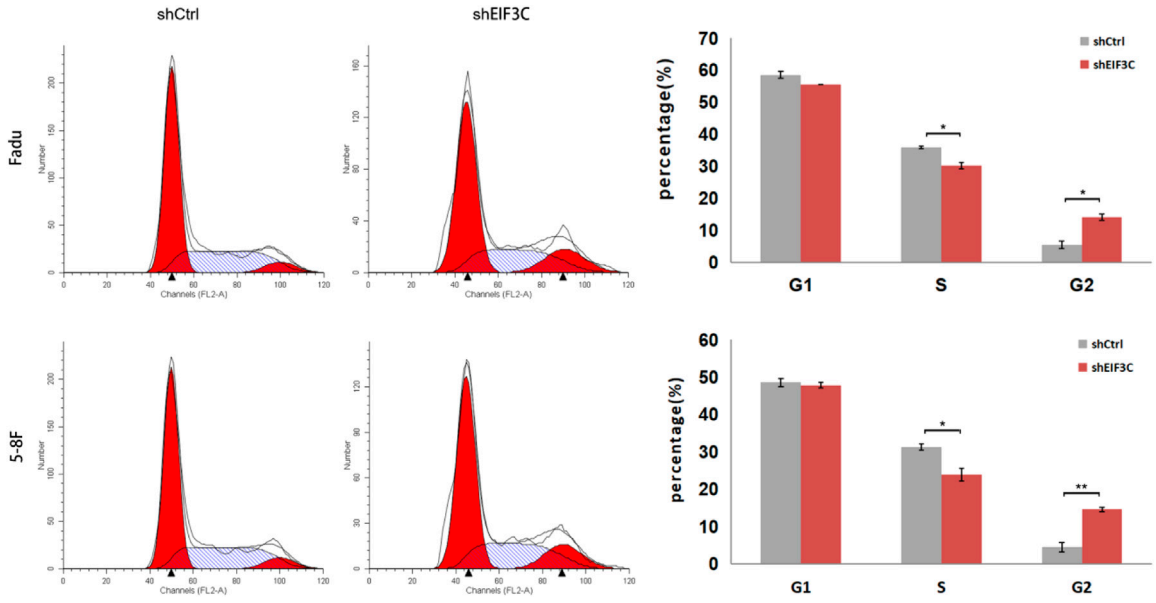

FIGURE 5
The L.v-shEIF3C triggered cell cycle arrest in FaDu and 5-8F cells. The flow cytometry analysis showed that the number of cells increased in G2 phase and decreased in S phase in L.v-shEIF3C group compared with the L.v-shCtrl group. The data is the means ± SDs of three independent experiments. The differences were statistically significant. *$p < 0.05$.

Down-regulation of EIF3C promoted the apoptosis of FaDu and 5-8F cells by regulating the protein expression of key genes in the signaling pathways

Flow cytometry was used to analyze the apoptosis when FaDu and 5-8F cells were infected with L.v-shEIF3C and L.v-shCtrl, it was found that the number of apoptotic cells in L.v-shEIF3C group was significantly more than that in L.v-shCtrl group (Figure 4A), indicating that down-regulation of EIF3C can promote apoptosis of tumor cells. In order to further study the regulation mechanism of EIF3C on apoptosis, we used PathScan® Stress and Apoptosis Signaling Antibody Array Kit to detect the protein expression of key genes in apoptosis-related signaling pathways, and found that the expression of six key genes was affected after the down-regulation of EIF3C (Figures 4B,C). The expression of phospho-P44/P42 MAPK, phospho-Akt, and phospho-Smad2 was decreased, the expression of cleaved-PARP, cleaved-Caspase3 and cleaved-Caspase7 was increased, which provided strong evidence that EIF3C regulated cell apoptosis.

Downregulation of EIF3C triggered cell cycle arrest in FaDu and 5-8F cells

The cell cycle of FaDu and 5-8F cells infected with L.v-shEIF3C and L.v-shCtrl were analyzed by Flow cytometry, the results showed that the number of cells in the G2 phase increased and the number of cells in the S phase decreased in L.v-shEIF3C group compared with the L.v-shCtrl group (Figure 5), suggesting that EIF3C was significantly correlated with the cell cycle distribution of FaDu and 5-8F cells, and down-regulation of EIF3C could trigger the cell cycle arrest of tumor cells.

L.v-shEIF3C suppressed tumor formation and growth in a FaDu cancer cell xenograft animal model

A FaDu mouse xenograft model was constructed to study the effect of EIF3C on tumor *in vivo*, FaDu cells were inoculated into the back of mice, tumor size was measured and recorded with vernier calipers every 3 days from the 14th day after inoculation until the 32nd day. On the last day, the tumor growth in mice was observed by small animal imager, and the fluorescence intensity of tumor was statistically analyzed. It was found that the fluorescence intensity of tumor in the control group was significantly higher than that in the experimental group (Figure 6A). Then the mice were sacrificed, the tumor masses were taken out and photographed, and the tumor masses were weighed. Through photo observation and volume and weight analysis of the tumor masses (Figure 6B), it was found that the tumor masses in the experimental group were small in size and low in weight, indicating that down-regulation of EIF3C could inhibit the formation and growth of tumor cells in mice.

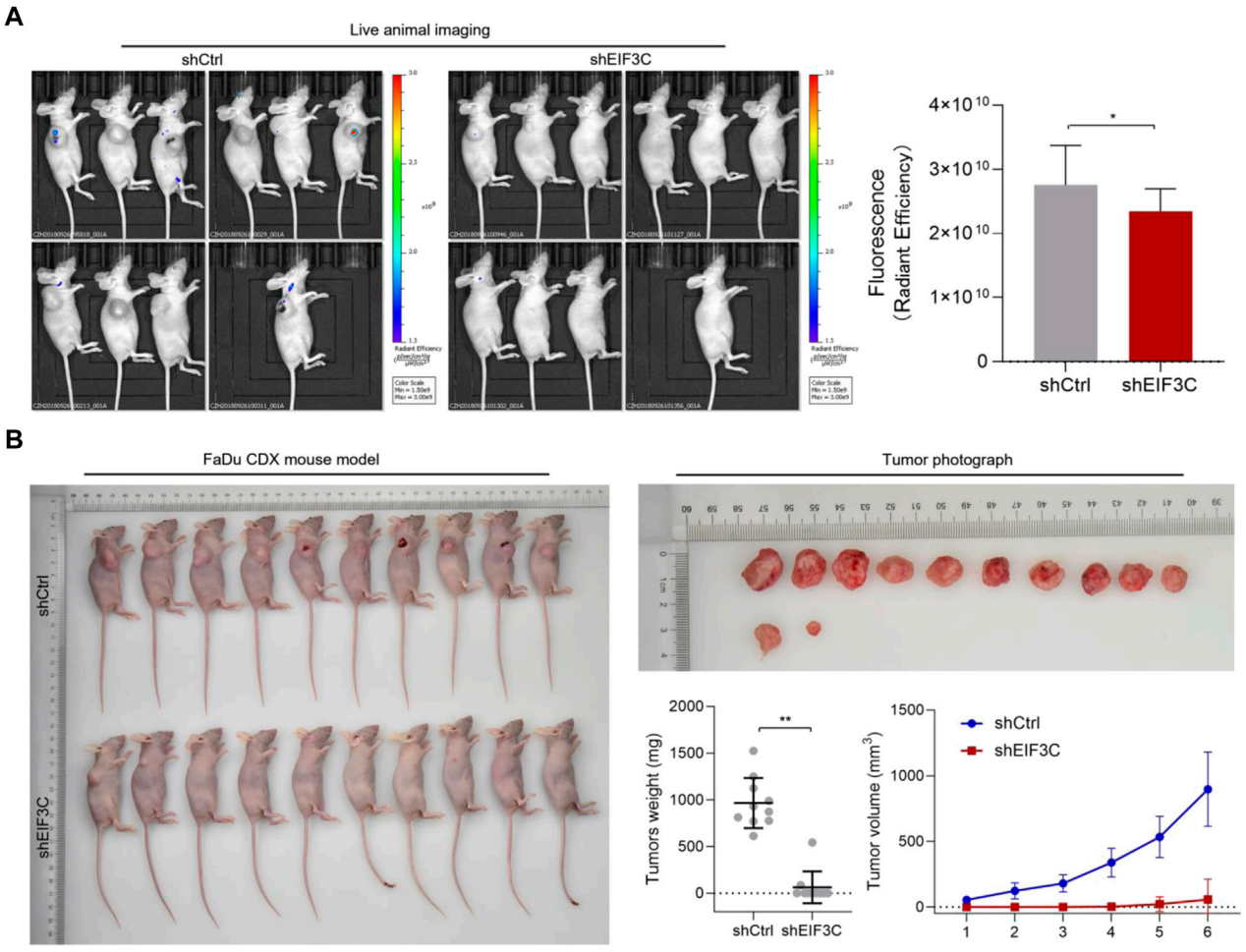

FIGURE 6
L.v-shEIF3C suppressed tumor formation in a FaDu cancer cell xenograft animal model. **(A)** live animal imaging images and the analysis showed that the fluorescence intensity of tumor in the L.v-shCtrl group was higher than that in L.v-shEIF3C group. **(B)** The photos of mice and tumors, as well as tumor weight and size statistics showed that the tumors were small in size and low in weight in L.v-shEIF3C group compared with the L.v-shCtrl group. The data is the means ± SDs. The differences were statistically significant. $*p < 0.05$, $**p < 0.01$.

Discussion

In this study, the role of EIF3C in head and neck cancer was investigated by constructing shRNA to down-regulate EIF3C expression. The results showed that down-regulating EIF3C inhibited the proliferation of FaDu and 5-8F cells, promoted their apoptosis, induced cycle arrest, and inhibited tumor growth in a mouse xenograft model. It has been shown that reduced EIF3C expression in melanoma and ovarian adenocarcinoma can mediate G0/G1 or G2/M phase arrest and lead to reduced cell proliferation and ultimately cell death in a tissue-dependent manner (Emmanuel et al., 2013), which was consistent with our findings in head and neck cancer, and thus, our study also provided another important evidence for the role of EIF3C in tumor development.

Recent studies have shown that the main reason of poor outcomes of patients with advanced head and neck cancer is the uncontrolled migration and invasion of cancer cells, the metastases of cancer cells make it difficult to eradicate with a single surgical treatment or regional chemoradiotherapy (Bossola, 2015; Kaidar-Person et al., 2018). At present, it has become a hot research direction to search for tumor differential genes and diagnostic markers. It is significant to study the biological process precisely regulated by cytokines in tumor formation and development and the regulation of gene translation for the diagnosis and treatment of tumors (Konings et al., 2020; Kordbacheh and Farah, 2021).

EIF3C, one of the core subunits of the eukaryotic translation initiation factor EIF3 complex, is critical in the process of translation initiation, and studies have shown that down-regulation of EIF3C affects overall cellular protein synthesis, thereby interfering with cellular function. Therefore, we examined the protein expression levels of several genes in the apoptosis-related signaling pathway through pathscan sandwich ELISA in this study, and found that the

expressions of phosphorylated P44/p42MAPK, phosphorylated AKT and phosphorylated Smad2 were down-regulated. P44 and P42 MAP kinase (ERK1 and ERK2) play important roles in regulating cell growth and differentiation (Plotnikov et al., 2011; Sabio and Davis, 2014). The serine/threonine kinase AKT is a proto-oncogene and a major medical concern that plays an important role in regulating multiple different cellular functions, including metabolism, growth, proliferation, survival, transcription, and protein synthesis (Porta et al., 2014; Ersahin et al., 2015). The protein encoded by Smad2 gene belongs to the SMAD protein family, which is a regulator of signal transduction and transcription in a variety of signaling pathways, and the proteins can regulate a variety of cellular processes, such as cell proliferation, apoptosis and differentiation by mediating transforming growth factor (TGF-β) signaling (Yang et al., 2019). Therefore, down-regulating EIF3C affected the expression of phosphorylated P44/p42 MAPK, phosphorylated AKT and phosphorylated SMad2, which promoted the FaDu cells apoptosis by down-regulating the protein expression of these three genes. In contrast, when cell apoptosis occurs, PARP, an inhibitor of DNA damage repair enzymes, was cleaved, and caspase-3 and caspase-7 were activated, the protein expression of cleaved-PARP, cleaved-caspase-3 and cleaved-caspase-7 was up-regulated, all indicating the onset of apoptosis (Shi, 2002; Cohausz and Althaus, 2009; Zhang et al., 2015; Xu et al., 2019).

In summary, we investigated the role of EIF3C in pharyngeal squamous carcinoma and nasopharyngeal carcinoma cells, and combined with animal models, we found that down-regulation of EIF3C could inhibit tumor progression in head and neck cancer, which provides a basis for evaluating EIF3C as a potential diagnostic or prognostic marker of head and neck cancer. The pathscan sandwich ELISA also preliminarily explored the protein expression signaling pathway associated with EIF3C affecting the apoptosis in pharyngeal squamous carcinoma cells, however, the specific regulatory mechanism of EIF3C in head and neck cancer remains to be further investigated.

Data availability statement

The original contributions presented in the study are included in the article/supplementary material, further inquiries can be directed to the corresponding author.

Ethics statement

The animal study was reviewed and approved by The ethics committee of Xi'an Jiaotong University.

Author contributions

QZ: Complete experimental design and manuscripts. XL, HL, and YB: Data analysis. QC, MY, BP, and CX: Literature collation. SH: Revision and review of the manuscripts. All authors contributed to this study and approved the submitted article.

Funding

This work was supported by the Shaanxi provincial innovation capacity support program (No. 2018TD-002) and Institutional foundation of the first affiliated hospital of Xi'an Jiaotong University (2019ZYTS-13).

Acknowledgments

We appreciate all your time and effort in helping us improve and clarify our manuscript.

Conflict of interest

The authors declare that the research was conducted in the absence of any commercial or financial relationships that could be construed as a potential conflict of interest.

Publisher's note

References

Aupérin, A. (2020). Epidemiology of head and neck cancers: An update. *Curr. Opin. Oncol.* 32 (3), 178–186. doi:10.1097/cco.0000000000000629

Bossola, M. (2015). Nutritional interventions in head and neck cancer patients undergoing chemoradiotherapy: A narrative review. *Nutrients* 7 (1), 265–276. Epub 20150105. doi:10.3390/nu7010265

Chen, Y. P., Chan, A. T. C., Le, Q. T., Blanchard, P., Sun, Y., and Ma, J. (2019). Nasopharyngeal carcinoma. *Lancet* 394 (10192), 64–80. Epub 20190606. doi:10.1016/s0140-6736(19)30956-0

Cohausz, O., and Althaus, F. R. (2009). Role of parp-1 and parp-2 in the expression of apoptosis-regulating genes in hela cells. *Cell Biol. Toxicol.* 25 (4), 379–391. Epub 20080628. doi:10.1007/s10565-008-9092-8

Emmanuel, R., Weinstein, S., Landesman-Milo, D., and Peer, D. (2013). Eif3c: A potential therapeutic target for cancer. *Cancer Lett.* 336 (1), 158–166. Epub 20130425. doi:10.1016/j.canlet.2013.04.026

Ersahin, T., Tuncbag, N., and Cetin-Atalay, R. (2015). The pi3k/akt/mtor interactive pathway. *Mol. Biosyst.* 11 (7), 1946–1954. doi:10.1039/c5mb00101c

Gao, W., Hu, Y., Zhang, Z., Du, G., Yin, L., and Yin, Z. (2019). Knockdown of Eif3c promotes human U-2os cells apoptosis through increased casp3/7 and Chk1/2 by upregulating sapk/jnk. *Onco. Targets. Ther.* 12, 1225–1235. Epub 20190214. doi:10.2147/ott.S187209

Gavrielatou, N., Doumas, S., Economopoulou, P., Foukas, P. G., and Psyrri, A. (2020). Biomarkers for immunotherapy response in head and neck cancer. *Cancer Treat. Rev.* 84, 101977. Epub 20200124. doi:10.1016/j.ctrv.2020.101977

Horton, J. D., Knochelmann, H. M., Day, T. A., Paulos, C. M., and Neskey, D. M. (2019). Immune evasion by head and neck cancer: Foundations for combination therapy. *Trends Cancer* 5 (4), 208–232. Epub 20190320. doi:10.1016/j.trecan.2019.02.007

Hsieh, J. C-H., Wang, H-M., Wu, M-H., Chang, K-P., Chang, P-H., Liao, C-T., et al. (2019). Review of emerging biomarkers in head and neck squamous cell carcinoma in the era of immunotherapy and targeted therapy. *Head Neck* 41 (1), 19–45. doi:10.1002/hed.25932

Hu, C., Wang, Y., Li, A., Zhang, J., Xue, F., and Zhu, L. (2019). Overexpressed Circ_0067934 acts as an oncogene to facilitate cervical cancer progression via the mir-545/eif3c Axis. *J. Cell. Physiol.* 234 (6), 9225–9232. Epub 20181026. doi:10.1002/jcp.27601

Huang, T., Debelius, J. W., Ploner, A., Xiao, X., Zhang, T., Hu, K., et al. (2021). Radiation therapy-induced changes of the nasopharyngeal commensal microbiome in nasopharyngeal carcinoma patients. *Int. J. Radiat. Oncol. Biol. Phys.* 109 (1), 145–150. Epub 20200828. doi:10.1016/j.ijrobp.2020.08.054

Jackson, R. J., Hellen, C. U., and Pestova, T. V. (2010). The mechanism of eukaryotic translation initiation and principles of its regulation. *Nat. Rev. Mol. Cell Biol.* 11 (2), 113–127. doi:10.1038/nrm2838

Johnson, D. E., Burtness, B., Leemans, C. R., Lui, V. W. Y., Bauman, J. E., and Grandis, J. R. (2020). Head and neck squamous cell carcinoma. *Nat. Rev. Dis. Prim.* 6 (1), 92. doi:10.1038/s41572-020-00224-3

Kaidar-Person, O., Gil, Z., and Billan, S. (2018). Precision medicine in head and neck cancer. *Drug resist. updat.* 40, 13–16. Epub 20180925. doi:10.1016/j.drup.2018.09.001

Kawakita, D., and Matsuo, K. (2017). Alcohol and head and neck cancer. *Cancer Metastasis Rev.* 36 (3), 425–434. doi:10.1007/s10555-017-9690-0

Konings, H., Stappers, S., Geens, M., De Winter, B. Y., Lamote, K., van Meerbeeck, J. P., et al. (2020). A literature review of the potential diagnostic biomarkers of head and neck neoplasms. *Front. Oncol.* 10, 1020. Epub 20200626. doi:10.3389/fonc.2020.01020

Kordbacheh, F., and Farah, C. S. (2021). Current and emerging molecular therapies for head and neck squamous cell carcinoma. *Cancers (Basel)* 13 (21), 5471. Epub 20211030. doi:10.3390/cancers13215471

Kristensen, M. B., Isenring, E., and Brown, B. (2020). Nutrition and swallowing therapy strategies for patients with head and neck cancer. *Nutrition* 69, 110548. Epub 20190702. doi:10.1016/j.nut.2019.06.028

Lam, W. K. J., and Chan, J. Y. K. (2018). Recent advances in the management of nasopharyngeal carcinoma. *F1000Res* 7, 1829. Epub 20181121. doi:10.12688/f1000research.15066.1

Lee, A. S., Kranzusch, P. J., and Cate, J. H. (2015). Eif3 targets cell-proliferation messenger rnas for translational activation or repression. *Nature* 522 (7554), 111–114. Epub 20150406. doi:10.1038/nature14267

Li, T., Li, S., Chen, D., Chen, B., Yu, T., Zhao, F., et al. (2017). Transcriptomic analyses of rna-binding proteins reveal Eif3c promotes cell proliferation in hepatocellular carcinoma. *Cancer Sci.* 108 (5), 877–885. Epub 20170426. doi:10.1111/cas.13209

Liao, S., Xie, Y., Feng, Y., Zhou, Y., Pan, Y., Fan, J., et al. (2020). Superiority of intensity-modulated radiation therapy in nasopharyngeal carcinoma with skull-base invasion. *J. Cancer Res. Clin. Oncol.* 146 (2), 429–439. Epub 20191101. doi:10.1007/s00432-019-03067-y

Luo, X., Qiu, Y., Jiang, Y., Chen, F., Jiang, L., Zhou, Y., et al. (2018). Long non-coding rna implicated in the invasion and metastasis of head and neck cancer: Possible function and mechanisms. *Mol. Cancer* 17 (1), 14. doi:10.1186/s12943-018-0763-7

Plotnikov, A., Zehorai, E., Procaccia, S., and Seger, R. (2011). The mapk cascades: Signaling components, nuclear roles and mechanisms of nuclear translocation. *Biochimica Biophysica Acta - Mol. Cell Res.* 1813 (9), 1619–1633. Epub 20101216. doi:10.1016/j.bbamcr.2010.12.012

Porta, C., Paglino, C., and Mosca, A. (2014). Targeting pi3k/akt/mtor signaling in cancer. *Front. Oncol.* 4, 64. Epub 20140414. doi:10.3389/fonc.2014.00064

Robichaud, N., Sonenberg, N., Ruggero, D., and Schneider, R. J. (2019). Translational control in cancer. *Cold Spring Harb. Perspect. Biol.* 11 (7), a032896. Epub 20190701. doi:10.1101/cshperspect.a032896

Rosenberg, A. J. (2020). Multimodality therapy for locoregional nasopharyngeal carcinoma-a decision tool for treatment optimization. *JAMA Netw. Open* 3 (12), e2030672. Epub 20201201. doi:10.1001/jamanetworkopen.2020.30672

Sabio, G., and Davis, R. J. (2014). Tnf and map kinase signalling pathways. *Semin. Immunol.* 26 (3), 237–245. Epub 20140316. doi:10.1016/j.smim.2014.02.009

Saloura, V., Langerman, A., Rudra, S., Chin, R., and Cohen, E. E. (2013). Multidisciplinary care of the patient with head and neck cancer. *Surg. Oncol. Clin. N. Am.* 22 (2), 179–215. Epub 20130204. doi:10.1016/j.soc.2012.12.001

Shi, Y. (2002). Mechanisms of caspase activation and inhibition during apoptosis. *Mol. Cell* 9 (3), 459–470. doi:10.1016/s1097-2765(02)00482-3

Sung, H., Ferlay, J., Siegel, R. L., Laversanne, M., Soerjomataram, I., Jemal, A., et al. (2021). Global cancer statistics 2020: Globocan estimates of incidence and mortality worldwide for 36 cancers in 185 countries. *Ca. A Cancer J. Clin.* 71 (3), 209–249. doi:10.3322/caac.21660

Xu, X., Lai, Y., and Hua, Z. C. (2019). Apoptosis and apoptotic body: Disease message and therapeutic target potentials. *Biosci. Rep.* 39 (1), BSR20180992. Epub 20190118. doi:10.1042/bsr20180992

Yang, Q., Ren, G. L., Wei, B., Jin, J., Huang, X. R., Shao, W., et al. (2019). Conditional knockout of tgf-ßrii/Smad2 signals protects against acute renal injury by alleviating cell necroptosis, apoptosis and inflammation. *Theranostics* 9 (26), 8277–8293. Epub 20191021. doi:10.7150/thno.35686

Zhang, D., Tang, B., Xie, X., Xiao, Y. F., Yang, S. M., and Zhang, J. W. (2015). The interplay between DNA repair and autophagy in cancer therapy. *Cancer Biol. Ther.* 16 (7), 1005–1013. Epub 20150518. doi:10.1080/15384047.2015.1046022

Zhao, W., Li, X., Wang, J., Wang, C., Jia, Y., Yuan, S., et al. (2017). Decreasing eukaryotic initiation factor 3c (Eif3c) suppresses proliferation and stimulates apoptosis in breast cancer cell lines through mammalian target of rapamycin (mtor) pathway. *Med. Sci. Monit.* 23, 4182–4191. Epub 20170830. doi:10.12659/msm.906389

frontiers | Frontiers in Bioengineering and Biotechnology

TYPE Review
PUBLISHED 19 October 2022
DOI 10.3389/fbioe.2022.1023700

OPEN ACCESS

EDITED BY
Jin Yan,
Xi'an Jiaotong University, China

REVIEWED BY
Junling Wu,
School of Stomatology, Shandong University, China
Muhammad Nawaz,
University of Gothenburg, Sweden
Lei Cheng,
Sichuan University, China

*CORRESPONDENCE
Ke Zhang,
orthozhangke@mail.ccmu.edu.cn
Yuxing Bai,
byuxing@ccmu.edu.cn

SPECIALTY SECTION
This article was submitted to Biomaterials, a section of the journal Frontiers in Bioengineering and Biotechnology

RECEIVED 20 August 2022
ACCEPTED 04 October 2022
PUBLISHED 19 October 2022

CITATION
Yu W, Li S, Zhang G, Xu HHK, Zhang K and Bai Y (2022), New frontiers of oral sciences: Focus on the source and biomedical application of extracellular vesicles.
Front. Bioeng. Biotechnol. 10:1023700. doi: 10.3389/fbioe.2022.1023700

New frontiers of oral sciences: Focus on the source and biomedical application of extracellular vesicles

Wenting Yu[1], Shengnan Li[1], Guohao Zhang[2], Hockin H. K. Xu[3,4,5], Ke Zhang[1]* and Yuxing Bai[1]*

[1]Department of Orthodontics, Beijing Stomatological Hospital, School of Stomatology, Capital Medical University, Beijing, China, [2]Department of Oral and Maxillofacial Surgery, Peking University School and Hospital of Stomatology and National Center of Stomatology and National Clinical Research Center for Oral Diseases and National Engineering Research Center of Oral Biomaterials and Digital Medical Devices, Beijing, China, [3]Biomaterials and Tissue Engineering Division, Department of Advanced Oral Sciences and Therapeutics, University of Maryland School of Dentistry, Baltimore, MD, United States, [4]Center for Stem Cell Biology and Regenerative Medicine, University of Maryland School of Medicine, Baltimore, MD, United States, [5]Marlene and Stewart Greenebaum Cancer Center, University of Maryland School of Medicine, Baltimore, MD, United States

Extracellular vesicles (EVs) are a class of nanoparticles that are derived from almost any type of cell in the organism tested thus far and are present in all body fluids. With the capacity to transfer "functional cargo and biological information" to regulate local and distant intercellular communication, EVs have developed into an attractive focus of research for various physiological and pathological conditions. The oral cavity is a special organ of the human body. It includes multiple types of tissue, and it is also the beginning of the digestive tract. Moreover, the oral cavity harbors thousands of bacteria. The importance and particularity of oral function indicate that EVs derived from oral cavity are quite complex but promising for further research. This review will discuss the extensive source of EVs in the oral cavity, including both cell sources and cell-independent sources. Besides, accumulating evidence supports extensive biomedical applications of extracellular vesicles in oral tissue regeneration and development, diagnosis and treatment of head and neck tumors, diagnosis and therapy of systemic disease, drug delivery, and horizontal gene transfer (HGT). The immune cell source, odontoblasts and ameloblasts sources, diet source and the application of EVs in tooth development and HGT were reviewed for the first time. In conclusion, we concentrate on the extensive source and potential applications offered by these nanovesicles in oral science.

KEYWORDS

extracellular vesicles, exosomes, oral cavity, source, EVs-based biomedical application

1 Introduction

Extracellular vesicles (EVs) research, particularly exosomes research, is one of the most rapidly growing biomedical fields. This area of research has attracted extensive attention recently due to EVs having the capacity to transfer "functional cargo and biological information" to regulate local and distant intercellular communication and the potential of EVs as diagnostic and therapeutic tools for the treatment of diverse diseases and the adjustable of EVs functions. The term "EVs" encompasses a heterogeneous group of cell-derived membrane vesicles that are present in all body fluids due to membrane shedding by any cell type in the organism tested thus far, including bacteria (van der Pol, et al., 2012). The first story about these tiny phospholipid bilayer-covered particles can be traced back to 1946, with EVs were referred to pro-coagulant platelet-derived particles (Chargaff and West, 1946). Later, Peter Wolf called EVs "platelet dust", referring to them as a garbage bin (Wolf, 1967). Since the 1970s–1980s, EVs biology began to attract more attention. Researchers claim that EVs can be found in serum (Benz and Moses, 1974) and the cell medium of reticulocytes (Johnstone, et al., 1987). Promisingly, scientists in the field of oral science isolated extracellular vesicles from *bacteroides gingivalis* at almost

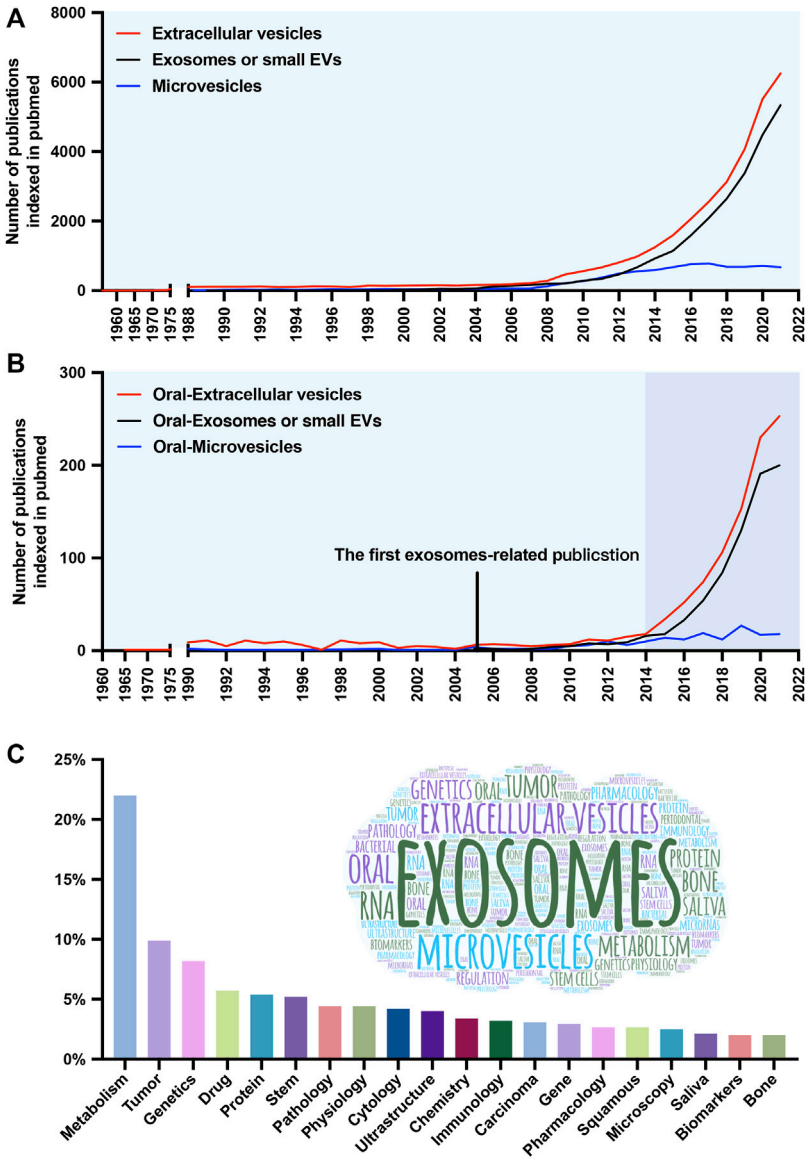

FIGURE 1
Number and keyword analysis of publications. **(A)** Timeline (1960–2021) of the publications referring to extracellular vesicles (EVs) (red line), exosomes or small EVs (black line), and microvesicles (blue line). **(B)** Timeline of the publications referring to oral-extracellular vesicles (red line), oral-exosomes or small EVs (black line), and oral-microvesicles (blue line). **(C)** The frequency distribution and cloud maps of keywords in the publications.

the same time (Grenier and Mayrand, 1987). Although related studies started early, they were interrupted, and at least another 15 years elapsed until investigators refocused on the oral region, primarily exosomes in saliva (Kapsogeorgou, et al., 2005) (Figure 1). The oral cavity is a special part of the human organ. It includes multiple types of tissue, is the beginning of the digestive tract, and it is also harboring up to 1,000 bacterial species that maintenance of both oral and systemic health (Soro, et al., 2014). The research on EVs in oral cavity is important because complexity and particularity of oral function. However, a literature search revealed few systematic review on the source and biomedical applications of EVs in oral cavity.

According to their size distribution and biogenesis, EVs can be divided into exosomes, microvesicles (MVs), and apoptotic bodies. Exosomes are the most specialized subgroup, generated by the inward budding of endosomal membranes and having a minimum diameter (almost 30–150 nm) in EVs. In contrast, MVs (100 nm-1 μm) and apoptotic bodies (1–5 μm) originate from outward budding (Akers, et al., 2013; Tkach and Thery, 2016). Notably, these sizes overlap, so it is challenging to separate these three subgroups both in experiments and descriptions. Moreover, the protein markers used to identify exosomes (such as ALIX and TSG101) can be found in MVs. Therefore, the International Society for Extracellular Vesicles suggested EVs as a preferential term used to describe all the previously mentioned types (Gould and Raposo, 2013), and the term "small EVs" is sometimes used to describe the exosomes. This review mainly concentrates on exosomes and microvesicles, and EVs serve as a general term referring to all subtypes.

Growing evidence suggests that extracellular vesicles exert their function mainly *via* the targeted transfer of functional cargo to promote intercellular communication. Novel biological functions of EVs continue to be described, including cancer treatment, early diagnosis, tissue regeneration, and drug delivery (Huang, et al., 2019; Wiklander, et al., 2019; Kalluri and LeBleu, 2020). Research also shows that mesenchymal stem cell (MSC)-derived exosomes have no adverse effects on toxicological testing (Ha, et al., 2020a). Even xenogeneic extracullular vesicles have shown a therapeutic effect similar to that of allogeneic EVs in soft tissue repair (Dong, et al., 2020). These findings imply that the extracellular vesicles not only exhibit potential for clinical applications but are also relatively safe. Therefore, the objectives of this paper were to review current knowledge on both cell source and cell-independent source of EVs in oral cavity, highlight the research directions of biomedical application of EVs, and elucidate the mechanisms of extracellular vesicles-based horizontal gene transfer for the first time.

2 Isolation and characterization of extracellular vesicles

Although exosomes, microvesicles, and apoptotic bodies are all membrane trafficking vesicles, they have a totally different biogenesis pattern. As shown in Figure 2, Exosomes originate through endocytosis, which means that the plasma membrane invaginates from outside to inside to raise vesicles. As a result, exosomes contain extracellular materials and cellular membrane constituents (Hessvik and Llorente, 2018). MVs and apoptotic bodies, conversely, are generated *via* outward budding by pinching off from the plasma membrane surface (inside to outside). Therefore, MVs and apoptotic bodies are known collectively as ectosomes (Colombo, et al., 2014; Teng and Fussenegger, 2020).

It is usually considered that EVs biofunctions based on their specific bioactive cargo, including lipids, proteins and genetic material. The lipids usually have the same function, providing structural stability, encapsulating EVs functional cargo and protecting it from enzymatic digestion (Kourembanas, 2015). The proteins in EVs reflect the vesicle's mechanism of biogenesis and fusion, and also serve as markers to identify EVs and represent their cellular origin (Simpson, et al., 2008; Keerthikumar, et al., 2016). The functional genetic materials, including RNA (mRNA, miRNA, and other noncoding RNA), DNA, and other cytosolic molecules and ingredients. Several studies have shown that packed genetic material in EVs is exchanged between cells and subsequently translated to induce the reprogramming of EVs target cells (Valadi, et al., 2007; Ekstrom, et al., 2012). Numerous researchers have applied themselves to providing a more exhaustive and comprehensive characterization of EVs content. There are at least two public online databases: Evpedia (Kim, et al., 2013) and Vesiclepedia (Pathan, et al., 2019) (previously Exocarta), which are constantly updated and are crucial tools to improving our understanding of the EVs complexity.

It is worth noting that disease-related and specific active genetic molecules can be encapsulated in EVs. Hence, there are two promising directions for the application of EVs. On the one hand, in light of the RNA content of EVs changes with the pathological condition, they have become an interesting origin of biomarkers for diagnosing human disease (Momen-Heravi et al., 2018). On the other hand, exploiting the biological characteristics that EVs are able to modulate the phenotype and behavior of recipient cells, EVs are widely applied in disease therapeutics (Phinney and Pittenger, 2017; Lasser, et al., 2018).

3 Sources of extracellular vesicles in the oral cavity

The biological efficacy of extracellular vesicles mainly depends on the cellular origin and physiological condition of the parent cells (Tkach and Thery, 2016). Thus, the potential sources of EVs in the oral cavity and the specificity of their donor cells are discussed in detail in this section. To appreciate the EVs in oral cavity, the complexities and particularities of oral cavity need to be taken into consideration first. The mouth cavity itself

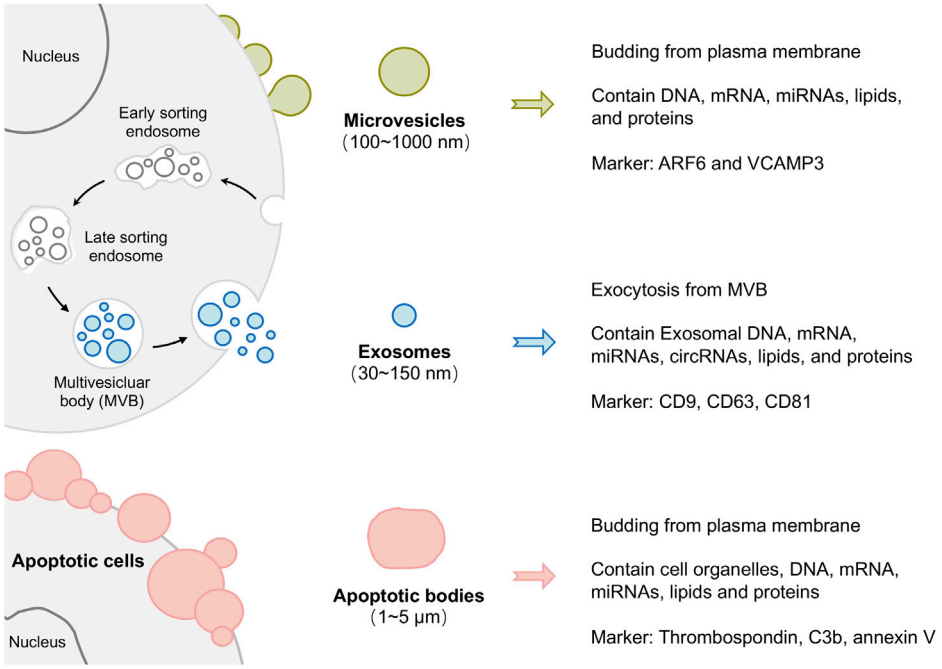

FIGURE 2
Schematic representation of extracellular vesicle (EVs) biogenesis and heterogeneity. According to their size distribution and biogenesis, EVs can be divided into exosomes, microvesicles, and apoptotic bodies.

is complex, including various hard tissue (teeth and bones), soft tissue (lip, cheek, tongue, and palate), nerves, and blood vessels (Madani, et al., 2014). Furthermore, the mouth is the beginning of the digestive tract through which numerous diets obtain access to the human body. It cannot be ignored that the oral cavity is one of the four major bacterial banks of the human body too (Gao, et al., 2018). There are two disparate sources may contribute to secrete EVs in oral cavity: cell source (dental tissue-derived cells, bone marrow mesenchymal stem cells, cancer cells, and immune cells) (Table 1) and cell-independent sources (microbiome, saliva, and diet) (Table 2). In the following sections, each of these sources will be reviewed.

3.1 Extracellular vesicles released by cell sources

3.1.1 Dental tissue-derived cells

3.1.1.1 Gingival mesenchymal stem cells

Gingival mesenchymal stem cells (GMSCs) can be isolated from gingival lamina propria. GMSCs are characterized by markedly reduced inflammation, notable fast wound-healing aptitude, and easily accessible during dental surgery (El-Sayed, et al., 2015). EVs in oral cavity were first discovered in GMSCs, and they can be traced back to 1990 (Trabandt, et al., 1990). GMSC-derived exosomes have been verified to induce anti-inflammatory M2 macrophage polarization and this effect can be reinforced through tumor necrosis factor-alpha (TNF-α) in the microenvironment (Wang, et al., 2020a; Nakao, et al., 2020). EVs derived from GMSCs also have great potential in tissue regeneration. GMSC-exosomes have been demonstrated the encapsulate of several growth factors, such as transforming growth factor-beta (TGF-β) and vascular endothelial growth factors (VEGF), promoting the migration and osteogenic differentiation of preosteoblast MC3T3-E1, and accelerating wound healing in the diabetic skin defect model (Shi, et al., 2017; Jiang and Xu, 2020).

3.1.1.2 Periodontal ligament stem cells

Periodontal ligament stem cells (PDLSCs) are the most extensively studied EVs source in oral cavity. PDLSCs, a subgroup of cells from periodontal ligament, are considered a traditional source of multipotential stem cells to direct regeneration (Seo, et al., 2004). Derivatives of PDLSCs (such as culture mediums or EVs) have been confirmed to promote calvarial bone regeneration (Liu, et al., 2020a) and to possess immunomodulatory and neuroprotective effects in relapsing remitting multiple sclerosis (RR-MS) patients (Rajan, et al., 2016). Similarly, the inflammatory microenvironment has been shown to increase exosomes secretion and enhance VEGFA transfer in exosomes to promote angiogenesis in periodontal ligaments (Zhang, et al., 2020a). Moreover,

TABLE 1 The cell sources and features of extracellular vesicles (EVs).

Original of EVs	Recipient of EVs	Content profile	Functions	References
Dental tissue-derived cells				
GMSCs	Macrophages	CD73, miR-1260b	Modulation of the inflammatory phenotypes	Jiang and Xu (2020); Nakao, et al. (2020); Shi, et al. (2017); Wang, et al. (2020a)
	MC3T3-E1	TGF-β, VEGF	Bone regeneration	
			Wound healing	
PDLSCs	BMSCs	miRNAs	Bone regeneration	Kanjanamekanant, et al. (2014); Liu, et al. (2020a); Rajan, et al. (2016); Zhang, et al. (2020a)
	Macrophages	IL-10, TGF-β	Anti-inflammation and immunosuppressive effects	
	HUVECs	VEGFA	Angiogenesis	
	PDLs	IL-1b	Response mechanical stress	
DPCs	DPCs		Dental tissue regeneration	Couble, et al. (2000); Huang, et al. (2016); Wen, et al. (2021); Zhou, et al. (2020)
	ECs		Angiogenesis	
Odontoblasts and ameloblasts	Mineralized dentin	DPP	Construct well-mineralized tooth structures	Kidd and Fejerskov (2004); Matsuo, et al. (1986); Rabie and Veis (1995); Wang, et al. (2019a); Zhang, et al. (2014)
	ECM			
	SCAPs		Maintain tooth homeostasis	
SHEDs	BMSCs	miR-100-5p	Dental tissue regeneration	Jarmalaviciute, et al. (2015); Luo, et al. (2019); Zhuang, et al. (2020)
	Neural stem cells		Treatment Parkinson's disease	
	Chondrocytes		Suppress inflammation in TMJ	
Other Cells	Such as Hertwig's epithelial root sheath cells (HERS), periapical cyst-mesenchymal stem cells (PCy-MSCs), dental follicle cells (DFCs), oral keratinocyte (OKEx), oral mucosa lamina propria-progenitor cells (OMLP-PCs), and salivary gland epithelial cells. However, EVs from these sources have not been broadly studied due to the particularity of the cells.			Kapsogeorgou, et al. (2005); Shi, et al. (2020); Sjoqvist, et al. (2019a); Tatullo, et al. (2019); Yang, et al. (2020a); Zhang, et al. (2020b)
BMSCs	HUVECs	miR-146a	Bone regeneration	Davis, et al. (2017); Liu, et al. (2020b); Liu, et al. (2020c); Liu, et al. (2020d); Liu, et al. (2021); Yang, et al. (2020b)
	Macrophages		Wound healing	
	ECs	miR-125a, miR-125b	Improve cardiac function	
	PDLSCs		Immunomodulation	
	T cells	miR-183 cluster	Induces senescence	
	BMSCs			
Cancer cells				
OSCC	Stromal cells around cancer tissues	hsp90	Tumor treatment	Ono, et al. (2018); Zhao, et al. (2020)
ACC	HPLF	MRPL23-AS1	Facilitate tumor metastasis	Chen, et al. (2020); Xu, et al. (2019)
	Microvascular endothelial cells			
Immune cells				
Macrophages	BMSCs	miR-378a	Bone regeneration	Kang, et al. (2020); Liu, et al. (2020e)
T cells	Jurkat cells	microRNA-21	Immunomodulation	Dou, et al. (2020); Yang, et al. (2020b)
	Macrophages	Curcumin		

PDLSCs are the critical response cells to mechanical force during the orthodontic tooth movement (OTM) process. Mechanical stress induces IL-1 beta release *via* EVs and IL-1 beta expression through Pannexin 1 and P2X7 receptor associated (Kanjanamekanant, et al., 2014).

3.1.1.3 Dental pulp cells

Dental pulp cells (DPCs) are the predominant cells within the dental pulp of permanent teeth. DPC-EVs appear to be the potential biomimetic tool for tooth regeneration. First, EVs induce the odontogenic differentiation of stem cells, including pushing the differentiation of mesenchymal stem cells (MSCs) into odontoblasts and triggering the regeneration of dental pulp-like tissue *in vivo* (Couble, et al., 2000; Huang, et al., 2016). Exosomes bind linked to biomaterials even efficiently promote the formation of continuous reparative dentin in the minipig model of pulp injury (Wen, et al., 2021), which may be applied as a bioactive pulp-capping material in the future.

TABLE 2 The cell-independent sources and features of extracellular vesicles (EVs).

Original of EVs	Recipient of EVs	Content profile	Functions	References
Microbiome				
P.g.	HPLF	LPS	Accelerate ECM degradation prevents osteogenic differentiating	Fleetwood, et al. (2017); He, et al. (2020); Sang, et al. (2014); Singhrao and Olsen (2018)
	Macrophages		Active inflammation	
	Brain		Contribute to AD development	
	Lung epithelial cells		Induce cell death	
A.a.	HGF	CDT	Deliver virulence factors	Ha, et al. (2020a); Nice, et al. (2018); Rompikuntal, et al. (2012)
	THP-1 cells	LtxA	Cause neuroinflammation	
	Brain monocyte and microglial cells	IL-6 and TNF-α		
G. adiacens	PBMCs	Virulent proteins	Elicit inflammation	Alkandari, et al. (2020)
S. mutans	C. albicans		Facilitate bacteria cross-kingdom interactions	Wu, et al. (2020); Wu, et al. (2022b)
			Enhancing candida albicans cariogenic ability	
Saliva		DPP IV miRNA/ proteins	Influence immune response	Chaparro Padilla, et al. (2020); Kim, et al. (2017); Li, et al. (2020); Yakob, et al. (2014)
			Diagnosis	
Diet				
milk	Osteocytes	CD9, CD81, NT5E, CD59	Bone regeneration	Oliveira, et al. (2020); Sadri, et al. (2020); Tong, et al. (2020)
	Murine placenta and embryos		Facilitate embryo survival	
	Gut Microbiota		Immune regulation	
Plant	P.g.	Lipids, PA, miR159a	Inhibit pathogenicity of P.g.	Sundaram, et al. (2019)
Other sources	EVs have also been isolated from gingival crevicular fluid, junctional epithelium, and periosteum. Perhaps because these sources are not representative, related researches are very limited.			Atsawasuwan, et al. (2018); Shimono, et al. (1991); Sun, et al. (2019)

Moreover, these vesicles also have vital roles in angiogenesis by promoting proangiogenic factor expression and tube formation (Zhou, et al., 2020), which are necessary for functional tooth regeneration.

3.1.1.4 Odontoblasts and ameloblasts

Enamel and dentin are the primary hard tissue that make up the teeth. They are located outside of the dental pulp and play an essential role in protecting the entire tooth from external stimuli, especially the inflammation caused by caries (Kidd and Fejerskov, 2004). Previous findings suggest that these dental hard tissue-derived EVs may maintain tooth homeostasis by modulating the dentin crystal growth pattern and regulating enamel resorption and extracellular organic material digestion (Matsuo, et al., 1986; Rabie and Veis, 1995). Under healthy conditions, exosomes transport dentin phosphophoryn (DPP) to the extracellular matrix to construct well-mineralized tooth structures (Zhang, et al., 2014). Under diseases conditions, exosomes derived from severely inflamed odontoblasts attenuate apoptosis of mildly inflamed neighboring cells to protect the dentin (Wang, et al., 2019a).

3.1.1.5 Stem cells from human exfoliated deciduous teeth

Deciduous and permanent tooth replacement is a special and actional process. It may take almost 6 years for humans to achieve the ordered transition of twenty deciduous teeth, which means that there are several opportunities to access sufficient Stem cell from exfoliated deciduous teeth (SHEDs) fairly easy in a period of up to 6 years. In addition to DPCs, SHEDs are another source of exosomes for dentine and dental pulp regeneration (Zhuang, et al., 2020). Moreover, SHED-EVs are even considered to provide an effective therapeutic tool in the treatment of Parkinson's disease and TMJ inflammation, as their productive neuroprotective potential on human dopaminergic neurons and inflammation-suppressive potential on temporomandibular joint chondrocytes (Jarmalaviciute, et al., 2015; Luo, et al., 2019). The use of SHED-EVs, similar to the reuse of "biological wastes", provides hope in zero biological cost regenerative medicine.

3.1.1.6 Other cells

In addition to the above cells, several reports have shown that the oral cavity contains other uncommon cell sources of EVs, such as Hertwig's epithelial root sheath cells (HERS) and human periapical cyst-mesenchymal stem cells (PCy-MSCs). HERS-secreted exosomes are a proven biomimetic tool in promoting odontogenic differentiation, neural differentiation, and tube formation *in vitro*, and regeneration of dental pulp-dentin-like tissue *in vivo*. Based on the roles of HERS in development, EVs might be considered as a mediator facilitating epithelial-mesenchymal interactions (Zhang, et al., 2020b). Researchers have found a novel MSCs community settled in the inner wall of dental periapical inflammatory cysts. Interestingly, naïve PCy-MSCs express primary neuronal markers and the main astrocyte markers. hPCy-MSC-derived EVs could also provide a wise "lab-on-cell" strategy to assess neurodegenerative disease therapies based on alterations in extracellular vesicle content (Tatullo, et al., 2019).

Furthermore, EVs have also been isolated from dental follicle cells (DFCs) (Shi, et al., 2020), oral keratinocytes (Sjoqvist, et al., 2019a), oral mucosa lamina propria-progenitor cells (OMLP-PCs) (Yang, et al., 2020a), and salivary gland epithelial cells (Kapsogeorgou, et al., 2005). However, EVs from these sources have not been broadly studied due to the particularity of the cells. Theoretically, EVs can be secreted by almost all types of cells. It is believed that a more extensive source of EVs will become available in the future.

3.1.2 Bone marrow mesenchymal stem cells

Bone marrow mesenchymal stem cells (BMSCs) are highly effective cell sources of EVs. BMSCs can be harvested from maxilla or mandible bone marrow (Ding, et al., 2010), and can differentiate into osteogenic, chondrogenic, adipogenic, myogenic, or neurogenic lineages (Charbord, 2010). Based on the potent stemness of BMSCs, EVs have shown great potential for tissue regeneration and disease therapy. Several studies have illustrated that BMSC-EVs play crucial roles in vascularized bone regeneration (Liu, et al., 2021), cutaneous wound healing (Liu, et al., 2020b), cardiac functional recovery (Liu, et al., 2020c) and as immunomodulatory and anti-inflammatory agents for the management of periodontitis and colitis (Yang, et al., 2020b; Liu, et al., 2020d). These properties of BMSCs may provide advantages for EVs-based craniofacial tissue engineering and regeneration.

Bone is also a critical organ for the corresponding aging. *In vitro* experiments have shown that aged EVs are internalized by young bone marrow mesenchymal stem cells and inhibit the osteogenic differentiation of young BMSCs (Davis, et al., 2017). From this perspective, BMSC-EVs may have potential applications in antiaging interventions.

3.1.3 Cancer cells

Similar to other cell types in physiological states, cancer cells in the oral cavity are also able to produce EVs in pathological conditions. To date, the majority of vesicles associated with cancer have been isolated from oral squamous cell carcinoma (OSCC) (Ono, et al., 2018; Zhao, et al., 2020) and adenoid cystic carcinoma (ACC) (Xu, et al., 2019; Chen, et al., 2020). It has been demonstrated that cancer cell-derived EVs can significantly increase cancer cell proliferation, migration, and invasion through the autocrine pathway, and the PI3K/Akt, MAPK/ERK, and JNK-1/2 pathways have been closely interrelated with EVs function in the tumor site (Sento, et al., 2016; Ono, et al., 2020). Simultaneously, as a critical component of the tumor microenvironment, EVs are highly involved in creating a favorable microenvironment to facilitate tumor progression and metastasis (Li and Nabet, 2019). It is worth mentioning that EVs also have "various tumor marker cargo" of early-stage tumor cells. Therefore, exosomes and other EVs are considered as potential biomarkers of liquid biopsy and may act as an innovative noninvasive diagnostic system for early cancer diagnosis (Zhang, et al., 2020c).

3.1.4 Immune cells

Many chronic inflammatory diseases in the oral cavity such as periodontitis and oral mucosal infectious diseases often progressed by the acute immune responses to microbial. Previous investigations have demonstrated that a significant infiltration of immunes cells (*e.g.,* T cell and macrophage) in chronic inflammation of the gingiva, periapical tissues and alveolar bone (Hasiakos, et al., 2021). In inflammatory diseases, T cell-exosomes have been demonstrated to elicit the development of oral lichen planus (OLP) by increasing the infiltration of T lymphocytes in lesional sites (Yang, et al., 2020c). In the field of osteoimmunology, macrophage-derived exosomes have been shown to carry miR-378a to regulate the BMP2/Smad5 pathway for bone regeneration and even endogenous bone regeneration (Liu, et al., 2020e; Kang, et al., 2020). To pursue the optimal functionally engineered extracellular vesicles, researchers have designed T cell-derived chimeric apoptotic bodies (cABs) for on-demand inflammation regulation, which achieve accurate agent release at designated locations (Dou, et al., 2020). All these immune cell-EVs have shown diverse immunomodulatory properties and may act as modulators to affect the inflammatory response.

3.2 Extracellular vesicles released by cell-independent sources

3.2.1 Microbiome

The dynamic microbiome in the oral cavity, mainly located in the saliva and plaque, is a direct cause of dental periodontitis and caries. Bacteria are the most common microorganisms in the oral cavity. It is worth noting that among extracellular vesicles, EVs derived from Gram-negative bacteria are often named outer membrane vesicles (OMVs) (Sartorio, et al., 2021). OMVs produced by *Porphyromonas gingivalis* (*P.g.*) (Sang, et al.,

2014; Fleetwood, et al., 2017) and *Aggregatibacter actinomycetemcomitans* (*A.a.*) (Rompikuntal, et al., 2012; Nice, et al., 2018) are the most extensively investigated bacterial vesicles to date. Bacteria package and transfer genes and key virulence factors (LPS, gingipains, and fimbriae) through OMVs (Schwechheimer and Kuehn, 2015). Given the presence of the phospholipid bilayer membrane, these contents are protected from harsh conditions (Kadurugamuwa and Beveridge, 1999). Thus, bacterial EVs resemble a destructive bullet, promoting proinflammatory signaling cascades and long-distance microbiota-host communication (Jones, et al., 2020) to cause oral disease (Peng, et al., 2020) and systemic diseases such as Alzheimer's disease (AD) (Singhrao and Olsen, 2018), neuroinflammatory diseases (Ha, et al., 2020b), infective endocarditis (Alkandari, et al., 2020) and respiratory system diseases (He, et al., 2020).

In addition to bacteria, the fungus *Candida albicans* is considered an important part of the healthy flora in the oral cavity. Once opportunistic infection occurs, it is often accompanied by oral candidiasis even potentially oral cancer (Lamont, et al., 2018). Although the mechanism(s) by which the fungal EVs across the thick cell wall remain unclear, *Candida albicans*-derived EVs have been identified and characterized, and were also shown to influence host immune response (Martinez-Lopez, et al., 2022), regulate biofilm formation (Honorato, et al., 2022), and confer drug resistance (Zarnowski, et al., 2018). State-of-the-art research suggests that EVs also play an important role in bacteria-fungi interactions and in turn impact oral disease progression. EVs derived from *Streptococcus mutans* augmented the virulence of *Candida albicans* by enhancing *Candida albicans* exopolysaccharides synthesis and biofilm development (Wu, et al., 2020), and subsequently increasing the dentin demineralization and *Candida albicans* cariogenic ability (Wu, et al., 2022a). These studies further suggest that extracellular vesicles released by the microbiome represent a novel potential target for the treatment of oral disease and system disorders.

3.2.2 Saliva

Compared with the cellular supernatant, body fluids such as saliva, plasma, amniotic fluid, and breast milk are more common EVs sources. Ogawa, Y found exosome-like vesicles in human saliva for the first time and demonstrated that salivary EVs might play an administrative role in local immunity and participate in the catabolism of bioactive peptides (Ogawa, et al., 2008). Given the characterization of saliva, salivary vesicles show many advantages. Its collection is fast, simple, inexpensive, painless, and can be performed several times. In fact, the extracellular vesicles in saliva have diverse origins, including salivary glands, the oral flora, and any cells in the oral cavity. Furthermore, since EVs are believed to cross the epithelial barriers, which implies that they transport multitudinous components of systemic origin from the blood into saliva (Han, et al., 2018). Therefore, an analysis of EVs cargos circulating in salivary actually reflects the altered state of their diverse origins. Salivary EVs serve as a "mirror of the human body", Proteins and miRNAs present in them offer insights into the clinical applications of oral diseases (Chaparro Padilla, et al., 2020), head and neck tumors (Yakob, et al., 2014), and systemic diseases (Kim, et al., 2017; Li, et al., 2020).

3.2.3 Diet

The oral cavity is the start of the digestive tract, chewing and digesting numerous foods over an organism's lifetime. Plant-based diets and milk are most frequently consumed foods. Researchers have found diet-derived miRNAs in mammalian cells and their modulation of mammalian genes, challenging the consensus (Yang, et al., 2015). A novel study has shown that milk-derived EVs have osteoprotective properties, these EVs initiate a decrease in osteoclast number, improving the bone microarchitecture (Oliveira, et al., 2020). Milk-EVs also reveal a potential capacity for involvement in embryo development (Sadri, et al., 2020) and immune regulation (Tong, et al., 2020). Edible plant-derived exosomes have been demonstrated as a potential therapeutic agent to treat periodontitis by significantly reducing the pathogenic mechanisms of *P.g.* (Sundaram, et al., 2019). These emerging findings may reveal a new potential source of EVs.

Extracellular vesicles have also been isolated from gingival crevicular fluid (Atsawasuwan, et al., 2018), junctional epithelium (Shimono, et al., 1991) and periosteum (Sun, et al., 2019). Perhaps because these sources are not representative, related studies are very limited. It is noteworthy that because of the sources and technical difficulty of exploring related research, cell-independent source is in its initial phases. Existing studies have shown that cell-independent sources mainly play a vital role in linking the oral cavity and systemic disease and may even be a mechanism of horizontal gene transfer. Thus, cell-independent sources are promising sources and cannot be ignored.

4 Biomedical applications of extracellular vesicles in the oral cavity

Recent studies have shown that EVs exert their function mainly by transmitting their "cargo" to target cells, activating different signaling pathways, and modifying target cell biology (Raposo and Stoorvogel, 2013). The rich sources of EVs in oral cavity have made them acting different biological effects in many ways, and promising cell-free strategy for applications in clinical medicine. The function of extracellular vesicles in oral cavity will be reviewed in the following five sections from the perspective of clinical applications (Figure 3).

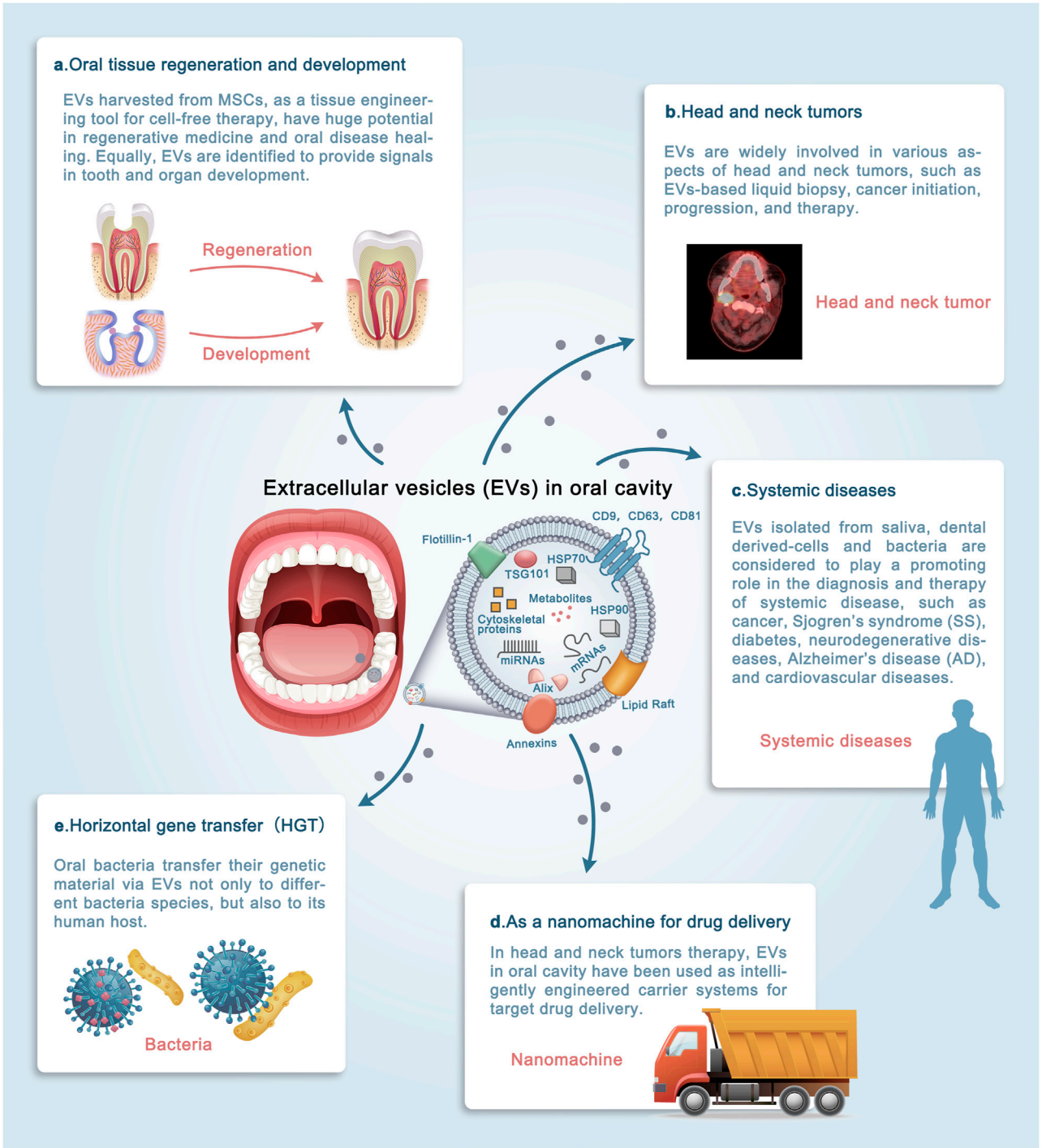

FIGURE 3
The roles of extracellular vesicles (EVs) in the oral cavity. The diverse sources of EVs in the oral cavity have allowed their involvement in a wide variety of physiological and pathological processes. **(A–E)** Schematic illustrating the promising clinical applications by which EVs may contribute to the diagnosis and treatment of diseases. Evidence supporting these applications is discussed in detail in the text. Note that EVs exert their function mainly in three ways: 1. source of EVs; 2. microenvironment in which EVs parent cells are located; 3. engineering of bilayer membrane vesicles structure. It is increasingly apparent that the clinical applications of EVs in the oral cavity are widespread, and the underlying signaling network needs to be deciphered. (MSCs: Mesenchymal stem cells).

4.1 Application of extracellular vesicles in oral tissue regeneration and development

4.1.1 Extracellular vesicles in craniofacial tissue regeneration

Extracellular vesicles harvested from dental tissue-derived cells have immense potential as a tissue engineering tool in regenerative medicine. Bone tissue engineering is the primary potential field. Exosomes have been demonstrated to accelerate bone formation even in rat osteoporosis, and this osteogenesis function will increase with the differentiation of osteoblasts (Wei, et al., 2019a). Mechanistic studies suggest that EVs may regulate angiogenesis-related genes (SDF-1, FGF2, and KDR), the BMP/Smad signaling pathway, and the Wnt/beta-catenin pathway (Wu, et al., 2019; Wang, et al., 2020b). The change of microenvironments in which parent cells are situated also impacts the osteoinductivity of EVs. Previous studies have shown that three-dimensional (3D) strain microenvironment influence PDLSC-derived exosomes, significantly improving the pro-osteogenicity of exosomes both *via* altering miRNA expression profile (miR-10a, miR-10b), and consequently improving the proliferation, migration, and osteogenic differentiation of target BMSCs (Yu, et al., 2021). The engineering of vesicles has further expanded their biomedical applications. EVs engineered with titanium nanotubes activate autophagy during osteogenic differentiation and show an effect on bone regeneration, thus facilitating the biofunctionality of titanium implants (Wei, et al., 2019b). Three-dimensional polyglycolic acid and polylactide (PLA)-engineered EVs (3D PLA-EVs) also show the activation effect of the osteogenic process (Diomede, et al., 2018).

Wound healing is another frequent medical problem. The facial skin and oral mucosa typically represent sites of injury, which may lead to an unattractive esthetic appearance and perhaps psychological issues. Several studies suggest that EVs are able to rapidly and substantially reduce wound size and structure (Sjoqvist, et al., 2019b). Apoptotic bodies derived from MSCs trigger the polarization of macrophages toward the M2 phenotype, and the resulting functional M2 phenotype increases the migration and proliferation of fibroblasts may represent the potential mechanism (Liu, et al., 2020a).

The tongue can be typically damaged in patients with oral cancer, but few studies have focused on tongue regeneration, especially tongue sensation. Surprisingly, EVs harvested from gingival mesenchymal stem cells are able to benefit taste bud regeneration and reinnervation (Zhang, et al., 2019). This impressive regenerative capacity may be related to the embryonic origin of oral tissue-derived cells is the neural crest (Stanko, et al., 2018). The similar potential of EVs in oral cavity for nerve be overlooked in neurological diseases.

4.1.2 Extracellular vesicles in oral disease healing

Periodontal disease is a prevalent chronic inflammatory disease caused by microbe infection and destruction of tooth-supporting structures. Dynamic changes in the microbiome and phenotypic shifts of PDLSCs in the proinflammatory environment have led to the progression of periodontitis (Hasiakos, et al., 2021). EVs have been reported to have promising potential in periodontitis diagnosis and therapy. The detection of EV-related biomarkers in saliva will help to distinguish diseased from healthy tissues (Yu, et al., 2019). As periodontitis initiation and progression, the level of exosomes-based PD-L1 mRNA increased in saliva. Conversely, the level of miR-126 and miR-199a was reduced (Yu, et al., 2019; Nik Mohamed Kamal, et al., 2020). These findings highlight the potential of EVs as a biomarker in diagnosis. In view of microbes, vesicles are both a part and a toxic complex of bacteria. The vesicles derived from periodontitis-related bacterial species *P.g.* and *A. a.*, have been suggested to function as immunogens in developing periodontal disease vaccines (Sang, et al., 2014; Nice, et al., 2018). From the perspective of the inflammatory environment, vesicles secreted from MSCs and edible plants have shown strong modulation of inflammation and matrix degradation to prevent/treat periodontal disease (Sundaram, et al., 2019; Čebatariuniene et al., 2019).

Dental caries and endodontic disease are diseases that happen on the teeth themselves. Similar to periodontitis, bacteria are also an essential factor in the pathogenesis of dental caries. The short-size DNAs associated with *Streptococcus mutans* membrane vesicles, the principal pathogens of dental caries, are important contributors to the biofilm formation (Senpuku, et al., 2019). Thus, EVs may serve as an additional target for the prevention of caries. Irreversible pulp disease is another dismal disease. Once dental pulp is infected due to trauma or bacteria, the existing treatment such as root canal therapy cannot restore the function of the dental pulp and therefore causes a permanently devitalized tooth. Fortunately, exosome-like vesicles (ELVs) derived from Hertwig's epithelial root sheath cells (HERS) significantly enhance pulp-dentin complex regeneration, as shown in the tooth root slice model in Figure 4 (Zhang, et al., 2020a). HE staining and immunofluorescence analysis demonstrated that HER-ELVs induced regenerated tooth structures (*e.g.*, polarizing odontoblast-like cells, predentin-like tissue, and collagen fibers) were close to the first molars levels of normal 4-week-old rats (Figure 4C). However, without ELVs, the Gel + DPCs group only displayed the formation of collagen and the deposition of extracellular matrix (ECM). The upregulated expression of dentin sialophosphoprotein (DSPP) and dentin matrix protein 1 (DMP1) indicated that ELVs treatment induced odontogenic differentiation in the tooth root slice model. Moreover, exosomes derived from DPCs and SCAP also show their potential on functional pulp-dentin complex regeneration.

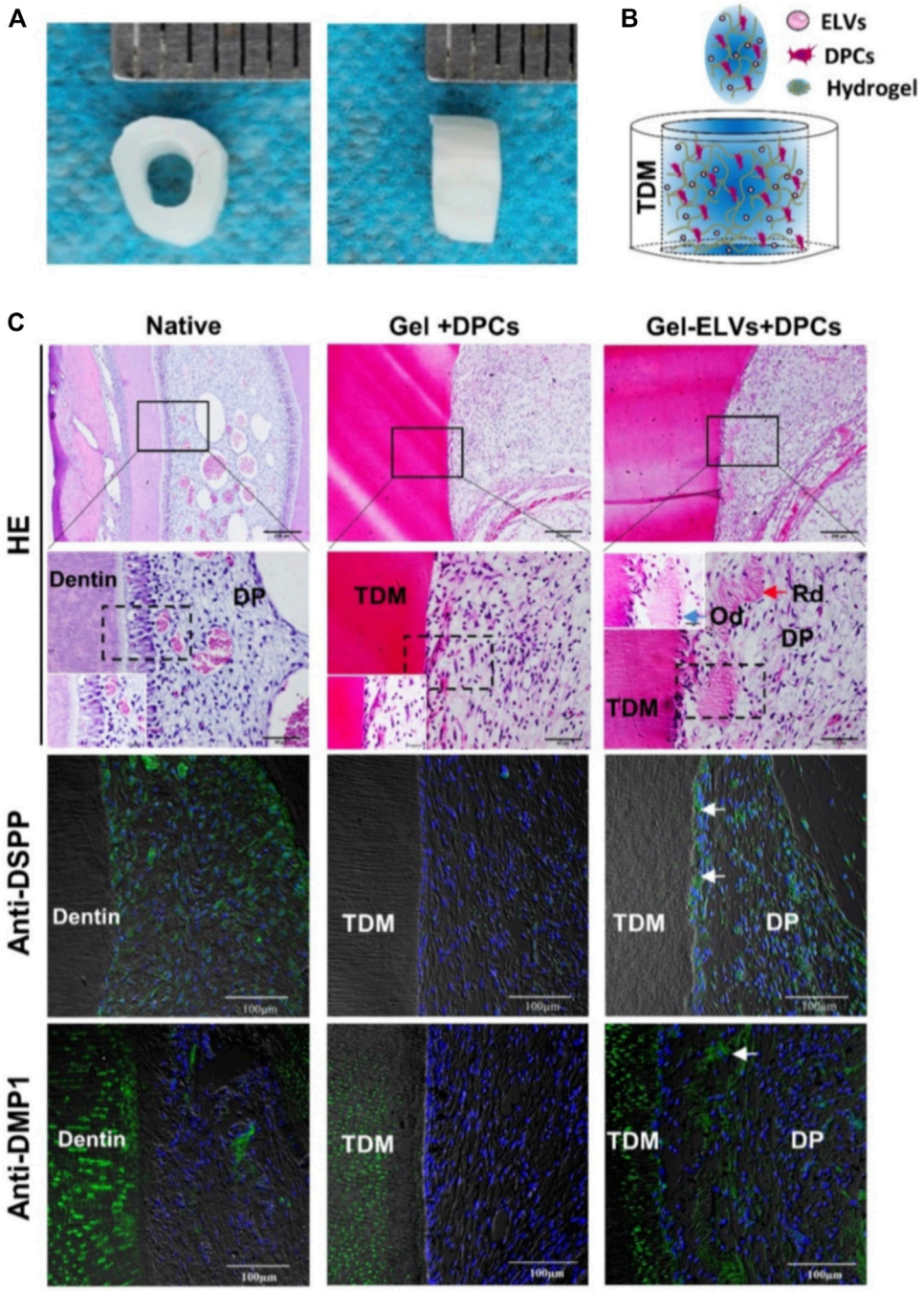

FIGURE 4
Hertwig's epithelial root sheath cell-derived exosome-like Vesicles (ELVs) accelerate the formation of pulp-detin complexes *in vivo*. **(A)** The treated dentin matrix (TDM) canal obtained from extracted incisors of pigs formed a tooth root slice with an internal diameter of 2 mm and a height of 3 mm. **(B)** Schematic of the contents of TDM. Exosome-like vesicles were resuspended in DPC cells mixed with collagen hydrogel and then injected into the tooth root slice model. **(C)** HE staining showing newly regenerated tooth structures (e.g., polarizing odontoblast-like cells and predentin-like tissue) at the interface between the pulp-like tissue and the dentin. Immunofluorescence analysis revealing the increased expression of odontogenic differentiation markers (DSPP and DMP1) in the ELV-treated group, with white arrows indicating positive green staining. (DPCs: Dental pulp cells; DSPP: dentin sialophosphoprotein; DMP1: dentin matrix protein 1; Rd: regenerated dentin-like tissue; Od: odontoblast-like cell; DP: dental pulp-like tissue). Scale bars are shown. (Zhang, et al., 2020a Copyright; ivyspring).

Oral mucosal infectious diseases like leukoplakia and oral lichen planus (OLP) are potentially malignant oral disorders (OPMDs) that may develop into oral cancer. Investigators found that genetically modified EVs enriched with miR-185 are able to attenuate the malignant transformation risk of OPMDs by decreasing the inflammatory response and inhibiting cell proliferation and angiogenesis (Wang, et al., 2019b). Mucosal disease is often related to immune disorders. Circulating exosomes from OLP are not only able to be a biomarker for disease diagnosis (Byun, et al., 2015) but are also involved in the immunomodulatory functions of T cells (Peng, et al., 2019), suggesting a novel therapeutic option for oral mucosal disease.

The application of proper mechanical forces during orthodontic tooth movement (OTM) helps maintain periodontal tissue homeostasis and tissue remodeling surrounding the teeth. Recent studies have shown that EVs specifically express the miRNA-29 family during OTM in humans (Atsawasuwan, et al., 2018). Moreover, mechanical strain enhances the exosomal pro-proliferating effect *via* the miR-181b-5p/PTEN/AKT signaling pathway and enhances the osteogenic differentiation capability of PDLSCs by BMP2/Runx2, suggesting a potential mechanism for orthodontic tooth movement (Lv, et al., 2020). These studies on the character of EVs in OTM will afford novel insight that may identify means to achieving faster OTM procedures. Mechanical force (MF)-induced root resorption is a pathological side effect of orthodontic treatment, and the osteoclast and odontoclast biomarker RANKL in EVs may allow the detection of root resorption in the early stage to obtain a more secure orthodontic treatment (Cappariello, et al., 2018).

Bisphosphonates (BPs) are widely used in treating bone metastasis of cancer and osteoporosis. However, bisphosphonate-related osteonecrosis of the jaw (BRONJ) has been recognized as one of the most disabling disorders associated with BPs. Although little is known about the pathogenesis and treatment of BRONJ, Watanabe et al. showed that MSC-EVs are able to prevent BP-induced senescence and decrease the spread of chronic inflammation, thus promoting bone regeneration and preventing BRONJ (Watanabe, et al., 2020).

4.1.3 Extracellular vesicles in tooth development

Recently, EVs were identified to provide tooth development signals based on the exquisite coordination of epithelial-mesenchymal interactions. Dentin matrix protein 1 (DMP1), present during the biogenic formation of mineral deposits, is a critical regulatory protein in dentinogenesis. It has been reported that EVs containing DMP1 are routed to the nucleus along microtubules during tooth development, and the GRP-78 receptor is also involved in this process (Ravindran, et al., 2008). Another dentinogenesis-related protein, dentin phosphophoryn (DPP), was demonstrated to be transported to the extracellular matrix through exosomes (Zhang, et al., 2014). For enamel development, Rab27a/b knockdown will alleviate EVs secretion and thus disrupt basement membranous formation and reduce enamel and dentin production (Jiang, et al., 2017). Additionally, vesicles are also observed in angiogenic regions, lining the luminal plasma membrane and formating capillary sprouts, which is a critical morphological event in dental organ development (Tsuzuki and Sasa, 1994). Mechanistically, the miRNAs in EVs influence development by regulating the expression of genes involved in DNA methylation in progenitor cells (Hayashi and Hoffman, 2017).

4.2 Application of extracellular vesicles in head and neck tumors

To date, application of EVs in oral cancer is the most investigated field of oral science. The tumor microenvironment is complex, with various cells and mechanisms involved. Previous reviews have detailed the role of extracellular vesicles in head and neck tumors (Xie, et al., 2019), so we just outline a few of important findings at this part.

EV-based liquid biopsy has unique advantages over traditional tissue biopsy as a noninvasive, real-time diagnostic technique (Colombo, et al., 2014). EVs provide better stability, contain high stocks of the original cellular biological information, thus providing better diagnostic accuracy. Substantial evidence has shown that salivary EVs are ideal diagnostic biomarkers. Compared with healthy populations, salivary exosomes show significantly increased concentrations, irregular morphologies, larger particle diameters and differentially expressed immune-related proteins in oral cancer patients (Zlotogorski-Hurvitz, et al., 2016). Recent studies have shown that miR-302b-3p and miR-517b-3p are expressed only in saliva EVs of oral squamous cell carcinoma (OSCC) patient. Excellent discrimination power for OSCC diagnosis based on exosomal miRNAs has been indicated by the ROC curve (Gai, et al., 2018). At the single vesicle and single protein levels, the significantly increased CD63 densities exhibited on the surface could also act as an index for cancer, even in the early stages (Sharma, et al., 2011).

Extracellular vesicles, which serve as intercellular information "trucks", have great application potential in tumor therapy. To date, the application of EVs in clinical treatment can be divided into three areas. First, EV-based immune regulation methods. Programmed death-ligand 1 (PD-L1) is a crucial regulator by which tumor cells evade immunity. Compared with parent tumor cells, the level of PD-L1 in EVs significantly decreases in the early treatment stages and varies during anti-PD-1 therapy (Chen, et al., 2018). Second, EV-based drug-related methods. In view of the overall biocompatibility, membrane-based stability, and low immunogenicity of EVs, EVs can also be referred to as drug delivery vehicles. EVs have been used as a vehicle for the most

common anticancer drugs of oral cavity cancer, such as doxorubicin (DOX) (Tian, et al., 2014), paclitaxel (PTX) (Batrakova and Kim, 2015) and curcumin (Sun, et al., 2010), increasing their therapeutic efficiency while reducing their side effects. Third, cancer cell-derived EVs are associated with decreased sensitivity of cancer cells to anticancer drugs. Downregulation of EVs may help solve the problem of anticancer drug resistance (Shedden, et al., 2003). It is believed that the application of EVs may be a promising field of cancer treatment due to their unique host fingerprint, ideal biocompatibility, and nanolevel molecular structure.

4.3 Application of extracellular vesicles in systemic disease

Accumulating evidence has revealed that extracellular vesicles derived from oral cavity are correlated with systemic diseases, such as Alzheimer's disease (AD) (Hassan, et al., 2020), Sjogren's syndrome (SS) (Kyriakidis, et al., 2014), foot-and-mouth disease virus (FMDV) (Wang, et al., 2020c), inflammation-related diseases (Pivoraite, et al., 2015), allergy-mediating diseases (Nazimek, et al., 2016) and aging (Machida, et al., 2015).

As an attractive EVs source with the advantage of noninvasiveness, human saliva is a unique medium for systemic disease diagnosis. Tumor-derived exosomes can be transported to and promptly detected in saliva upon cancer development. Like oral cancer, salivary EVs are a candidate for any cancer diagnosis (such as lung cancer, pancreatic cancer, and ovarian cancer) (Lau, et al., 2013). Sjogren's syndrome is a common systemic autoimmune disease targeting salivary and lacrimal glands. The progressive damage of salivary glands will lead to dryness of the mouth and glazed tongue (Du, et al., 2019). Long-lasting, noninvasive, and more accurate diagnostic techniques are essential when evaluating primary Sjogren's syndrome (pSS) patients. Research shows that salivary EVs can provide increased diagnostic accuracy in pSS (Li, et al., 2020) and can also be used to monitor the disease and staging (Aqrawi, et al., 2019). Altered bone metabolism as one of the long-term complications related to diabetes mellitus, usually increases alveolar bone loss and advances the progress of the periodontal disease. Due to the particular physiological condition of pregnancy, it often introduces difficulties in diagnosing and treating many diseases. Extracellular vesicles isolated from gingival crevicular fluid show a capacity to predict gestational diabetes mellitus in presymptomatic women (Monteiro, et al., 2019). Regarding technical aspects, the affinity chromatography column combined with a filter system (ACCF) as a simple approach has already been explored to efficiently remove the interference of saliva to obtain further purified salivary EVs (Sun, et al., 2016).

EVs isolated from dental tissue-derived cells and bacteria are considered to play a promoting role in systemic disease treatments due to the complexity of the oral environment and the special tissue origin of the oral cavity. Most dental MSCs exhibit convincing therapeutic functions in neurodegenerative diseases considering their neural crest cell origination. DPC-EVs even show the same neuroprotective efficacy as the neuron-MSC coculture system (Venugopal, et al., 2018). For specific diseases, PDLSC-EVs vesicles have been demonstrated to block experimental autoimmune encephalomyelitis and reverse disorder progression by reinforcing spinal cord integrity *via* remyelination (Rajan, et al., 2016). Among oral tissue, the dental pulp contains a rich nerve, this neuroprotective efficacy is also advantageous for the regeneration of functional tooth roots. The consensus that Alzheimer's disease and periodontal disease have a bidirectional relationship means that treating periodontitis in AD patients will improve their memory. *Porphyromonas gingivalis* (*P.g.*) is the critical virulence factor of periodontitis. Recent studies indicated that the inhibition of *P.g.*, outer vesicles can modulate the progress of AD (Singhrao and Olsen, 2018). The membrane vesicles of *P.g.* also play a critical role in the pathogenesis of cardiovascular diseases by inducing inflammation (Yang, et al., 2016). These results suggest that the inhibition of EVs derived from bacteria will be a potential treatment target for several systemic diseases and systemic diseased-related oral diseases.

4.4 Application of extracellular vesicles as nanomachines for drug delivery

Given that EVs have relatively strong protective ability and ligand combining ability, it is hopeful that they will be developed into intelligently engineered nanovesicles for precision drug delivery. EV-based nanodrug delivery systems have multiple advantages over traditional drugs, including easier escape phagocytosis, enhanced targeting efficiency, prolonged drug release and reduced drug degradation (Vader, et al., 2016). Oral cancer-associated fibroblast-derived EVs have been used as a nanovehicle for miR-196a to mediate the cisplatin resistance of head and neck cancer, and this mediating effect is targeting CDKN1B and ING5 (Qin, et al., 2019). Additionally, encapsulation of anticancer agents such as paclitaxel into exosomes show significant accumulation in drug-resistant cancer and was 50 times more cytotoxic than conventional drugs *in vitro* (Kim, et al., 2016). It is worth mentioning that paclitaxel displayed the best potency to induce the apoptosis of oral squamous cell carcinoma cells compared to daunorubicin, doxorubicin and vincristine (Robert, et al., 2018). All the results imply the emerging strategy for EV-based therapy, may be promising for head and neck tumors treatment in the future.

Currently, oral drug delivery is the most commonly used administration system for the treatment of diverse diseases. Although EV-based targeted drug delivery systems overcome the limitations of traditional methods, they still have some barriers to clinical applications, such as difficulties harvesting sufficient EVs in a cost-effective manner. Recent studies have indicated that bovine milk may serve as a natural source for cost-effective and large-scale EVs production. Milk-derived EVs can be profitably used for oral drug administration of paclitaxel, affording desirable antitumor activity with high cross-species tolerance (Agrawal, et al., 2017). Further mechanism studies showed that the origin of distinguished oral-performance of milk-derived EVs including pH adaptation, intestinal mucus penetration and multi-targeting uptake (Wu, et al., 2022b).

4.5 Extracellular vesicles involved in horizontal gene transfer

Horizontal gene transfer (HGT) is the sharing of genetic material between organisms without a parent-offspring relationship. HGT is not only a widely recognized mechanism for drug resistance in bacteria but also builds the web of life even between multicellular eukaryotes (Soucy, et al., 2015). Several findings suggest oral biofilm-related bacteria release extracellular DNA (eDNA) *via* extracellular vesicles to other microbial (Liao, et al., 2014), and the EVs upregulate the transcriptional regulators expression of other microorganisms to influence the progression of caries (Wu, et al., 2020; Wu, et al., 2022a). Doxycycline resistance encoding transposons even can be transferred between different bacterial species *via* EVs in periodontitis patients (Warburton, et al., 2007). It is therefore plausible to speculate that EVs equipped with the specific antimicrobial target, may be promising for bacteria-associated caries and periodontitis treatment in the future.

The coevolution of the microbiome and its human host has led to refined interactions to maintain a sophisticated homeostasis. Studies on saliva indicate that *F. nucleatum* trigger the EV-mediated release of host transfer RNA-derived small RNAs (tsRNAs), and these tsRNAs in turn exerted a protein biosynthesis inhibition and growth inhibition effect on *F. nucleate* (He, et al., 2018). These findings suggest that the oral cavity as essential habitat for bacteria may also play a role in the long periods of evolution.

5 Conclusion and perspective

In this review, we focus on extracellular vesicles in the oral cavity. These EVs have several unique advantages, such as easy access, extensive sources, noninvasiveness, and broad application prospects. We discuss the extensive source of EVs in the oral cavity, including both cell and cell-independent sources. Then, the biomedical application roles of extracellular vesicles in craniofacial tissue regeneration and development, diagnosis and treatment of head and neck tumors, diagnosis and therapy of systemic disease, drug delivery, and horizontal gene transfer are introduced in detail. This paper represents the first effort on reviewing immune cells, odontoblasts, ameloblasts and diet EVs sources in the oral cavity, and applications of EVs in tooth development and bacteria mediated-horizontal gene transfer. Taken together, EVs in the oral cavity are a versatile communication device, and an in-depth realization of the source and roles of EVs under physiological/pathophysiological conditions may pave the way for the construction of diagnostic and therapeutic tools involving EVs. In the area of oral science, EVs still represent a most promising and exciting world that we are dedicated to pioneering.

However, several open questions remain to deserve further exploration. First, the oral cavity is an extremely complex environment that changes constantly. The influence and underlying mechanism of changing factors, including temperature, pH, oxygen, inflammation, and flora species, on EVs in oral cavity remain unclear. The second issue concerns the extracellular vesicles research itself. Supraphysiological numbers of cells were used to isolate EVs for experiments, but it remains unclear whether unpreconditional, physiological levels of EVs exert homeostatic or pathological functions (or neither) *in vivo*. Notably, the translation of findings from the laboratory to clinical practice is still challenging. The last but not least, our current knowledge of the cellular and molecular mechanisms that govern EV biogenesis, cargo sorting, release, and uptake remains limited. Inherent technical bottlenecks of precise isolating, quantifying, and characterizing pure populations of specific subtypes of EVs were a key limitation (Ramirez, et al., 2018). To facilitate and promote the EVs field, comprehensive studies in this EVs area are warranted. The safety, homogeneity, and standardized characterization of EVs should attract more attention in the future.

Author contributions

WY collected data and prepared the draft. SL and GZ retrieved and analyzed literatures. HX gave advice to the final version of this manuscript. YB and KZ supervised the study and gave advice to the final version of this manuscript. All authors have read and approved the final manuscript.

Funding

This work was supported by the National Natural Science Foundation of China (No. 81901028); Beijing Municipal Administration of Hospitals, Youth Program (QML20201503);

Young Scientist Program of Beijing Stomatological Hospital, Capital Medical University, NO. YSP202206.

Conflict of interest

The authors declare that the research was conducted in the absence of any commercial or financial relationships that could be construed as a potential conflict of interest.

Publisher's note

References

Agrawal, A. K., Aqil, F., Jeyabalan, J., Spencer, W. A., Beck, J., Gachuki, B. W., et al. (2017). Milk-derived exosomes for oral delivery of paclitaxel. *Nanomedicine Nanotechnol. Biol. Med.* 13 (5), 1627–1636. doi:10.1016/j.nano.2017.03.001

Akers, J. C., Gonda, D., Kim, R., Carter, B. S., and Chen, C. C. (2013). Biogenesis of extracellular vesicles (EV): Exosomes, microvesicles, retrovirus-like vesicles, and apoptotic bodies. *J. Neurooncol.* 113 (1), 1–11. doi:10.1007/s11060-013-1084-8

Alkandari, S. A., Bhardwaj, R. G., Ellepola, A., and Karched, M. (2020). Proteomics of extracellular vesicles produced by Granulicatella adiacens, which causes infective endocarditis. *PLoS One* 15 (11), e0227657. doi:10.1371/journal.pone.0227657

Aqrawi, L. A., Galtung, H. K., Guerreiro, E. M., Ovstebo, R., Thiede, B., Utheim, T. P., et al. (2019). Proteomic and histopathological characterisation of sicca subjects and primary Sjogren's syndrome patients reveals promising tear, saliva and extracellular vesicle disease biomarkers. *Arthritis Res. Ther.* 21 (1), 181. doi:10.1186/s13075-019-1961-4

Atsawasuwan, P., Lazari, P., Chen, Y., Zhou, X., Viana, G., Evans, C. A., et al. (2018). Secretory microRNA-29 expression in gingival crevicular fluid during orthodontic tooth movement. *PLoS One* 13 (3), e0194238. doi:10.1371/journal.pone.0194238

Batrakova, E. V., and Kim, M. S. (2015). Using exosomes, naturally-equipped nanocarriers, for drug delivery. *J. Control. Release* 219, 396–405. doi:10.1016/j.jconrel.2015.07.030

Benz, E. W., and Moses, H. L. (1974). Brief communication: Small, virus-like particles detected in bovine sera by electron Microscopy2. *J. Natl. Cancer Inst.* 52 (6), 1931–1934. doi:10.1093/jnci/52.6.1931

Byun, J. S., Hong, S. H., Choi, J. K., Jung, J. K., and Lee, H. J. (2015). Diagnostic profiling of salivary exosomal microRNAs in oral lichen planus patients. *Oral Dis.* 21 (8), 987–993. doi:10.1111/odi.12374

Cappariello, A., Loftus, A., Muraca, M., Maurizi, A., Rucci, N., Teti, A., et al. (2018). Osteoblast-derived extracellular vesicles are biological tools for the delivery of active molecules to bone. *J. Bone Min. Res.* 33 (3), 517–533. doi:10.1002/jbmr.3332

Čebatariuniene, A., Kriaučiunaite, K., Prunskaite, J., Tunaitis, V., and Pivoriunas, A. (2019). Extracellular vesicles suppress basal and lipopolysaccharide-induced NFκB activity in human periodontal ligament stem cells. *Stem Cells Dev.* 28 (15), 1037–1049. doi:10.1089/scd.2019.0021

Chaparro Padilla, A., Weber Aracena, L., Realini Fuentes, O., Albers Busquetts, D., Hernández Ríos, M., Ramírez Lobos, V., et al. (2020). Molecular signatures of extracellular vesicles in oral fluids of periodontitis patients. *Oral Dis.* 26, 1318–1325. doi:10.1111/odi.13338

Charbord, P. (2010). Bone marrow mesenchymal stem cells: Historical overview and concepts. *Hum. Gene Ther.* 21 (9), 1045–1056. doi:10.1089/hum.2010.115

Chargaff, E., and West, R. (1946). The biological significance of the thromboplastic protein of blood. *J. Biol. Chem.* 166 (1), 189–197. doi:10.1016/s0021-9258(17)34997-9

Chen, G., Huang, A. C., Zhang, W., Zhang, G., Wu, M., Xu, W., et al. (2018). Exosomal PD-L1 contributes to immunosuppression and is associated with anti-PD-1 response. *Nature* 560 (7718), 382–386. doi:10.1038/s41586-018-0392-8

Chen, C. W., Fu, M., Du, Z. H., Zhao, F., Yang, W. W., Xu, L. H., et al. (2020). Long noncoding RNA MRPL23-AS1 promotes adenoid cystic carcinoma lung metastasis. *Cancer Res.* 80 (11), 2273–2285. doi:10.1158/0008-5472.Can-19-0819

Colombo, M., Raposo, G., and Thery, C. (2014). "Biogenesis, secretion, and intercellular interactions of exosomes and other extracellular vesicles,". *Annual review of cell and developmental biology*. Editors R. Schekman, and R. Lehmann, 30, 255–289.

Couble, M. L., Farges, J. C., Bleicher, F., Perrat-Mabillon, B., Boudeulle, M., Magloire, H., et al. (2000). Odontoblast differentiation of human dental pulp cells in explant cultures. *Calcif. Tissue Int.* 66 (2), 129–138. doi:10.1007/pl00005833

Davis, C., Dukes, A., Drewry, M., Helwa, I., Johnson, M. H., Isales, C. M., et al. (2017). MicroRNA-183-5p increases with age in bone-derived extracellular vesicles, suppresses bone marrow stromal (stem) cell proliferation, and induces stem cell senescence. *Tissue Eng. Part A* 23 (21-22), 1231–1240. doi:10.1089/ten.TEA.2016.0525

Ding, G., Wang, W., Liu, Y., An, Y., Zhang, C., Shi, S., et al. (2010). Effect of cryopreservation on biological and immunological properties of stem cells from apical papilla. *J. Cell. Physiol.* 223 (2), 415–422. doi:10.1002/jcp.22050

Diomede, F., Gugliandolo, A., Cardelli, P., Merciaro, I., Ettorre, V., Traini, T., et al. (2018). Three-dimensional printed PLA scaffold and human gingival stem cell-derived extracellular vesicles: A new tool for bone defect repair. *Stem Cell Res. Ther.* 9 (1), 104. doi:10.1186/s13287-018-0850-0

Dong, J., Wu, Y., Zhang, Y., Yu, M., and Tian, W. (2020). <p>Comparison of the therapeutic effect of allogeneic and xenogeneic small extracellular vesicles in soft tissue repair</p>. *Int. J. Nanomedicine* 15, 6975–6991. doi:10.2147/ijn.S269069

Dou, G., Tian, R., Liu, X., Yuan, P., Ye, Q., Liu, J., et al. (2020). Chimeric apoptotic bodies functionalized with natural membrane and modular delivery system for inflammation modulation. *Sci. Adv.* 6, eaba2987. doi:10.1126/sciadv.aba2987

Du, Z. H., Ding, C., Zhang, Q., Zhang, Y., Ge, X. Y., Li, S. L., et al. (2019). Stem cells from exfoliated deciduous teeth alleviate hyposalivation caused by Sjogren syndrome. *Oral Dis.* 25 (6), 1530–1544. doi:10.1111/odi.13113

Ekstrom, K., Valadi, H., Sjostrand, M., Malmhall, C., Bossios, A., Eldh, M., et al. (2012). Characterization of mRNA and microRNA in human mast cell-derived exosomes and their transfer to other mast cells and blood CD34 progenitor cells. *J. Extracell. Vesicles* 1, 18389. doi:10.3402/jev.v1i0.18389

El-Sayed, K. M., Paris, S., Graetz, C., Kassem, N., Mekhemar, M., Ungefroren, H., et al. (2015). Isolation and characterisation of human gingival margin-derived STRO-1/MACS(+) and MACS(-) cell populations. *Int. J. Oral Sci.* 7 (2), 80–88. doi:10.1038/ijos.2014.41

Fleetwood, A. J., Lee, M. K. S., Singleton, W., Achuthan, A., Lee, M. C., O'Brien-Simpson, N. M., et al. (2017). Metabolic remodeling, inflammasome activation, and pyroptosis in macrophages stimulated by Porphyromonas gingivalis and its outer membrane vesicles. *Front. Cell. Infect. Microbiol.* 7, 351. doi:10.3389/fcimb.2017.00351

Gai, C., Camussi, F., Broccoletti, R., Gambino, A., Cabras, M., Molinaro, L., et al. (2018). Salivary extracellular vesicle-associated miRNAs as potential biomarkers in oral squamous cell carcinoma. *BMC Cancer* 18 (1), 439. doi:10.1186/s12885-018-4364-z

Gao, L., Xu, T., Huang, G., Jiang, S., Gu, Y., Chen, F., et al. (2018). Oral microbiomes: More and more importance in oral cavity and whole body. *Protein Cell* 9 (5), 488–500. doi:10.1007/s13238-018-0548-1

Gould, S. J., and Raposo, G. (2013). As we wait: Coping with an imperfect nomenclature for extracellular vesicles. *J. Extracell. Vesicles* 2, 20389. doi:10.3402/jev.v2i0.20389

Grenier, D., and Mayrand, D. (1987). Functional characterization of extracellular vesicles produced by Bacteroides gingivalis. *Infect. Immun.* 55 (1), 111–117. doi:10.1128/iai.55.1.111-117.1987

Ha, D. H., Kim, S. D., Lee, J., Kwon, H. H., Park, G. H., Yang, S. H., et al. (2020a). Toxicological evaluation of exosomes derived from human adipose tissue-derived mesenchymal stem/stromal cells. *Regul. Toxicol. Pharmacol.* 115, 104686. doi:10.1016/j.yrtph.2020.104686

Ha, J. Y., Choi, S. Y., Lee, J. H., Hong, S. H., and Lee, H. J. (2020b). Delivery of periodontopathogenic extracellular vesicles to brain monocytes and microglial IL-6 promotion by RNA cargo. *Front. Mol. Biosci.* 7, 596366. doi:10.3389/fmolb.2020.596366

Han, Y., Jia, L., Zheng, Y., and Li, W. (2018). Salivary exosomes: Emerging roles in systemic disease. *Int. J. Biol. Sci.* 14 (6), 633–643. doi:10.7150/ijbs.25018

Hasiakos, S., Gwack, Y., Kang, M., and Nishimura, I. (2021). Calcium signaling in T cells and chronic inflammatory disorders of the oral cavity. *J. Dent. Res.* 100 (7), 693–699. doi:10.1177/0022034521990652

Hassan, R., Rabea, A. A., Ragae, A., and Sabry, D. (2020). The prospective role of mesenchymal stem cells exosomes on circumvallate taste buds in induced alzheimer's disease of ovariectomized albino rats: (Light and transmission electron microscopic study). *Arch. Oral Biol.* 110, 104596. doi:10.1016/j.archoralbio.2019.104596

Hayashi, T., and Hoffman, M. P. (2017). Exosomal microRNA communication between tissues during organogenesis. *RNA Biol.* 14 (12), 1683–1689. doi:10.1080/15476286.2017.1361098

He, X., Li, F., Bor, B., Koyano, K., Cen, L., Xiao, X., et al. (2018). Human tRNA-derived small RNAs modulate host–oral microbial interactions. *J. Dent. Res.* 97 (11), 1236–1243. doi:10.1177/0022034518770605

He, Y., Shiotsu, N., Uchida-Fukuhara, Y., Guo, J., Weng, Y., Ikegame, M., et al. (2020). Outer membrane vesicles derived from Porphyromonas gingivalis induced cell death with disruption of tight junctions in human lung epithelial cells. *Arch. Oral Biol.* 118, 104841. doi:10.1016/j.archoralbio.2020.104841

Hessvik, N. P., and Llorente, A. (2018). Current knowledge on exosome biogenesis and release. *Cell. Mol. Life Sci.* 75 (2), 193–208. doi:10.1007/s00018-017-2595-9

Honorato, L., de Araujo, J. F. D., Ellis, C. C., Piffer, A. C., Pereira, Y., Frases, S., et al. (2022). Extracellular vesicles regulate biofilm formation and yeast-to-hypha differentiation in Candida albicans. *mBio* 13 (3), e0030122. doi:10.1128/mbio.00301-22

Huang, C. C., Narayanan, R., Alapati, S., and Ravindran, S. (2016). Exosomes as biomimetic tools for stem cell differentiation: Applications in dental pulp tissue regeneration. *Biomaterials* 111, 103–115. doi:10.1016/j.biomaterials.2016.09.029

Huang, T., Song, C., Zheng, L., Xia, L., Li, Y., Zhou, Y., et al. (2019). The roles of extracellular vesicles in gastric cancer development, microenvironment, anti-cancer drug resistance, and therapy. *Mol. Cancer* 18 (1), 62. doi:10.1186/s12943-019-0967-5

Jarmalaviciute, A., Tunaitis, V., Pivoraite, U., Venalis, A., and Pivoriunas, A. (2015). Exosomes from dental pulp stem cells rescue human dopaminergic neurons from 6-hydroxy-dopamine-induced apoptosis. *Cytotherapy* 17 (7), 932–939. doi:10.1016/j.jcyt.2014.07.013

Jiang, N., Xiang, L., He, L., Yang, G., Zheng, J., Wang, C., et al. (2017). Exosomes mediate epithelium-mesenchyme crosstalk in organ development. *ACS Nano* 11 (8), 7736–7746. doi:10.1021/acsnano.7b01087

Jiang, S., and Xu, L. (2020). Exosomes from gingival mesenchymal stem cells enhance migration and osteogenic differentiation of pre-osteoblasts. *Pharmazie* 75 (11), 576–580. doi:10.1691/ph.2020.0652

Johnstone, R. M., Adam, M., Hammond, J. R., Orr, L., and Turbide, C. (1987). Vesicle formation during reticulocyte maturation. Association of plasma membrane activities with released vesicles (exosomes). *J. Biol. Chem.* 262 (19), 9412–9420. doi:10.1016/s0021-9258(18)48095-7

Jones, E. J., Booth, C., Fonseca, S., Parker, A., Cross, K., Miquel-Clopés, A., et al. (2020). The uptake, trafficking, and biodistribution of Bacteroides thetaiotaomicron generated outer membrane vesicles. *Front. Microbiol.* 11, 57. doi:10.3389/fmicb.2020.00057

Kadurugamuwa, J. L., and Beveridge, T. J. (1999). Membrane vesicles derived from *Pseudomonas aeruginosa* and Shigella flexneri can be integrated into the surfaces of other gram-negative bacteria. *Microbiol. Read.* 145, 2051–2060. doi:10.1099/13500872-145-8-2051

Kalluri, R., and LeBleu, V. S. (2020). The biology, function, and biomedical applications of exosomes. *Science* 367 (6478), eaau6977. doi:10.1126/science.aau6977

Kang, M., Huang, C. C., Lu, Y., Shirazi, S., Gajendrareddy, P., Ravindran, S., et al. (2020). Bone regeneration is mediated by macrophage extracellular vesicles. *Bone* 141, 115627. doi:10.1016/j.bone.2020.115627

Kanjanamekanant, K., Luckprom, P., and Pavasant, P. (2014). P2X7 receptor-Pannexin1 interaction mediates stress-induced interleukin-1 beta expression in human periodontal ligament cells. *J. Periodontal Res.* 49 (5), 595–602. doi:10.1111/jre.12139

Kapsogeorgou, E. K., Abu-Helu, R. F., Moutsopoulos, H. M., and Manoussakis, M. N. (2005). Salivary gland epithelial cell exosomes: A source of autoantigenic ribonucleoproteins. *Arthritis Rheum.* 52 (5), 1517–1521. doi:10.1002/art.21005

Keerthikumar, S., Chisanga, D., Ariyaratne, D., Al Saffar, H., Anand, S., Zhao, K., et al. (2016). ExoCarta: A web-based compendium of exosomal cargo. *J. Mol. Biol.* 428 (4), 688–692. doi:10.1016/j.jmb.2015.09.019

Kidd, E. A., and Fejerskov, O. (2004). What constitutes dental caries? Histopathology of carious enamel and dentin related to the action of cariogenic biofilms. *J. Dent. Res.* 83, C35–C38. doi:10.1177/154405910408301s07

Kim, D. K., Kang, B., Kim, O. Y., Choi, D. S., Lee, J., Kim, S. R., et al. (2013). EVpedia: An integrated database of high-throughput data for systemic analyses of extracellular vesicles. *J. Extracell. Vesicles* 2, 20384. doi:10.3402/jev.v2i0.20384

Kim, M. S., Haney, M. J., Zhao, Y., Mahajan, V., Deygen, I., Klyachko, N. L., et al. (2016). Development of exosome-encapsulated paclitaxel to overcome MDR in cancer cells. *Nanomedicine Nanotechnol. Biol. Med.* 12 (3), 655–664. doi:10.1016/j.nano.2015.10.012

Kim, J., Shin, H., and Park, J. (2017). RNA in salivary extracellular vesicles as a possible tool for systemic disease diagnosis. *J. Dent. Res.* 96 (8), 938–944. doi:10.1177/0022034517702100

Kourembanas, S. (2015). Exosomes: Vehicles of intercellular signaling, biomarkers, and vectors of cell therapy. *Annu. Rev. Physiol.* 77, 13–27. doi:10.1146/annurev-physiol-021014-071641

Kyriakidis, N. C., Kapsogeorgou, E. K., and Tzioufas, A. G. (2014). A comprehensive review of autoantibodies in primary sjogren's syndrome: Clinical phenotypes and regulatory mechanisms. *J. Autoimmun.* 51, 67–74. doi:10.1016/j.jaut.2013.11.001

Lamont, R. J., Koo, H., and Hajishengallis, G. (2018). The oral microbiota: Dynamic communities and host interactions. *Nat. Rev. Microbiol.* 16 (12), 745–759. doi:10.1038/s41579-018-0089-x

Lasser, C., Jang, S. C., and Lotvall, J. (2018). Subpopulations of extracellular vesicles and their therapeutic potential. *Mol. Asp. Med.* 60, 1–14. doi:10.1016/j.mam.2018.02.002

Lau, C., Kim, Y., Chia, D., Spielmann, N., Eibl, G., Elashoff, D., et al. (2013). Role of pancreatic cancer-derived exosomes in salivary biomarker development. *J. Biol. Chem.* 288 (37), 26888–26897. doi:10.1074/jbc.M113.452458

Li, F., Liu, Z., Zhang, B., Jiang, S., Wang, Q., Du, L., et al. (2020). Circular RNA sequencing indicates circ-IQGAP2 and circ-ZC3H6 as noninvasive biomarkers of primary Sjögren's syndrome. *Rheumatol. Oxf.* 59 (9), 2603–2615. doi:10.1093/rheumatology/keaa163

Li, I., and Nabet, B. Y. (2019). Exosomes in the tumor microenvironment as mediators of cancer therapy resistance. *Mol. Cancer* 18 (1), 32. doi:10.1186/s12943-019-0975-5

Liao, S., Klein, M. I., Heim, K. P., Fan, Y., Bitoun, J. P., Ahn, S. J., et al. (2014). Streptococcus mutans extracellular DNA is upregulated during growth in biofilms, actively released via membrane vesicles, and influenced by components of the protein secretion machinery. *J. Bacteriol.* 196 (13), 2355–2366. doi:10.1128/JB.01493-14

Liu, A., Jin, S., Fu, C., Cui, S., Zhang, T., Zhu, L., et al. (2020a). Macrophage-derived small extracellular vesicles promote biomimetic mineralized collagen-mediated endogenous bone regeneration. *Int. J. Oral Sci.* 12 (1), 33. doi:10.1038/s41368-020-00100-6

Liu, H., Liu, S., Qiu, X., Yang, X., Bao, L., Pu, F., et al. (2020b). Donor MSCs release apoptotic bodies to improve myocardial infarction via autophagy regulation in recipient cells. *Autophagy* 16 (12), 2140–2155. doi:10.1080/15548627.2020.1717128

Liu, J., Qiu, X., Lv, Y., Zheng, C., Dong, Y., Dou, G., et al. (2020c). Apoptotic bodies derived from mesenchymal stem cells promote cutaneous wound healing via regulating the functions of macrophages. *Stem Cell Res. Ther.* 11 (1), 507. doi:10.1186/s13287-020-02014-w

Liu, L., Guo, S., Shi, W., Liu, Q., Huo, F., Wu, Y., et al. (2020d). Bone marrow mesenchymal stem cell-derived small extracellular vesicles promote periodontal regeneration. *Tissue Eng. Part A* 27, 962–976. doi:10.1089/ten.TEA.2020.0141

Liu, T., Hu, W., Zou, X., Xu, J., He, S., Chang, L., et al. (2020e). Human periodontal ligament stem cell-derived exosomes promote bone regeneration by altering MicroRNA profiles. *Stem Cells Int.* 2020, 1–13. doi:10.1155/2020/8852307

Liu, L., Yu, F., Li, L., Zhou, L., Zhou, T., Xu, Y., et al. (2021). Bone marrow stromal cells stimulated by strontium-substituted calcium silicate ceramics: Release of exosomal miR-146a regulates osteogenesis and angiogenesis. *Acta Biomater.* 119, 444–457. doi:10.1016/j.actbio.2020.10.038

Luo, P., Jiang, C., Ji, P., Wang, M., and Xu, J. (2019). Exosomes of stem cells from human exfoliated deciduous teeth as an anti-inflammatory agent in temporomandibular joint chondrocytes via miR-100-5p/mTOR. *Stem Cell Res. Ther.* 10 (1), 216. doi:10.1186/s13287-019-1341-7

Lv, P. Y., Gao, P. F., Tian, G. J., Yang, Y. Y., Mo, F. F., Wang, Z. H., et al. (2020). Osteocyte-derived exosomes induced by mechanical strain promote human

periodontal ligament stem cell proliferation and osteogenic differentiation via the miR-181b-5p/PTEN/AKT signaling pathway. *Stem Cell Res. Ther.* 11 (1), 295. doi:10.1186/s13287-020-01815-3

Machida, T., Tomofuji, T., Ekuni, D., Maruyama, T., Yoneda, T., Kawabata, Y., et al. (2015). MicroRNAs in salivary exosome as potential biomarkers of aging. *Int. J. Mol. Sci.* 16 (9), 21294–21309. doi:10.3390/ijms160921294

Madani, M., Berardi, T., and Stoopler, E. T. (2014). Anatomic and examination considerations of the oral cavity. *Med. Clin. North Am.* 98 (6), 1225–1238. doi:10.1016/j.mcna.2014.08.001

Martinez-Lopez, R., Hernaez, M. L., Redondo, E., Calvo, G., Radau, S., Pardo, M., et al. (2022). Candida albicans hyphal extracellular vesicles are different from yeast ones, carrying an active proteasome complex and showing a different role in host immune response. *Microbiol. Spectr.* 10 (3), e0069822. doi:10.1128/spectrum.00698-22

Matsuo, S., Yamamoto, K., Nishikawa, S., Ichikawa, H., Wakisaka, S., Takano, Y., et al. (1986). Influence of colchicine on the distribution of horseradish peroxidase in the secretory ameloblast layer *in vitro*. *Anat. Rec. Hob.* 216 (1), 10–18. doi:10.1002/ar.1092160103

Momen-Heravi, F., Getting, S. J., and Moschos, S. A. (2018). Extracellular vesicles and their nucleic acids for biomarker discovery. *Pharmacol. Ther.* 192, 170–187. doi:10.1016/j.pharmthera.2018.08.002

Monteiro, L. J., Varas-Godoy, M., Monckeberg, M., Realini, O., Hernandez, M., Rice, G., et al. (2019). Oral extracellular vesicles in early pregnancy can identify patients at risk of developing gestational diabetes mellitus. *PLoS One* 14 (6), e0218616. doi:10.1371/journal.pone.0218616

Nakao, Y., Fukuda, T., Zhang, Q., Sanui, T., Shinjo, T., Kou, X., et al. (2020). Exosomes from TNF-α-treated human gingiva-derived MSCs enhance M2 macrophage polarization and inhibit periodontal bone loss. *Acta Biomater.* 122, 306–324. doi:10.1016/j.actbio.2020.12.046

Nazimek, K., Bryniarski, K., and Askenase, P. W. (2016). Functions of exosomes and microbial extracellular vesicles in allergy and contact and delayed-type hypersensitivity. *Int. Arch. Allergy Immunol.* 171 (1), 1–26. doi:10.1159/000449249

Nice, J. B., Balashova, N. V., Kachlany, S. C., Koufos, E., Krueger, E., Lally, E. T., et al. (2018). Aggregatibacter actinomycetemcomitans leukotoxin is delivered to host cells in an LFA-1-indepdendent manner when associated with outer membrane vesicles. *Toxins (Basel)* 10 (10), 414. doi:10.3390/toxins10100414

Nik Mohamed Kamal, N. N. S., Awang, R. A. R., Mohamad, S., and Shahidan, W. N. S. (2020). Plasma- and saliva exosome profile reveals a distinct MicroRNA signature in chronic periodontitis. *Front. Physiol.* 11, 587381. doi:10.3389/fphys.2020.587381

Ogawa, Y., Kanai-Azuma, M., Akimoto, Y., Kawakami, H., and Yanoshita, R. (2008). Exosome-like vesicles with dipeptidyl peptidase IV in human saliva. *Biol. Pharm. Bull.* 31 (6), 1059–1062. doi:10.1248/bpb.31.1059

Oliveira, M. C., Pieters, B. C. H., Guimarães, P. B., Duffles, L. F., Heredia, J. E., Silveira, A. L. M., et al. (2020). Bovine milk extracellular vesicles are osteoprotective by increasing osteocyte numbers and targeting RANKL/OPG system in experimental models of bone loss. *Front. Bioeng. Biotechnol.* 8, 891. doi:10.3389/fbioe.2020.00891

Ono, K., Eguchi, T., Sogawa, C., Calderwood, S. K., Futagawa, J., Kasai, T., et al. (2018). HSP-enriched properties of extracellular vesicles involve survival of metastatic oral cancer cells. *J. Cell. Biochem.* 119 (9), 7350–7362. doi:10.1002/jcb.27039

Ono, K., Sogawa, C., Kawai, H., Tran, M. T., Taha, E. A., Lu, Y., et al. (2020). Triple knockdown of CDC37, HSP90-alpha and HSP90-beta diminishes extracellular vesicles-driven malignancy events and macrophage M2 polarization in oral cancer. *J. Extracell. Vesicles* 9 (1), 1769373. doi:10.1080/20013078.2020.1769373

Pathan, M., Fonseka, P., Chitti, S. V., Kang, T., Sanwlani, R., Van Deun, J., et al. (2019). Vesiclepedia 2019: A compendium of RNA, proteins, lipids and metabolites in extracellular vesicles. *Nucleic Acids Res.* 47 (D1), D516–D519. doi:10.1093/nar/gky1029

Peng, Q., Yang, J. Y., and Zhou, G. (2020). Emerging functions and clinical applications of exosomes in human oral diseases. *Cell Biosci.* 10, 68. doi:10.1186/s13578-020-00424-0

Peng, Q., Zhang, J., and Zhou, G. (2019). Circulating exosomes regulate T-cell-mediated inflammatory response in oral lichen planus. *J. Oral Pathol. Med.* 48 (2), 143–150. doi:10.1111/jop.12804

Phinney, D. G., and Pittenger, M. F. (2017). Concise review: MSC-derived exosomes for cell-free therapy. *Stem Cells* 35 (4), 851–858. doi:10.1002/stem.2575

Pivoraite, U., Jarmalaviciute, A., Tunaitis, V., Ramanauskaite, G., Vaitkuviene, A., Kaseta, V., et al. (2015). Exosomes from human dental pulp stem cells suppress carrageenan-induced acute inflammation in mice. *Inflammation* 38 (5), 1933–1941. doi:10.1007/s10753-015-0173-6

Qin, X., Guo, H., Wang, X., Zhu, X., Yan, M., Wang, X., et al. (2019). Exosomal miR-196a derived from cancer-associated fibroblasts confers cisplatin resistance in head and neck cancer through targeting CDKN1B and ING5. *Genome Biol.* 20 (1), 12. doi:10.1186/s13059-018-1604-0

Rabie, A. M., and Veis, A. (1995). An immunocytochemical study of the routes of secretion of collagen and phosphophoryn from odontoblasts into dentin. *Connect. Tissue Res.* 31 (3), 197–209. doi:10.3109/03008209509010811

Rajan, T. S., Giacoppo, S., Diomede, F., Ballerini, P., Paolantonio, M., Marchisio, M., et al. (2016). The secretome of periodontal ligament stem cells from MS patients protects against EAE. *Sci. Rep.* 6, 38743. doi:10.1038/srep38743

Ramirez, M. I., Amorim, M. G., Gadelha, C., Milic, I., Welsh, J. A., Freitas, V. M., et al. (2018). Technical challenges of working with extracellular vesicles. *Nanoscale* 10 (3), 881–906. doi:10.1039/c7nr08360b

Raposo, G., and Stoorvogel, W. (2013). Extracellular vesicles: Exosomes, microvesicles, and friends. *J. Cell Biol.* 200 (4), 373–383. doi:10.1083/jcb.201211138

Ravindran, S., Narayanan, K., Eapen, A. S., Hao, J., Ramachandran, A., Blond, S., et al. (2008). Endoplasmic reticulum chaperone protein GRP-78 mediates endocytosis of dentin matrix protein 1. *J. Biol. Chem.* 283 (44), 29658–29670. doi:10.1074/jbc.M800786200

Robert, B. M., Dakshinamoorthy, M., Ganapathyagraharam Ramamoorthy, B., Dhandapani, M., Thangaiyan, R., Muthusamy, G., et al. (2018). Predicting tumor sensitivity to chemotherapeutic drugs in oral squamous cell carcinoma patients. *Sci. Rep.* 8 (1), 15545. doi:10.1038/s41598-018-33998-4

Rompikuntal, P. K., Thay, B., Khan, M. K., Alanko, J., Penttinen, A. M., Asikainen, S., et al. (2012). Perinuclear localization of internalized outer membrane vesicles carrying active cytolethal distending toxin from Aggregatibacter actinomycetemcomitans. *Infect. Immun.* 80 (1), 31–42. doi:10.1128/IAI.06069-11

Sadri, M., Shu, J., Kachman, S. D., Cui, J., and Zempleni, J. (2020). Milk exosomes and miRNA cross the placenta and promote embryo survival in mice. *Reproduction* 160 (4), 501–509. doi:10.1530/rep-19-0521

Sang, S. G., Rong, H., Wang, J. B., and Xie, Y. Q. (2014). Effects of Porphyromonas gingivalis extracellular vesicles on human periodontal ligament fibroblasts. *Int. J. Clin. Exp. Med.* 7 (2), 379–383.

Sartorio, M. G., Pardue, E. J., Feldman, M. F., and Haurat, M. F. (2021). Bacterial outer membrane vesicles: From discovery to applications. *Annu. Rev. Microbiol.* 75, 609–630. doi:10.1146/annurev-micro-052821-031444

Schwechheimer, C., and Kuehn, M. J. (2015). Outer-membrane vesicles from gram-negative bacteria: Biogenesis and functions. *Nat. Rev. Microbiol.* 13 (10), 605–619. doi:10.1038/nrmicro3525

Senpuku, H., Nakamura, T., Iwabuchi, Y., Hirayama, S., Nakao, R., and Ohnishi, M. (2019). Effects of complex DNA and MVs with GTF extracted from Streptococcus mutans on the oral biofilm. *Molecules* 24 (17), 3131. doi:10.3390/molecules24173131

Sento, S., Sasabe, E., and Yamamoto, T. (2016). Application of a persistent heparin treatment inhibits the malignant potential of oral squamous carcinoma cells induced by tumor cell-derived exosomes. *PLoS One* 11 (2), e0148454. doi:10.1371/journal.pone.0148454

Seo, B. M., Miura, M., Gronthos, S., Bartold, P. M., Batouli, S., Brahim, J., et al. (2004). Investigation of multipotent postnatal stem cells from human periodontal ligament. *Lancet* 364 (9429), 149–155. doi:10.1016/S0140-6736(04)16627-0

Sharma, S., Gillespie, B. M., Palanisamy, V., and Gimzewski, J. K. (2011). Quantitative nanostructural and single-molecule force spectroscopy biomolecular analysis of human-saliva-derived exosomes. *Langmuir* 27 (23), 14394–14400. doi:10.1021/la2038763

Shedden, K., Xie, X. T., Chandaroy, P., Chang, Y. T., and Rosania, G. R. (2003). Expulsion of small molecules in vesicles shed by cancer cells: Association with gene expression and chemosensitivity profiles. *Cancer Res.* 63 (15), 4331–4337.

Shi, Q., Qian, Z. Y., Liu, D. H., Sun, J., Wang, X., Liu, H. C., et al. (2017). GMSC-derived exosomes combined with a chitosan/silk hydrogel sponge accelerates wound healing in a diabetic rat skin defect model. *Front. Physiol.* 8, 904. doi:10.3389/fphys.2017.00904

Shi, W., Guo, S., Liu, L., Liu, Q., Huo, F., Ding, Y., et al. (2020). Small extracellular vesicles from lipopolysaccharide-preconditioned dental follicle cells promote periodontal regeneration in an inflammatory microenvironment. *ACS Biomater. Sci. Eng.* 6 (10), 5797–5810. doi:10.1021/acsbiomaterials.0c00882

Shimono, M., Hashimoto, S., Abiko, Y., Hamano, H., and Chen, S. H. (1991). Vacuoles and vesicles in the rat junctional epithelium: A study with serial ultrathin sections. *J. Periodontal Res.* 26 (2), 85–90. doi:10.1111/j.1600-0765.1991.tb01630.x

Simpson, R. J., Jensen, S. S., and Lim, J. W. (2008). Proteomic profiling of exosomes: Current perspectives. *Proteomics* 8 (19), 4083–4099. doi:10.1002/pmic.200800109

Singhrao, S. K., and Olsen, I. (2018). Are Porphyromonas gingivalis outer membrane vesicles microbullets for sporadic alzheimer's disease manifestation? *J. Alzheimers Dis. Rep.* 2 (1), 219–228. doi:10.3233/ADR-180080

Sjoqvist, S., Ishikawa, T., Shimura, D., Kasai, Y., Imafuku, A., Bou-Ghannam, S., et al. (2019a). Exosomes derived from clinical-grade oral mucosal epithelial cell sheets promote wound healing. *J. Extracell. Vesicles* 8 (1), 1565264. doi:10.1080/20013078.2019.1565264

Sjoqvist, S., Kasai, Y., Shimura, D., Ishikawa, T., Ali, N., Iwata, T., et al. (2019b). Oral keratinocyte-derived exosomes regulate proliferation of fibroblasts and epithelial cells. *Biochem. Biophys. Res. Commun.* 514 (3), 706–712. doi:10.1016/j.bbrc.2019.04.202

Soro, V., Dutton, L. C., Sprague, S. V., Nobbs, A. H., Ireland, A. J., Sandy, J. R., et al. (2014). Axenic culture of a candidate division TM7 bacterium from the human oral cavity and biofilm interactions with other oral bacteria. *Appl. Environ. Microbiol.* 80 (20), 6480–6489. doi:10.1128/AEM.01827-14

Soucy, S. M., Huang, J., and Gogarten, J. P. (2015). Horizontal gene transfer: Building the web of life. *Nat. Rev. Genet.* 16 (8), 472–482. doi:10.1038/nrg3962

Stanko, P., Altanerova, U., Jakubechova, J., Repiska, V., and Altaner, C. (2018). Dental mesenchymal stem/stromal cells and their exosomes. *Stem Cells Int.* 8, 1–8. doi:10.1155/2018/8973613

Sun, D. M., Zhuang, X. Y., Xiang, X. Y., Liu, Y. L., Zhang, S. Y., Liu, C. R., et al. (2010). A novel nanoparticle drug delivery system: The anti-inflammatory activity of curcumin is enhanced when encapsulated in exosomes. *Mol. Ther.* 18 (9), 1606–1614. doi:10.1038/mt.2010.105

Sun, Y., Xia, Z., Shang, Z., Sun, K., Niu, X., Qian, L., et al. (2016). Facile preparation of salivary extracellular vesicles for cancer proteomics. *Sci. Rep.* 6, 24669. doi:10.1038/srep24669

Sun, R., Xu, S., and Wang, Z. (2019). Rat sinus mucosa- and periosteum-derived exosomes accelerate osteogenesis. *J. Cell. Physiol.* 234 (12), 21947–21961. doi:10.1002/jcp.28758

Sundaram, K., Miller, D. P., Kumar, A., Teng, Y., Sayed, M., Mu, J., et al. (2019). Plant-derived exosomal nanoparticles inhibit pathogenicity of Porphyromonas gingivalis. *iScience* 21, 308–327. doi:10.1016/j.isci.2019.10.032

Tatullo, M., Codispoti, B., Spagnuolo, G., and Zavan, B. (2019). Human periapical cyst-derived stem cells can Be A smart "Lab-on-A-Cell" to investigate neurodegenerative diseases and the related alteration of the exosomes' content. *Brain Sci.* 9 (12), 358. doi:10.3390/brainsci9120358

Teng, F., and Fussenegger, M. (2020). Shedding light on extracellular vesicle biogenesis and bioengineering. *Adv. Sci. (Weinh).* 8 (1), 2003505. doi:10.1002/advs.202003505

Tian, Y. H., Li, S. P., Song, J., Ji, T. J., Zhu, M. T., Anderson, G. J., et al. (2014). A doxorubicin delivery platform using engineered natural membrane vesicle exosomes for targeted tumor therapy. *Biomaterials* 35 (7), 2383–2390. doi:10.1016/j.biomaterials.2013.11.083

Tkach, M., and Thery, C. (2016). Communication by extracellular vesicles: Where we are and where we need to go. *Cell* 164 (6), 1226–1232. doi:10.1016/j.cell.2016.01.043

Tong, L., Hao, H., Zhang, X., Zhang, Z., Lv, Y., Zhang, L., et al. (2020). Oral administration of bovine milk-derived extracellular vesicles alters the gut microbiota and enhances intestinal immunity in mice. *Mol. Nutr. Food Res.* 64 (8), e1901251. doi:10.1002/mnfr.201901251

Trabandt, A., Gay, R. E., Birkedal-Hansen, H., and Gay, S. (1990). Intracellular secretory pathway and ultrastructural localization of interstitial procollagenase in human gingival fibroblasts. *Matrix* 10 (5), 339–347. doi:10.1016/s0934-8832(11)80190-3

Tsuzuki, H., and Sasa, S. (1994). Ultrastructural observation of capillary sprouts in the dental organs of rat molars. *Kaib. Zasshi.* 69 (5), 684–696.

Vader, P., Mol, E. A., Pasterkamp, G., and Schiffelers, R. M. (2016). Extracellular vesicles for drug delivery. *Adv. Drug Deliv. Rev.* 106, 148–156. doi:10.1016/j.addr.2016.02.006

Valadi, H., Ekstrom, K., Bossios, A., Sjostrand, M., Lee, J. J., Lotvall, J. O., et al. (2007). Exosome-mediated transfer of mRNAs and microRNAs is a novel mechanism of genetic exchange between cells. *Nat. Cell Biol.* 9 (6), 654–659. doi:10.1038/ncb1596

van der Pol, E., Boing, A. N., Harrison, P., Sturk, A., and Nieuwland, R. (2012). Classification, functions, and clinical relevance of extracellular vesicles. *Pharmacol. Rev.* 64 (3), 676–705. doi:10.1124/pr.112.005983

Venugopal, C., K, S., Rai, K. S., Pinnelli, V. B., Kutty, B. M., Dhanushkodi, A., et al. (2018). Neuroprotection by human dental pulp mesenchymal stem cells: From billions to nano. *Curr. Gene Ther.* 18 (5), 307–323. doi:10.2174/1566523218666180913152615

Wang, H. S., Yang, F. H., Wang, Y. J., Pei, F., Chen, Z., Zhang, L., et al. (2019a). Odontoblastic exosomes attenuate apoptosis in neighboring cells. *J. Dent. Res.* 98 (11), 1271–1278. doi:10.1177/0022034519869580

Wang, L., Yin, P., Wang, J., Wang, Y., Sun, Z., Zhou, Y., et al. (2019b). Delivery of mesenchymal stem cells-derived extracellular vesicles with enriched miR-185 inhibits progression of OPMD. *Artif. Cells Nanomed. Biotechnol.* 47 (1), 2481–2491. doi:10.1080/21691401.2019.1623232

Wang, M., Li, J., Ye, Y., He, S., and Song, J. (2020a). SHED-derived conditioned exosomes enhance the osteogenic differentiation of PDLSCs via Wnt and BMP signaling *in vitro*. *Differentiation* 111, 1–11. doi:10.1016/j.diff.2019.10.003

Wang, R., Ji, Q., Meng, C., Liu, H., Fan, C., Lipkind, S., et al. (2020b). Role of gingival mesenchymal stem cell exosomes in macrophage polarization under inflammatory conditions. *Int. Immunopharmacol.* 81, 106030. doi:10.1016/j.intimp.2019.106030

Wang, Y., Zhang, S., Song, W., Zhang, W., Li, J., Li, C., et al. (2020c). Exosomes from EV71-infected oral epithelial cells can transfer miR-30a to promote EV71 infection. *Oral Dis.* 26, 778–788. doi:10.1111/odi.13283

Warburton, P. J., Palmer, R. M., Munson, M. A., and Wade, W. G. (2007). Demonstration of *in vivo* transfer of doxycycline resistance mediated by a novel transposon. *J. Antimicrob. Chemother.* 60 (5), 973–980. doi:10.1093/jac/dkm331

Watanabe, J., Sakai, K., Urata, Y., Toyama, N., Nakamichi, E., Hibi, H., et al. (2020). Extracellular vesicles of stem cells to prevent BRONJ. *J. Dent. Res.* 99 (5), 552–560. doi:10.1177/0022034520906793

Wei, F., Li, M., Crawford, R., Zhou, Y., and Xiao, Y. (2019a). Exosome-integrated titanium oxide nanotubes for targeted bone regeneration. *Acta Biomater.* 86, 480–492. doi:10.1016/j.actbio.2019.01.006

Wei, Y., Tang, C., Zhang, J., Li, Z., Zhang, X., Miron, R. J., et al. (2019b). Extracellular vesicles derived from the mid-to-late stage of osteoblast differentiation markedly enhance osteogenesis *in vitro* and *in vivo*. *Biochem. Biophys. Res. Commun.* 514 (1), 252–258. doi:10.1016/j.bbrc.2019.04.029

Wen, B., Huang, Y., Qiu, T., Huo, F., Xie, L., Liao, L., et al. (2021). Reparative dentin formation by dentin matrix proteins and small extracellular vesicles. *J. Endod.* 47 (2), 253–262. doi:10.1016/j.joen.2020.11.017

Wiklander, O. P. B., Brennan, M. A., Lotvall, J., Breakefield, X. O., and El Andaloussi, S. (2019). Advances in therapeutic applications of extracellular vesicles. *Sci. Transl. Med.* 11 (492), eaav8521. doi:10.1126/scitranslmed.aav8521

Wolf, P. (1967). The nature and significance of platelet products in human plasma. *Br. J. Haematol.* 13 (3), 269–288. doi:10.1111/j.1365-2141.1967.tb08741.x

Wu, J., Chen, L., Wang, R., Song, Z., Shen, Z., Zhao, Y., et al. (2019). Exosomes secreted by stem cells from human exfoliated deciduous teeth promote alveolar bone defect repair through the regulation of angiogenesis and osteogenesis. *ACS Biomater. Sci. Eng.* 5 (7), 3561–3571. doi:10.1021/acsbiomaterials.9b00607

Wu, R., Tao, Y., Cao, Y., Zhou, Y., and Lin, H. (2020). Streptococcus mutans membrane vesicles harboring glucosyltransferases augment Candida albicans biofilm development. *Front. Microbiol.* 11, 581184. doi:10.3389/fmicb.2020.581184

Wu, L., Wang, L., Liu, X., Bai, Y., Wu, R., Li, X., et al. (2022a). Milk-derived exosomes exhibit versatile effects for improved oral drug delivery. *Acta Pharm. Sin. B* 12 (4), 2029–2042. doi:10.1016/j.apsb.2021.12.015

Wu, R., Cui, G., Cao, Y., Zhao, W., and Lin, H. (2022b). Streptococcus mutans membrane vesicles enhance Candida albicans pathogenicity and carbohydrate metabolism. *Front. Cell. Infect. Microbiol.* 12, 940602. doi:10.3389/fcimb.2022.940602

Xie, C., Ji, N., Tang, Z., Li, J., and Chen, Q. (2019). The role of extracellular vesicles from different origin in the microenvironment of head and neck cancers. *Mol. Cancer* 18 (1), 83. doi:10.1186/s12943-019-0985-3

Xu, Z., Zheng, X., and Zheng, J. (2019). Tumor-derived exosomes educate fibroblasts to promote salivary adenoid cystic carcinoma metastasis via NGF-NTRK1 pathway. *Oncol. Lett.* 18 (4), 4082–4091. doi:10.3892/ol.2019.10740

Yakob, M., Fuentes, L., Wang, M. B., Abemayor, E., and Wong, D. T. (2014). Salivary biomarkers for detection of oral squamous cell carcinoma - current state and recent advances. *Curr. Oral Health Rep.* 1 (2), 133–141. doi:10.1007/s40496-014-0014-y

Yang, J., Hirschi, K. D., and Farmer, L. M. (2015). Dietary RNAs: New stories regarding oral delivery. *Nutrients* 7 (5), 3184–3199. doi:10.3390/nu7053184

Yang, W. W., Guo, B., Jia, W. Y., and Jia, Y. (2016). Porphyromonas gingivalis-derived outer membrane vesicles promote calcification of vascular smooth muscle cells through ERK1/2-RUNX2. *FEBS Open Bio* 6 (12), 1310–1319. doi:10.1002/2211-5463.12151

Yang, J. Y., Zhang, J., Lu, R., Tan, Y. Q., Du, G. F., Zhou, G., et al. (2020a). T cell-derived exosomes induced macrophage inflammatory protein-1α/β drive the

trafficking of CD8(+) T cells in oral lichen planus. *J. Cell. Mol. Med.* 24 (23), 14086–14098. doi:10.1111/jcmm.16020

Yang, R., Huang, H., Cui, S., Zhou, Y., Zhang, T., Zhou, Y., et al. (2020b). IFN-γ promoted exosomes from mesenchymal stem cells to attenuate colitis via miR-125a and miR-125b. *Cell Death Dis.* 11 (7), 603. doi:10.1038/s41419-020-02788-0

Yang, Y., Knight, R., Stephens, P., and Zhang, Y. (2020c). Three-dimensional culture of oral progenitor cells: Effects on small extracellular vesicles production and proliferative function. *J. Oral Pathol. Med.* 49 (4), 342–349. doi:10.1111/jop.12981

Yu, J., Lin, Y., Xiong, X., Li, K., Yao, Z., Dong, H., et al. (2019). Detection of exosomal PD-L1 RNA in saliva of patients with periodontitis. *Front. Genet.* 10, 202. doi:10.3389/fgene.2019.00202

Yu, W. T., Su, X. X., Li, M. X., Wan, W. T., Li, A., Zhou, H., et al. (2021). Three-dimensional mechanical microenvironment enhanced osteogenic activity of mesenchymal stem cells-derived exosomes. *Chem. Eng.J.* 417C.

Zarnowski, R., Sanchez, H., Covelli, A. S., Dominguez, E., Jaromin, A., Bernhardt, J., et al. (2018). Candida albicans biofilm-induced vesicles confer drug resistance through matrix biogenesis. *PLoS Biol.* 16 (10), e2006872. doi:10.1371/journal.pbio.2006872

Zhang, Y., Song, Y., Ravindran, S., Gao, Q., Huang, C. C., Ramachandran, A., et al. (2014). DSPP contains an IRES element responsible for the translation of dentin phosphophoryn. *J. Dent. Res.* 93 (2), 155–161. doi:10.1177/0022034513516631

Zhang, Y., Shi, S., Xu, Q., Zhang, Q., Shanti, R. M., Le, A. D., et al. (2019). SIS-ECM laden with GMSC-derived exosomes promote taste bud regeneration. *J. Dent. Res.* 98 (2), 225–233. doi:10.1177/0022034518804531

Zhang, S., Yang, Y., Jia, S., Chen, H., Duan, Y., Li, X., et al. (2020a). Exosome-like vesicles derived from Hertwig's epithelial root sheath cells promote the regeneration of dentin-pulp tissue. *Theranostics* 10 (13), 5914–5931. doi:10.7150/thno.43156

Zhang, Y., Tang, K., Chen, L., Du, M., and Qu, Z. (2020b). <p>Exosomal CircGDI2 suppresses oral squamous cell carcinoma progression through the regulation of MiR-424-5p/SCAI Axis</p>. *Cancer Manag. Res.* 12, 7501–7514. doi:10.2147/cmar.S255687

Zhang, Z., Shuai, Y., Zhou, F., Yin, J., Hu, J., Guo, S., et al. (2020c). PDLSCs regulate angiogenesis of periodontal ligaments via VEGF transferred by exosomes in periodontitis. *Int. J. Med. Sci.* 17 (5), 558–567. doi:10.7150/ijms.40918

Zhao, C., Zhang, G., Liu, J., Zhang, C., Yao, Y., Liao, W., et al. (2020). Exosomal cargoes in OSCC: Current findings and potential functions. *PeerJ* 8, e10062. doi:10.7717/peerj.10062

Zhou, H., Li, X., Yin, Y., He, X. T., An, Y., Tian, B. M., et al. (2020). The proangiogenic effects of extracellular vesicles secreted by dental pulp stem cells derived from periodontally compromised teeth. *Stem Cell Res. Ther.* 11 (1), 110. doi:10.1186/s13287-020-01614-w

Zhuang, X., Ji, L., Jiang, H., Liu, Y., Liu, X., Bi, J., et al. (2020). Exosomes derived from stem cells from the apical papilla promote dentine-pulp complex regeneration by inducing specific dentinogenesis. *Stem Cells Int.* 2020, 1–10. doi:10.1155/2020/5816723

Zlotogorski-Hurvitz, A., Dayan, D., Chaushu, G., Salo, T., and Vered, M. (2016). Morphological and molecular features of oral fluid-derived exosomes: Oral cancer patients versus healthy individuals. *J. Cancer Res. Clin. Oncol.* 142 (1), 101–110. doi:10.1007/s00432-015-2005-3

frontiers | Frontiers in Bioengineering and Biotechnology

TYPE Original Research
PUBLISHED 12 December 2022
DOI 10.3389/fbioe.2022.1087363

OPEN ACCESS

EDITED BY
Jin Yan,
Xi'an Jiaotong University, China

REVIEWED BY
Xiang Li,
Second Military Medical University, China
Guang Yang,
BenQ Medical Center, China
Xiaoxue Xing,
Fudan University, China

*CORRESPONDENCE
Yinong Huang,
ynhuang@xjtu.edu.cn
Hong Cai,
ch1031@163.com
Xiaojing Liu,
4511015055@xjtu.edu.cn
Jingyao Dai,
daijingyao2006@163.com

†These authors have contributed equally to this work and share first authorship

SPECIALTY SECTION
This article was submitted to Biomaterials, a section of the journal Frontiers in Bioengineering and Biotechnology

RECEIVED 07 November 2022
ACCEPTED 29 November 2022
PUBLISHED 12 December 2022

CITATION
Liu D, Huang Y, Mao J, Jiang C, Zheng L, Wu Q, Cai H, Liu X and Dai J (2022), A nanohybrid synthesized by polymeric assembling Au(I)-peptide precursor for anti-wrinkle function.
Front. Bioeng. Biotechnol. 10:1087363.
doi: 10.3389/fbioe.2022.1087363

A nanohybrid synthesized by polymeric assembling Au(I)-peptide precursor for anti-wrinkle function

Dan Liu[1†], Yinong Huang[2†*], Jian Mao[3,4], Cheng Jiang[3,4], Lei Zheng[3,4], Qimei Wu[3,4], Hong Cai[4*], Xiaojing Liu[1*] and Jingyao Dai[4,5*]

[1]Department of Talent Highland, The First Affiliated Hospital of Xi'an Jiaotong University, Xi'an, China, [2]Shaanxi Institute of Pediatric Diseases, Xi'an Children's Hospital, Xi'an, China, [3]Graduate School of China Medical University, Shenyang, China, [4]Air Force Medical Center, Beijing, China, [5]Air Force Medical Center, Fourth Military Medical University, Xi'an, China

A major sign of aging is wrinkles (dynamic lines and static lines) on the surface of the skin. In spite of Botulinum toxin's favorable therapeutic effect today, there have been several reports of its toxicity and side effects. Therefore, the development of an effective and safe wrinkle-fighting compound is imperative. An antioxidant-wrinkle effect was demonstrated by the peptide that we developed and synthesized, termed Skin Peptide. Aiming at the intrinsic defects of the peptide such as hydrolysis and poor membrane penetration, we developed a general approach to transform the Skin Peptide targeting intracellular protein-protein interaction into a bioavailable peptide-gold spherical nano-hybrid, Skin Pcluster. As expected, the results revealed that Skin Pcluster reduced the content of acetylcholine released by neurons *in vitro*, and then inhibit neuromuscular signal transmission. Additionally, human experiments demonstrated a significant de-wrinkle effect. Moreover, Skin Pcluster is characterized by a reliable safety profile. Consequently, anti-wrinkle peptides and Skin Pcluster nanohybrids demonstrated innovative anti-wrinkle treatments and have significant potential applications.

KEYWORDS

anti-wrinkle, anti-aging, peptide, nanohybrid, biomaterial

1 Introduction

Due to the rapid pace of modern life, the aging population, and our changing lifestyles (staying up late, eating irregularly, etc.), fine wrinkles and loose skin have become the most prevalent symptoms of aging (Spada et al., 2019). This is one of the most obvious signs of aging skin that brings forth aging-related concerns (Ganceviciene et al., 2012). As a result of wrinkles, anxiety, depression, and psychological and physiological inferiority can occur, affecting both work and personal lives negatively (Tomas-Aragones and Marron, 2016). At present,

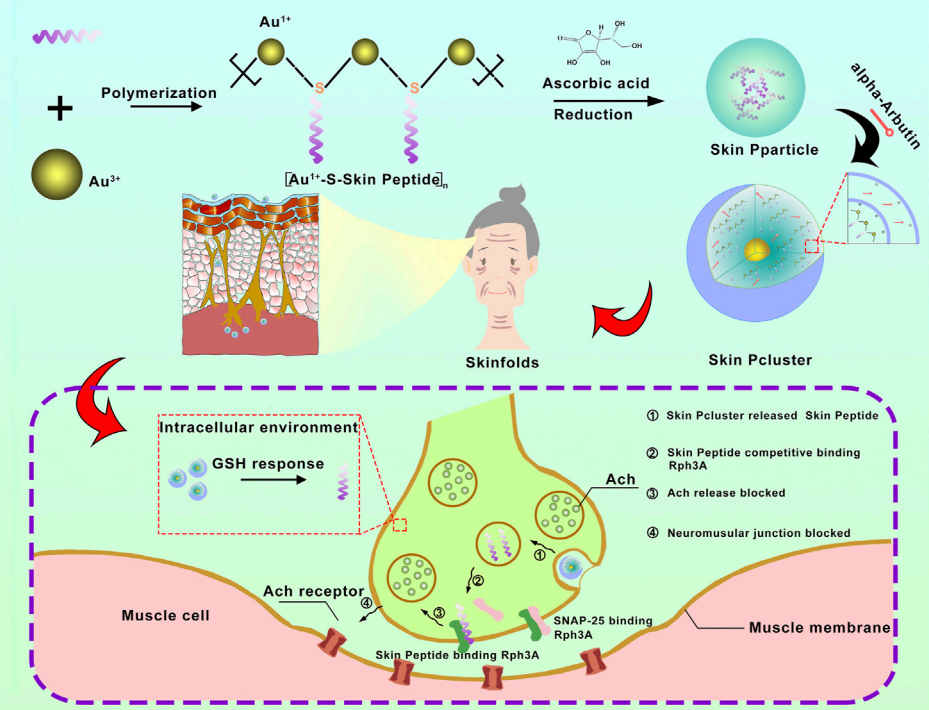

FIGURE 1
The schematic diagram for synthesis and biological function of Skin Pcluster. Firstly, a bionic peptide called Skin peptide was designed and synthesized. Then, the bioavailable peptide-gold spherical nano-hybrid, Skin Pcluster, was synthesized by self-assembled nanoengineering strategy. Skin Pcluster, similar to botulinum toxin and acetylhexapeptide-8, competitively binded Rph3A to inhibit the release of acetylcholine and then reduce wrinkles caused by excessive contraction of muscle.

Botulinum toxin (Botox), which inhibits muscle contractions by blocking acetylcholine, is the most widely used anti-aging modality (Nguyen et al., 2012; Tepper, 2020). However, Botox is expensive and has severe allergic reactions in humans, which cannot be ignored (Thanasarnaksorn et al., 2019). Therefore, the development of anti-wrinkle products is of great importance to address the issues of skin wrinkles.

There is an intrinsic factor that contributes significantly to the formation of wrinkles on the skin, which is the long-term muscle contraction by the facial muscles (Saluja and Fabi, 2017). By inhibiting the release of acetylcholine in nerve endings, neuromuscular signal transduction can be organized to paralyze muscles and reduce the formation of wrinkles. Rabphilin-3A (Rph3A) protein, which acts as a calcium-regulated nerve vesicle transporter on the inner membrane of nerve cells, can interact with SNAP25 to promote the release of acetylcholine. Blocking the interaction of Rph3A and SNAP25 can inhibit muscle fiber contraction and wrinkle formation (Nguyen et al., 2012; Ferrer-Orta et al., 2017; Stanic et al., 2017).

There are numerous types of external cosmetics or injectable pharmaceuticals in which peptides are widely used as major anti-wrinkle ingredients both at home and abroad (Kennedy et al., 2020; Lim et al., 2020). The biomimetic peptide called Skin Peptide was designed and synthesized by an automated synthesizer in our study (Figure 1). Similar to Botox and acetyl hexapeptide-8, Skin Peptide played a role of anti-wrinkles by competitively inhibiting the interaction between SNAP25 and Rph3A. In chromaffin cells, this suppresses catecholamine release regulated by Ca^{2+}, results in muscle to relax and paralysis, reduces the occurrence of dynamic lines and removes fine lines (Wang Y. et al., 2013; Multani et al., 2019a; Multani et al., 2019b). In addition, Skin Peptide has no risks of surgery, no restrictions on ages and no requirements for skin, which ensure a higher degree of safety than Botox. Due to inherent defects of peptide, such as low skin permeability, poor stability and rapid elimination, the clinical application of Skin Peptide is greatly limited (He et al., 2019a). To address these pharmacological barriers and improve clinical application of peptides, a growing number of optimizations for proteolytic resistance have been developed, including modifications and targeted delivery mechanisms (Lim et al., 2018). Although in optimizing peptide therapeutics, these two approaches have achieved some success, the translational applications of intracellular protein-protein interactions (PPI) remain a challenge (Katz et al., 2011).

As recent advances in nanotechnology, peptides are able to overcome inherent barriers more readily (Habibi et al., 2016; Li et al., 2017; Wei et al., 2017; Yuan et al., 2019). Through covalent or non-covalent modifications, the polypeptide has a stable structure with proteolytic resistance and cytomembrane permeability (Nevola and Giralt, 2015; Acar et al., 2017; Li et al., 2019). It has been demonstrated that peptide-derived nanomedicines, such as macromolecule-derived peptide nano micelles (Ying et al., 2016), peptide-coated nanoparticles (She et al., 2020), and peptide-based self-assembling nanostructures (He et al., 2019c; He et al., 2020), have attractive biological benefits including extended circulation times in the bloodstream, enhanced disease specificity and proteolytic stability (Yan et al., 2018; He et al., 2020; Zheng et al., 2021). The gold nanoparticle-conjugated peptides have the advantages of inherent inertia, low cytotoxicity and affordability, and have been more and more exploited and applied in clinical trials. In the past, AuNPs have been used as non-toxic vectors for the delivery of medicines and biomolecules. After conjugation, the complex structural characterizations of peptides (hydrophobicity, charge, and redox) are not conducive to the stable state of colloidal gold nanoparticles, resulting in subsequent aggregation and even sedimentation under the physiological conditions of increased ion concentration (Brinas et al., 2008). Thus, diminished colloidal stability usually results in prolonged release of therapeutic peptides, coupled with increased uptake by the reticuloendothelial system, ultimately leading to off-target toxicity and therapeutic failure (Ganceviciene et al., 2012).

In order to solve this problem, nanoengineering technology offers an attractive potential option (Yan et al., 2020a; Yan et al., 2021; Li et al., 2022). In mild conditions, the reducing agent transforms the peptide and $HAucl_4$ into $[Au(I)\text{-}S\text{-}peptide]_n$ and assembles the particles into a stable gold nanohybrid, a nanoscale gold sphere with a narrow distribution of gold particles (He et al., 2019b; Zheng et al., 2021; Wang et al., 2022). As one component of the drug delivery system, polypeptides significantly increased the loading efficiency. Further, it overcomes the inherent obstacles of peptides such as low skin permeability and poor stability.

2 Materials and methods

2.1 General remarks

All of these chemical reagents used in these experiments were obtained from Sigma-Aldrich unless otherwise indicated. All commercial products were directly used without further purification.

2.2 Synthesis of Skin Peptide

All peptides were prepared on a CSbio336X automated synthesizer using the technology of total chemical synthesis. After cleavage and deprotection in HF (Boc chemistry) or a mixture of reagents containing 88% TFA, 5% phenol, 5%H2O, and 2%TIPS (Fmoc chemistry), the crude products were precipitated with chilled diethyl and purified to homogeneity by preparative reversed-phase High-performance liquid chromatography (HPLC) on C18 columns. The molecular weights were identified by electrospray ionization mass spectrometry.

2.3 Preparation of Skin Pparticle and Skin Pcluster

The 0.5 ml $HAuCl_4$ (10 mM) and 0.4 ml vitamin C ascorbic acid (0.2 M) were successively mixed with 4.5 ml of distilled water in a 50 ml beaker and stirred at a speed of 650 rpm for a few minutes. The above mixture solution gradually changed from colorless to wine red, indicating the formation of the solution of Au-nanoparticles. Subsequently, the 5.4 mg of peptide completely dissolved into the 21.6 ml distilled water under the ultrasonic condition. The solution of peptide was added into the solution of Au-nanoparticles and mixed evenly to obtain the solution of Skin Pparticle. Finally, the solution of Skin Pcluster was synthesized by adding 2% alpha-arbutin on the basis of solution of Skin Pparticle.

2.4 Physicochemical characterization of Skin Pparticle and Skin Pcluster

The morphology and dimensions were recorded on Transmission electron microscopy (TEM) (HT7700, 120 kV) at an acceleration voltage of 120 kV. These size distribution and zeta potential of nanoparticles were measured by dynamic light scattering (DLS). The surface chemical structure of nanoparticles was observed by Fourier transform infrared (FT-IR) spectroscopy (Nicolet 6700) and UV-vis spectroscopy (Shimadzu 3000).

2.5 GSH-triggered Skin Pcluster release Skin Peptide

Skin Pcluster and alpha-Arbutin standard were centrifuged at a speed of 12,000 rpm for 10 min, respectively. The release of alpha-Arbutin was qualitatively detected in the supernatant by UV-vis spectroscopy (Shimadzu 3000).

To illustrate the release of Skin Pcluster by GSH-triggered, the Skin Pcluster was dissolved in PBS buffer (pH 7.4) containing 10 mM or 10 μM glutathione (GSH) and incubated at 37°C for 1 h, 2 h, 3 h, 6 h and 12 h, respectively. Following this, the release of Skin Peptide in supernatants was quantified by HPLC. (Mobile phase A: 0.1% TFA/H_2O, mobile phase B: 0.1% TFA/CH3CN, the flow rate of 1 ml/min, the gradient of 5–65%).

2.6 Study of acetylcholine release *in vitro*

The cultured neuron cells were induced by Skin Peptide and Botox respectively to detect the content of acetylcholine released in the supernatant. Untreated neuronal cell culture medium was used as negative control and Botox as positive control.

2.7 Study of paralytic relaxation of the gastrocnemius muscle in mice

The experiments involving animals were approved by the Xi'an Jiao tong University Ethics committee and followed the principles of the Laboratory Animal Center of Xi'an Jiao tong University.

C57BL/6 mice (aged 5–6 weeks) were randomly divided into the WT group (control group), Skin Pcluster group, Botox 0.004 U group, and Botox 0.008 U group, with no less than 3 mice in each group. The method of administration was intramuscular injection in the gastrocnemius muscle of mice with a dose of 20 μg per mouse (Cornet et al., 2020a; Cornet et al., 2020b). The images of the morphology were recorded by camera at 1 h and 2 h after injection. The effect of Skin Pcluster on gastrocnemius paralysis in mice was measured with force and drop distance by a digital force gauge.

2.8 Anti-wrinkle effect studies on humans

The experiments involving human were approved by the Air Force Medical University Ethics committee. Healthy subjects were recruited and randomly assigned to the group with/without anti-wrinkles treatment. The eye cream, face cream, essence and mask containing 10% Skin Pcluster were used on the skin of eyes, face, hands and neck respectively. The eye cream, face cream and essence were used twice a day and mask were used twice a week for 4 weeks. Pre- and post-treatment images were acquired by VISIA.

2.9 Statistics

The experimental results were compared between the two groups of data by independent sample *t*-test. One-way ANOVA and Tukey post-analysis, or logarithmic rank test was used to compare more than three groups ($^*p < 0.05$, $^{**}p < 0.01$, and $^{***}p < 0.001$).

3 Results

3.1 Design and synthesis of Skin Peptide

According to the report, Rph3A is a calcium-regulated neural vesicle transporter on the inner membrane of nerve cells, which interacts with SNAP25 to block the release of intracellular acetylcholine, and then inhibit the contraction of muscle and achieve the effect of anti-wrinkle (Lee et al., 2008). Hence, we focused on Rph3A as the target protein (PDB code: 5LOW) and synthesized Skin Peptide with the help of total chemical synthesis technology utilizing native chemical ligation. Subsequently, the relative molecular weight of the peptide was determined to be 1947 Da by mass spectrometry (Figure 2A), which further confirmed that the sequence of the synthesized peptide was consistent with our design, namely the Skin Peptide. The purity of the Skin Peptide was determined by HPLC. As shown in Figure 2B, the synthesized Skin Peptide showed a single chromatographic peak with a 13.61 min retention time. These results illustrated that Skin Peptide was successfully synthesized.

3.2 Synthesis and characterization of Skin Pcluster

According to the previous report (Yan et al., 2020b), the preparation of Skin Pcluster was conducted under mild conditions by a three-step "one-pot" reaction. Specifically speaking, in step 1) the reduction of the flavescent Au^{3+} by mercaptan in Skin Peptide-SH forms a polymerized structure of [Au (I)-SH-Skin Peptide] n, termed (Au^{1+}-S-Skin Peptide); step 2), subsequently, (Au^{1+}-S-Skin Peptide) is reduced to polymerized Au-peptide nanoparticles Skin Peptide Nanoparticles, termed Skin Pparticle. Finally, to endow nanoparticles with more biological properties and improve the physical stability of Skin Pparticle, in step 3), add alpha-Arbutin to trigger the Skin Pparticle into the Skin Pcluster in an electrostatic absorption manner (Figure 1).

In the first step, (Au^{1+}-S-Skin Peptide) was formed by spontaneous coordination between Au^{3+} in $HAucl_4$ and sulfated Skin Peptide. As shown in Figures 2C, D, the disappearance of the characteristic absorption peak of sulfhydryl groups in Skin Peptide-SH and the appearance of Au-SH absorption peak in Skin Pparticle and Skin Pcluster were confirmed by UV-Vis and FT-IR spectroscopy, which indicated successful synthesis of the (Au^{1+}-S-Skin Peptide).

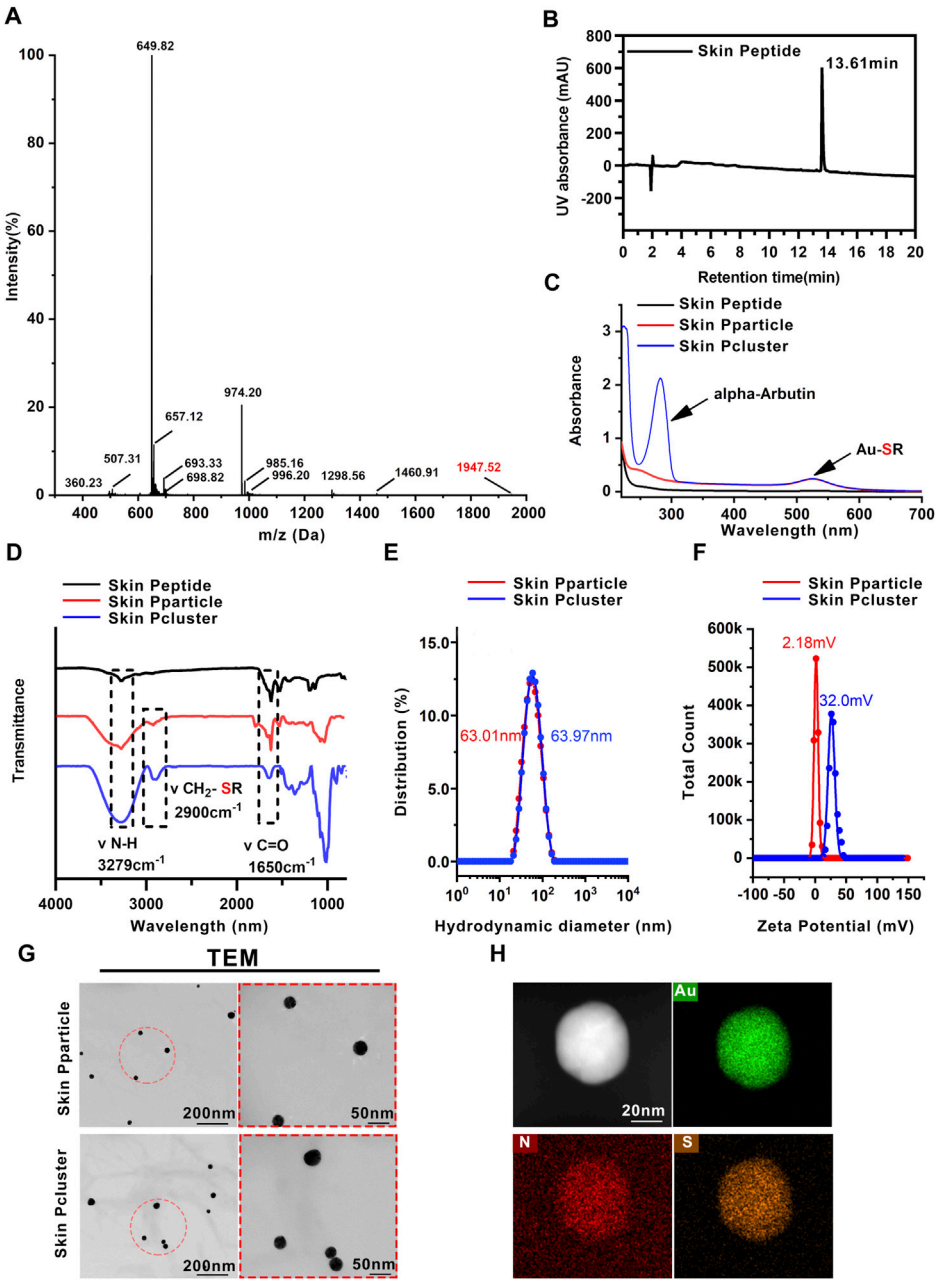

FIGURE 2
Characterization of Skin Pcluster. **(A)** The molecular weight of the Skin Peptide was identified by electrospray ionization mass spectrometry. **(B)** Retention time and purity of Skin Peptide was quantitatively analyzed by high performance liquid chromatography (HPLC) on a C18 column at 214 nm. **(C)** UV-vis spectra of Skin Peptide, Skin Pparticle and Skin Pcluster. The characteristic absorption peaks of Au-SR and alpha-Arbutin (aromatic compound) were visualized at 520 nm and 283nm, respectively. **(D)** FTIR spectra of the Skin Peptide, Skin Pparticle and Skin Pcluster were determined after lyophilization. Three absorption peaks at 3279 cm^{-1}, 2900 cm^{-1} and 1650 cm^{-1} demonstrated the stretching vibration of N-H, CH_2-SR, and C=O, respectively. **(E)** Hydrodynamic diameter distributions of the Skin Pparticle and Skin Pcluster were performed by dynamic light scattering. **(F)** The surface charge (Zeta potential) of the Skin Pparticle and Skin Pcluster was measured in PBS at pH7.4. **(G)** TEM images of the Skin Pparticle and Skin Pcluster were obtained by a CCD camera. The red circles represent magnification-related regions of the Skin Pparticle and Skin Pcluster. **(H)** Elemental analysis of Skin Pcluster was recorded by HRTEM.

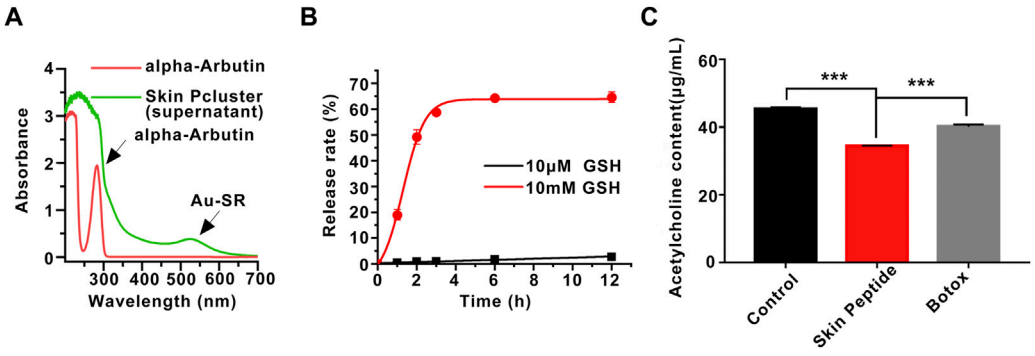

FIGURE 3
Stability of Skin Pcluster and the release of acetylcholine induced by Skin Peptide. **(A)** The release of alpha-Arbutin from Skin Pcluster in the supernatant was determined by UV-vis spectroscopy. **(B)** The release of Skin Peptide was detected in PBS containing 10 μM or 10 mM GSH at different times. **(C)** The measurement of acetylcholine in the supernatant. Data were shown as mean ± sem (n = 3). *P* values were obtained by *t*-test.

In the second step, the solution containing Vitamin C-ascorbic acid was reduced to the Skin Pparticle, and then was changed from colorless to wine-red to form the Skin Pparticle. The characteristic absorption peaks of peptides were found in the FT-IR spectrum (Figure 2D). In addition, as illustrated in Figure 2G, TEM images of the Skin Pparticle showed that the average size and shape distribution of particles was homogeneous at about 30 nm. It was worth noting that, in Figure 2E, the sizes of Skin Pparticle measured by dynamic light scattering (DLS) were 63.01 nm larger than that observed by TEM, which was attributed to the fact tant particles are easily stretched in solution.

In the third step, alpha-Arbutin was added into the two-step solution inducing the Skin Pparticles to form a more stable Skin Pcluster in a manner of electrostatic assembly. As shown in Figure 2C, the characteristic absorption peak of alpha-Arbutin was observed at 283 nm. With the addition of alpha-Arbutin, the zeta potential was gradually increased from 2.18 mV to 32.0 mV, indicating that the Skin Pcluster had excellent colloidal stability (Figure 2F). Additionally, the size distribution of the Skin Pcluster was homogenous and at approximately 30–40 nm observed by TEM (Figure 2G). The element overlay and TEM images presented the uniform distribution of nitrogen (N), sulfur (S), and gold (Au) in the Skin Pcluster indicating the good uniformity of Skin Pcluster (Figure 2H). The elements constituent of Skin Pcluster were consistent with the constituents of $HAuCl_4$, Skin Peptide, alpha-Arbutin, and Vitamin C-ascorbic acid by Energy dispersive X-ray spectroscopy (EDS) analysis (Supplementary Figure S1). Taken together, these results demonstrated that Skin Pclusters were successfully prepared and were homogeneous spherical gold-peptide nanohybrids.

3.3 Skin Pcluster can respond to GSH-triggered to release Skin Peptide

To endow nanoparticles with more biological properties and improve their physical stability, alpha-arbutin was added to induce the assembly of Skin Pparticle to form Skin Pcluster by electrostatic adsorption (Shin et al., 2019). The alpha-Arbutin can be qualitatively released in the supernatant of the Skin Pcluster. As demonstrated in Figure 3A, compared with the standard of alpha-arbutin, there was no characteristic absorption peak of alpha-arbutin at 283 nm in the supernatant of Skin Pcluster, indicating that the alpha-arbutin in Skin Pcluster was easily released. Additionally, the characteristic absorption peak of Au-SR can still be observed in the supernatant of Skin Pcluster, which is consistent with the result described above that Au-S bond was relatively stable.

The therapeutic effect of Skin Pcluster targeting intracellular PPI is related to the effective concentration of Skin Peptide in the cytoplasm (Yan et al., 2020a). Therefore, another essential function of the Skin Pcluster is the efficient release of functional Skin Peptide into the targeted cells. According to the literature (He et al., 2020), the Au-S bond is a robust chemical linkage in extracellular physiological environment, and it can be disrupted by a high concentration of thiol. GSH, as a general non-protein mercaptan in organisms, was discovered in intracellular at a concentration of millimoles and extracellular at a concentration of micromoles (Wang X. et al., 2013). To further simulate the high concentration of GSH could stimulate the quantitative release of Skin Peptide from the Skin Pcluster, Skin Peptide was monitored by analytical high-performance liquid chromatography (HPLC) at different time points.

As shown in Figure 3B, Skin Pcluster maintained basically intact after incubation in the PBS containing 10 μM GSH (pH7.4) for 12h, and release of Skin Peptides were much lower than 10%. In stark contrast, the release of Skin Peptides had reached 20% after Skin Pcluster incubated with 10 mM GSH for 1 h. Meanwhile, with the extension of incubation time, the release of Skin Peptides gradually increased. When Skin Pcluster was incubated for 12 h, the release of Skin Peptides reached 65%.

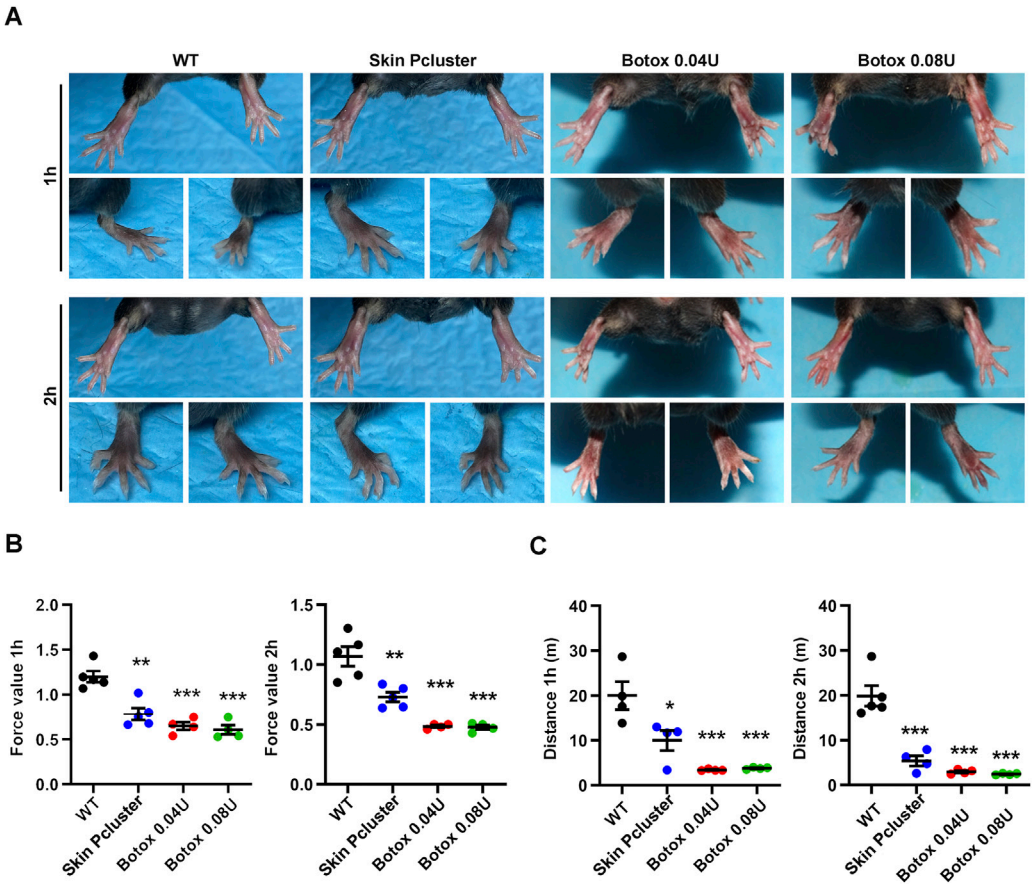

FIGURE 4
Study on paralytic relaxation of gastrocnemius in C57BL/6 mice. **(A)** The photographs of feet were recorded at 1h and 2 h after injection. **(B,C)** The effects of Skin Pcluster on gastrocnemius paralysis in mice were measured by force and drop distance with a digital force gauge. Statistic data were represented as mean ± sem (n = 4 or 5/group). *P* values were obtained by *t*-test.

These results illustrated that Skin Peptide can be released under high GSH conditions.

3.4 *In vitro* inhibition of acetylcholine release

Previous findings have indicated that Skin Peptide can be released in response to GSH. Based on this, we further investigated whether the released Skin Peptide could affect the content of the neurotransmitter acetylcholine. It has been reported that Botox can inhibit the release of acetylcholine, and thus Botox was used as a positive control. As shown in Figure 3C, Skin Peptide remarkably inhibited the released acetylcholine compared with the Control group, which was consistent with our previous speculation. Excitingly, in contrast to the Botox group, Skin Peptide significantly suppressed the release of acetylcholine. Collectively, these results demonstrated that Skin Peptide could decrease the release of the neurotransmitter acetylcholine.

3.5 Study of paralytic relaxation of the gastrocnemius muscle in mice

On previous study, the Skin Pcluster could inhibit the release of the neurotransmitter acetylcholine. To further confirm whether the Skin Pcluster had secondary effects on muscle movement in mice, such as muscle expansion and relaxation. The healthy mice were randomly divided into four groups, and were injected intramuscular with PBS(WT), Skin Pcluster (1 mg/kg), Botox (0.04U/Kg) or Botox (0.08U/Kg) at different time points, respectively. As shown in Figure 4A, compared with WT group, toes gradually converged and gastrocnemius relaxed in the hindlimbs of Skin Pcluster-treated mice after 1 h injection. Additionally, there was no significant difference in muscle relaxation between Botox (0.08 U/Kg, 0.04 U/Kg) and Skin

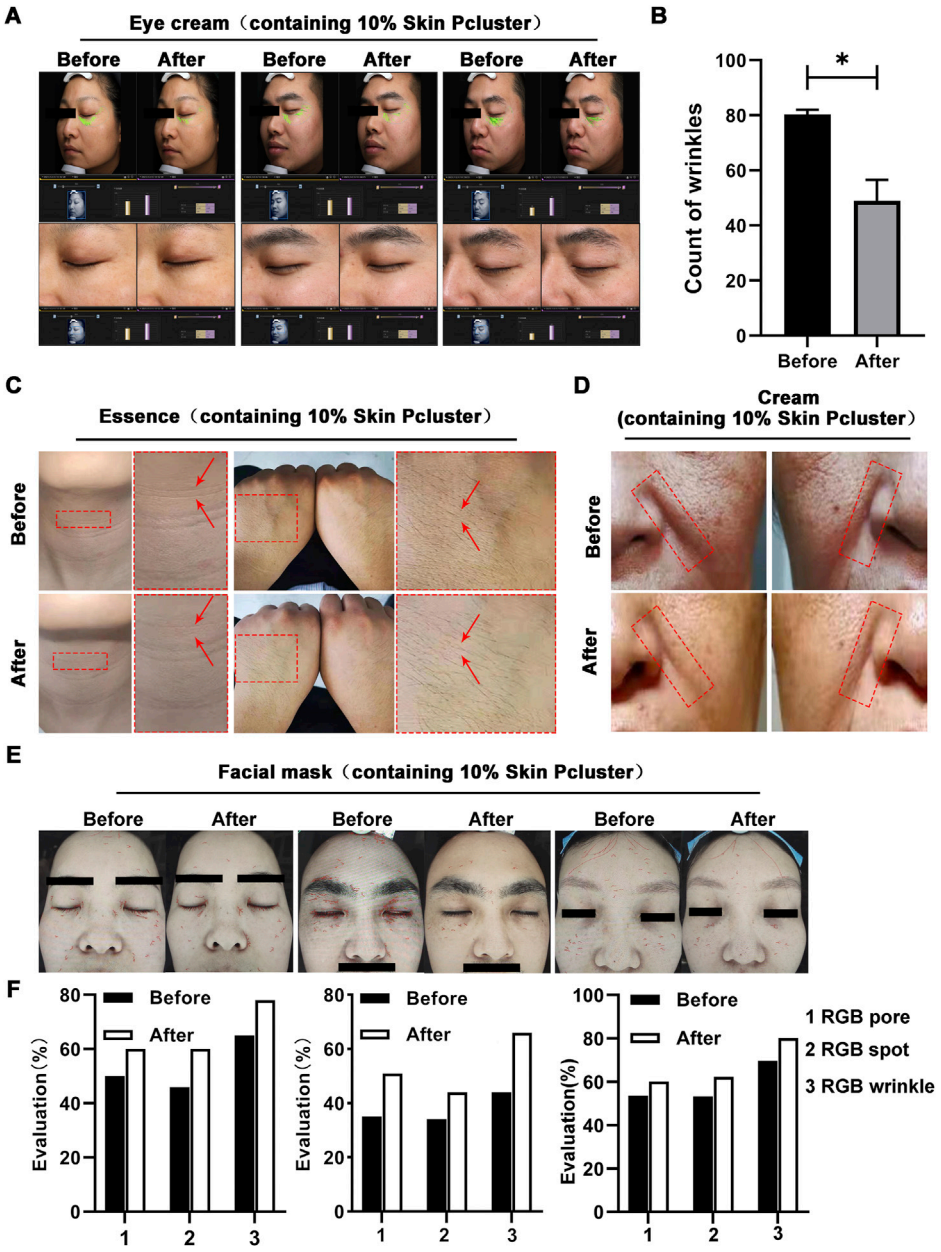

FIGURE 5
Anti-wrinkle effect of Skin Pcluster in humans. **(A,B)** Before and after the treatment with eye cream (including 10% Skin Pcluster), VISIA was used to visualize the wrinkles around the eyes of the recruited volunteers. The number of wrinkles was quantified. **(C)** The representative photographs of healthy subjects' neck and hand before and after treatment with essence containing 10% Skin Pcluster. **(D)** Images of facial wrinkles treated with a cream containing 10% Skin Pcluster. **(E,F)** Images of wrinkles around the eyes and on the forehead of the recruited volunteers were obtained by VISIA before and after treatment with eye cream containing 10% Skin Pcluster. p values were obtained by *t*-test.

Pcluster (1 mg/kg). Two hours after injection, the hindlimbs of the mice with Skin Pcluster-treatment displayed visible gastrocnemius weakness and toe aggregation.

Then, the test of mouse grasping power and the measurement of running distance were further used to quantitatively evaluate the muscle relaxation degree of the hindlimbs of mice after administration. As shown in Figure 4B, compared with WT group, the grasping power of Skin Pcluster group was significantly decreased 1h and 2 h after injection, respectively. Meanwhile, the grasping force values of Botox positive control group (0.04 U/Kg and 0.08 U/Kg) were also lower than those of WT group, indicating that the quantitative evaluation of the

degree of muscle relaxation in the hindlimbs of mice was feasible. As expected, after 1h and 2 h treatment, the running distance of Skin Pcluster group was significantly less than the WT group, which was consistent with the results of the grasping force (Figure 4C). In conclusion, these results suggested that the Skin Pcluster, as a novel self-assembling nanomedicine, produced a relaxant effect on the movement of gastrocnemius muscle.

3.6 Anti-wrinkles evaluation in humans

Previous studies have revealed that injection with Skin Pcluster can exert an inhibitory effect on the release of the neurotransmitter acetylcholine, which in turn blocks neuromuscular signaling. We further examined whether the suppression of neuromuscular transmission signaling can reduce or eliminate wrinkles caused by prolonged contractions of muscle. As expected, a significant reduction in eye wrinkle texture (marked in green) was observed in three subjects after treatment with eye cream containing 10% Skin Pcluster (Figure 5A). Using the VISIA Skin analysis system to further quantify the results of eye wrinkle improvement, it was found that when subjects applied an eye cream containing 10% Skin Pcluster, the number of wrinkle textures was reduced by half and the crow's feet texture covering the eye area was significantly improved (Figure 5B). Furthermore, none of the subjects experienced significant discomfort or allergic reactions after using the eye cream containing 10% Skin Pcluster.

To further confirm the reliability of Skin Pcluster's anti-wrinkle effect, essence containing 10% Skin Pcluster was applied to subjects' neck and hands respectively. As expected, the wrinkle texture of neck became lighter by visual inspection (marked by red arrows) when the neck was treated with essence containing 10% Skin Pcluster compared to the skin before application essence. Meanwhile, it was observed that in the hand, skin pores narrowed and skin tightened after application of essence (Figure 5C). In addition, there was no obvious discomfort or allergic reaction for all subjects after using the essence containing 10% Skin Pcluster. Next, the subjects with deep nasolabial folds were selected to receive a cream containing the 10% Skin Pcluster. Comparing the face area marked by the red dashed box, the nasolabial folds gradually became lighter after usage of the cream (Figure 5D).

Finally, VISIA skin analysis system was used to detect wrinkles across the face. It was consistently found that in subjects who applied mask with 10% Skin Pcluster, not only the number of wrinkles (red) was reduced, but also the pores and pigmentation of the skin were improved (Figures 5E, F). Moreover, in the analysis system, the higher value of RGB spots, RGB pores and RGB texture, the better the skin condition is. And it could be seen that these three indicators increased after the use of the mask. Furthermore, all the above subjects had no obvious discomfort or allergic reaction after using the mask. Taken together, the above results illustrated that the Skin Pcluster had an obvious anti-wrinkle effect. Notably, even intraperitoneal administration of Skin Pcluster did not result in loss of body weight, changes in H&E staining of organs and the function of liver and kidney (Supplementary Figure S2), suggesting the safety of the Skin Pcluster.

4 Discussion

Wrinkles (dynamic texture and static wrinkles) originate from the excessive contraction of muscle fibers, and the key to reduce wrinkles is to block the excessive contraction of muscle fibers. Rph3A, a calcium-regulated vesicle transporter located on the cell membrane of neurons, is involved in the release of neurotransmitters by interacting with SNAP25 (Ferrer-Orta et al., 2017). Therefore, we first designed and synthesized a bionic peptide that competitively binds to Rph3A for anti-wrinkle. However, due to the inherent defects of peptide (easy hydrolysis, poor membrane permeability, etc.), the further development and clinical application of it are limited. Here, we have developed a general nano-engineering technology to convert biomimetic peptides into stable and bioavailable peptide-gold spherical nanohybrids, called Skin Pcluster, under simple and mild chemical reaction conditions. According to previous TEM images, the Skin Pcluster had a particle size distribution of 30–40 nm and easily penetrated the skin. Additionally, Skin Peptide was covalently bound with Au^{1+} and was not easily degraded by the proteasome in skin. When the Skin Pcluster entered the neurons on muscle layer, Skin Peptides could be released in response to the intracellular higher GSH, competitively binds to Rph3A. Furthermore, the interaction of SNAP25-Rph3A was inhibited and the release of neurotransmitter acetylcholine was reduced, thus inhibiting excessive contraction of muscle to achieve anti-wrinkle effects. Through nano-engineering modification, Skin Pcluster was enhanced on the performance of penetrating skin, which can be applied on the surface of skin to play the role of anti-wrinkle. Compared with invasive operation of intramuscular injection, Skin Pcluster is more convenient, comfortable and safe to apply on the surface of skin, which further expands the possibility of widespread application of Skin Pcluster in the market in the future.

In this study, with the aid of computer-aided drug design, a biomimetic peptide was designed to target the interaction between intracellular proteins and proteins (Yu and MacKerell, 2017; Battini et al., 2021). There is no doubt that peptide-based nanostructures have increased exponentially over the past few decades, which is attributed to their bio-inspired properties. Biomimetic strategies have been widely used in various types of research, such as tumor therapy (He et al., 2022; Peng et al., 2022; Wu et al., 2022), vaccination (Peng et al.,

2022) and wound dress (Mirhaj et al., 2022). And it has been reported that nanocarriers with bionic cell membranes were an effective and safe delivery system for osteosarcoma therapy (Huang and Kiick, 2022). The shell of ZIF-8 has multiple functions to develop as a safe and effective platform for novel spore-based vaccine. In addition, the biomimetic strategies were applied to the preparation of bi-layer chitosan wound dressings. Generally speaking, the bionic strategy opens the way for a more systematic study of protein-protein interaction or nanoscale, which may eventually lead to the development of rationally designed engineered nanoparticles for biosynthesis. In the further continuation, our team will utilize bionic strategies to focus on the development of a new generation of collagen technology.

Data availability statement

The original contributions presented in the study are included in the article/Supplementary Material, further inquiries can be directed to the corresponding authors.

Ethics statement

The studies involving human participants were reviewed and approved by The human studies were approved by the Air Force Medical Center Ethics committee (No. 2022-193-YJ01). The patients/participants provided their written informed consent to participate in this study. The animal study was reviewed and approved by Xi'an Jiao tong University Ethics committee (No. 2021-1736). Written informed consent was obtained from the individual(s) for the publication of any potentially identifiable images or data included in this article.

Author contributions

JD designed the research, provided funding, and performed the final manuscript revision for the manuscript. HC collected experimental data and involved technical supervision. DL, JM, and YH fully participated in the research and preparation of the manuscript. CJ analyzed the data. LZ, QW, and XL were in charge of the experiments involving in animal and humans. All authors approved this final version of the manuscript.

Funding

This work was supported by Medical Improvement Plan (No.2021JSTS05) of Air Force Medical Center (For JD).

Acknowledgments

We thank Instrument Analysis Center of Xi'an Jiaotong University for their assistance with TEM, DLS, FT-IR and XPS analysis.

Conflict of interest

The authors declare that the research was conducted in the absence of any commercial or financial relationships that could be construed as a potential conflict of interest.

The handling editor JY declared a shared parent affiliation with the authors DL and XL at the time of the review.

Publisher's note

All claims expressed in this article are solely those of the authors and do not necessarily represent those of their affiliated organizations, or those of the publisher, the editors and the reviewers. Any product that may be evaluated in this article, or claim that may be made by its manufacturer, is not guaranteed or endorsed by the publisher.

Supplementary material

The Supplementary Material for this article can be found online at: https://www.frontiersin.org/articles/10.3389/fbioe.2022.1087363/full#supplementary-material

References

Acar, H., Ting, J. M., Srivastava, S., LaBelle, J. L., and Tirrell, M. V. (2017). Molecular engineering solutions for therapeutic peptide delivery. *Chem. Soc. Rev.* 46 (21), 6553–6569. doi:10.1039/c7cs00536a

Battini, L., Fidalgo, D. M., Alvarez, D. E., and Bollini, M. (2021). Discovery of a potent and selective chikungunya virus envelope protein inhibitor through computer-aided drug design. *ACS Infect. Dis.* 7 (6), 1503–1518. doi:10.1021/acsinfecdis.0c00915

Brinas, R. P., Hu, M., Qian, L., Lymar, E. S., and Hainfeld, J. F. (2008). Gold nanoparticle size controlled by polymeric Au(I) thiolate precursor size. *J. Am. Chem. Soc.* 130 (3), 975–982. doi:10.1021/ja076333e

Cornet, S., Perier, C., and Kalinichev, M. (2020a). Optimization of the rat digit abduction score (DAS) assay: Evaluation of botulinum neurotoxin activity in the gastrocnemius lateralis, peronei, and extensor digitorum longus. *Toxicon. X* 6, 100029. doi:10.1016/j.toxcx.2020.100029

Cornet, S., Perier, C., Wagner, S., Andriambeloson, E., Pouzet, B., and Kalinichev, M. (2020b). The use of the dynamic weight bearing test to assess the effects of acute, intramuscularly administered botulinum neurotoxin type A1 in rats. *Toxicon. X* 7, 100041. doi:10.1016/j.toxcx.2020.100041

Ferrer-Orta, C., Perez-Sanchez, M. D., Coronado-Parra, T., Silva, C., Lopez-Martinez, D., Baltanas-Copado, J., et al. (2017). Structural characterization of the

Rabphilin-3A-SNAP25 interaction. *Proc. Natl. Acad. Sci. U. S. A.* 114 (27), E5343–E5351. doi:10.1073/pnas.1702542114

Ganceviciene, R., Liakou, A. I., Theodoridis, A., Makrantonaki, E., and Zouboulis, C. C. (2012). Skin anti-aging strategies. *Dermatoendocrinol.* 4 (3), 308–319. doi:10.4161/derm.22804

Habibi, N., Kamaly, N., Memic, A., and Shafiee, H. (2016). Self-assembled peptide-based nanostructures: Smart nanomaterials toward targeted drug delivery. *Nano Today* 11 (1), 41–60. doi:10.1016/j.nantod.2016.02.004

He, S., Fang, J., Zhong, C., Wang, M., and Ren, F. (2022). Spatiotemporal delivery of pBMP2 and pVEGF by a core-sheath structured fiber-hydrogel gene-activated matrix loaded with peptide-modified nanoparticles for critical-sized bone defect repair. *Adv. Healthc. Mat.* 11, e2201096. doi:10.1002/adhm.202201096

He, W., Mazzuca, P., Yuan, W., Varney, K., Bugatti, A., Cagnotto, A., et al. (2019a). Identification of amino acid residues critical for the B cell growth-promoting activity of HIV-1 matrix protein p17 variants. *Biochimica Biophysica Acta - General Subj.* 1863 (1), 13–24. doi:10.1016/j.bbagen.2018.09.016

He, W., Wang, S., Yan, J., Qu, Y., Jin, L., Sui, F., et al. (2019b). Self-assembly of therapeutic peptide into stimuli-responsive clustered nanohybrids for cancer-targeted therapy. *Adv. Funct. Mat.* 29 (10), 1807736. doi:10.1002/adfm.201807736

He, W., Yan, J., Li, Y., Yan, S., Wang, S., Hou, P., et al. (2020). Resurrecting a p53 peptide activator - an enabling nanoengineering strategy for peptide therapeutics. *J. Control. Release* 325, 293–303. doi:10.1016/j.jconrel.2020.06.041

He, W., Yan, J., Wang, L., Lei, B., Hou, P., Lu, W., et al. (2019c). A lanthanide-peptide-derived bacterium-like nanotheranostic with high tumor-targeting, -imaging and -killing properties. *Biomaterials* 206, 13–24. doi:10.1016/j.biomaterials.2019.03.026

Huang, H., and Kiick, K. (2022). Peptide-based assembled nanostructures that can direct cellular responses. *Biomed. Mat.* 17 (6), 062002. doi:10.1088/1748-605X/ac92b5

Katz, C., Levy-Beladev, L., Rotem-Bamberger, S., Rito, T., Rudiger, S. G., and Friedler, A. (2011). Studying protein-protein interactions using peptide arrays. *Chem. Soc. Rev.* 40 (5), 2131–2145. doi:10.1039/c0cs00029a

Kennedy, K., Cal, R., Casey, R., Lopez, C., Adelfio, A., Molloy, B., et al. (2020). The anti-ageing effects of a natural peptide discovered by artificial intelligence. *Int. J. Cosmet. Sci.* 42 (4), 388–398. doi:10.1111/ics.12635

Lee, J. D., Huang, P. C., Lin, Y. C., Kao, L. S., Huang, C. C., Kao, F. J., et al. (2008). In-depth fluorescence lifetime imaging analysis revealing SNAP25A-Rabphilin 3A interactions. *Microsc. Microanal.* 14 (6), 507–518. doi:10.1017/S1431927608080628

Li, L., He, W., You, W., Yan, J., and Liu, W. (2022). Turing miRNA into infinite coordination supermolecule: A general and enabling nanoengineering strategy for resurrecting nuclear acid therapeutics. *J. Nanobiotechnology* 20 (1), 10. doi:10.1186/s12951-021-01212-9

Li, M., Guan, Y., Zhao, A., Ren, J., and Qu, X. (2017). Using multifunctional peptide conjugated Au nanorods for monitoring beta-amyloid aggregation and chemo-photothermal treatment of alzheimer's disease. *Theranostics* 7 (12), 2996–3006. doi:10.7150/thno.18459

Li, X., Tolbert, W. D., Hu, H. G., Gohain, N., Zou, Y., Niu, F., et al. (2019). Dithiocarbamate-inspired side chain stapling chemistry for peptide drug design. *Chem. Sci.* 10 (5), 1522–1530. doi:10.1039/c8sc03275k

Lim, S. H., Sun, Y., Thiruvallur Madanagopal, T., Rosa, V., and Kang, L. (2018). Enhanced skin permeation of anti-wrinkle peptides via molecular modification. *Sci. Rep.* 8 (1), 1596. doi:10.1038/s41598-017-18454-z

Lim, S. H., Tiew, W. J., Zhang, J., Ho, P. C., Kachouie, N. N., and Kang, L. (2020). Geometrical optimisation of a personalised microneedle eye patch for transdermal delivery of anti-wrinkle small peptide. *Biofabrication* 12 (3), 035003. doi:10.1088/1758-5090/ab6d37

Mirhaj, M., Tavakoli, M., Varshosaz, J., Labbaf, S., Salehi, S., Talebi, A., et al. (2022). Preparation of a biomimetic bi-layer chitosan wound dressing composed of A-PRF/sponge layer and L-arginine/nanofiber. *Carbohydr. Polym.* 292, 119648. doi:10.1016/j.carbpol.2022.119648

Multani, I., Manji, J., Hastings-Ison, T., Khot, A., and Graham, K. (2019a). Botulinum toxin in the management of children with cerebral palsy. *Pediatr. Drugs* 21 (4), 261–281. doi:10.1007/s40272-019-00344-8

Multani, I., Manji, J., Tang, M. J., Herzog, W., Howard, J. J., and Graham, H. K. (2019b). Sarcopenia, cerebral palsy, and botulinum toxin type A. *JBJS Rev.* 7 (8), e4. doi:10.2106/JBJS.RVW.18.00153

Nevola, L., and Giralt, E. (2015). Modulating protein-protein interactions: The potential of peptides. *Chem. Commun.* 51 (16), 3302–3315. doi:10.1039/c4cc08565e

Nguyen, A. T., Ahmad, J., Fagien, S., and Rohrich, R. J. (2012). Cosmetic medicine: Facial resurfacing and injectables. *Plastic Reconstr. Surg.* 129 (1), 142e–153e. doi:10.1097/PRS.0b013e3182362c63

Peng, F., Xiang, Y., Wang, H., Hu, Y., Zhou, R., and Hu, Y. (2022). Biomimetic assembly of Spore@ZIF-8 microspheres for vaccination. *Small* 18 (38), e2204011. doi:10.1002/smll.202204011

Saluja, S. S., and Fabi, S. G. (2017). A holistic approach to antiaging as an adjunct to antiaging procedures: A review of the literature. *Dermatol. Surg.* 43 (4), 475–484. doi:10.1097/DSS.0000000000001027

She, J., Li, Y., Yan, S., Yan, Y., Liu, D., Li, S., et al. (2020). De novo supraparticle construction by a self-assembled Janus cyclopeptide to tame hydrophilic microRNA and hydrophobic molecule for anti-tumor cocktail therapy and augmented immunity. *Chem. Eng. J.* 401, 126080. doi:10.1016/j.cej.2020.126080

Shin, J. W., Kwon, S. H., Choi, J. Y., Na, J. I., Huh, C. H., Choi, H. R., et al. (2019). Molecular mechanisms of dermal aging and antiaging approaches. *Int. J. Mol. Sci.* 20 (9), 2126. doi:10.3390/ijms20092126

Spada, F., Lui, A. H., and Barnes, T. M. (2019). <p>Use of formulations for sensitive skin improves the visible signs of aging, including wrinkle size and elasticity</p>. *Clin. Cosmet. Investig. Dermatol.* 12, 415–425. doi:10.2147/CCID.S212240

Stanic, J., Mellone, M., Napolitano, F., Racca, C., Zianni, E., Minocci, D., et al. (2017). Rabphilin 3A: A novel target for the treatment of levodopa-induced dyskinesias. *Neurobiol. Dis.* 108, 54–64. doi:10.1016/j.nbd.2017.08.001

Tepper, D. (2020). *OnabotulinumtoxinA. Headache* 60 (10), 2649–2650. doi:10.1111/head.13955

Thanasarnaksorn, W., Rattakul, B., Suvanasuthi, S., and Sutthipisal, N. (2019). Botulinum toxin type A injection-related suppurative granuloma: A case report. *J. Cosmet. Laser Ther.* 21 (7-8), 422–424. doi:10.1080/14764172.2019.1690663

Tomas-Aragones, L., and Marron, S. E. (2016). Body image and body dysmorphic concerns. *Acta Derm. Venereol.* 96 (217), 47–50. doi:10.2340/00015555-2368

Wang, J., Yang, W., He, X., Zhang, Z., and Zheng, X. (2022). Assembling p53 activating peptide with CeO2 nanoparticle to construct a metallo-organic supermolecule toward the synergistic ferroptosis of tumor. *Front. Bioeng. Biotechnol.* 10, 929536. doi:10.3389/fbioe.2022.929536

Wang, X., Cai, X., Hu, J., Shao, N., Wang, F., Zhang, Q., et al. (2013a). Glutathione-triggered "off-on" release of anticancer drugs from dendrimer-encapsulated gold nanoparticles. *J. Am. Chem. Soc.* 135 (26), 9805–9810. doi:10.1021/ja402903h

Wang, Y., Wang, M., Xiao, S., Pan, P., Li, P., and Huo, J. (2013b). The anti-wrinkle efficacy of argireline, a synthetic hexapeptide, in Chinese subjects: A randomized, placebo-controlled study. *Am. J. Clin. Dermatol.* 14 (2), 147–153. doi:10.1007/s40257-013-0009-9

Wei, G., Su, Z., Reynolds, N. P., Arosio, P., Hamley, I. W., Gazit, E., et al. (2017). Self-assembling peptide and protein amyloids: From structure to tailored function in nanotechnology. *Chem. Soc. Rev.* 46 (15), 4661–4708. doi:10.1039/c6cs00542j

Wu, W., Guo, H., Jing, D., Zhang, Z., Zhang, Z., Pu, F., et al. (2022). Targeted delivery of PD-L1-derived phosphorylation-mimicking peptides by engineered biomimetic nanovesicles to enhance osteosarcoma treatment. *Adv. Healthc. Mat.* 2022, e2200955. doi:10.1002/adhm.202200955

Yan, J., He, W., Yan, S., Niu, F., Liu, T., Ma, B., et al. (2018). Self-assembled peptide-lanthanide nanoclusters for safe tumor therapy: Overcoming and utilizing biological barriers to peptide drug delivery. *ACS Nano* 12 (2), 2017–2026. doi:10.1021/acsnano.8b00081

Yan, J., Ji, F., Yan, S., You, W., Ma, F., Li, F., et al. (2020a). A general-purpose Nanohybrid fabricated by Polymeric Au(I)-peptide precursor to wake the function of Peptide Therapeutics. *Theranostics* 10 (19), 8513–8527. doi:10.7150/thno.47243

Yan, J., Yao, Y., Yan, S., Gao, R., Lu, W., and He, W. (2020b). Chiral protein supraparticles for tumor suppression and synergistic immunotherapy: An enabling strategy for bioactive supramolecular chirality construction. *Nano Lett.* 20 (8), 5844–5852. doi:10.1021/acs.nanolett.0c01757

Yan, S., Yan, J., Liu, D., Li, X., Kang, Q., You, W., et al. (2021). A nano-predator of pathological MDMX construct by clearable supramolecular gold(I)-thiol-peptide complexes achieves safe and potent anti-tumor activity. *Theranostics* 11 (14), 6833–6846. doi:10.7150/thno.59020

Ying, M., Zhan, C., Wang, S., Yao, B., Hu, X., Song, X., et al. (2016). Liposome-based systemic glioma-targeted drug delivery enabled by all-d peptides. *ACS Appl. Mat. Interfaces* 8 (44), 29977–29985. doi:10.1021/acsami.6b10146

Yu, W., and MacKerell, A. D., Jr. (2017). Computer-aided drug design methods. *Methods Mol. Biol.* 1520, 85–106. doi:10.1007/978-1-4939-6634-9_5

Yuan, Q., Gao, F., Yao, Y., Cai, P., Zhang, X., Yuan, J., et al. (2019). Gold clusters prevent inflammation-induced bone erosion through inhibiting the activation of NF-κB pathway. *Theranostics* 9 (7), 1825–1836. doi:10.7150/thno.31893

Zheng, X., Yan, J., You, W., Li, F., Diao, J., He, W., et al. (2021). De novo nano-erythrocyte structurally braced by biomimetic Au(I)-peptide skeleton for MDM2/MDMX predation toward augmented pulmonary adenocarcinoma immunotherapy. *Small* 17 (20), e2100394. doi:10.1002/smll.202100394

frontiers | Frontiers in Bioengineering and Biotechnology

TYPE Original Research
PUBLISHED 26 January 2023
DOI 10.3389/fbioe.2023.1124944

OPEN ACCESS

EDITED BY
Jin Yan,
Xi'an Jiaotong University, China

REVIEWED BY
Zhimin Tian,
Northwestern Polytechnical University, China
Jinran Lin,
Fudan University, China

*CORRESPONDENCE
Hang Liu,
liuhang@xjtu.edu.cn
Weinan Guo,
guown@fmmu.edu.cn

SPECIALTY SECTION
This article was submitted to Biomaterials, a section of the journal Frontiers in Bioengineering and Biotechnology

RECEIVED 15 December 2022
ACCEPTED 13 January 2023
PUBLISHED 26 January 2023

CITATION
Yang N, Shi N, Yao Z, Liu H and Guo W (2023), Gallium-modified gelatin nanoparticles loaded with quercetin promote skin wound healing *via* the regulation of bacterial proliferation and macrophage polarization. *Front. Bioeng. Biotechnol.* 11:1124944. doi: 10.3389/fbioe.2023.1124944

Gallium-modified gelatin nanoparticles loaded with quercetin promote skin wound healing *via* the regulation of bacterial proliferation and macrophage polarization

Ning Yang[1], Nianyuan Shi[2], Zhou Yao[1], Hang Liu[3]* and Weinan Guo[4]*

[1]Xijing Hospital, Fourth Military Medical University, Xi'an, China, [2]The Key Laboratory of Biomedical Information Engineering of Ministry of Education, Xi'an Jiaotong University School of Life Science and Technology, Xi'an, China, [3]State Key Laboratory for Mechanical Behavior of Materials, Xi'an Jiaotong University, Xi'an, China, [4]Department of Dermatology, Xijing Hospital, Fourth Military Medical University, Xi'an, China

Background: Wound healing is a complicated process involving multiple cell components and can help the re-establishment of the skin's barrier function. Previous studies have pointed out that bacterial infection and sustained inflammatory reactions are the main causes of the delay of wound closure and scar formation during wound healing. The effect of current approaches for scar-free wound repair still faces many challenges, and alternative therapeutic methods are urgently needed to be established.

Methods: The basic characteristics of the new-designed nanoparticles were clarified through the characterization of the material. The biocompatibility of the nanoparticles, as well as its effect on fibroblast function, anti-bacterial capacity, inflammation suppressive role, and the underlying mechanism were further verified by a panel of biochemical assays *in vitro*. Ultimately, pre-clinical rat model was employed to testify its role in wound healing and scar formation *in vivo*.

Results: Firstly, gallium-modified gelatin nanoparticles loaded with quercetin was successfully established, displaying good biocompatibility and facilitative effect on fibroblast function. In addition, the nanoparticles showed prominent anti-bacterial and inflammation-suppressive effects. What's more important, the nanoparticles could also induce the polarization of macrophages from M1 to M2 phenotype to exert its inflammatory inhibitory role through TGF-β/Smad signaling pathway. Ultimately, *in vivo* experiment showed that the nanoparticles could effectively promote wound repair and inhibit scar formation during the process of wound healing.

Conclusion: Taken together, the new nanoparticles have good anti-bacterial and anti-scar formation effects and great potential in the field of skin wound repair, which provides a promising therapeutic strategy for wound treatment.

KEYWORDS

Gallium, nanoparticles, Quercetin, wound healing, macrophage

Introduction

Wound healing is a complicated process involving multiple cell components and can help the re-establishment of the skin's barrier function (Gurtner et al., 2008). Impaired function of fibroblast, bacterial proliferation, and prolonged activation of inflammatory reactions at the wound site are the major reasons for delayed wound healing and excess scar formation (Morris et al., 2014; Nanditha and Kumar, 2022; Shams et al., 2022). Delayed wound healing and the resultant occurrence of hypertrophic scar (HS) not only leads to a reduction in cosmetic effects, but also might result in impaired function of adjacent joints, greatly affecting patients' quality of life (QOL). Of note, HS has been identified as one of the major unaddressed functional and psychosocial challenges facing global health (Ogawa et al., 2021). Previously, several agents like corticosteroids, bleomycin and verapamil have been reported to ameliorate scarring during the process of wound healing (Giugliano et al., 2003; Yamamoto, 2006; Atiyeh, 2020). Nevertheless, since that skin wound healing is a complicated process with risks of infection, as well as the detailed mechanism underlying wound healing and scar formation remains far from understood, the effect of current approaches for scar-free wound repair still faces many challenges (Alster, 2003), and alternative therapeutic methods are needed to be established.

In recent years, accumulative evidence has demonstrated that some types of new biomaterials, such as hydrogel nanoparticles, are of great therapeutic potential in wound healing repair and anti-scar treatment. Hydrogel nanoparticles are an emerging biomaterial technology, displaying advantages including relatively larger coverage area, strong absorbability, strong slow-release capacity, and minor side effects, and have great application prospect in tissue repair, targeted drug delivery and regenerative medicine (Huang et al., 2022). It has also been reported that the injectable hydrogel nanoparticle preparation is suitable for closure of irregular wound and wound surface (Tariq et al., 2022), indicating the potential of hydrogel nanoparticle in repairing skin wound. Of note, impaired function of fibroblast, bacterial proliferation, and prolonged activation of inflammatory reactions are among the most important causes of the delay of wound healing and excessive scar formation (Morris et al., 2014; Nanditha and Kumar, 2022; Shams et al., 2022). Therefore, if any hydrogel nanoparticles preparation with the capacity to potentiate fibroblast function, suppress bacterial proliferation and inhibit excess inflammation can be developed, it will be an ideal method for wound treatment with simultaneous effects on promoting wound closure and inhibiting scar formation.

Gallium composite is an international emerging anti-bacterial material (Clarkin et al., 2019). The iron-eating property of bacteria is utilized to make the gallium ion that is highly similar to iron ion enter cells in place of iron, and then disrupt the iron metabolism of bacteria to reduce their survival rate to achieve the anti-bacterial effect (Wang et al., 2020). Of note, the anti-bacterial property of gallium ion has been verified in many studies (Qi et al., 2022; Zheng et al., 2022), and the Food and Drug Administration (FDA) also affirmed that gallium has good anti-bacterial activity and can be used in medicine (Rossato et al., 2022). While gallium ion-coated nanoparticles have been prepared in some studies and used to treat diseases like liver abscess and cancer (Xie et al., 2021; Yang et al., 2021). Their anti-bacterial effects on biological wound remain elusive. Quercetin is a

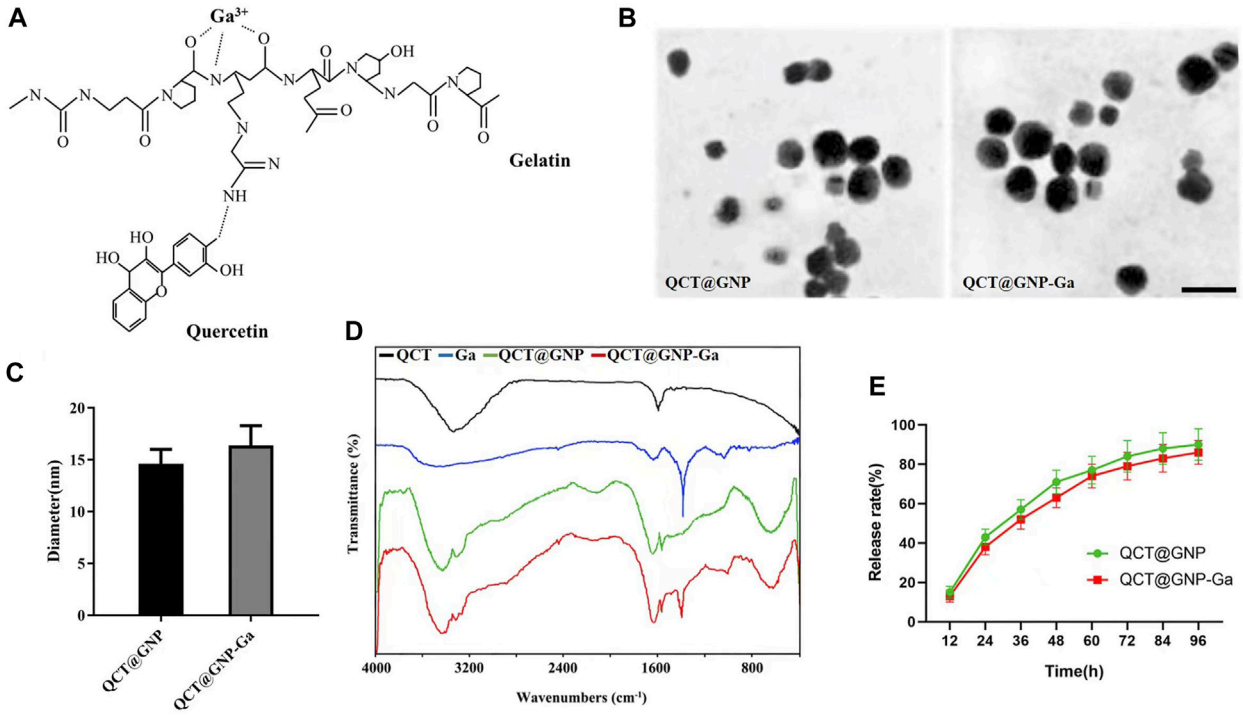

FIGURE 1
Characterization of QCT@GNP-Ga. **(A)** A schematic view of the design of gallium-modified gelatin nanoparticles loaded with quercetin. **(B)** Representative image TEM images of QCT@GNP and QCT@GNP-Ga, Scale bar = 20 nm. **(C)** Particle size of QCT@GNP and QCT@GNP-Ga. **(D)** FTIR spectra of QCT, Ga, QCT@GNP, and QCT@GNP-Ga. **(E)** QCT release from QCT@GNP and QCT@GNP-Ga.

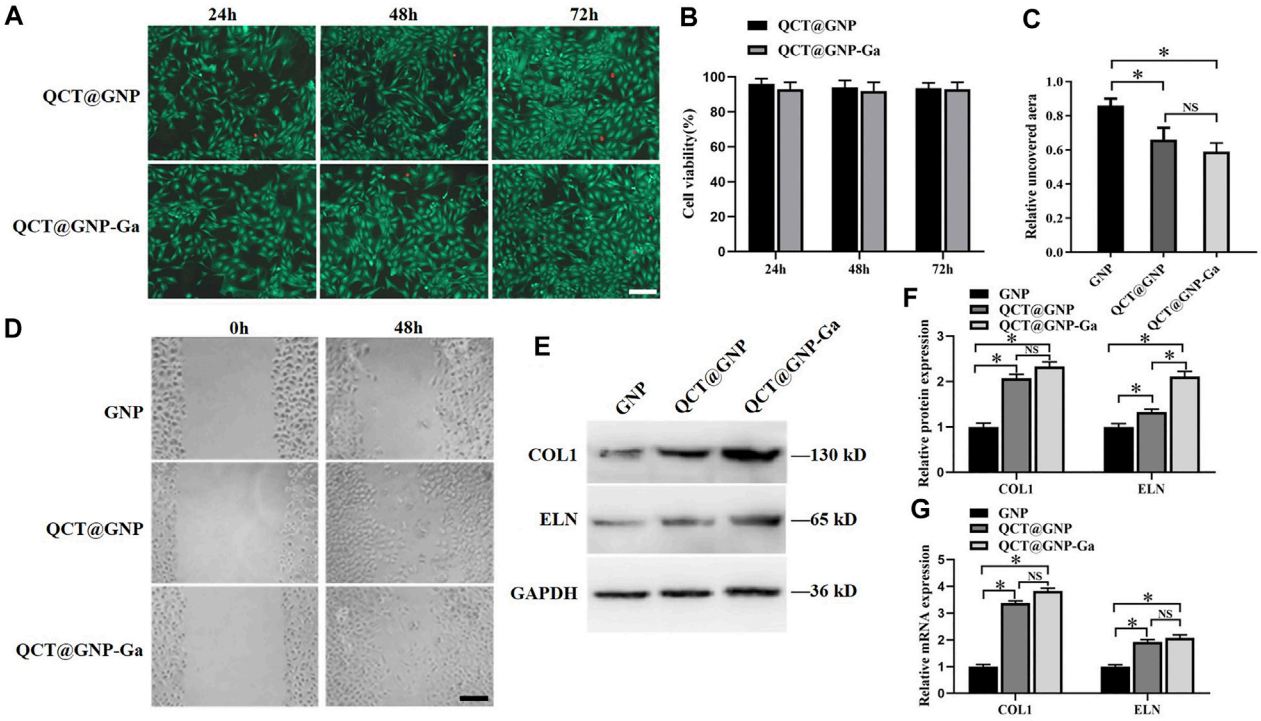

FIGURE 2
Effect of QCT@GNP-Ga on the cell function of primary fibroblasts. **(A)** Live/dead staining of fibroblasts treated with QCT@GNP or QCT@GNP-Ga. Scale bar = 100 μm. **(B)** Cell viability of fibroblasts treated with QCT@GNP or QCT@GNP-Ga for 24, 48, and 72 h. **(C)** The uncovered aera and **(D)** representative images of wound-healing assay of fibroblasts treated with GNP, QCT@GNP or QCT@GNP-Ga. **(E)** Western blot analysis and **(E)** statistical results of COL1, ELN protein expressions in fibroblasts treated with GNP, QCT@GNP or QCT@GNP-Ga. **(G)** qRT-PCR analysis of COL1, ELN mRNA expressions in fibroblasts treated with GNP, QCT@GNP or QCT@GNP-Ga for 48 h. Data are shown as mean ± SD, $*p < 0.05$ compared with GNP group.

flavonol compound among flavonoids, mainly exists in the form of glycosides, is widely distributed in multiple plants, fruits and traditional Chinese medicine and rick in red wine, and has anti-inflammatory, anti-oxidant, anti-bacterial, anti-cancer and anti-viral effects (Pinheiro et al., 2021). Some studies have suggested that the anti-inflammatory effect of quercetin is associated with its mechanisms of inhibiting the secretion of inflammatory factors and interfering with inflammatory signaling pathways (Chanjitwiriya et al., 2020; Dehghani et al., 2021). In previous studies, quercetin has been used to prevent peritoneal scar adhesion in abdominal surgery (Zeng et al., 2022). Nevertheless, its effect on suppressing sustained inflammation and preventing scar formation during skin wound healing warrants further investigation.

Inflammatory response is greatly implicated in the process of wound healing and scar formation, in which macrophage undergoing specific phenotypic and functional changes plays a cardinal role in all stages of the healing process. The dysregulation of the macrophages' function is highly correlated with delayed wound healing and scarring (Sim et al., 2022). While the infiltration of the pro-inflammatory macrophage in the early phase of wound healing is necessary for the wound-healing progression, sustained existence of pro-inflammatory macrophages in remodeling phase could delay re-epithelialisation accompanied by an increased frequency of vascular leakage, immature granulation, and the persistence of neutrophils, which all contribute to delayed wound healing and increased scar formation (Ishida et al., 2008). Therefore, to suppress the infiltration of pro-inflammatory macrophage and induce macrophage polarization from M1 to M2 type in late phase is beneficial for wound healing.

In the present study, gallium-modified gelatin nanoparticles loaded with quercetin were firstly established, and its anti-bacterial and healing-promoting effects were testified *in vitro*. Then, its role in suppressing sustained inflammation and the underlying mechanism was investigated, focusing on the regulation of macrophage polarization. Furthermore, the therapeutic effect of this preparation on skin wound healing was examined in pre-clinical rats *in vivo*.

Material and methods

Agents, antibodies and animals

Gelatin (Gel), quercetin (QCT), gallium nitrate hydrate, and common chemical reagents were purchased from Sigma-Aldrich (United States). Dulbecco's modified eagle medium (DMEM) and fetal bovine serum (FBS) were purchased from Gibco (United States). The following primary antibodies were purchased from Abcam (United States): Collagen 1 (COL1) (ab270993), Elastin (ab307151), Arginase 1 (Arg1) (ab203490), TGF beta Receptor II (TGFβR2) (ab259360), Smad2 (ab40855), p-Smad2 (ab280888). The following primary antibodies were purchased from Invitrogen (United States): CD206 (17-2061-82), CD86 (12-0862-82). TGFβR2 inhibitor LY2109761 were purchased from Selleck (United States). Cell viability/cytotoxicity detection kit were purchased from Solarbio

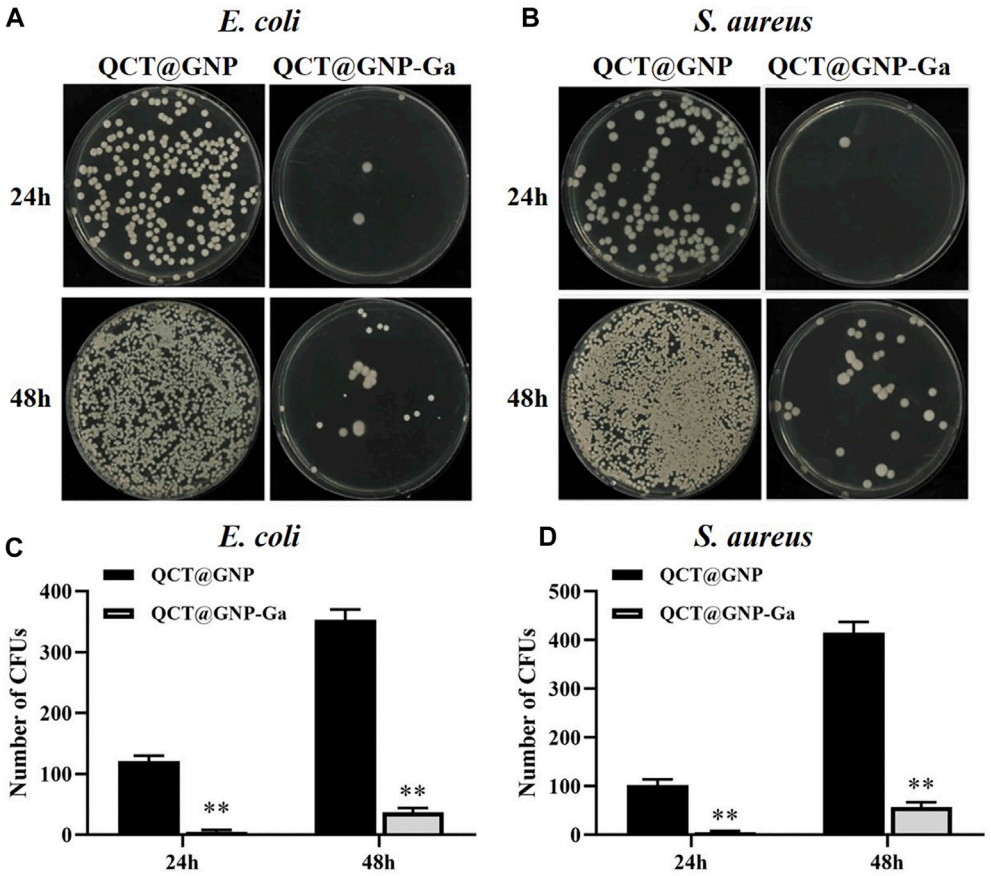

FIGURE 3
Anti-bacterial activity of QCT@GNP-Ga. **(A, B)** Images and **(C, D)** statistical results of colony forming unit (CFU) of *E. coli* and *S. aureus* treated with QCT@GNP or QCT@GNP-Ga. Data are shown as mean ± SD, $*p < 0.05$ compared with QCT@GNP group.

(China). TNF-α, MCP-1, TGF-β3, IL-4 ELISA kit were purchased from eBioscience (United States).

Sprague-Dawley (SD) rats were purchased from Air Force Medical University. RAW264.7 cell line was obtained from National Collection of Authenticated Cell Cultures, The Academy of Sciences of China (SCSP-5036). *E. coli* and (ATCC 8739) and *S. aureus* (ATCC 6538) were obtained from the American Type Culture Collection (ATCC). All animal procedures were approved by the Experimental Animal Ethics Committee of Air Force Medical University.

Synthesis of QCT@GNP-Ga

GNP was synthesized according to a previous protocol (Xu et al., 2013). Briefly, 0.1 g of gelatin (225 Bloom strength) was dissolved in 10 mL of deionized water at 50°C. The gelatin solution's pH value was adjusted to 7.0 by 0.1 M NaOH. The nanoparticles forming procedure was conducted by adding acetone dropwise to the gelatin solution under continuous stirring. Then, 200 μL of 40% w/w glyoxal was added and mixed by stirring for 3 h at 100 g to crosslink the nanoparticles. 1 mM glycine was used to quench the surface-accessible aldehyde groups of glyoxal. The nanoparticles were obtained by centrifugation at 10,000 g for 20 min and re-suspended in PBS. QCT was added when the pH of the gelatin solution was adjusted to 7.0. The gallium ionic-GNPs were prepared by placing 3 wt % GNP solution in a grooved mold. When dialysis membrane (MWCO 3500 Da) was covered, 0.1 M $Ga(NO_3)_3$ aqueous solution was added. After soaking for 4 h, $Ga3^+$-cross-linked GNPs were finally produced.

Characterization of QCT@GNP-Ga

The chemical group alterations in the QCT@GNP and QCT@GNP-Ga were tested by a Fourier transform infrared (FTIR, Bruker, Germany) spectrometer with a wavenumber range of 4,000–500 cm^{-1}. The morphologies of QCT@GNP and QCT@GNP-Ga samples were recorded by a transmission microscope (TEM, JEM-2100, JEOL, Japan).

Drug release from QCT@GNP-Ga

The medium was prepared with 1 mg/mL lysozyme phosphate-buffered saline (PBS) solution (pH = 7.4, pH = 6.8). 0.5 g of QCT@GNP or QCT@GNP-Ga samples were soaked in 10 mL of the medium, agitating at 100 rpm and 37°C. At certain time intervals (12 h, 24 h, 36 h, 48 h, 60 h, 72 h, 84 h, and 96 h), a 3-mL volume was taken for measurement, and fresh medium was added to replenish. To

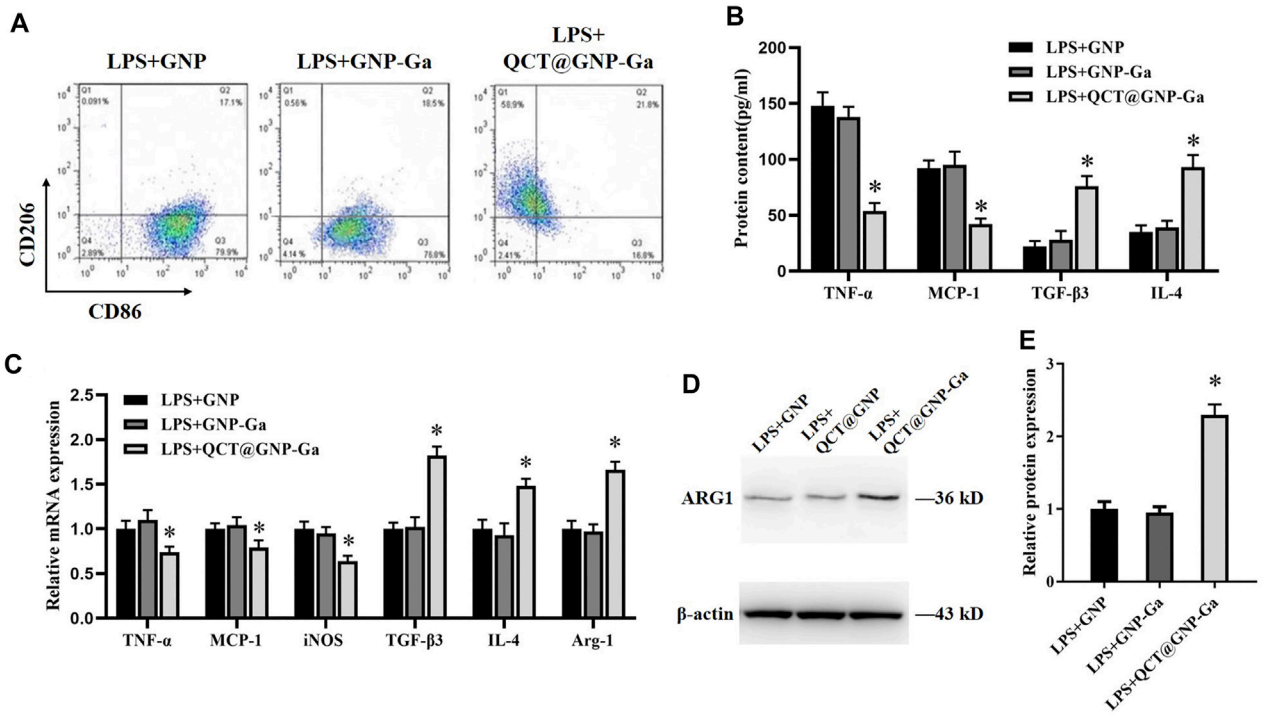

FIGURE 4
Induction of macrophages from M1 to M2 phenotype by QCT@GNP-Ga. **(A)** Representative images of FCM analysis of LPS induced RAW264.7 cells treated with GNP, GNP-Ga, or QCT@GNP-Ga. **(B)** EILSA analysis of TNF-α, MCP-1, TGF-β3, and IL-4 protein expressions in LPS induced RAW264.7 cells treated with GNP, GNP-Ga, or QCT@GNP-Ga. **(C)** qPCR analysis of TNF-α, MCP-1, iNOS, TGF-β3, IL-4, Arg-1 mRNA expressions in LPS induced RAW264.7 cells treated with GNP, GNP-Ga, or QCT@GNP-Ga. **(D)** Western blot analysis and **(E)** statistical results of ARG1 protein expressions in LPS induced RAW264.7 cells treated with GNP, GNP-Ga, or QCT@GNP-Ga. Data are shown as mean ± SD, $*p < 0.05$ compared with LPS + GNP group.

remove the interference of the BSA, high-performance liquid chromatography was performed to test the concentration of QCT at 355 nm. The accumulated release was calculated to clarify the drug release profile and explore the drug release mechanism.

Cell toxicity examination

The cells were seeded into 48-well plates at a density of 1.5×10^4 cells/well and became adherent in 6 h. Discarded the medium and replaced with 10% of QCT@GNP or QCT@GNP-Ga extract. After 24, 48, and 72 h of co-culture, the cells were stained with calcein-AM/propidium iodide to observe the morphology and proliferation *via* confocal laser microscopy (Lecia, Germany).

RNA extraction and qRT-PCR

Total RNA was extracted using EZNA Total RNA Kit II (OMEGA Bio-tek) and reverse transcription was performed using PrimeScript RTase (Takara Bio Inc.). The mRNA expression levels were measured with real-time quantitative reverse transcription PCR (qRT-PCR) using Premix Ex Taq (Takara) and standardized according to the endogenous control (β-actin) expression level. The cycle conditions were as follows: 95°C for 2 min, denaturation at 95°C for 5 s, annealing at 55°C for 10 s and finally extension at 72°C for 45 s. All the reactions were conducted in triplicate. The amplification and melt curves were used to identity the consistency of specific PCR product. The results were analyzed by using the $2^{-\Delta\Delta CT}$ method.

Protein extraction and immunoblotting analysis

After cells were lysed by RIPA buffer (Beyotime) added with PMSF (Beyotime), protein concentration was identified by the BCA method kit (Solarbio). Protein samples were collected using 10% SDS-PAGE (Beyotime) and transferred to the polyvinylidene fluoride membranes (PVDF, Millipore). After blocked with 5% skim milk for 1 h, the membrane was incubated with primary antibodies overnight at 4°C and then with the corresponding horse radish peroxidase (HRP)-conjugated secondary antibody (1:2000 dilution) for 1 h at RT. Finally, enhanced chemiluminescence substrate (ECL kit, Millipore) were used for visualization.

Immunohistochemical staining

Scar tissues were obtained, soaked in 4% paraformaldehyde fixative, and then embedded by paraffin and finally cut into 4 μm slices. The following procedures were performed using biotin-streptavidin peroxidase method (SPlink Detection Kit, ZSGB-Bio). According to the manufacturer's instruction, the paraffin-embedded slices were dewaxed, rehydrated using graded ethanol diluent, subjected to antigen restoration, incubated with

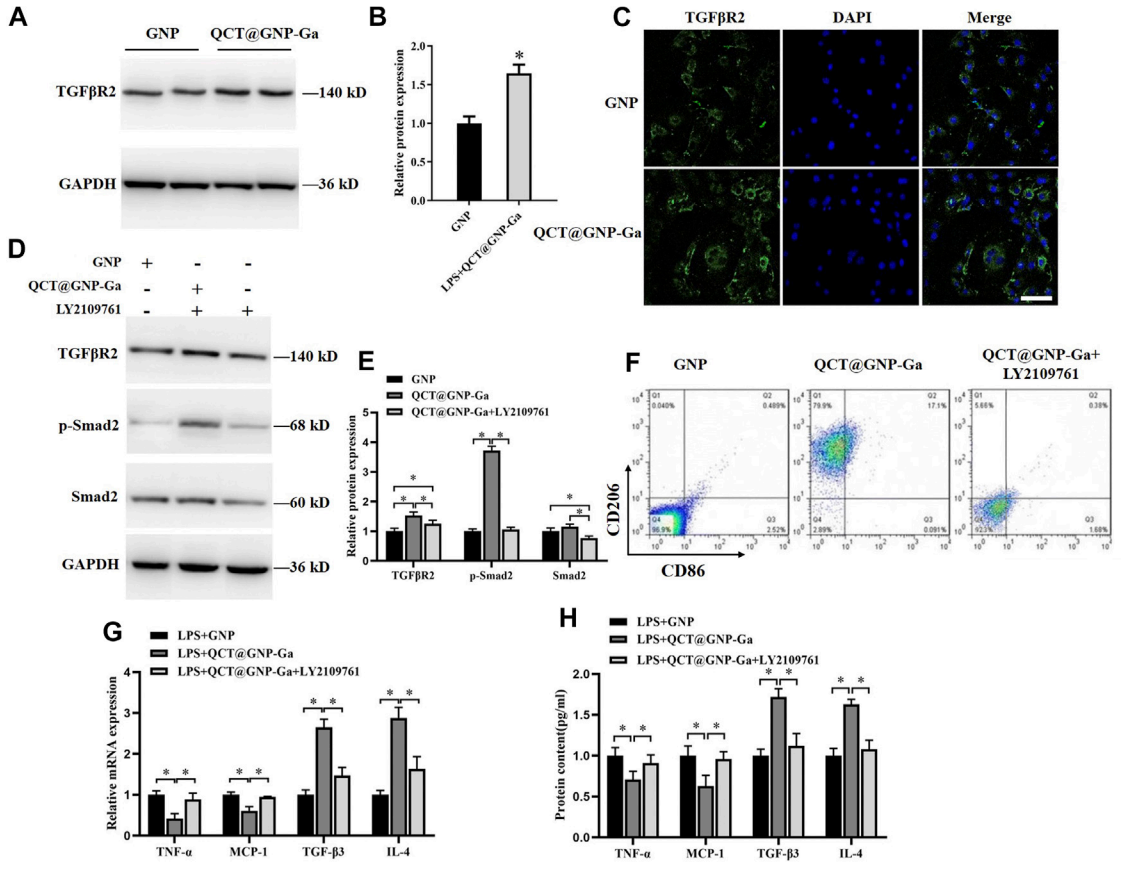

FIGURE 5
Regulation of polarization of macrophages by QCT@GNP-Ga through TGFβ/Smad pathway. **(A)** Western blot analysis, **(B)** statistical results, and **(C)** immunofluorescent staining analysis of TGFβR2 protein expressions in RAW264.7 cells treated with GNP or QCT@GNP-Ga. **(D)** Western blot analysis and **(E)** statistical results of TGFβR2, p-Smad2, and Smad2 protein expressions in RAW264.7 cells treated with GNP or QCT@GNP-Ga. **(F)** Representative images of FCM analysis of RAW264.7 cells treated with GNP or QCT@GNP-Ga or LY2109761. **(G, H)** Relative expression and secretion of TNF-α, MCP-1, TGF-β3 and IL-4 after the treatment with GNP or QCT@GNP-Ga or with LY2109761 in LPS-stimulated macrophage. Data are shown as mean ± SD, $*p < 0.05$, Scale bar = 20 μm.

30% H_2O_2-CH_3OH, and blocked with goat serum. Then the slices were incubated with the corresponding primary antibodies, followed by the biotinylated goat anti-rabbit IgG and HRP-conjugated streptomycin. Finally, Diaminobenzidine (ZSGB-Bio) was used for chromogenic reaction. The slices were observed using optical microscope (Olympus).

Flow cytometry analysis

The cells treated with LPS and GNP-Ga or QCT@GNP-Ga were dissociated and resuspended. Fc block (Biosciences, United States) was used to prevent non-specific binding. All the detecting cells were stained with anti-CD86 and CD-206. Analysis was processed on a flow cytometer (BD Biosciences) with the FlowJo software (Tommy Digital Biology, Tokyo, Japan).

ELISA

Cell supernatants were used to quantify the TNF-α, MCP-1, TGF-β3, and IL-4 with the detection limits of 7 pg/mL. Total protein was examined using a commercial kit (BCA protein assay kit, Pierce, Rockford, IL).

Statistical analysis

Each experiment was performed at least three times, and statistical analyses of the data were performed using unpaired, two-tailed Student's *t*-tests built into GraphPad Prism (GraphPad Software 8.0; San Diego, CA, United States). Data were presented as the mean ± S.D. *p* values of<0.05 were considered statistically significant.

Results

Characterization of QCT@GNP-Ga

The quercetin (QCT)-loaded gelatin nanoparticles (QCT@GNP) were prepared by dissolving, and then gallium ions were crosslinked onto the surface of nanoparticles by ion cross-linking to establish QCT@GNP-Ga (Figure 1A). Firstly, nanoparticles were observed

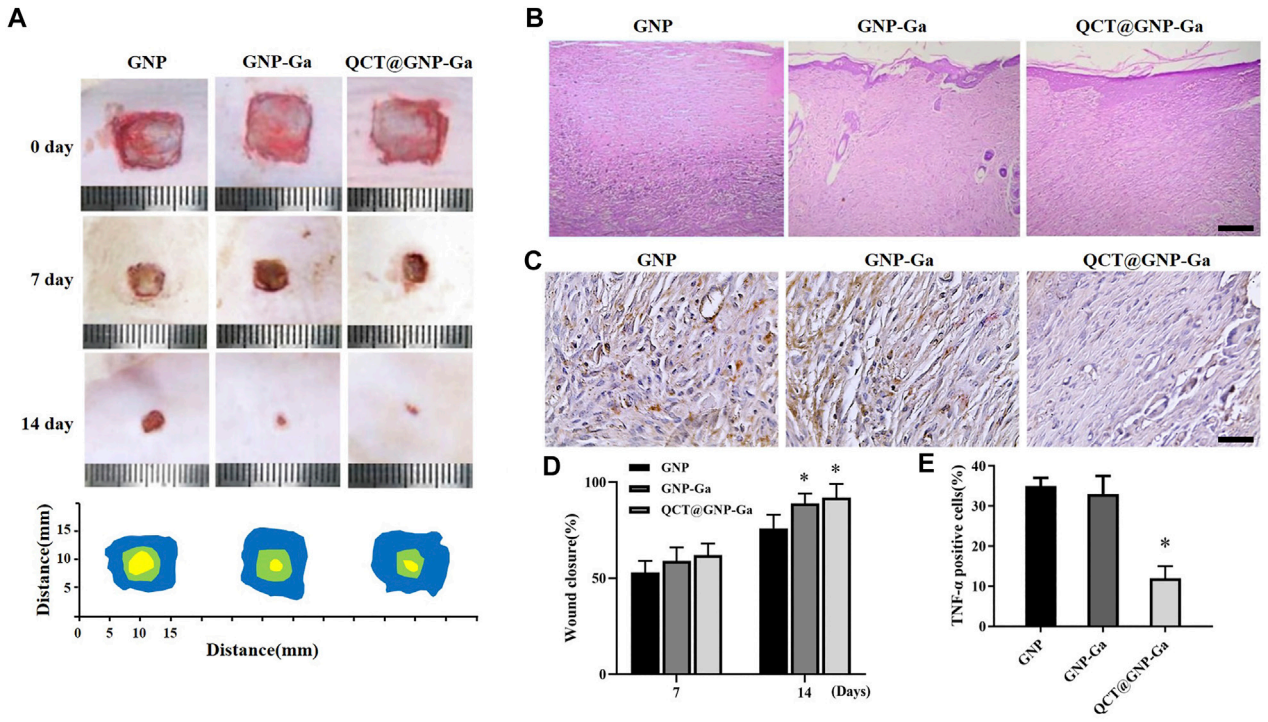

FIGURE 6
In vivo repair effect of QCT@GNP-Ga on rat skin wounds. **(A)** Representative images of wound healing covered by GNP, GNP-Ga or QCT@GNP-Ga from 0 to 14 days and **(D)** quantitative results. **(B)** Representative HE staining images of tissue from healing wounds of GNP, GNP-Ga, or QCT@GNP-Ga group, Scale bar = 100 μm. **(C)** Representative TNF-α immunohistochemical staining images and **(E)** quantitative results of tissue from healing wounds of GNP, GNP-Ga or QCT@GNP-Ga group, Scale bar = 20 μm. Data are shown as mean ± SD, $*p < 0.05$ compared with GNP group.

under a transmission electron microscope (TEM), which showed that both QCT@GNP and QCT@GNP-Ga were of uniform and smooth spherical structures. The diameter of QCT@GNP and QCT@GNP-Ga was 14.6 ± 1.4 nm and 16.3 ± 1.9 nm, respectively (Figures 1B, C). Further, the molecular structure of the nanoparticle was detected by Fourier transform infrared spectrum. The results showed that the characteristic peak of gallium ion (Ga^{3+}) was at 1,380 cm^{-1}, while that of QCT was at 1,600 cm^{-1}. The characteristic peaks of QCT@GNP were at 1,600 and 1,680 cm^{-1}. Combined with the characteristics of the three above, the characteristic peaks of QCT@GNP-Ga were at 1,380, 1,600 and 1,680 cm^{-1}. Of note, the characteristic peak of QCT@GNP at 1,600 cm^{-1} was shifted, indicating that the amido bonds in gelatin nanoparticles were strengthened under the action of gallium ion (Figure 1D). The controlled release of drugs by nanoparticles was further detected, which revealed that both QCT@GNP and QCT@GNP-Ga can be released stably in PBS solution for 96 h. The release curve of QCT@GNP-Ga is gentler (Figure 1E).

Biocompatibility of QCT@GNP-Ga and its effect on function of fibroblasts

QCT@GNP-Ga was added to the medium of the mouse primary skin fibroblasts cultured *in vitro* to observe its effect on the function of fibroblasts. Firstly, the results of cell survival/death staining showed that there was no significant difference in the cell survival between the QCT@GNP group and the QCT@GNP-Ga group, indicating that both QCT@GNP and QCT@GNP-Ga have good biocompatibility with mouse fibroblasts and are not cytotoxic (Figures 2A, B). Besides, cell wound-healing assay showed that the cell migration in the QCT@GNP group and the QCT@GNP-Ga group at 48 h was significantly greater than that in the GNP group. However, the difference between the QCT@GNP group and the QCT@GNP-Ga group was insignificant (Figures 2C, D). Human skin is constructed with many proteins, among which Type I collagen (COL1) and elastin (ELN) that are derived from fibroblasts and constitute extracellular matrix (ECM) play a key role in providing strength and elasticity to the human skin and body (Lee et al., 2022). The expressions of COL1 and ELN can well reflect the ability of fibroblast to produce ECM that is related to process of wound healing and scar formation (Bui et al., 2022). qPCR and WB analysis showed that 48 h after the treatment with QCT@GNP or QCT@GNP-Ga, both the mRNA and protein levels of COL1 and ELN were significantly higher than those in the GNP group (Figures 2E–G). The above results showed that QCT@GNP-Ga has no cytotoxicity to mouse fibroblasts and can promote fibroblast migration and matrix secretion.

Anti-bacterial activity of QCT@GNP-Ga

Since that bacterial proliferation at the wound site is one of the major reasons for delayed healing and abnormal scarring (Frykberg and Banks, 2015; Zhang et al., 2022), and Gallium and Quercetin are documented of anti-bacterial property (Hu et al., 2022; Qin J. et al., 2022), we went on to investigate whether QCT@GNP-Ga exerted great anti-bacterial effect. The surface of the agarose

medium was coated with QCT@GNP-Ga and then inoculated with *S. aureus* and *E. coli* to observe its anti-bacterial activity. After 24 h of constant temperature culture at 37°C, many bacterial colonies were observed on the culture dish in the QCT@GNP group, while only a few bacterial colonies were observed in the QCT@GNP-Ga group. At 48 h, the culture dish in the QCT@GNP was covered with bacterial colonies, while only a few bacterial colonies were formed in the QCT@GNP-Ga group (Figures 3A, B). Further statistics analysis showed that the number of bacterial colonies formed in the QCT@GNP-Ga group at either 24 or 48 h was significantly smaller than that in the QCT@GNP group. The same results were obtained for *S. aureus* and *E. coli* (Figures 3C, D).

Induction of macrophages from M1 to M2 phenotype by QCT@GNP-Ga

It has been demonstrated that a proper inflammatory response is required for skin wound repair (Xu et al., 2010), while prolonged inflammation leads to pathological healing especially scarring (Morris et al., 2014). Macrophages are the most functionally diverse cells for generation and resolution of inflammation by phenotype polarization. Classically-activated macrophages (M1) secrete high levels of pro-inflammatory cytokines like IL-1β, IL-6, and TNF-α to exhibit pro-inflammatory properties (Koh and DiPietro, 2011), whereas alternatively-activated macrophages (M2) that secret high level IL-10 and TGF-β and low-level IL-12 play a role in resolution of inflammation (Gensel and Zhang, 2015). High population of macrophages could lead to sustained inflammation that might delay the process of wound healing (Guo et al., 2016). Therefore, we wondered whether QCT@GNP-Ga played a role in the regulation of macrophage polarization. To this end, mouse RAW264.7 macrophages were cultured *in vitro* and induced to polarize to M1 by LPS. Afterwards, these macrophages were treated with QCT@GNP-Ga for 5 days to observe its effect on the polarization of mouse macrophages. Flow cytometry analysis revealed that, after the induction by LPS, CD86 was highly-expressed in cells, while CD206 was merely expressed. After the treatment with QCT@GNP-Ga, the expression of CD86 in RAW264.7 cells decreased, while the expression of CD206 increased, indicating the polarization of macrophages from M1 to M2 phenotype (Figure 4A). Further ELISA assay showed that, in response to LPS stimulation, the expression of TNF-α and MCP-1 was significantly lower in the QCT@GNP-Ga group than that in the GNP group and GNP-Ga group, while the expression of TGF-β3 and IL-4 was prominently increased in QCT@GNP-Ga group (Figure 4B). In addition, qRT-PCR analysis showed that in response to LPS stimulation, the mRNA levels of TNF-α, MCP-1 and iNOS were significantly lower in the QCT@GNP-Ga group than those in the GNP group and GNP-Ga group, while the mRNA levels of TGF-β3, IL-4 and Arg-1 were significantly higher than those in the GNP group and GNP-Ga group (Figure 4C). Similarly, immunoblotting analysis proved that the expression of Arg-1 was prominently increased after the treatment with QCT@GNP-Ga (Figures 4D, E). Taken together, these results demonstrated that QCT@GNP-Ga could induce the phenotype switch of macrophages from M1 to M2, so that sustained inflammation could be mitigated to facilitate the process of wound healing.

Regulation of polarization of macrophages by QCT@GNP-Ga through TGF-β/Smad pathway

Thereafter, we went on to elucidate the mechanism underlying the role of QCT@GNP-Ga in the regulation of macrophages polarization. To this end, QCT@GNP-Ga was added to the medium of the RAW264.7 cells cultured *in vitro* for 48 h, after which the expressions of related signaling pathways were detected. It was found that the protein expression of TGFβR2 was increased after the treatment with QCT@GNP-Ga compared with control GNP group (Figures 5A, B). In consistent, immunofluorescence staining analysis also showed that the expression of TGFβR2 was enhanced after the treatment with QCT@GNP-Ga (Figure 5C). In line with the upregulation of TGFβR2 after QCT@GNP-Ga treatment, the phosphorylation of Smad2 was also increased, indicating the activation of TGFβ-Smad signaling by QCT@GNP-Ga, and this effect could be effectively blocked by TGFβR2 inhibitor LY2109761 (Figures 5D, E). Flow cytometry analysis revealed that the expression of CD206 in cells increased after the treatment with QCT@GNP-Ga, while its expression was significantly reduced by the inhibitor LY2109761 (Figure 5F). In addition, while QCT@GNP-Ga treatment induced prominent downregulation of the expression and secretion of TNF-α and MCP-1, as well as the upregulation of the expression and secretion of TGF-β3 and IL-4, co-treatment with TGFβR2 inhibitor LY2109761 was capable of reversing this alteration trend (Figures 5G, H). Therefore, these results suggested that the activation of TGF-β/Smad pathway mediated the role of QCT@GNP-Ga in macrophages polarization from M1 to M2.

In vivo repair effect of QCT@GNP-Ga on rat skin wound

Given that QCT@GNP-Ga could simultaneously potentiate fibroblast function, exert anti-bacterial property, and induce macrophages polarization from M1 to M2 to suppress sustained inflammation, we proposed that QCT@GNP-Ga might play a cardinal role in facilitating wound healing and restraining scar formation *in vivo*. A skin wound model was established on the back skin of SD rats, and then the injectable material for repairing skin wound prepared with the gelatin hydrogel loaded with QCT@GNP-Ga. After 14 days of injection, the average rates of wound healing in both the GNP-Ga group and the QCT@GNP-Ga groups were higher than that in the GNP group (Figures 6A, D). The results of HE staining showed that many fibrous scars were formed at wound locations in the GNP group, and local fibrocytes proliferated and were arranged in a compact and disordered manner. In contrary, the scar tissues in the GNP-Ga group were partially reduced, and were further reduced in the QCT@GNP-Ga group (Figure 6B). Concurrent immunohistochemical staining analysis showed that the TNFα-positive cells in the control group were distributed in scar tissues, while the TNFα-positive cells in the QCT@GNP-Ga group were significantly reduced (Figures 6C, E), indicating that the reduction of scar tissues was associated with the inhibition of inflammatory reactions. Taken together, QCT@GNP-Ga exerts great potential in facilitating wound healing and restraining scar formation in pre-clinical rat model.

Discussion

With the improvement of people's living standard, the attention to efficient wound healing paralleled with reduced scar formation has been gradually increased. In case of an open skin wound, it is often accompanied with bacterial attachment, causing wound infection and resultant severe scars (Leng et al., 2022). In addition, the impaired wound-healing function of fibroblast and sustained inflammatory reactions also restrain the process of wound closure and increase the incidence or severity of scar (Morris et al., 2014; Shams et al., 2022). In the present study, a novel anti-bacterial drug-loaded hydrogel nanoparticle was developed, which could effectively facilitate wound closure, inhibit bacterial proliferation, and ameliorate scar formation, which was related to its role in regulating macrophage polarization, providing a promising choice for the treatment of wound.

Since that nanoparticles have multiple advantages including high drug loading capacity, good biocompatibility, and the ability of the controlling drug release, they have been widely employed in investigations on tissue repair. As a drug carrier or antibacterial active substance, nanoparticles are applied to skin damage repair by mixing with hydrogel to form composite hydrogel (Sun et al., 2021; Burdusel et al., 2022; Qin P. et al., 2022). Silver particles, titanium oxide, gentamicin-containing nanoparticles, curcumin-containing nanoparticles, and other composite hydrogels have been confirmed to have anti-bacterial and wound healing-promoting effects (Javanmardi et al., 2018; Zahiri et al., 2020; Xiang et al., 2022). In recent years, gallium ion has been found to be advantageous in the field of antibacterial materials (Vinuesa and McConnell, 2021). Due to the unique anti-microbial mechanism of gallium, it can overcome the problem of resistance to traditional antibiotics, such as the prevention of drug absorption due to the permeability of bacterial cell wall. Gallium ions can imitate the metabolic pathway of iron ions to promote cell absorption, whereas cannot be reduced like iron ions (Kurtuldu et al., 2022). Therefore, the proliferation of bacteria is inhibited when the oxidation-reduction process necessary for the synthesis of the DNA and protein of bacteria is interrupted. In addition to the recognized broad-spectrum bactericidal activity of gallium ions, small doses of gallium ions can also suppress inflammatory reactions (Ma and Fu, 2010; Goss et al., 2018). Besides, some studies have demonstrated that gallium ions can also promote collagen synthesis and cell migration, thus facilitating the process of wound healing (Kircheva and Dudev, 2019; Castilla-Amoros et al., 2020). In this study, our data proved that the gallium ion-modified gelatin nanoparticles were efficient in promoting the wound-healing function of fibroblast, suppressing bacterial proliferation and inhibiting inflammatory reactions, providing an experimental foundation for wound treatment.

Quercetin is flavonoid rich in a variety of foods and has multiple biological characteristics, including anti-inflammatory reaction, anti-oxidative and some other properties (Liu et al., 2019; Mi et al., 2022). Some studies have pointed out that quercetin can reduce the generation of TNF-α, IL-6 and IL-1 in mononuclear U937 cells induced by LPS (Okoko and Oruambo, 2009). In addition, quercetin can inhibit the expressions of inflammation-related genes in RAW264.7 macrophages (Cui et al., 2019). The study by Gupta et al. (2016) proved that quercetin can effectively ameliorate the eosinophilic airway inflammation in allergic asthma. Moreover, Guan et al. (2021) demonstrated that quercetin can relieve rheumatoid arthritis (RA) by promoting the apoptosis of neutrophils. Supplementary to these previous reports, our data for the first time proved that quercetin was also effective in inhibiting the inflammatory reactions during skin scar formation. Inflammatory response participates in wound healing and scar formation, and macrophages that undergo phenotypic and functional changes play a critical role. The persistent existence of pro-inflammatory M1 macrophage in regional skin could prominently delay would healing (Ishida et al., 2008; Sim et al., 2022). To suppress the infiltration of pro-inflammatory macrophage and induce macrophage polarization from M1 to M2 type in late phase is beneficial for wound healing and reduced scar formation. To be specific, quercetin regulated the polarization of macrophages towards M2 through TGF-β/Smad signaling pathway to inhibit inflammation and thereby reduce scar formation, further supporting that the intervention of macrophages polarization might be a useful strategy to reduce scar formation risk during the process of wound healing.

Conclusion

In the present study, a new gallium ion-modified drug-loaded hydrogel nanoparticle was developed aiming to ameliorate infection and scar formation during the process of wound healing. The anti-bacterial, healing-promoting and scar formation-inhibitory effects of the nanoparticles were verified both *in vitro* and *in vivo*, with particular emphasis on the regulation of macrophages polarization *via* TGF-β/Smad pathway to suppress sustained inflammatory reactions at wounds. Our data demonstrated that gallium-modified gelatin nanoparticles loaded with quercetin could promote skin wound healing *via* the regulation of bacterial proliferation and macrophage polarization, and this preparation might be a promising choice to treat wound and suppress scar formation simultaneously, which needs further confirmation by clinical trial in the future.

Data availability statement

The raw data supporting the conclusion of this article will be made available by the authors, without undue reservation.

Ethics statement

The animal study was reviewed and approved by Laboratory Animal Welfare and Ethics Committee of Fourth Military Medical University.

Author contributions

NY: Methodology, investigation, formal analysis, writing—Original draft. NS: Methodology, investigation, writing—Original draft. ZY: Conceptualization, resources, methodology. HL: Conceptualization, supervision, resources, funding acquisition. WG: Conceptualization, writing—Original draft, writing—Review and editing, supervision, funding acquisition.

Funding

This work was supported by Natural Science Foundation of China (52150221), Natural Science Foundation of Shaanxi Province (2021JQ-015), Natural Science Foundation of Jiangsu Province (BK20200242), and Postdoctoral Science Foundation of China (2021M692546).

Conflict of interest

The authors declare that the research was conducted in the absence of any commercial or financial relationships that could be construed as a potential conflict of interest.

The handling editor, KL, declared a shared affiliation with the authors NS and HL at the time of review.

Publisher's note

References

Alster, T. (2003). Laser scar revision: Comparison study of 585-nm pulsed dye laser with and without intralesional corticosteroids. *Dermatol Surg.* 29 (1), 25–29. doi:10.1046/j.1524-4725.2003.29024.x

Atiyeh, B. S. (2020). Nonsurgical management of hypertrophic scars: Evidence-based therapies, standard practices, and emerging methods. *Aesthetic Plast. Surg.* 44 (4), 1320–1344. doi:10.1007/s00266-020-01820-0

Bui, V. D., Son, S., Xavier, W., Nguyen, V. Q., Jung, J. M., Lee, J., et al. (2022). Dissolving microneedles for long-term storage and transdermal delivery of extracellular vesicles. *Biomaterials* 287, 121644. doi:10.1016/j.biomaterials.2022.121644

Burdusel, A. C., Gherasim, O., Andronescu, E., Grumezescu, A. M., and Ficai, A. (2022). Inorganic nanoparticles in bone healing applications. *Pharmaceutics* 14 (4), 770. doi:10.3390/pharmaceutics14040770

Castilla-Amoros, L., Stoian, D., Pankhurst, J. R., Varandili, S. B., and Buonsanti, R. (2020). Exploring the chemical reactivity of gallium liquid metal nanoparticles in galvanic replacement. *J. Am. Chem. Soc.* 142, 19283–19290. doi:10.1021/jacs.0c09458

Chanjitwiriya, K., Roytrakul, S., and Kunthalert, D. (2020). Quercetin negatively regulates IL-1β production in Pseudomonas aeruginosa-infected human macrophages through the inhibition of MAPK/NLRP3 inflammasome pathways. *PLoS One* 15 (8), e0237752. doi:10.1371/journal.pone.0237752

Clarkin, O. M., Wu, B., Cahill, P. A., Brougham, D. F., Banerjee, D., Brady, S. A., et al. (2019). Novel injectable gallium-based self-setting glass-alginate hydrogel composite for cardiovascular tissue engineering. *Carbohydr. Polym.* 217, 152–159. doi:10.1016/j.carbpol.2019.04.016

Cui, S., Wu, Q., Wang, J., Li, M., Qian, J., and Li, S. (2019). Quercetin inhibits LPS-induced macrophage migration by suppressing the iNOS/FAK/paxillin pathway and modulating the cytoskeleton. *Cell Adh Migr.* 13, 1–12. doi:10.1080/19336918.2018.1486142

Dehghani, F., Sezavar Seyedi Jandaghi, S. H., Janani, L., Sarebanhassanabadi, M., Emamat, H., and Vafa, M. (2021). Effects of quercetin supplementation on inflammatory factors and quality of life in post-myocardial infarction patients: A double blind, placebo-controlled, randomized clinical trial. *Phytother. Res.* 35, 2085–2098. doi:10.1002/ptr.6955

Frykberg, R. G., and Banks, J. (2015). Challenges in the treatment of chronic wounds. *Adv. Wound Care (New Rochelle)* 4, 560–582. doi:10.1089/wound.2015.0635

Gensel, J. C., and Zhang, B. (2015). Macrophage activation and its role in repair and pathology after spinal cord injury. *Brain Res.* 1619, 1–11. doi:10.1016/j.brainres.2014.12.045

Giugliano, G., Pasquali, D., Notaro, A., Brongo, S., Nicoletti, G., D'andrea, F., et al. (2003). Verapamil inhibits interleukin-6 and vascular endothelial growth factor production in primary cultures of keloid fibroblasts. *Br. J. Plast. Surg.* 56, 804–809. doi:10.1016/s0007-1226(03)00384-9

Goss, C. H., Kaneko, Y., Khuu, L., Anderson, G. D., Ravishankar, S., Aitken, M. L., et al. (2018). Gallium disrupts bacterial iron metabolism and has therapeutic effects in mice and humans with lung infections. *Sci. Transl. Med.* 10 (460), eaat7520. doi:10.1126/scitranslmed.aat7520

Guan, F., Wang, Q., Bao, Y., and Chao, Y. (2021). Anti-rheumatic effect of quercetin and recent developments in nano formulation. *RSC Adv.* 11, 7280–7293. doi:10.1039/d0ra08817j

Guo, Y., Lin, C., Xu, P., Wu, S., Fu, X., Xia, W., et al. (2016). AGEs induced autophagy impairs cutaneous wound healing via stimulating macrophage polarization to M1 in diabetes. *Sci. Rep.* 6, 36416. doi:10.1038/srep36416

Gupta, K., Kumar, S., Gupta, R. K., Sharma, A., Verma, A. K., Stalin, K., et al. (2016). Reversion of asthmatic complications and mast cell signalling pathways in BALB/c mice model using quercetin nanocrystals. *J. Biomed. Nanotechnol.* 12, 717–731. doi:10.1166/jbn.2016.2197

Gurtner, G. C., Werner, S., Barrandon, Y., and Longaker, M. T. (2008). Wound repair and regeneration. *Nature* 453, 314–321. doi:10.1038/nature07039

Hu, Y., Huang, D., Li, Y., Li, Z., Cai, X., and Wang, F. (2022). Investigation on characterization of novel anti-bacterial chitosan/gelatin composite membranes loaded with quercetin via electrophoretic deposition. *J. Biomater. Sci. Polym. Ed.*, 1–19. doi:10.1080/09205063.2022.2145701

Huang, S., Hong, X., Zhao, M., Liu, N., Liu, H., Zhao, J., et al. (2022). Nanocomposite hydrogels for biomedical applications. *Bioeng. Transl. Med.* 7, e10315. doi:10.1002/btm2.10315

Ishida, Y., Gao, J. L., and Murphy, P. M. (2008). Chemokine receptor CX3CR1 mediates skin wound healing by promoting macrophage and fibroblast accumulation and function. *J. Immunol.* 180, 569–579. doi:10.4049/jimmunol.180.1.569

Javanmardi, S., Ghojoghi, A., Divband, B., and Ashrafi, J. (2018). Titanium dioxide nanoparticle/gelatin: A potential burn wound healing biomaterial. *Wounds* 30, 372–379.

Kircheva, N., and Dudev, T. (2019). Novel insights into gallium's mechanism of therapeutic action: A DFT/PCM study of the interaction between Ga(3+) and ribonucleotide reductase substrates. *J. Phys. Chem. B* 123, 5444–5451. doi:10.1021/acs.jpcb.9b03145

Koh, T. J., and Dipietro, L. A. (2011). Inflammation and wound healing: The role of the macrophage. *Expert Rev. Mol. Med.* 13, e23. doi:10.1017/S1462399411001943

Kurtuldu, F., Mutlu, N., Boccaccini, A. R., and Galusek, D. (2022). Gallium containing bioactive materials: A review of anticancer, antibacterial, and osteogenic properties. *Bioact. Mater* 17, 125–146. doi:10.1016/j.bioactmat.2021.12.034

Lee, S., Choi, Y. J., Lee, S., Kang, K. S., Jang, T. S., and Kim, K. H. (2022). Protective effects of withagenin A diglucoside from Indian ginseng (withania somnifera) against human dermal fibroblast damaged by TNF-α stimulation. *Antioxidants (Basel)* 11 (11), 2248. doi:10.3390/antiox11112248

Leng, T., Wang, Y., Cheng, W., Wang, W., Qu, X., and Lei, B. (2022). Bioactive anti-inflammatory antibacterial metformin-contained hydrogel dressing accelerating wound healing. *Biomater. Adv.* 135, 212737. doi:10.1016/j.bioadv.2022.212737

Liu, X., Sun, N., Mo, N., Lu, S., Song, E., Ren, C., et al. (2019). Quercetin inhibits kidney fibrosis and the epithelial to mesenchymal transition of the renal tubular system involving suppression of the Sonic Hedgehog signaling pathway. *Food Funct.* 10, 3782–3797. doi:10.1039/c9fo00373h

Ma, Z., and Fu, Q. (2010). Comparison of the therapeutic effects of yeast-incorporated gallium with those of inorganic gallium on ovariectomized osteopenic rats. *Biol. Trace Elem. Res.* 134, 280–287. doi:10.1007/s12011-009-8472-0

Mi, Y., Zhong, L., Lu, S., Hu, P., Pan, Y., Ma, X., et al. (2022). Quercetin promotes cutaneous wound healing in mice through Wnt/β-catenin signaling pathway. *J. Ethnopharmacol.* 290, 115066. doi:10.1016/j.jep.2022.115066

Morris, M. W., Allukian, M., 3R. D., Herdrich, B. J., Caskey, R. C., Zgheib, C., Xu, J., et al. (2014). Modulation of the inflammatory response by increasing fetal wound size or interleukin-10 overexpression determines wound phenotype and scar formation. *Wound Repair Regen.* 22, 406–414. doi:10.1111/wrr.12180

Nanditha, C. K., and Kumar, G. S. V. (2022). Bioactive peptides laden nano and micro-sized particles enriched ECM inspired dressing for skin regeneration in diabetic wounds. *Mater Today Bio* 14, 100235. doi:10.1016/j.mtbio.2022.100235

Ogawa, R., Dohi, T., Tosa, M., Aoki, M., and Akaishi, S. (2021). The latest strategy for keloid and hypertrophic scar prevention and treatment: The nippon medical school (NMS) protocol. *J. Nippon. Med. Sch.* 88, 2–9. doi:10.1272/jnms.JNMS.2021_88-106

Okoko, T., and Oruambo, I. F. (2009). Inhibitory activity of quercetin and its metabolite on lipopolysaccharide-induced activation of macrophage U937 cells. *Food Chem. Toxicol.* 47, 809–812. doi:10.1016/j.fct.2009.01.013

Pinheiro, R. G. R., Pinheiro, M., and Neves, A. R. (2021). Nanotechnology innovations to enhance the therapeutic efficacy of quercetin. *Nanomater. (Basel)* 11, 2658. doi:10.3390/nano11102658

Qi, X., Zhang, H., Li, Y., Zhang, X., Ma, H., and Zhang, L. (2022). Nonfouling and antibacterial zwitterionic contact lenses loaded with heme-mimetic gallium porphyrin for treating keratitis. *Langmuir* 38, 14335–14344. doi:10.1021/acs.langmuir.2c02433

Qin J., J., Li, M., Yuan, M., Shi, X., Song, J., He, Y., et al. (2022). Gallium(III)-Mediated dual-cross-linked alginate hydrogels with antibacterial properties for promoting infected wound healing. *ACS Appl. Mater Interfaces* 14, 22426–22442. doi:10.1021/acsami.2c02497

Qin P., P., Tang, J., Sun, D., Yang, Y., Liu, N., Li, Y., et al. (2022). Zn(2+) cross-linked alginate carrying hollow silica nanoparticles loaded with RL-QN15 peptides provides promising treatment for chronic skin wounds. *ACS Appl. Mater Interfaces* 14, 29491–29505. doi:10.1021/acsami.2c03583

Rossato, L., Arantes, J. P., Ribeiro, S. M., and Simionatto, S. (2022). Antibacterial activity of gallium nitrate against polymyxin-resistant *Klebsiella pneumoniae* strains. *Diagn Microbiol. Infect. Dis.* 102, 115569. doi:10.1016/j.diagmicrobio.2021.115569

Shams, F., Moravvej, H., Hosseinzadeh, S., Mostafavi, E., Bayat, H., Kazemi, B., et al. (2022). Overexpression of VEGF in dermal fibroblast cells accelerates the angiogenesis and wound healing function: *In vitro* and *in vivo* studies. *Sci. Rep.* 12, 18529. doi:10.1038/s41598-022-23304-8

Sim, S. L., Kumari, S., Kaur, S., and Khosrotehrani, K. (2022). Macrophages in skin wounds: Functions and therapeutic potential. *Biomolecules* 12 (11), 1659. doi:10.3390/biom12111659

Sun, L., He, L., Wu, W., Luo, L., Han, M., Liu, Y., et al. (2021). Fibroblast membrane-camouflaged nanoparticles for inflammation treatment in the early stage. *Int. J. Oral Sci.* 13, 39. doi:10.1038/s41368-021-00144-2

Tariq, L., Arafah, A., Ali, S., Beigh, S., Dar, M. A., Dar, T. U. H., et al. (2022). Nanogel-Based transdermal drug delivery system: A therapeutic strategy with under discussed potential. *Curr. Top. Med. Chem.* 23, 44–61. doi:10.2174/1568026622666220818112728

Vinuesa, V., and Mcconnell, M. J. (2021). Recent advances in iron chelation and gallium-based therapies for antibiotic resistant bacterial infections. *Int. J. Mol. Sci.* 22, 2876. doi:10.3390/ijms22062876

Wang, X., Liu, X., Bi, P., Zhang, Y., Li, L., Guo, J., et al. (2020). Electrochemically enabled embedded three-dimensional printing of freestanding gallium wire-like structures. *ACS Appl. Mater Interfaces* 12, 53966–53972. doi:10.1021/acsami.0c16438

Xiang, J., Bai, Y., Huang, Y., Lang, S., Li, J., Ji, Y., et al. (2022). A zwitterionic silver nanoparticle-incorporating injectable hydrogel with a durable and efficient antibacterial effect for accelerated wound healing. *J. Mater Chem. B* 10, 7979–7994. doi:10.1039/d2tb01493a

Xie, T., Qi, Y., Li, Y., Zhang, F., Li, W., Zhong, D., et al. (2021). Ultrasmall Ga-ICG nanoparticles based gallium ion/photodynamic synergistic therapy to eradicate biofilms and against drug-resistant bacterial liver abscess. *Bioact. Mater* 6, 3812–3823. doi:10.1016/j.bioactmat.2021.03.032

Xu, J. H., Gao, F. P., Liu, X. F., Zeng, Q., Guo, S. S., Tang, Z. Y., et al. (2013). Supramolecular gelatin nanoparticles as matrix metalloproteinase responsive cancer cell imaging probes. *Chem. Commun. (Camb)* 49, 4462–4464. doi:10.1039/c3cc00304c

Xu, Z., Xu, H., Ploplis, V. A., and Castellino, F. J. (2010). Factor VII deficiency impairs cutaneous wound healing in mice. *Mol. Med.* 16, 167–176. doi:10.2119/molmed.2009.00171

Yamamoto, T. (2006). Bleomycin and the skin. *Br. J. Dermatol* 155, 869–875. doi:10.1111/j.1365-2133.2006.07474.x

Yang, N., Gong, F., Zhou, Y., Hao, Y., Dong, Z., Lei, H., et al. (2021). A general *in-situ* reduction method to prepare core-shell liquid-metal/metal nanoparticles for photothermally enhanced catalytic cancer therapy. *Biomaterials* 277, 121125. doi:10.1016/j.biomaterials.2021.121125

Zahiri, M., Khanmohammadi, M., Goodarzi, A., Ababzadeh, S., Sagharjoghi Farahani, M., Mohandesnezhad, S., et al. (2020). Encapsulation of curcumin loaded chitosan nanoparticle within poly (epsilon-caprolactone) and gelatin fiber mat for wound healing and layered dermal reconstitution. *Int. J. Biol. Macromol.* 153, 1241–1250. doi:10.1016/j.ijbiomac.2019.10.255

Zeng, H., Liu, X., Zhang, Z., Song, X., Quan, J., Zheng, J., et al. (2022). Self-healing, injectable hydrogel based on dual dynamic covalent cross-linking against postoperative abdominal cavity adhesion. *Acta Biomater.* 151, 210–222. doi:10.1016/j.actbio.2022.08.030

Zhang, C., Yang, D., Wang, T. B., Nie, X., Chen, G., Wang, L. H., et al. (2022). Biodegradable hydrogels with photodynamic antibacterial activity promote wound healing and mitigate scar formation. *Biomater. Sci.* 11 (1), 288–297. doi:10.1039/d2bm01493a

Zheng, H., Huang, Z., Chen, T., Sun, Y., Chen, S., Bu, G., et al. (2022). Gallium ions incorporated silk fibroin hydrogel with antibacterial efficacy for promoting healing of Pseudomonas aeruginosa-infected wound. *Front. Chem.* 10, 1017548. doi:10.3389/fchem.2022.1017548

frontiers | Frontiers in Bioengineering and Biotechnology

TYPE Original Research
PUBLISHED 14 March 2023
DOI 10.3389/fbioe.2023.1119639

OPEN ACCESS

EDITED BY
Jin Yan,
Xi'an Jiaotong University, China

REVIEWED BY
Yi Guo,
Xi'an Medical University, China
Elisa López-Dolado,
Fundación del Hospital Nacional de Parapléjicos, Spain

*CORRESPONDENCE
Zhongquan Qi,
yxyyz@gxu.edu.cn

SPECIALTY SECTION
This article was submitted to Biomaterials, a section of the journal Frontiers in Bioengineering and Biotechnology

RECEIVED 09 December 2022
ACCEPTED 27 February 2023
PUBLISHED 14 March 2023

CITATION
Mi S, Wang X, Gao J, Liu Y and Qi Z (2023), Implantation with SHED sheet induced with homogenate protein of spinal cord promotes functional recovery from spinal cord injury in rats.
Front. Bioeng. Biotechnol. 11:1119639.
doi: 10.3389/fbioe.2023.1119639

Implantation with SHED sheet induced with homogenate protein of spinal cord promotes functional recovery from spinal cord injury in rats

Sisi Mi, Xue Wang, Jiaxin Gao, Yu Liu and Zhongquan Qi*

Medical College, Guangxi University, Nanning, China

Introduction: After spinal cord injury (SCI) occurs, the lesion is in a growth inhibitory microenvironment that severely hinders neural regeneration. In this microenvironment, inhibitory factors are predominant and factors that promote nerve regeneration are few. Improving neurotrophic factors in the microenvironment is the key to treating SCI.

Methods: Based on cell sheet technology, we designed a bioactive material with a spinal cord-like structure –SHED sheet induced with homogenate protein of spinal cord (hp–SHED sheet). Hp–SHED sheet was implanted into the spinal cord lesion for treating SCI rats with SHED suspensions as a control to investigate the effects on nerve regeneration.

Results: Hp–SHED sheet revealed a highly porous three–dimensional inner structure, which facilitates nerve cell attachment and migration. Hp-SHED sheet *in vivo* restored sensory and motor functions in SCI rats by promoting nerve regeneration, axonal remyelination, and inhibiting glial scarring.

Discussion: Hp–SHED sheet maximally mimics the microenvironment of the natural spinal cord and facilitate cell survival and differentiation. Hp–SHED sheet could release more neurotrophins and the sustained action of neurotrophins improves the pathological microenvironment, which effectively promotes nerve regeneration, axonal extension, and inhibits glial scarring, thereby promoting the *in situ* centralis neuroplasticity. Hp–SHED sheet therapy is a promising strategy for effective treatment of SCI based on neurotrophins delivery.

KEYWORDS

spinal cord injury, cell sheet technology, spinal cord homogenate, neurotrophins, neuroplasticity, regeneration

1 Introduction

Spinal cord injury (SCI) is a serious and highly disabling disease of the central nervous system. More than 20 million patients worldwide currently suffer from SCI, with an annual increase of approximately 700,000 individuals (Global et al., 2018). SCI is divided into primary and secondary injuries. Primary injury directly causes neuron death and axon disruption. Secondary injury involves a series of biological cascades caused by primary injury, such as inflammatory responses, apoptosis, gray matter breakdown, white matter demyelination, and glial scar formation (Tran et al., 2018; Yu and Fehlings, 2011).

Essentially, secondary injury is a complex process of multicellular and multimolecular interactions (Rubiano et al., 2015). The lesions are infiltrated by a large number of dead cells as well as inflammatory cells, while microglia activation transforms into macrophages to phagocyte debris and degenerate myelin sheaths (Lin et al., 2021) and astrocytes proliferate to form glial scars. The glial scar is a physical barrier to nerve regeneration and axonal growth (Anderson et al., 2016; Dias et al., 2018). The factors above allow the establishment of a local growth inhibitory microenvironment within the lesion, which severely hinders nerve regeneration after SCI. Moreover, the intrinsic repair capacity of the central nervous system is highly limited. Current clinical therapies are not yet able to achieve effective functional recovery and it is difficult to achieve effective neurological recovery by targeting a single factor (Thuret et al., 2006). Thus, comprehensive regulation of the lesion microenvironment is key for SCI treatment (Li et al., 2019; Wang et al., 2021).

Stem cells from human exfoliated deciduous teeth (SHED) are mesenchymal stem cells (MSCs) derived from neural crest, which is homologous to central nervous system tissue (Miura et al., 2003). Compared with MSCs from other sources, SHED display stronger neurotropic characteristics, including the ability to migrate to sites of neural injury and differentiate into neurons and oligodendrocytes (Hochuli et al., 2021; Huang et al., 2009). Accordingly, SHED have been used to treat a variety of neurological diseases (Fujii et al., 2015; Huang et al., 2022; Pereira et al., 2019). Currently, SHED are used for treatment of SCI with some efficacy (Nicola et al., 2017; Sakai et al., 2012). The therapeutic neurotrophic effects of SHED have been attributed to a paracrine role *via* the paracrine factors including cytokines, growth factors, immune-modulatory proteins, and exosomes (Chen et al., 2020; Sugimura-Wakayama et al., 2015).

The type of cells that MSCs differentiate into is closely related to the microenvironment in which they live (Tang et al., 2020). The microenvironment in which the cells of different tissues are located differs, most notably in various factors. This is one of the main reasons for the differentiation of stem cells to other tissue cells (Hwang et al., 2009). The component of spinal cord homogenate is complex and includes some chemical substances or cytokines. Previous studies showed that spinal cord homogenate could be used as an effective inducer to induce BMSCs to differentiate into neuronal cells and secrete brain-derived neurotrophic factor (Liu et al., 2011; WU et al., 2009). Studies previously found that inoculation of DCs pulsed with homogenate proteins of the spinal cord (hpDCs) promotes functional recovery from SCI in mice. Application of hpDCs can improve hindlimb motor function after SCI in rats by increasing the expression of neurotrophic factors and cytokines at the injury site (Liu et al., 2009; Wang et al., 2013).

Cell sheet technology (CST) refers to the inoculation of high-density cells *in vitro*, culturing them and growing them in layers to form a dense membrane-like structure rich in cells and extracellular matrix (ECM) (Yang et al., 2005). CST completely retains the rich signal transmission between cells and their ECM, and can mimic the *in vivo* microenvironment to maximize the biological properties of cells (Elloumi-Hannachi et al., 2010; Lin et al., 2013). Compared to cell suspensions, CST facilitates cell survival, migration, proliferation, and differentiation (Lin et al., 2013; Takeuchi et al., 2016). Nowadays, CST has become a popular research topic in the field of tissue engineering, and been successfully applied to the repair of periodontal (Iwata et al., 2018), cornea (Nishida et al., 2004), bone (Liu et al., 2013), cartilage (Sato et al., 2014), esophagus (Ohki et al., 2012), heart (Shimizu et al., 2003), and other tissues. In addition, CST has been shown to promote nerve regeneration and functional recovery after SCI (Fan et al., 2020; Yamazaki et al., 2021).

Based on the above techniques, a scheme is proposed. SHED sheet is cultured with homogenate proteins of the spinal cord (hp-SHED sheet). In the microenvironment rich in spinal cord homogenate, SHED differentiate into neural cells. Hp-SHED sheet can release more cytokines and neurotrophins with neuroprotective functions. In this project, hp-SHED sheet was implant into the spinal cord lesion for treating SCI rats with SHED suspensions as a control to investigate the effects on neural regeneration and repair.

2 Results

2.1 Cell identification

SHED were obtained from donors. The morphology of cells was irregular, mostly spindle or polygonal shapes. The cell bodies were small, the cytoplasm was abundant and transparent, and there were almost no protrusions (Figure 1B). The identity of SHED was confirmed by evaluating expression of specific marker proteins by flow cytometry. Percentages of cells expressing positive markers CD44, CD73, CD90, and CD105 were 99.57%, 97.27%, 99.54%, and 99.91%, respectively. Furthermore, the percentage of cells expressing the negative marker human leukocyte antigen was 0.10%, indicating successful isolation of SHED (Figure 1A). In a colony-formation assay, SHED proliferated after 10 days and cell clone formation was visible under light microscopy. After crystalline violet staining, multiple cell colonies were visible (Figure 1C). Following induction of osteogenic differentiation of SHED for 21 days, calcium nodule deposition was visible and Alizarin Red staining was positive (Figure 1D). Following induction of lipogenic differentiation of SHED for 28 days, lipid droplets were observed in the cytoplasm, which stained positive for Oil Red O (Figure 1E). In summary, the extracted cells were SHED with the potential for unlimited proliferation, osteogenic differentiation, and lipogenic differentiation.

2.2 Hp-SHED sheet preparation and characterization

To optimize the formation of SHED sheet, we assayed the effect of varying AA concentrations on the proliferation of SHED. The results show that 240 μg/mL AA obviously inhibited proliferation, and while 120 μg/mL AA promoted cell proliferation and facilitated cell sheet formation. Thus, we chose 120 μg/mL AA for cell sheet construction ($p < 0.001$, Figure 1F). After SHED were cultured with complete medium containing AA for 1 week, SHED sheet was incubated with homogenate protein of spinal cord for 1 week to

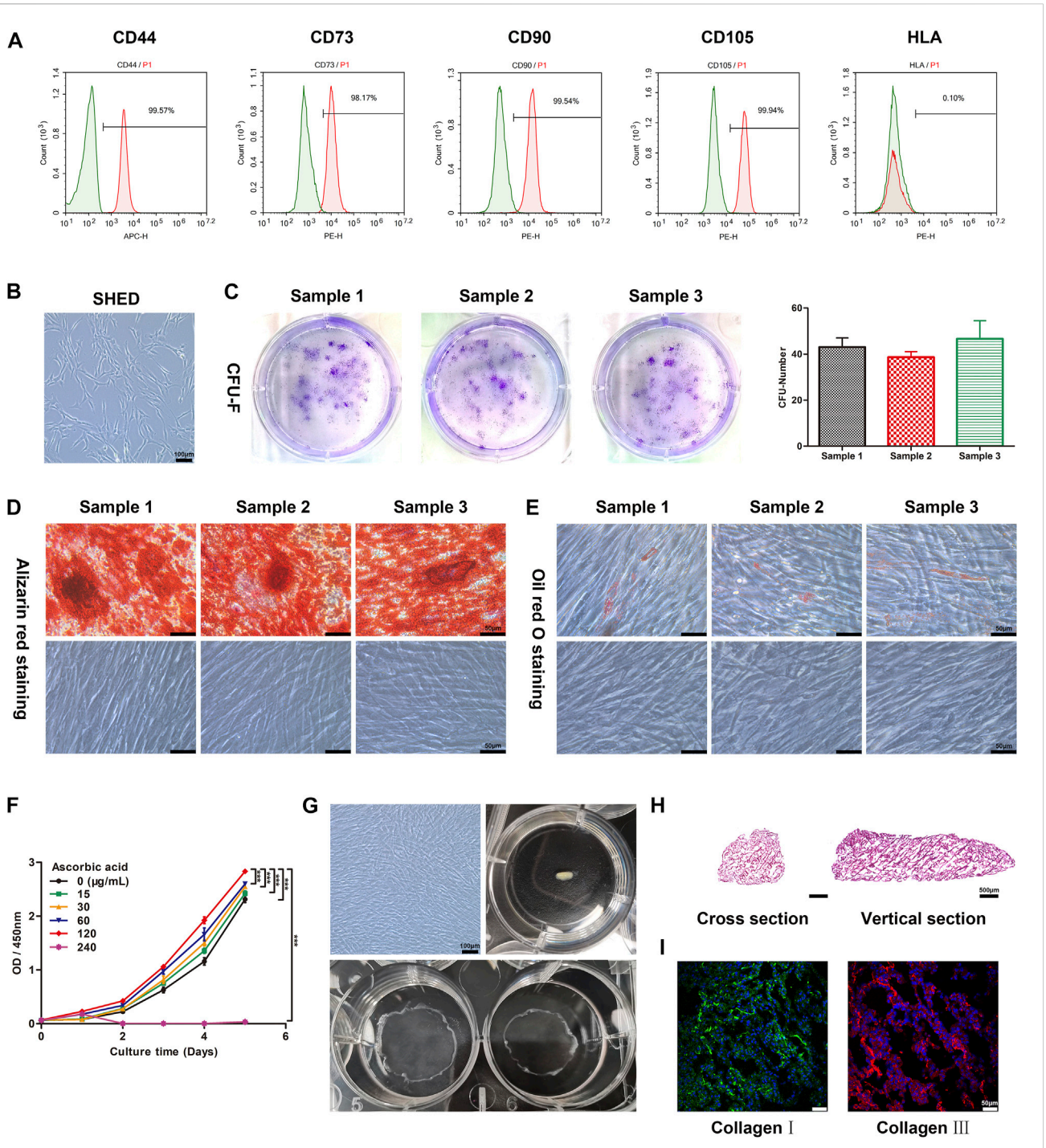

FIGURE 1
The construction and characteristics of hp-SHED sheet, which possesses a geometric structure similar to that of spinal cord tissue. **(A)** The surface markers of SHED, including CD44, CD73, CD90, CD105 and HLA were analyzed by flow cytometry. **(B)** Map of the morphology of the SHED. **(C)** SHED formed single CFU clusters in culture, the quantitative result was indicated in right panel. Data shown as mean ± SD. **(D)** Osteogenic differentiation of SHED. Alizarin red staining was performed at day 21 after osteogenic induction. **(E)** Adipogenic differentiation of SHED. Oil Red O staining was performed at day 28 after adipogenic induction. **(F)** The proliferation curve of SHED with different concentrations of ascorbic acid (AA) was analyzed by CCK8 assay. (mean ± SD, ***$p < 0.001$). **(G)** Construction of hp-SHED sheet. **(H)** Representative images of hp-SHED sheet sections. **(I)** Collagens in hp-SHED sheet were characterized by CLSM.

differentiate into neural cells. Finally, hp-SHED sheet peeled off the culture dish and self-assembled into a spinal cord-like shape, forming the bioactive filling material (Figure 1G).

First, hp-SHED sheet can serve as a biological scaffold, providing a structural basis for cell growth, differentiation, migration, and axonal extension. Cross and vertical sections

10.3389/fbioe.2023.1119639

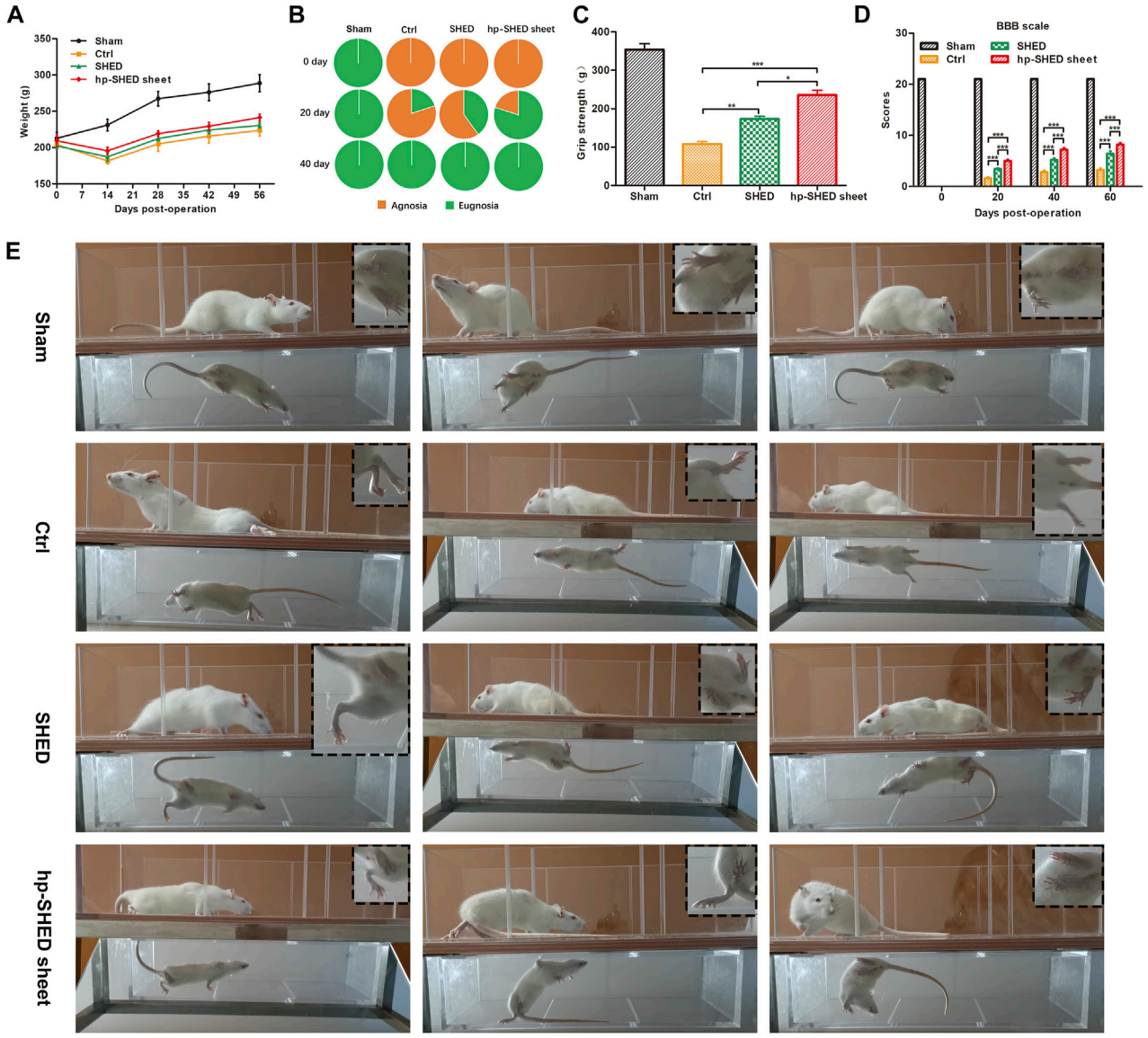

FIGURE 2
Hp-SHED sheet was more active than SHED to recover the sensory and motor in complete SCI rats. **(A)** The weight change in SCI rat model with indicated treatments. **(B)** The percentage of sensory restorative rats at days 0, 20, and 40 post-treatment. **(C)** Grip strength of each group at 60 days post-treatment. **(D)** BBB scores of sham operated rats (Sham) and complete SCI rats upon PBS (Ctrl), SHED, or hp-SHED sheet treatment. **(E)** Representative crawling photos of rats in the indicated group at day 60 post-treatment. (mean ± SD, $*p < 0.05$, $**p < 0.01$, $***p < 0.001$).

of hp-SHED sheet revealed a highly porous three-dimensional inner structure, which facilitates nerve cell attachment, migration, and nerve axon regeneration and extension (Figure 1H). In addition, our results show that both collagens Ⅰ and Ⅲ were positively expressed in hp-SHED sheet. Cells in the hp-SHED sheet were tightly arranged, had a "honeycomb" structure, and regular ECM distribution (Figure 1I). High expression of collagen provides stability to the ECM microenvironment, enhancing intercellular interactions within hp-SHED sheet. Stable ECM is essential for sustained and stable cytokines and neurotrophins production in hp-SHED sheet.

2.3 Hp-SHED sheet effectively restored sensory and motor functions in SCI rats

To systematically and comprehensively explore the biological functions of hp-SHED sheet, 20 rats were divided into four groups: Sham, Control (Ctrl), SHED, and hp-SHED sheet ($n = 5$ per group). The spinal cord at T9–T10 was cut in rats to establish a complete SCI model. After modeling, the lesion cavity was filled with SHED or hp-SHED sheet in experimental groups, and PBS in the Ctrl group (Supplementary Figure S1). During the 60-day recovery period, all rats were subjected to body weight measurements, Von Frey testing, BBB scoring and grip strength

10.3389/fbioe.2023.1119639

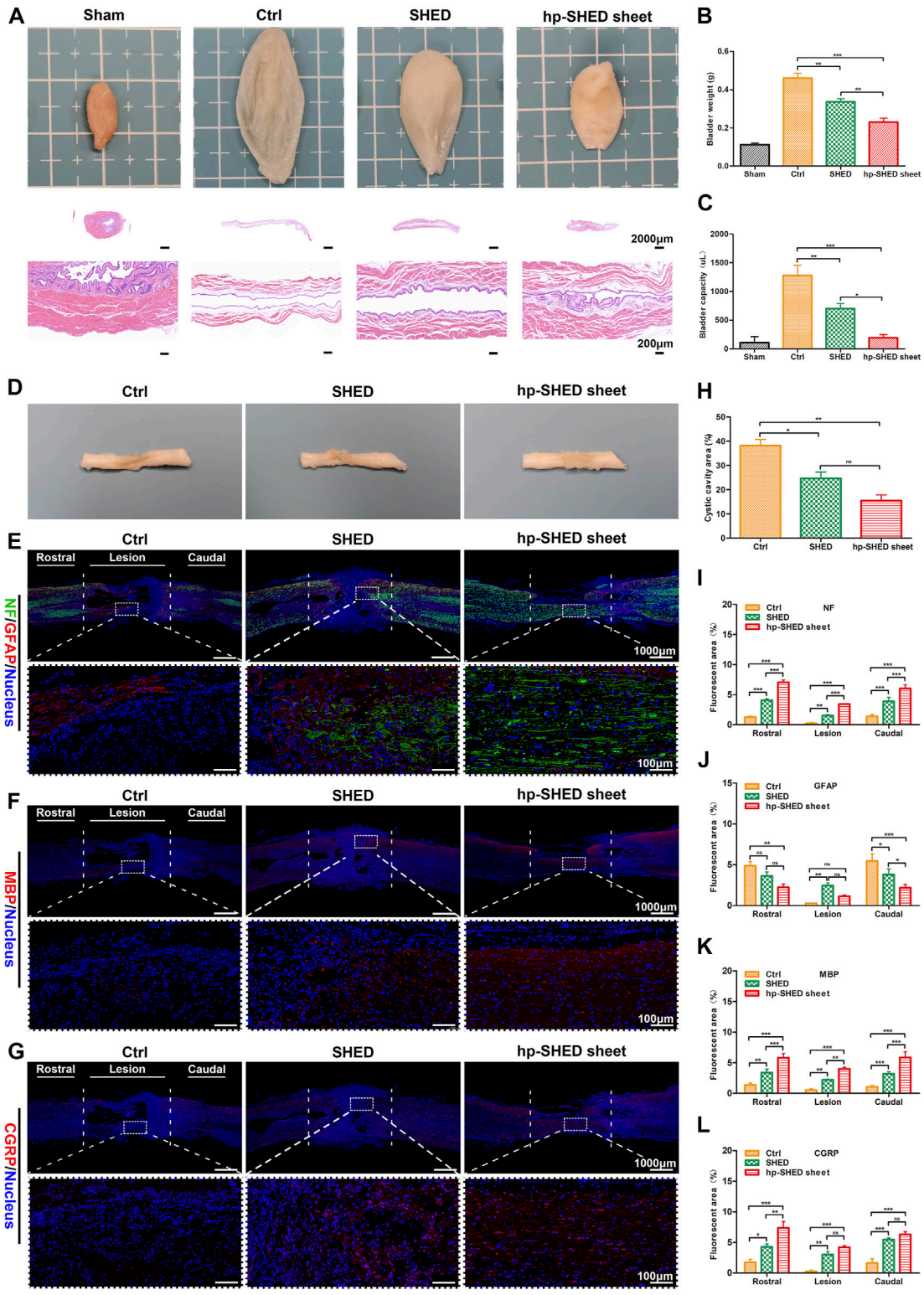

FIGURE 3
Histological mechanisms underlying sensory and motor recovery. **(A)** Representative images and HE staining of bladders from rats in the indicated group. **(B–C)** Quantification and comparison of bladder weight and capacity in the indicated groups. **(D–G)** Spinal cord representative images and IF staining of NF (green) and GFAP (red), MBP (red), CGRP (red), in Ctrl, SHED and hp-SHED sheet. Images below showed the magnified views of the lesion area that are boxed in the above images. **(H–L)** Quantification and comparison of NF, GFAP, MBP, CGRP expression and cystic cavity area. (mean ± SD, $*p < 0.05$, $**p < 0.01$, $***p < 0.001$, ns = no significance).

test every 20 days. Before surgery, rats in each group were weighed. After surgery, rats lost weight because of the effects of spinal cord trauma. However, several days later, the weight of rats started to recover and gradually increased. Weight recovery was faster and more evident in the hp-SHED sheet group, followed by the SHED group, and poorest in the Ctrl group. However, differences between groups were not statistically significant. The rats in the hp-SHED sheet group recovered better and had better appetite, but with an increase in locomotion. The rats in the Ctrl group recovered less and had a poor appetite, but with less locomotion due to poor recovery of the hind limbs. The SHED group was in between. Eating and energy expenditure were in balance, so there was no significant difference in body weight (Figure 2A).

Von Frey filaments were used to detect the sensory recovery of rat hindlimbs. On the second day after surgery, all three groups of SCI rats had complete sensory deficits and negative hindlimb sensory ratings; whereas, rats in the Sham group had sensitive hindlimb sensation, with all rats responding positively. Twenty days after surgery, 20% of Ctrl rats recovered sensation, 40% of SHED rats recovered sensation, and 80% hp-SHED sheet rats recovered sensation (Figure 2B). Thus, the hp-SHED sheet group had a higher proportion of rats with sensory recovery compared with the SHED group, was both were significantly higher than Ctrl group. Rats in the hp-SHED sheet group recovered earlier and more completely.

The recovery of sensation was always accompanied by the recovery of motor ability. At 60 days, average grip strengths were 107.80 g ± 14.81 g in the Ctrl group, 173.00 g ± 16.70 g in the SHED group, and 235.40 g ± 27.93 g in the hp-SHED sheet group ($p < 0.05$, Figure 2C). At 60 days, average BBB locomotor scores were 3.20 ± 0.84 in the Ctrl group, 6.40 ± 1.14 in the SHED group, and 8.20 ± 0.84 in the hp-SHED sheet group ($p < 0.001$, Figure 2D). After 60 days of treatment, Ctrl rats were still unable to crawl on their hind legs and had only slight movement of the hindlimb joints. While SHED rats showed extensive movement of the three joints in the hindlimbs. Hp-SHED sheet rats could land on the plantar placement of the paw with no weight support (Figure 2E; Supplementary Video S1). Compared with the Ctrl group, the joint movement of both hp-SHED sheet and SHED groups showed significant improvement, although the treatment effect of hp-SHED sheet was more significant. In conclusion, hp-SHED sheet produced more significant neurorestorative effects in terms of both sensory and joint movement recovery.

2.4 Hp-SHED sheet *in vivo* restored sensory and motor functions in SCI rats by promoting nerve fiber regeneration and axonal remyelination, and inhibiting glial scarring

We analyzed the recovery of spontaneous urination in rats from histological characteristics of the bladder. Compared with the Sham group, the Ctrl group had overly enlarged bladders due to urinary retention and loss of medial bladder folds, along with abnormally large bladder volumes and increased bladder weights. In contrast, following treatment with SHED or hp-SHED sheet, there were significant improvements in various aspects of bladder size, fold texture, bladder volume, and bladder weight. Notably, for all these observations, hp-SHED sheet was more effective ($p < 0.05$, Figures 3A–C). The analysis of bladder mucosal folds, weight, and capacity revealed that both hp-SHED sheet and SHED had therapeutic effects compared with the Ctrl group, although bladders in the hp-SHED sheet group were more like the Sham group. These results demonstrate that rats in the hp-SHED sheet group recovered spontaneous urination function earlier.

After spinal cord sampling at 60 days postoperatively, it was found that the recovery at the spinal cord lesion differed significantly between the groups (Figure 3D). To compare groups, pathological analysis of the spinal cord was performed. Specifically, the spinal cord lesion, as well as rostral and caudal stumps, were stained for markers of neurons (NF), astrocytes (GFAP), myelin (MBP), and regenerating peripheral nerves (CGRP) to detect neuronal regeneration, glial scar production, and neuronal axonal remyelination. The results revealed an absence of NF staining at the site of SCI in Ctrl rats, and there were obvious voids at the damage site. In SHED rats, there was a small amount of positive NF staining at the damage site. In hp-SHED sheet rats, a large amount of NF positive staining was clearly observable at the injury site, and there was no obvious cavity at the damage site (Figure 3E). Quantification of NF-positive areas at the lesion site shows that the hp-SHED sheet group had the largest area of positive neuron staining (3.43% ± 0.04%) compared to the Ctrl (0.21% ± 0.17%) and SHED groups (1.52% ± 0.16%), indicating that more neurons regenerated, matured, and formed nerve fibers in the SCI lesion this group ($p < 0.01$, Figure 3I).

High numbers of astrocytes promote glial scar deposition, which in turn prevents nerve fiber growth into and extension of nerve axons. To detect astrocyte formation, GFAP staining was performed. In Ctrl rats, the least GFAP staining was observed at the SCI lesion site because of the massive cell death (0.26% ± 0.08%) (Figure 3J). In SHED rats, positive GFAP staining was increased at the damage site as treatment inhibits cell death. In contrast, only weak GFAP-positive staining was observed in hp-SHED sheet rats because the treatment allowed more cells to survive and to differentiate towards non-astrocyte (Figure 3E). Quantification of GFAP-positive areas at the lesion site shows that hp-SHED sheet rats had less GFAP staining (1.15% ± 0.12%) than SHED rats (2.46% ± 0.31%) (Figure 3J). As shown by percentages of GFAP-positive cells, at the rostral and caudal site, astrocyte formation and glial scar deposition were reduced in SHED and hp-SHED sheet rats compared with Ctrl rats, with hp-SHED sheet having the most evident inhibitory effect. At the lesion site, besides the massive cell death in Ctrl rats, hp-SHED sheet rats effectively inhibited astrocyte production compared to SHED rats. Thus, hp-SHED sheet reduced glial scar deposition to mitigate its inhibitory effect on nerve regeneration by decreasing astrocyte production.

During the early stages of SCI, axonal demyelination occurs. Regeneration of myelin can be determined by assessing MBP expression. We did not observe MBP staining in spinal cords of Ctrl rats, while SHED rats displayed small amounts of MBP-positive staining. In hp-SHED sheet rats, large amounts of MBP-positive staining could be observed (Figure 3F). Quantification of MBP-positive areas at the lesion site shows that myelin-positive areas were significantly larger in SHED rats (2.22% ± 0.09%) than Ctrl rats (0.51% ± 0.25%), and significantly higher in hp-SHED sheet rats

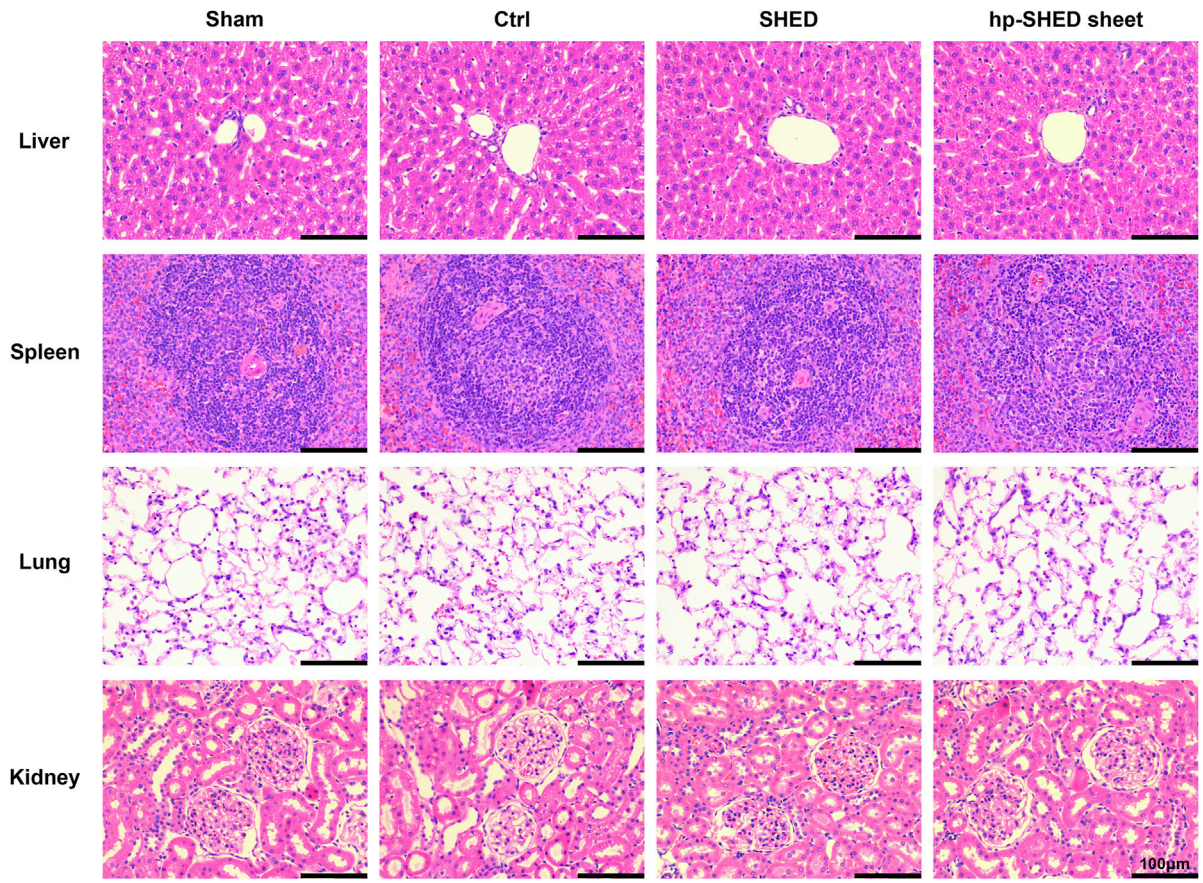

FIGURE 4
The HE staining of liver, spleen, lung and kidney in each group of rats on the 60th day postoperatively.

(3.99% ± 0.28%) than SHED rats, with hp-SHED sheet rats exhibiting the densest myelin structures ($p < 0.01$, Figure 3K).

CGRP is a marker of nerve regeneration, especially early nerve regeneration, that is often used as a rating index for spinal cord repair and regeneration. Our results show that Ctrl rats had almost no CGRP-positive cells, while CGRP-positive staining was increased in the SHED group and highest in the hp-SHED sheet group (Figure 3G). When areas of CGRP-positive staining in each group were quantified, the hp-SHED sheet group had the highest CGRP expression (4.18% ± 0.49%) compared to the Ctrl (0.25% ± 0.15%) and SHED groups (2.98% ± 0.92%) at the lesion site (Figure 3L). Increased numbers of CGRP-positive neurons in hp-SHED sheet rats suggests that hp-SHED sheet can promote neural regeneration earlier and better.

NeuN is a neuron-specific nuclear protein. NeuN staining was performed on the spinal cord, and it was found that there were a large number of neurons at the lesion in the hp-SHED sheet group. In SHED group, there were a few neurons in the lesion. The Ctrl group saw almost no neurons (Supplementary Figure S2A). When areas of NeuN-positive staining in each group were quantified, the hp-SHED sheet group had the highest NeuN expression (2.96% ± 0.69%) compared to the Ctrl (1.01% ± 0.22%) and SHED groups (1.79% ± 0.67%) at the lesion site (Supplementary Figure S2B). IBA1, a 143 amino acid cytoplasmic, inflammation response scaffold protein, is the microglia-specific marker. We stained the spinal cord for IBA1 and found a small distribution of microglia at the lesion in the hp-SHED sheet group. There were more microglia at the lesion in the SHED group. In the Ctrl group, microglial cell expression varied greatly, with some rats having significant microglia expression at the spinal cord lesions, while others had almost no positive expression due to massive cell death (Supplementary Figure S2A). When the Iba1-positive staining area was quantified for each group, the hp-SHED sheet group had the lowest Iba1 expression at the lesion site (0.68% ± 0.28%) compared to the Ctrl group (1.42% ± 1.14%) and the SHED group (1.89% ± 0.29%) (Supplementary Figure S2C).

Persistent inflammatory cell infiltration after SCI leads to further cell death and destruction of cellular and extracellular structures, resulting in the formation of cystic cavities at the lesion. After 60 days of treatment in SCI rats, spinal cord lesions displayed different degrees of cavities among the three groups. Quantification of these cavity areas reveals that hp-SHED sheet rats had the smallest average cavity area (15.49% ± 4.09%), followed by SHED rats (24.64% ± 4.58%) and Ctrl rats (38.23% ± 4.37%) which had the largest cavity area (Figure 3H). Following hp-SHED sheet treatment, more neurons, Schwann cells, and oligodendrocytes regenerated, and regenerated nerve fibers and nerve axons could

extend to the lesion area, reducing the cystic area of the spinal cord lesion and promoting reconstruction of spinal cord neural circuits.

2.5 Hp-SHED sheet maintained a favorable safety profile

To further explore the potential of this bioactive filling material for clinical applications, we examined potential histological changes of several major organs of rats after transplantation. As expected, histopathological sections of the liver, spleen, lung, and kidney showed no abnormalities by HE staining, indicating that hp-SHED sheet and SHED are non-immunotoxic and preliminarily safe as human filler materials (Figure 4).

3 Discussion

After SCI occurs, the lesion is in a growth inhibitory microenvironment that severely hinders neural regeneration. In this microenvironment, inhibitory factors are predominant and factors that promote nerve regeneration are few (Rubiano et al., 2015). Some evidence suggests that neurotrophic cytokines and neurotrophins play a dominant role in the protection of the nervous system (Moalem et al., 2000). Improving neurotrophic factors in the microenvironment is the key to treating SCI. Therefore, an effective delivery strategy to achieve high retention and sustained release of neurotrophins into spinal cord lesion is urgently needed.

MSC transplantation replenishes the large number of cells that die after the occurrence of SCI and has a therapeutic effect. However, numerous studies have shown that cell survival is low after MSC transplantation, and it is the paracrine secreted neurotrophic factors that play the main therapeutic role (Chen et al., 2020; Sugimura-Wakayama et al., 2015). CST overcomes the problem of low survival rate of single-cell suspension. With CST, the cells remain active and are able to continuously secrete neurotrophic factors by paracrine (Yan et al., 2022). Indeed, the cell sheet can be regarded as a structural platform for natural, stable, and sustained release of neurotrophins. In addition, compared to cell suspensions, CST facilitates cell migration, proliferation, and differentiation (Lin et al., 2013; Takeuchi et al., 2016). The component of spinal cord homogenate proteins is complex and includes some chemical substances or cytokines. Previous studies showed that spinal cord homogenate proteins could be used as an effective inducer to induce BMSCs to differentiate into neuronal cells and secrete brain-derived neurotrophic factor (Liu et al., 2011; WU et al., 2009). In this study, SHED sheet was induced with homogenate proteins of the spinal cord to induce more cytokines and neurotrophins production for treating SCI mice with SHED suspensions as a control.

Hp-SHED sheet can serve as a biological scaffold, providing a structural basis for cell growth, differentiation, migration, and axonal extension. Ascorbic acid (AA) has been shown to promote intercellular adhesion *via* collagen to stimulate SHED self-assembly into flexible cell sheet structures (Yan et al., 2022). Collagen has good biocompatibility and degradability, and its collagen-binding domain and ordered structure provide a suitable basis for accommodating neurotrophic factors within a certain area, thus guiding neuronal axons to grow in a certain direction in an orderly manner (Li and Dai, 2018). In summary, hp-SHED sheet maximally mimics the microenvironment of spinal cord development.

Hp-SHED sheet not only serves as a biological scaffold to provide a structural basis for neural cell regeneration and axonal extension. It also secretes various neurotrophic factors related to nerve growth through the paracrine pathway. In the lesion microenvironment of SCI, neural stem cells were more inclined to differentiate into astrocytes and form scar tissue, which inhibits nerve cell regeneration and the reconstruction of neural circuits (Cao et al., 2001; Wang et al., 2008). SHED may act as neuroprotective agents after transplantation, possibly through paracrine signaling, to reduce glial scar formation and induce tissue plasticity and functional recovery (Nicola et al., 2019). While studies shown that compared with undifferentiated SHED, implantation of induced neural differentiated SHED had a stronger ability to promote nerve regeneration, axonal remyelination, and to inhibit astrocyte generation, glial scar formation in animal models of SCI (Fujii et al., 2015; Taghipour et al., 2012). In our study, SHED sheet was induced with homogenate proteins of spinal cord. The differentiated SHED can continuously secrete cytokines and neurotrophins to promote functional recovery.

Persistent inflammatory cell infiltration after SCI leads to further neural cell death and destruction of cellular and extracellular structures, resulting in the formation of cystic cavities at the lesion. In addition, astrocyte proliferation and ECM deposition promote glial scarring. The formation of cystic cavities and glial scarring after SCI severely hinders nerve regeneration and axonal extension (Alizadeh et al., 2019). During the early stages of SCI, axonal demyelination occurs. The absence of myelin sheath inhibits nerve impulse conduction and affects nerve function (Plemel et al., 2014). Microglia are the resident immune cells of CNS. After SCI, microglia are activated and transformed into macrophages, which colonize the damaged area to phagocytose cell debris and degenerated myelin sheaths (Lin et al., 2021). Microglia phagocytosis of myelin is a feature of neurological disease and injury (Neumann et al., 2009). SCI induces scar formation consisting of multiple cell types (astrocytes, fibroblasts, microglia, macrophages) without spontaneous neuronal regeneration and axonal growth. Hp-SHED sheet group could better promote nerve regeneration and could reduce the inflammatory response and scar formation caused by injury by inhibiting microglia proliferation. Hp-SHED sheet improved the microenvironment by secreting cytokines and neurotrophins to promote nerve regeneration, axonal extension, myelin regeneration and to inhibit astrocyte generation, glial scar formation. Previous studies have shown that hpDCs promote functional recovery from SCI in mice by upregulating neurotrophic cytokines and neurotrophins at the injury site. hpDCs decrease the areas of cysts and exhibit good tissue preservation in SCI mice, which is consistent with our present findings (Liu et al., 2009; Wang et al., 2013).

After spinal cord injury, primary and secondary injuries result in massive neuronal cell death at the lesion as well as destruction of extracellular structures, and a cystic cavity is formed at the injury site. The surviving neural stem cells are more likely to differentiate into astrocytes in the lesion microenvironment, and the proliferation of astrocytes promotes the formation of glial scar (Cao et al., 2001;

Wang et al., 2008). The cystic cavity and glial scar formed after SCI severely impede neural regeneration and axonal extension (Alizadeh et al., 2019). Common filler materials can reduce the cystic cavity area by adding exogenous cells or reducing cell death. But the surviving neural stem cells eventually differentiated into astrocytes due to insufficient neurotrophic factors in the lesion microenvironment and formed a glial scar in other studies (Dominguez-Bajo et al., 2019, 2020). Studies have shown that Implantation of SHED with induced neural differentiation has a stronger ability to promote neural regeneration, axonal remyelination and inhibit astrocyte generation and glial scar formation in animal models of SCI (Taghipour et al., 2012; Fujii et al., 2015). Spinal homogenins act as an effective inducer to induce differentiation of stem cells into neuronal cells (Wu et al., 2009; Liu et al., 2011). In this paper, hp-SHED sheet has stronger neurotrophic properties compared to other filler materials. Hp-SHED sheet can inhibit the differentiation of neural stem cells into astrocytes and promote their differentiation into neurons, as evidenced by increased NF expression and decreased GFAP expression at the lesion site. In this way, hp-SHED sheet facilitates the construction of neural networks by reducing glial scar generation and promoting neural axon extension. This is supported by results in other study (Yan et al., 2022).

Nerve regeneration and axonal remyelination promoted the repair and reconstruction of neural networks, which in turn promoted the recovery of sensory and motor functions in SCI rats. Hp-SHED sheet rats had earlier hindlimb sensory repair and earlier recovery of urinary reflex than SHED rats. In addition, the rats in hp-SHED sheet group had better recovery of hindlimb grip strength and better recovery of hindlimb joint functions. Moreover, hp-SHED sheet maintained a favorable safety profile.

Hp-SHED sheet can continuously secrete cytokines and neurotrophins. The neuroprotective factors can improve the pathological microenvironment of spinal cord lesions, promote *in situ* centralis neuroplasticity, allowing regeneration after SCI. Thus, hp-SHED sheet is conducive to enhancing the reconstruction of spinal cord and an ideal bioactive material for filling injuries in the spinal cord.

4 Materials and methods

4.1 Cell extraction and culture

SHED were obtained from exfoliated deciduous teeth of clinical patients, and teeth were repeatedly flushed with phosphate-buffered saline (PBS). The pulp was removed under aseptic conditions, mechanically sheared, and then digested with type I collagenase (3 mg/mL; Sigma-Aldrich, St. Louis, MO, United States) for 1 h at 37°C to prepare a single-cell suspension. After centrifugation, cells were resuspended in α-Minimum Essential Media (Gibco, Grand Island, NY, United States) containing 10% fetal bovine serum (Hyclone, Logan, UT, United States) and 1% penicillin/streptomycin (Invitrogen, Carlsbad, CA, United States). Cells were incubated in T75 cm^2 flasks, allowed to grow to 80%–90% confluence, and then passaged normally.

4.2 Flow cytometry

Cells in logarithmic growth phase were removed and digested with trypsin into single-cell suspension. Adjust the cell concentration to 1×10^7 cells/mL. Prepare 6 EP tubes and add 0.1 mL of cell suspensions to each tube. Under light-proof conditions, 1 μl of antibodies were added to each EP tube, Anti-Human CD73 PE, Anti-Human CD105 (Endoglin) PE, Anti-Human/Mouse CD44 APC, Anti-Human CD90 (Thy-1) PE, Anti-Human HLA-DR FITC (BioGems, United States), control group plus PBS. Mix well and incubate for 30 min at 4°C away from light. Vortex shaking was removed every 10 min for 5 s to bring the cells into full contact with the antibody. At the end of incubation, the cells were washed 2–3 times with PBS. Then 0.5 mL of PBS was added to resuspend the cells, filtered through a copper mesh and assayed by flow cytometry (Agilent, United States).

4.3 Colony formation assay

SHED in single-cell suspension were seeded into six-well plates at a density of 200 cells per well. Then the cells were cultured in α-MEM at 37°C. The medium was changed every 3 days. The cells were cultured for 10 days. Then the colonies were washed by PBS and fixed in 4% paraformaldehyde (PFA) solution 10 min. After washed by PBS the cells were incubated in 0.1% crystal violet for 20 min (Beyotime, China). Then colonies were observed. Finally, calculate the number of colonies under an inverted light microscope (Leica, Germany).

4.4 Osteogenic differentiation

SHED were seeded into 0.1% gelatin-coated six-well plates at a density of 2×10^4 cells/cm^2. The cells were cultured in α-MEM at 37°C. When the degree of cell fusion reached 70%, the cells were cultured with osteogenic induction medium (OriCell®, China). Cells in control group were cultured in α-MEM. The medium was changed every 3 days. After 21 days of induction, alizarin red was used for staining. The osteogenesis staining was observed under the inverted light microscope.

4.5 Adipogenic differentiation

SHED were seeded into 0.1% gelatin-coated six-well plates at a density of 2×10^4 cells/cm^2. The cells were cultured in α-MEM at 37°C. When the degree of cell fusion reached 100%, the cells were cultured with adipogenic induction medium A (OriCell®, China). The medium was changed to adipogenic induction medium B after 3 days. After 1 day of maintenance, solution B was replaced with solution A. Solution A and solution B are used alternately as above. Cells in control group were cultured in α-MEM. After 28 days of induction, Oil Red O solution was used for staining. The lipid-forming staining was observed under the inverted light microscope.

4.6 CCK-8 assay

Cell proliferation was detected with the CCK-8 kit (DOjinDO, Japan). Each 96-well plate was divided into seven groups, with six replicate wells in each group. In six groups, each well was inoculated with 1000 cells in a volume of 200 μL of culture medium with ascorbic acid (AA) concentrations of 0, 15, 30, 60, 120, and 240 μg/mL. The other group was not inoculated with cells, and only the culture medium was added as a blank control. Cells were incubated in a CO_2 incubator at 37°C. A 96-well plate was removed at 0 h, 24 h, 48 h, 72 h, 96 h and 120 h, and CCK-8 solution (20 μL/well) was added to the culture medium. After incubation for 2 h in the incubator at 37°C, the absorbance was measured at 450 nm.

4.7 Preparation of homogenate proteins of spinal cord

Homogenate proteins of the spinal cord were harvested from Sprague-Dawley rats (aged 8–10 weeks) that had been anesthetized. Briefly, spinal cords at the T8–10 levels were resected, ground, filtered (200 mm), disrupted with an ultrasonic homogenizer, and finally centrifuged at 15,000 g for 20 min. The supernatant was collected as the protein homogenate and the protein concentration was measured. The concentration of total protein used here was 1 mg/mL.

4.8 Construction of hp-SHED sheet

SHED were cultured in medium containing ascorbic acid (AA), which was changed every 2–3 days. A cell sheet was formed after 1 week of culture. Then, the culture medium was changed to α-MEM containing homogenate proteins of spinal cord for 1 week. Finally, the cell sheet at the bottom of the dish was gently peeled off and curled by self-assembly into a bioactive filler shaped like the spinal cord. This filling material, termed hp-SHED sheet.

4.9 Spinal cord injury model and postoperative care

The animal study was reviewed and approved by the Animal Studies Committee of Guangxi University. Twenty female Sprague-Dawley rats, aged 8–10 weeks and weighing 180–230 g, were purchased from the Laboratory Animal Center. In this exploratory study, we utilized female rats, which are commonly used in spinal cord injury studies because of their better compliance with surgical procedures and low rate of self-mutilation compared to males. Besides female rats are superior to male rats in terms of postoperative care due to low urinary infection rate. Rats were housed in animal rooms with sterilized bedding, water, and feed, in a quiet environment with appropriate temperature and humidity. Before the experiment, all rats were subjected to routine behavioral tests to ensure that their motor functions were normal. Rats were numbered sequentially and randomly divided into four groups (n = 5 per group): 1) Sham, laminectomy only without spinal cord transection; 2) Ctrl, spinal cord transection with implantation replaced by PBS; 3) SHED, spinal cord transection with SHED implanted at the lesion gap; and 4) hp-SHED sheet, spinal cord transection with hp-SHED sheet implanted at the lesion gap. Rats were fasted for 12 h before surgery and drank water freely. Rats were weighed and anesthetized with 1% pentobarbital sodium (0.4 mL/100 g) by intraperitoneal injection. Under deep anesthesia, each rat was fixed in a prone position on the operating table, and the hair near the T8–T10 spinous process on the back of the rat was shaved, prepared, and positioned to make a posterior median incision centered on T10. At this position, the skin, fascia, and muscle tissues were separated layer by layer to expose the T10 spinous process and transverse process. The T10 spinous process was clipped, the transverse process was held in place with forceps, and the T10 lamina was bitten off with a miniature biting forceps to expose the spinal cord. Care was taken not to touch the spinal cord throughout this process. The spinal cord of the T10 segment was completely transected using ophthalmic scissors. After cutting, the severed end was trimmed slightly to regularize the cut surface for better anastomosis with the filler. The section trimming and the retraction of both rostral and caudal tissue endings produced a gap of 2.0 ± 0.5 mm. Immediately after transection, both lower limbs of the rat were observed to twitch and the rat wagged its tail and then completely relaxed. A filler was implanted into the spinal cord gap to ensure anastomosis with the severed end of the spinal cord. The muscle, fascia, and skin tissues were sutured layer by layer at the end of the operation. The principle of asepsis was strictly observed during the operation. To avoid infection, penicillin was injected intramuscularly daily for 7 days after surgery, and the duration of use was extended in the presence of hematuria and pyuria. Manual urination was performed 2–3 times a day until the urination reflex was restored.

4.10 Sensory recovery analysis

Sensory recovery was assessed using the Von Frey test (North Coast Medical, Carlsbad, CA, United States). Briefly, filaments with stimulus force gradients (0.07, 0.4, 2, 4, 10, 60, 180, and 300 g) were applied to the paw to elicit a nociceptive response (rapid stimulus avoidance by the paw) for at least 30 s between trials. Scores were determined by a blinded method. Assessments were performed at 9: 00 p.m. due to wide variations in the diurnal activity of rats. Mechanical pain thresholds were assessed using the "Up and Down" method to calculate the 50% retraction-response threshold of rats. Rats with a 50% retraction threshold of 4 g or less were counted as positive for sensory function, and the percentage of positive rats was calculated. The baseline score was measured every 2–3 days after surgery, and then every 20 days until the end of the experiment (60 days).

4.11 Grip strength test

Starting 1 week prior to SCI surgery, each rat was trained for 2 min per day to familiarize itself with the grip strength meter (KEWBASIS®, KW-ZL-1, China). After 60 days of SCI, the grip

strength of the hindlimb was measured for each rat by a blinded method. If the hindlimb motor impairment was too severe for the rat to grasp the crossbar, the grip strength score was 0. The grip strength tests on the same rat were performed a few minutes apart. We made sure that each rat was performed grip test with relaxed muscles and without spasms. Each rat was tested more than three times and the average was taken. The above ensures that the test values are at normal grip levels.

4.12 Behavioral evaluation

The Basso-Beattie-Bresnahan (BBB) locomotion rating scale is a neurological assessment method used to evaluate motor function in the hindlimbs of rats. A score of 0 is considered complete paralysis, whereas 21 is considered normal. All animals were checked for bladder fullness prior to the assessment to prevent bladder fullness from interfering with movements. The baseline score was measured every 2–3 days after surgery. Thereafter, measurements were taken every 20 days until the end of the experiment (60 days). In addition, video was recorded for each rat. The results were analyzed and processed using GraphPad Prism 8.0 software (GraphPad, San Diego, CA, United States).

4.13 Specimen collection

Sixty days after surgery, rats were anesthetized and systemically perfused with saline. After the saline flow was free of blood, the tissues and organs were fixed with 4% PFA. Subsequently, samples of spinal cord from approximately 2 cm around the lesion site were obtained (including the lesion, as well as the rostral and caudal stumps). Similarly, the liver, spleen, lung, kidney, and bladder were removed and placed in 4% PFA for fixation.

4.14 Histological analysis

After self-assembly of hp-SHED sheet, frozen sections were stained with hematoxylin and eosin (HE). Fixed spinal cord samples were cryosectioned, immunofluorescently stained, and imaged by confocal laser-scanning microscope (CLSM) (Leica, Wetzlar, Germany). The bladder was weighed and its volume measured. Finally, the rat liver, spleen, lung, kidney, and bladder were subjected to HE staining. Briefly, PFA-fixed tissues were removed, washed, embedded in paraffin, sectioned, and stained with HE. Images were acquired using an inverted light microscope. Finally, histological analysis was performed.

4.15 Immunofluorescence staining

Hp-SHED sheet staining: Hp-SHED sheet was embedded in Optimal Cutting Temperature Compound and cryosectioned at a thickness of 10 μm. Sections were fixed in acetone for 5 min and then washed three times with PBS before incubation at 4°C overnight with one of the following primary antibodies: collagen Ⅰ (Abcam, Cambridge, UK), collagen Ⅲ (Abcam). The next day, an appropriate secondary antibody was added and incubated at room temperature for 1 h, and DAPI was used to stain cell nuclei. Samples were imaged under a CLSM.

Spinal cord staining: PFA-fixed spinal cords were embedded in Optimal Cutting Temperature Compound and sectioned on ice at a thickness of 10 μm. Subsequently, sections were fixed with 4% PFA, washed three times with PBS, and subjected to antigen repair in a cassette filled with EDTA antigen repair buffer (pH 8.0) in a microwave oven. Sections could cool naturally, blocked with 3% bovine serum albumin for 30 min, and incubated overnight at 4°C with one of the following primary antibodies: neurofilament (NF; Cell Signaling Technology), glial fibrillary acidic protein (GFAP; Millipore), calcitonin gene-related peptide (CGRP; GeneTex, Irvine, CA, United States), and myelin basic protein (MBP; Signalway Antibody, Baltimore, MD, United States). The next day, sections were incubated with a secondary antibody at room temperature for 1 h and DAPI was used to restain cell nuclei. After mounting, sections were observed and photographed with a CLSM. Quantitative histomorphometric analysis was performed using Image-Pro Plus software (Media Cybernetics, Rockville, MD, United States).

4.16 Statistical analysis

Experimental data were statistically analyzed using GraphPad Prism and SPSS 23.0 software (IBM, Chicago, IL, United States). Measurement data are described as mean ± standard deviation (SD) for $n \geq 3$. Differences between two groups were compared utilizing t tests, while those among multiple groups were compared by ANOVA, followed by Tukey's test for multiple comparisons. BBB scores at different time points were analyzed by repeated measures ANOVA, followed by Tukey's test for multiple comparisons. $^{*}p < 0.05$ was considered statistically significant. Significance levels: $^{*}p < 0.05$, $^{**}p < 0.01$, $^{***}p < 0.001$.

Data availability statement

The original contributions presented in the study are included in the article/Supplementary Material, further inquiries can be directed to the corresponding author.

Ethics statement

The animal study was reviewed and approved by the Animal Studies Committee of Guangxi University.

Author contributions

ZQ conceived the idea for the study, provided a retrieval strategy. SM conducted the experiments and analyzed the data. SM drafted the first draft of the manuscript that was iteratively improved by XW, JG, and YL.

Funding

This work was supported by the National Key Research and Development Program of China (2018YFA0108304); the National Natural Science Foundation of China (81971505).

Conflict of interest

The authors declare that the research was conducted in the absence of any commercial or financial relationships that could be construed as a potential conflict of interest.

Publisher's note

All claims expressed in this article are solely those of the authors and do not necessarily represent those of their affiliated organizations, or those of the publisher, the editors and the reviewers. Any product that may be evaluated in this article, or claim that may be made by its manufacturer, is not guaranteed or endorsed by the publisher.

Supplementary material

The Supplementary Material for this article can be found online at: https://www.frontiersin.org/articles/10.3389/fbioe.2023.1119639/full#supplementary-material

SUPPLEMENTARY VIDEO S1
Locomotion of rats in each group on the 60th day postoperatively.

SUPPLEMENTARY FIGURE S1
The surgery process of SCI modeling.

SUPPLEMENTARY FIGURE S2
IF staining of NeuN and Iba1 in Ctrl, SHED and hp SHED sheet.

References

Alizadeh, A., Dyck, S. M., and Karimi-Abdolrezaee, S. (2019). Traumatic spinal cord injury: An overview of pathophysiology, models and acute injury mechanisms. *Front. Neurol.* 10, 282. doi:10.3389/fneur.2019.00282

Anderson, M. A., Burda, J. E., Ren, Y., Ao, Y., O'Shea, T. M., Kawaguchi, R., et al. (2016). Astrocyte scar formation aids central nervous system axon regeneration. *Nature* 532 (7598), 195–200. doi:10.1038/nature17623

Cao, Q. L., Zhang, Y. P., Howard, R. M., Walters, W. M., Tsoulfas, P., and Whittemore, S. R. (2001). Pluripotent stem cells engrafted into the normal or lesioned adult rat spinal cord are restricted to a glial lineage. *Exp. Neurol.* 167 (1), 48–58. doi:10.1006/exnr.2000.7536

Chen, Y. R., Lai, P. L., Chien, Y., Lee, P. H., Lai, Y. H., Ma, H. I., et al. (2020). Improvement of impaired motor functions by human dental exfoliated deciduous teeth stem cell-derived factors in a rat model of Parkinson's disease. *Int. J. Mol. Sci.* 21 (11), 3807. doi:10.3390/ijms21113807

Dias, D. O., Kim, H., Holl, D., Werne, S. B., Lundeberg, J., Carlen, M., et al. (2018). Reducing pericyte-derived scarring promotes recovery after spinal cord injury. *Cell* 173 (1), 153–165.e22. doi:10.1016/j.cell.2018.02.004

Dominguez-Bajo, A., Gonzalez-Mayorga, A., Guerrero, C. R., Palomares, F. J., Garcia, R., Lopez-Dolado, E., et al. (2019). Myelinated axons and functional blood vessels populate mechanically compliant rgo foams in chronic cervical hemisected rats. *Biomaterials* 192, 461–474. doi:10.1016/j.biomaterials.2018.11.024

Dominguez-Bajo, A., Gonzalez-Mayorga, A., Lopez-Dolado, E., Munuera, C., Garcia-Hernandez, M., and Serrano, M. C. (2020). Graphene oxide microfibers promote regenerative responses after chronic implantation in the cervical injured spinal cord. *ACS Biomater. Sci. Eng.* 6 (4), 2401–2414. doi:10.1021/acsbiomaterials.0c00345

Elloumi-Hannachi, I., Yamato, M., and Okano, T. (2010). Cell sheet engineering: A unique nanotechnology for scaffold-free tissue reconstruction with clinical applications in regenerative medicine. *J. Intern. Med.* 267 (1), 54–70. doi:10.1111/j.1365-2796.2009.02185.x

Fan, Z., Liao, X., Tian, Y., Xuzhuzi, X., and Nie, Y. (2020). A prevascularized nerve conduit based on a stem cell sheet effectively promotes the repair of transected spinal cord injury. *Acta Biomater.* 101, 304–313. doi:10.1016/j.actbio.2019.10.042

Fujii, H., Matsubara, K., Sakai, K., Ito, M., Ohno, K., Ueda, M., et al. (2015). Dopaminergic differentiation of stem cells from human deciduous teeth and their therapeutic benefits for parkinsonian rats. *Brain Res.* 1613, 59–72. doi:10.1016/j.brainres.2015.04.001

Global, R., Abate, D., Abate, K. H., Abay, S. M., Abbafati, C., Abbasi, N., et al. (2018). Global, regional, and national incidence, prevalence, and years lived with disability for 354 diseases and injuries for 195 countries and territories, 1990–2017: A systematic analysis for the global burden of disease study 2017. *Lancet* 392 (10159), 1789–1858. doi:10.1016/S0140-6736(18)32279-7

Hochuli, A., Senegaglia, A. C., Selenko, A. H., Fracaro, L., and Brofman, P. (2021). Dental pulp from human exfoliated deciduous teeth-derived stromal cells demonstrated neuronal potential: *In vivo* and *in vitro* studies. *Curr. Stem Cell Res. Ther.* 16 (5), 495–506. doi:10.2174/1574888X16666210215160402

Huang, G. T., Gronthos, S., and Shi, S. (2009). Mesenchymal stem cells derived from dental tissues vs. Those from other sources: Their biology and role in regenerative medicine. *J. Dent. Res.* 88 (9), 792–806. doi:10.1177/0022034509340867

Huang, L., Zheng, Z., Bai, D., and Han, X. (2022). Stem cells from human exfoliated deciduous teeth and their promise as preventive and therapeutic strategies for neurological diseases and injuries. *Curr. Stem Cell Res. Ther.* 17 (6), 527–536. doi:10.2174/1574888X17666211229155533

Hwang, N. S., Zhang, C., Hwang, Y. S., and Varghese, S. (2009). Mesenchymal stem cell differentiation and roles in regenerative medicine. *Wiley Interdiscip. Rev.-Syst. Biol.* 1 (1), 97–106. doi:10.1002/wsbm.26

Iwata, T., Yamato, M., Washio, K., Yoshida, T., Tsumanuma, Y., Yamada, A., et al. (2018). Periodontal regeneration with autologous periodontal ligament-derived cell sheets - a safety and efficacy study in ten patients. *Regen. Ther.* 9, 38–44. doi:10.1016/j.reth.2018.07.002

Li, L., Xiao, B., Mu, J., Zhang, Y., Zhang, C., Cao, H., et al. (2019). A mno2 nanoparticle-dotted hydrogel promotes spinal cord repair via regulating reactive oxygen species microenvironment and synergizing with mesenchymal stem cells. *ACS Nano* 13 (12), 14283–14293. doi:10.1021/acsnano.9b07598

Li, X., and Dai, J. (2018). Bridging the gap with functional collagen scaffolds: Tuning endogenous neural stem cells for severe spinal cord injury repair. *Biomater. Sci.* 6 (2), 265–271. doi:10.1039/c7bm00974g

Lin, S., Zhou, Z., Zhao, H., Xu, C., Guo, Y., Gao, S., et al. (2021). Tnf promotes m1 polarization through mitochondrial metabolism in injured spinal cord. *Free Radic. Biol. Med.* 172, 622–632. doi:10.1016/j.freeradbiomed.2021.07.014

Lin, Y. C., Grahovac, T., Oh, S. J., Ieraci, M., Rubin, J. P., and Marra, K. G. (2013). Evaluation of a multi-layer adipose-derived stem cell sheet in a full-thickness wound healing model. *Acta Biomater.* 9 (2), 5243–5250. doi:10.1016/j.actbio.2012.09.028

Liu, M., Zhao, J., Liang, H., and Bian, X. (2009). Vaccination with dendritic cells pulsed with homogenate protein of spinal cord promotes functional recovery from spinal cord injury in mice. *Spinal Cord.* 47 (5), 360–366. doi:10.1038/sc.2008.112

Liu, R., Fan, D., Jin, P., Fan, H., and Wang, P. (2011). Effects of injured spinal cord extracts on brain-derived neurotropic factor and myelin proteolipid protein in bone marrow mesenchymal stem cells. *Chin. J. Tissue Eng. Res.* 15 (1), 7.

Liu, Y., Ming, L., Luo, H., Liu, W., Zhang, Y., Liu, H., et al. (2013). Integration of a calcined bovine bone and bmsc-sheet 3d scaffold and the promotion of bone regeneration in large defects. *Biomaterials* 34 (38), 9998–10006. doi:10.1016/j.biomaterials.2013.09.040

Miura, M., Gronthos, S., Zhao, M., Lu, B., Fisher, L. W., Robey, P. G., et al. (2003). Shed: Stem cells from human exfoliated deciduous teeth. *Proc. Natl. Acad. Sci. U. S. A.* 100 (10), 5807–5812. doi:10.1073/pnas.0937635100

Moalem, G., Gdalyahu, A., Shani, Y., Otten, U., Lazarovici, P., Cohen, I. R., et al. (2000). Production of neurotrophins by activated t cells: Implications for neuroprotective autoimmunity. *J. Autoimmun.* 15 (3), 331–345. doi:10.1006/jaut.2000.0441

Neumann, H., Kotter, M. R., and Franklin, R. J. (2009). Debris clearance by microglia: An essential link between degeneration and regeneration. *Brain* 132, 288–295. doi:10.1093/brain/awn109

Nicola, F., Marques, M. R., Odorcyk, F., Arcego, D. M., Petenuzzo, L., Aristimunha, D., et al. (2017). Neuroprotector effect of stem cells from human exfoliated deciduous teeth transplanted after traumatic spinal cord injury involves inhibition of early neuronal apoptosis. *Brain Res.* 1663, 95–105. doi:10.1016/j.brainres.2017.03.015

Nicola, F., Marques, M. R., Odorcyk, F., Petenuzzo, L., Aristimunha, D., Vizuete, A., et al. (2019). Stem cells from human exfoliated deciduous teeth modulate early astrocyte response after spinal cord contusion. *Mol. Neurobiol.* 56 (1), 748–760. doi:10.1007/s12035-018-1127-4

Nishida, K., Yamato, M., Hayashida, Y., Watanabe, K., Yamamoto, K., Adachi, E., et al. (2004). Corneal reconstruction with tissue-engineered cell sheets composed of autologous oral mucosal epithelium. *N. Engl. J. Med.* 351 (12), 1187–1196. doi:10.1056/NEJMoa040455

Ohki, T., Yamato, M., Ota, M., Takagi, R., Murakami, D., Kondo, M., et al. (2012). Prevention of esophageal stricture after endoscopic submucosal dissection using tissue-engineered cell sheets. *Gastroenterology* 143 (3), 582–588.e2. doi:10.1053/j.gastro.2012.04.050

Pereira, L. V., Bento, R. F., Cruz, D. B., Marchi, C., Salomone, R., Oiticicca, J., et al. (2019). Stem cells from human exfoliated deciduous teeth (shed) differentiate *in vivo* and promote facial nerve regeneration. *Cell Transpl.* 28 (1), 55–64. doi:10.1177/0963689718809090

Plemel, J. R., Keough, M. B., Duncan, G. J., Sparling, J. S., Yong, V. W., Stys, P. K., et al. (2014). Remyelination after spinal cord injury: Is it a target for repair? *Prog. Neurobiol.* 117, 54–72. doi:10.1016/j.pneurobio.2014.02.006

Rubiano, A. M., Carney, N., Chesnut, R., and Puyana, J. C. (2015). Global neurotrauma research challenges and opportunities. *Nature* 527 (7578), S193–S197. doi:10.1038/nature16035

Sakai, K., Yamamoto, A., Matsubara, K., Nakamura, S., Naruse, M., Yamagata, M., et al. (2012). Human dental pulp-derived stem cells promote locomotor recovery after complete transection of the rat spinal cord by multiple neuro-regenerative mechanisms. *J. Clin. Invest.* 122 (1), 80–90. doi:10.1172/JCI59251

Sato, M., Yamato, M., Hamahashi, K., Okano, T., and Mochida, J. (2014). Articular cartilage regeneration using cell sheet technology. *Anat. Rec.* 297 (1), 36–43. doi:10.1002/ar.22829

Shimizu, T., Yamato, M., Kikuchi, A., and Okano, T. (2003). Cell sheet engineering for myocardial tissue reconstruction. *Biomaterials* 24 (13), 2309–2316. doi:10.1016/s0142-9612(03)00110-8

Sugimura-Wakayama, Y., Katagiri, W., Osugi, M., Kawai, T., Ogata, K., Sakaguchi, K., et al. (2015). Peripheral nerve regeneration by secretomes of stem cells from human exfoliated deciduous teeth. *Stem Cells Dev.* 24 (22), 2687–2699. doi:10.1089/scd.2015.0104

Taghipour, Z., Karbalaie, K., Kiani, A., Niapour, A., Bahramian, H., Nasr-Esfahani, M. H., et al. (2012). Transplantation of undifferentiated and induced human exfoliated deciduous teeth-derived stem cells promote functional recovery of rat spinal cord contusion injury model. *Stem Cells Dev.* 21 (10), 1794–1802. doi:10.1089/scd.2011.0408

Takeuchi, R., Kuruma, Y., Sekine, H., Dobashi, I., Yamato, M., Umezu, M., et al. (2016). *In vivo* vascularization of cell sheets provided better long-term tissue survival than injection of cell suspension. *J. Tissue Eng. Regen. Med.* 10 (8), 700–710. doi:10.1002/term.1854

Tang, S. W., Tong, W. Y., Pang, S. W., Voelcker, N. H., and Lam, Y. W. (2020). Deconstructing, replicating, and engineering tissue microenvironment for stem cell differentiation. *Tissue Eng. Part b-rev.* 26 (6), 540–554. doi:10.1089/ten.TEB.2020.0044

Thuret, S., Moon, L. D., and Gage, F. H. (2006). Therapeutic interventions after spinal cord injury. *Nat. Rev. Neurosci.* 7 (8), 628–643. doi:10.1038/nrn1955

Tran, A. P., Warren, P. M., and Silver, J. (2018). The biology of regeneration failure and success after spinal cord injury. *Physiol. Rev.* 98 (2), 881–917. doi:10.1152/physrev.00017.2017

Wang, B., Xiao, Z., Chen, B., Han, J., Gao, Y., Zhang, J., et al. (2008). Nogo-66 promotes the differentiation of neural progenitors into astroglial lineage cells through mtor-stat3 pathway. *PLoS One* 3 (3), e1856. doi:10.1371/journal.pone.0001856

Wang, K., Chao, R., Guo, Q. N., Liu, M. Y., Liang, H. P., Liu, P., et al. (2013). Expressions of some neurotrophins and neurotrophic cytokines at site of spinal cord injury in mice after vaccination with dendritic cells pulsed with homogenate proteins. *Neuroimmunomodulation* 20 (2), 87–98. doi:10.1159/000345522

Wang, L., Gu, S., Gan, J., Tian, Y., Zhang, F., Zhao, H., et al. (2021). Neural stem cells overexpressing nerve growth factor improve functional recovery in rats following spinal cord injury via modulating microenvironment and enhancing endogenous neurogenesis. *Front. Cell. Neurosci.* 15, 773375. doi:10.3389/fncel.2021.773375

Wu, J., Li, L. X., and Wu, X. (2009). An experimental study on neuron-like cells from mesenchymal stem cells induced by spinal cord supernatant. *Prog. Mod. Biomed.* 9 (06), 1085–1088.

Yamazaki, K., Kawabori, M., Seki, T., Takamiya, S., Konno, K., Watanabe, M., et al. (2021). Mesenchymal stem cell sheet promotes functional recovery and palliates neuropathic pain in a subacute spinal cord injury model. *Stem Cells Int.* 2021, 1–18. doi:10.1155/2021/9964877

Yan, J., Zhang, L., Li, L., He, W., and Liu, W. (2022). Developmentally engineered bio-assemblies releasing neurotrophic exosomes guide *in situ* neuroplasticity following spinal cord injury. *Mat. Today Bio* 16, 100406. doi:10.1016/j.mtbio.2022.100406

Yang, J., Yamato, M., Kohno, C., Nishimoto, A., Sekine, H., Fukai, F., et al. (2005). Cell sheet engineering: Recreating tissues without biodegradable scaffolds. *Biomaterials* 26 (33), 6415–6422. doi:10.1016/j.biomaterials.2005.04.061

Yu, W. R., and Fehlings, M. G. (2011). Fas/fasl-mediated apoptosis and inflammation are key features of acute human spinal cord injury: Implications for translational, clinical application. *Acta Neuropathol.* 122 (6), 747–761. doi:10.1007/s00401-011-0882-3

frontiers | Frontiers in Oncology

TYPE Review
PUBLISHED 04 April 2023
DOI 10.3389/fonc.2023.1122322

OPEN ACCESS

EDITED BY
Sen Hou,
Beihang University, China

REVIEWED BY
Yumeng Xue,
Northwestern Polytechnical University, China
John Morton,
University of Colorado Anschutz Medical Campus, United States

*CORRESPONDENCE
Xiaoqiang Zheng
zhengxiaoqiang@xjtu.edu.cn

SPECIALTY SECTION
This article was submitted to Cancer Immunity and Immunotherapy, a section of the journal Frontiers in Oncology

RECEIVED 23 December 2022
ACCEPTED 24 March 2023
PUBLISHED 04 April 2023

CITATION
Zhang W and Zheng X (2023) Patient-derived xenografts or organoids in the discovery of traditional and self-assembled drug for tumor immunotherapy. *Front. Oncol.* 13:1122322. doi: 10.3389/fonc.2023.1122322

Patient-derived xenografts or organoids in the discovery of traditional and self-assembled drug for tumor immunotherapy

Wei Zhang[1] and Xiaoqiang Zheng[2,3]*

[1]Department of Talent Highland, The First Affiliated Hospital of Xi'an Jiaotong University, Xi'an, China, [2]Department of Medical Oncology, The First Affiliated Hospital of Xi'an Jiaotong University, Xi'an, China, [3]Institute for Stem Cell & Regenerative Medicine, The Second Affiliated Hospital of Xi'an Jiaotong University, Xi'an, China

In addition to the rapid development of immune checkpoint inhibitors, there has also been a surge in the development of self-assembly immunotherapy drugs. Based on the immune target, traditional tumor immunotherapy drugs are classified into five categories, namely immune checkpoint inhibitors, direct immune modulators, adoptive cell therapy, oncolytic viruses, and cancer vaccines. Additionally, the emergence of self-assembled drugs with improved precision and environmental sensitivity offers a promising innovation approach to tumor immunotherapy. Despite rapid advances in tumor immunotherapy drug development, all candidate drugs require preclinical evaluation for safety and efficacy, and conventional evaluations are primarily conducted using two-dimensional cell lines and animal models, an approach that may be unsuitable for immunotherapy drugs. The patient-derived xenograft and organoids models, however, maintain the heterogeneity and immunity of the pathological tumor heterogeneity.

KEYWORDS

drug discovery, PDO, PDX, tumor immunotherapy, tumor microenvironment

1 Introduction

Clinical sample sequencing and experiments using animal models have demonstrated that the molecular mechanism of tumorigenesis is due to gene mutations induced by oncogene and anti-oncogene. However, oncogene mutation is not the only factor that eventually causes the development of cancer (1–3). Several preclinical and clinical studies have reported that multiple factors exist between the occurrence of oncogene mutations in cells and the tumors *in situ*, such as the tumor microenvironment (TME) (4–6).TME as a concept was proposed by Ioannides in 1993 (7). Currently, TME is regarded as the presentation of non-tumor cells and their components in tumors, including the protein molecules produced and released by them(8). Furthermore, the metabolic disorders of TME cells result in the consumption of nutrients, acidification of environmental pH,

hypoxia, and the production of regulatory metabolites, thus influencing the immune response to tumors as well as the overexpression of immune checkpoint molecules and tumor metastasis (9–11). The abortive phenomenon of various tumor therapy drugs in previous preclinical and clinical trials has been explained by the discovery of TME.

The concept of immunotherapy was first introduced by William Coley in the 1890s(12). Later, Honjo discovered that programmed death receptor 1 (PD-1) is an inducible gene on activated T lymphocytes, which led to the discovery of cancer immunotherapy through blocking PD-1 (13). Meanwhile, a protein on the molecular surface of immune cells called cytotoxic T lymphocyte-associated antigen 4 (CTLA-4) was discovered by James P. Allison to act as a "molecular brake" that prevents the immune system from responding. Inhibition of CTLA-4 can make T cells proliferate and attack tumor cells (14). The Nobel Prize in Physiology or Medicine was awarded to them in recognition of their contribution to tumor immunotherapy in 2018. Currently, tumor immunotherapy drugs can be mainly divided into five categories: antibody drugs such as immune checkpoint inhibitors (ICIs) (15), direct immune modulators (16–19), chimeric antigen receptor (CAR) -T cells(20), oncolytic viruses (OVs) (21) and cancer vaccines (22).Despite this progress, contributing to off-target toxicity, tissue heterogeneity, poor immunogenicity and tumor infiltration, the clinical use of tumor immunotherapy remains limited to a small subset of cancers. The development of self-assembly nanotechnology provides an opportunity for enhancing the effectiveness and reducing the toxicity of traditional drugs, and a series of nanomaterials were used in the preclinical study of cancer (23). This technology assembles molecules with different functions into highly ordered nanosystems with non-covalent bonds, which is a strategy for building powerful drugs (24).

In recent years, the development of experimental models to accurately replicate the pathophysiology of tumors has become one of the main challenges in the development of new drugs. Researchers emphasize patient-derived tumor xenografts (PDXs) (25)and patient-derived organoids (PDOs) (26) as potential solutions to these problems. PDX preserves the histological structure, degree of differentiation, morphological features, and molecular characteristics of most primary tumors and can better mimic their response to treatment. PDO models and three-dimensional (3D) culture can reproduce TME and biological behavior of tumor cells *in vitro* by reconstructing 3D communication networks of cell-cell and cell-extracellular matrix (ECM) interactions (16–19). Drug research and development have benefited greatly from the PDX and PDO models (27).

In this review, we discuss the latest advances of the technology in PDX and PDO models for tumor immunotherapy research. We emphasize the use of these preclinical setting to study tumor cell-immune cell interactions and to explore immunotherapeutic drug screens. We also investigate the application of these preclinical models to novel self-assembling drug development and discuss the challenges that need to be overcome to make possible a more widespread and rationalized use of PDX and PDO models. A careful consideration and evaluation must be given to the complexity of humanized PDX and PDO mice and their limitations. As a result, there will be a greater chance of achieving effective research results. In any case, we hope that the optimization of humanized PDX and PDO mouse models will make significant contributions to tumor immunotherapy and personalized medicine for improving the outcome of cancer patients in the future.

2 PDXs and PDOs models

2.1 PDXs

Over the years, PDXs have been used to study several aspects of oncological diseases, especially for individualized drug development. It has been proposed that PDX models not only recapitulate key characteristics of human tumors with high fidelity, but also exhibit treatment responses that are concordant with human responses(28–30). In recent years, breakthroughs in tumor immunotherapy have placed increased demands on the development of appropriate preclinical assessment models to evaluate tumor immune responses. Therefore, humanized PDX models have been developed to evaluate the efficacy of immunotherapeutic approaches in cancer. The fundamentals of the humanized PDX model are as follow. In summary, pieces of solid tumors are obtained through surgery or biopsy procedures, and these samples are implanted into the dorsal region or the same organ of immunocompromised mice. To simulate a more realistic state of functional human immune system (HIS), human peripheral blood mononuclear cells (PBMC), CD34+ hematopoietic stem cells (HSC), or other immune cells can be transplanted into immunodeficient mice such as non-obese diabetes (NOD)- severe combined immune deficiency (SCID) gamma(NSG)mice. After human immune reconstruction, patient-derived tumor tissues can be transplanted to create a dual immunogenic model with similar heterogeneity and tumor immune microenvironment (TIME) as patients. This model can not only simulate the growth process of tumors in patients, but also simulate the interaction between a cancer cell and the HIS. The construction process of humanized PDX models is presented in Figure 1.

Humanized PDX models have provided a tremendous boost to the study of tumor pathogenesis and drug development. However, there are still limitations of humanized PDX models: 1) the time period required to build PDX models from patients is long and may take up to 6 months (or longer), 2) the high cost and low throughput, 3) lack of maturation of innate immune cells, coupled with insufficient ability to generate antigen-specific antibodies, 4) limited education of T cells in absence of murine thymus, 5)deficient HLA molecules, and 6) the difficulty in generating lymph node structures and germinal centers(31). These limitations have led to several ongoing efforts to develop novel humanized preclinical models and platforms to develop therapeutic strategies that enhance response to immunotherapy. In general, it is believed that the robustness of drug-screening data will increase when both human-derived immune reconstruction and data analysis become more standardized.

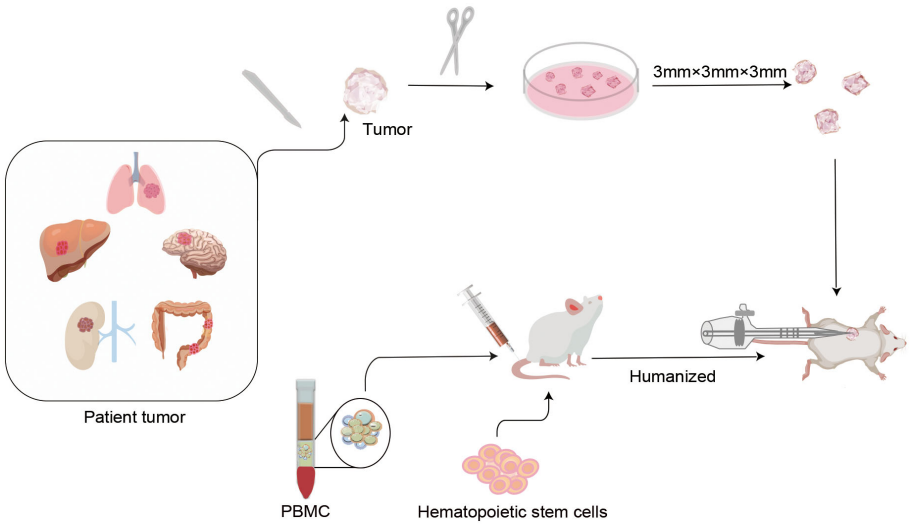

FIGURE 1
Protocols of humanized patient-derived tumor xenografts (PDX) model construction. In the first step, humanized mice were established by transplanting isolated human peripheral blood mononuclear cells (PBMC) or CD34+ human hematopoietic stem cells (HSC), etc. into severely combined immunodeficient mice. After the human immune system is successfully implanted, a novel humanized PDX model is established by inoculating patient-derived tumor tissues into humanized mice. These types of models not only mimic the phenotypic and molecular characteristics of the original tumor in the patient, but also reproduce the cross-talk between the tumor and the immune system. This is of critical significance for individualized drug marker screening and drug development for tumor immunotherapy.

2.2 PDOs

In 2009, Hans Clevers' team successfully cultured mouse intestinal organoids that self-renew and maintain the villous structure of intestinal gland pits *in vitro*, bringing new starting for development of cancer therapeutic approaches (32). As an *in vitro* 3D organ, PDO can not only mimic the cell composition and structure in tumor growth, but also perform specific gene editing, which can satisfy complex tumor microenvironment research and potential drug screening. PDO and organoid-derived PDX(PDOX), as an emerging field, have attracted much attention since they can provide a cancer pre-clinical platform to recapitulate the patient's tumor and promote translating novel treatments from bench to bedside (33–35). Over the past decades, several PDOs have been successfully cultured, including gastric tumors (36), breast tumors (37), bladder tumors (38), and ovarian tumors (39). The establishment and subsequent screening of PDO/PDOX can generally be completed in a shorter period than for PDX. The model construction process for PDO and PDOX is depicted in Figure 2.

Numerous studies in the past decades have demonstrated how using organoids enhances the accuracy of the drug screening system (37, 40). These PDOs have been widely employed in the research of anti-tumor drugs. There are many advantages associated with organoids, primarily in the realization of individualized precision medicine, the reduction of modeling time, high throughput screening, genomic screening, and drug screening(41, 42). Unfortunately, no single mouse model can capture every aspect of the parent tumor and immune landscape. Some major drawbacks should be considered. Organoids cannot perfectly replicate the microenvironment *in vivo*, they lack tumor blood vessels and immune cells, and the co-culture system with other cell types is not yet well established. There are difficulties in studying the role of other systems and organs within the body. A global standard for organoids establishment and quality control does not yet exist. Despite its limitations, it still provides an extremely valuable contribution to the research and development of cancer drugs (43). In any case, to maximize the potential for translational research, it is imperative to select the most suitable humanized mouse model (44).

3 PDX and PDO models in the discovery of traditional tumor immunotherapy drugs

3.1 Immune checkpoint inhibitors

Immune surveillance is a vital tool for inhibiting tumorigenesis and maintaining the body's internal environment's homeostasis. A tumor cell can self-modify or release factors that influence TIME, such as engaging immune checkpoint pathways, to evade immune surveillance. Several immune checkpoints have been identified, including PD-1 and its ligand (PD-L1), which regulate the activity of T cells and cancer growth (45). Since the development and clinical application of ICIs, cancer immunotherapy has significantly expanded our toolkit for fighting the disease. At present, ICIs primarily consist of antibodies against CTLA-4 (ipilimumab), PD-1 (nivolumab, pembrolizumab, cemiplimab) and PD-L1 (atezolizumab, durvalumab, avelumab) (15, 46, 47).

Researchers recently established a humanized mouse NPC-PDX model by engrafting nasopharyngeal carcinoma (NPC) biopsies in

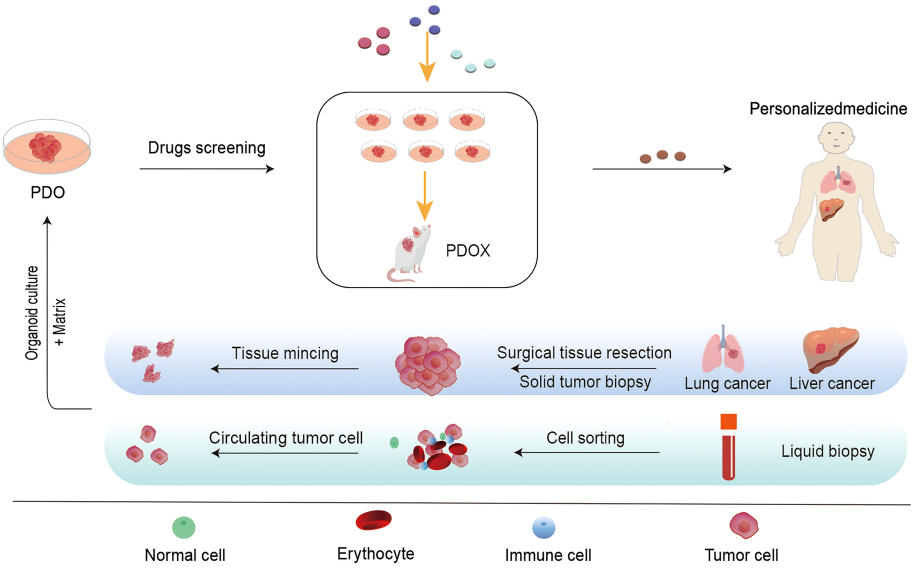

FIGURE 2
The flow chart of the establishment of patient-derived tumor organoid (PDO) models and the application of PDO in personalized treatment. It is commonly used to obtain primary tumor samples from surgical resections, puncture samples, or circulating tumor cells (CTCs) isolated from blood samples. Patient-derived cancer cells can be propagated *in vitro* on an enriched Matrigel matrix and cultured into three-dimensional tumor-like organs for *in vitro* and *in vivo* applications. These tumor models can be used for drug screening, gene analysis, immunotherapy, and other studies to accurately detect drug efficacy and toxicity. Furthermore, we are able to develop effective individualized treatment strategies for patients.

NSG mice. This model was used to investigate the anti-tumor efficacy of nivolumab and ipilimumab (48). A study published in 2019 evaluated the efficacy of nivolumab against colorectal cancer (CRC) in a hematopoietic humanized PDX mouse model (hu-CB-BRGS). It was observed that PD-1 blockade therapy induced the immune system to kill tumors in this mode of action (49). Kleinmanns et al. established a HIS-PDX model of ovarian carcinoma *in situ* of NSG mice, which were injected with CD34+HSC *via* the vein beforehand. They further investigated the change in immune cells by flow cytometry after the animal was treated with nivolumab. The results indicated that the overall response to monotherapy was modest, and the combination therapy might be more effective (50). Here, we summarized the conditions in which PDX models were used in the preclinical evaluation of immune checkpoint mAb drugs that are currently available, to better understand the utilization of the PDX model in drug development (Table 1).

To enable PDOs reproduce the TIME, researchers have developed a number of novel platforms to evaluate the efficacy of

TABLE 1 Patient-derived tumor xenografts (PDX) models in preclinical evaluation of immune checkpoint monoclonal antibody drugs.

Target	Name of drug	Type of tumor	Model and Strain	Reference
PD-1	Pembrolizumab and Nivolumab	TNBC	Hu-HSC-PDX (NSG mice)	(51)
PD-1	Pembrolizumab and Nivolumab	NSCLC	Hu-HSC-PDX (NSG mice)	(52)
PD-1	Pembrolizumab	NSCLC	Hu-PBMC-PDX (NSG mice)	(53)
PD-1	Pembrolizumab	HCC	Hu-HSC-PDX (NSG mice)	(54)
PD-1	Nivolumab	NSCLC	Hu-HSC-PDX (NSG mice)	(55)
PD-1	Nivolumab	MRCC	Hu-HSC-PDX (NSG mice)	(56)
PD-1	Nivolumab	CCA	Hu-PBMC-PDX (NSG mice)	(57)
PD-1	Pembrolizumab	Liposarcoma	Hu-HSC-PDX (NSG mice)	(58)
CTLA-4	Ipilimumab and Nivolumab	NPC	Hu-HSC-PDX (NSG mice)	(48)
PD-L1	Atezolizumab	NSCLC	Hu-PBL-PDX (NSG mice)	(59)
PD-L1	Durvalumab	NMIBC	Hu-PBMC-PDX (NOG mice)	(59)
PD-L1	Durvalumab	NMIBC	Hu-PBMC-PDX (NOG mice)	(60)

NSCLC, Non-small cell lung cancer; HCC, Hepatic cell carcinoma; TNBC, Triple-negative breast cancer; MRCC Metastatic renal cell carcinoma; CCA, Clear cell adenocarcinoma; Squamous cell carcinoma; NPC, Nasopharyngeal carcinoma; NMIBC, Non-muscle invasive bladder cancer; BC, Breast cancer; Hu, Human; HSC, Human stem cell; PBL, Peripheral blood lymphocyte.

tumor immunotherapy in recent years. For example, researchers have constructed a complex air-liquid interface approach PDO from different cancer types, allowing *in vitro* preservation of the tumor epithelium and its stromal microenvironment, and even immunologically active CD8+ T cells, NK cells, etc. Using this model, it is possible to simulate the biological behavior and therapeutic response of tumors during anti-PD-1 therapy (61). By combining PDO and humanized mouse techniques, the investigators constructed a new model of spontaneous multi-organ metastasis from microsatellite instability-H CRC and also provided empirical evidence for a key role of B cells in generating site-dependent anti-tumor immunity after anti-CTLA-4 treatment (62). Researchers also demonstrated using a patient-derived organotypic tumor spheroids (PDOTS) and a matched PDO drug screening platform that inhibition of innate immune kinase TANK-binding kinase 1 coupled with PD-1 blockade was an effective strategy for overcoming tumor immunotherapy resistance (63). In addition, the investigators established a glioblastoma (GBO)-related organoid biobank for individualized therapeutic screening. This is a PDO model with significant clinical translational potential to simulate tumor response to CAR-T cell immunotherapy (64). These studies demonstrate that immuno-oncology studies can be successfully conducted using organoid models that may facilitate personalized immunotherapy testing. In order to better understand the advantages and disadvantages of the PDOs model. We also summarize the studies with the PDO model to evaluate ICIs drugs briefly (Table 2).

3.2 Direct immune modulators

Immunosuppressive cells (such as myeloid-derived suppressor cells and regulatory T cells) can release inhibitory cytokines in the TME to evade the immune system (71). Cytokines, such as interferon (INF)-alpha and interleukin (IL)-2, also play a crucial role in tumor immunotherapy. In 1986, the FDA approved INF-α as a cancer therapy drug for the treatment of leukemia. Currently, IFN-α and IL-2 have become the most widely used drugs in tumor immunotherapy strategies, however, several other cytokines are currently under clinical investigation (72, 73). Aside from cytokines, non-specific immune drugs also include target natural killer (NK) cells, macrophages, and immunomodulators. Pexidartinib, the first macrophage-targeting medicine approved by the FDA, is recommended for adult patients with symptomatic giant cell tumors of tenosynovitis because it restricts macrophage proliferation by blocking CSF cytokines (74). In a recent study on pexidartinib, researchers evaluated its impact on PDX and observed that pexidartinib can significantly inhibit osteosarcoma tumor growth (75). Immunotherapy with IL-2 and GM-CSF has significantly improved survival in children with high-risk neuroblastoma (76). Treatment failure and IL2-related toxicity, however, pose significant challenges to the treatment of one third of these patients. There has been evidence in recent clinical trials that NK cells hyperproliferate and acquire an activated phenotype in patients receiving recombinant human IL-15, resulting in NK cell expansion *in vivo* and tumor shrinkage in two patients. As a result, scholars validated the tumor suppressive effect of IL-15 on PDX models, and they demonstrated that the replacement of IL-2 with IL-15 was associated with significant tumor regression *in vivo*, supporting clinical trials of IL-15 for pediatric neuroblastoma (77). Additionally, related study has also demonstrated that IL-15 enhanced the anti-tumor activity of γδ T cells, and effectively suppressed tumor growth, and prolonged the survival of renal cancer-bearing PDX mice (78). Taking these results into consideration, it appears that cytokines might be able to have significant clinical implications in the future.

3.3 CAR-T/NK

CAR- T cell therapy, as a novel approach in anticancer therapy, in which T cells are retargeted against the tumor cell following the engineered expression of CARs (79). Currently, two CAR-T cell products have been used for the treatment of lymphoblastic leukemia and lymphoma (80). Besides, it has been reported that CAR-T cells engineered to simultaneously produce interleukin (IL)-7 and chemokine (C–C motif) ligand 19 (CCL19) were effective against solid tumors in pancreatic cancer (PC) PDX model (81). Additionally, other researchers have also verified CAR-T cells anti-tumor immunotherapy effects on triple-negative breast cancer (TNBC) (82). Other studies have found that in a patient with late-stage HCC, anti-GPC3 IL-7/CCL19 CAR-T therapy resulted in complete tumor disappearance 30 days post-intra-tumor injection. And in a patient with advanced PC, anti-MSLN-IL-7/CCL19 CAR-T cellular therapy resulted in almost complete tumor disappearance 240 days post-intravenous infusion (83). Both preclinical and clinical studies suggest that novel CAR-T cells have significant potential for the treatment of solid tumors.

TABLE 2 Patient-derived organoids (PDOs) models in preclinical evaluation of immune checkpoint monoclonal antibody drugs.

Target	Name of drug	Organoids	Reference
PD-1	Nivolumab	Patient-derived gastric cancer organoids	(65)
PD-1	Pembrolizumab and Nivolumab	Patient-derived lung cancer organoids	(66)
PD-1	Nivolumab	Patient-derived chordoma organoids	(67)
PD-1	Nivolumab	Patient-derived renal cell carcinoma organoids	(68)
PD-1	Pembrolizumab and Cabozantinib	Patient-derived renal cell carcinoma clusters	(69)
PD-L1	Atezolizumab	Patient-derived renal cell carcinoma organoids	(70)

In 2010, Zhao Y et al., reported that they developed a PDX model to evaluate CAR-T therapy (84). Jiang Z et al., reported that CAR T cells demonstrated a positive therapeutic effect on liver cancer in a PDX mouse model. They concluded that the growth of the tumor in the PDX model could be inhibited following CAR-T cells therapy (85). The investigators developed a highly specific SynNotch-CAR-T cells, which was validated using the PDX model to target gliomas and exert anti-tumor effects with reduced off-target toxicity (86).The emergence of adaptive therapy has stimulated the development of new CAR-NK cells therapy techniques (20). In 2021, Cao B and his team developed mesothelin (MSLN)-CAR NK cells, which were evaluated using PDX (NSG mice). According to the findings, these cells demonstrated strong anti-tumor properties and offer a promising treatment for gastric cancer (87). Although CAR-NK cells have obvious advantages in tumor therapy, the short life cycle of NK cells *in vivo* and the immunosuppression of the TME limit the clinical transformation of CAR-NK cells.

Ding S et al., generated thousands of micro-organ spheres from patient tissues and assessed tumor drug response (88). The establishment of an organoid biobank, as mentioned earlier, is a valuable platform for evaluating tumor treatment strategies such as CAR-T cell therapy (89). In addition, combining organoid and 3D imaging technologies, the investigators have provided a platform to reveal the mode of action of cellular anti-cancer immunotherapies in a patient-specific manner and apply them to develop multiple engineered T cell products(90). PDOs are ideal for short drug screening cycles and convenient sampling of the model, which can be achieved through several methods, including surgery, biopsy, urine, and lung lavage fluid (88, 91). The development of PDOs will greatly shorten preclinical study time and facilitate drug development.

3.4 Oncolytic viruses

More than a century ago, a phenomenon was observed in clinical therapy, that is some patients with cancer experience the cancer regression if they were infected with certain viruses (92). Based on this case, OVs therapy was further developed to advance cancer biological therapy. OVs possess excellent safety in clinical trials, which greatly promotes their research and development. A novel OV (OAd-MUC16-BiTE) with better anti-tumor characteristics was developed for treating ovarian cancer in PDX mice models (93). Other study evaluated the anticancer efficacy of VG161, a herpes virus type 1 (HSV-1), in HLA-matched CD34+ humanized PDX model. It was found that VG161 significantly inhibited tumor growth and would realize enhancement of OV-induced antitumor immunity for long-term maintenance treatment (94). In research by Quinn CH et al., oncolytic herpes simplex viruses (oHSVs) were demonstrated to be effective in treating high-risk neuroblastoma in PDX mice (NOD-SCID) (95). OVs therapy has the advantages of excellent replication efficiency, a potent killing effect, fewer adverse reactions, and inexpensive cost, making it one of the most promising tumor immunotherapy methods in the future (21, 33). In addition, exploring the anticancer activity of OVs based on pancreatic PDOs proved to be an effective predictive tool (96). However, the delivery of OVs was by intertumoral injection, which limited its clinical use. Therefore, how to deliver these OVs to the tumor tissue more effectively and how to improve the potential of these viruses to disseminate within the tumor tissue site may be the future focus of this therapy.

4 PDXs and PDOs in the discovery of self-assembled drugs for tumor immunotherapy

Tumor immunotherapy has changed the treatment of advanced tumors, however, the proportion of patients responding to immunotherapies remains low. In recent years, supramolecular chemistry and self-assembled systems have been extensively investigated in the field of cancer therapy and hold great promise for improving immunotherapeutic outcomes in tumor patients (97, 98). Unlike conventional cancer immunotherapy, rationally designed nano-self-assembled drugs can trigger specific tumoricidal effects, thereby improving infiltration of TIME such as killer immune T lymphocytes, optimizing antigen presentation, and inducing durable immune responses (23). The development of nanotechnology provides an opportunity for enhancing the effectiveness and reducing the toxicity of traditional drugs, and a series of nanomaterials were used in the preclinical study of cancer (24). In conclusion, self-assembled drugs have a broad potential for application in tumor immunotherapy, especially in refractory and recurrent cancers.

The self-assembled peptides can respond to various environmental conditions, such as pH, temperature, and molecular interactions, while also possessing high biocompatibility and drug loading capabilities(99, 100). According to current research, self-assembly peptides can be classified into two main categories for tumor immunotherapy research: 1) Self-assembly into nanodrugs using their drug loading capacity, delivering molecules such as peptides or siRNA, inhibiting specific proteins or genes in tumor cells to enhance tumor immunotherapy response. 2) Using peptide self-assembly to simulate tumor antigens as tumor vaccines to stimulate the body to produce anti-tumor antibodies(101, 102). In short, self-assembling peptide drugs may improve the treatment of tumors immune therapy significantly in future.

Self-assembled nanomedicines have received significant attention due to their excellent biocompatibility, high modification versatility and ease of synthesis, controllable and adaptive nanostructures(103). Recently, a study pointed out that through targeted inhibition of MDM2, p53 can be activated, the tumor immune microenvironment can be reprogramed, and immunotherapy resistance can be overcome (104). Researchers created TPA, a combined targeted peptide that inhibited the PD-1/PD-L1 axis, activated p53, and showed tumor killing and immunotherapeutic sensitization effects on a humanized PBMC-engrafted PDX model. There is now a potential pathway for the development of self-assembled peptide drugs for cancer therapy

(105). For tumor targeting, the researchers synthesized size-tunable nanostructures with a spherical morphology by combining partially reductive HSA with hydrophobic Fluvastatin, known as AB-Flu. According to the study, these nanodrugs effectively enhanced the potency of Anti-PD1 antibodies against colon cancer in a humanized CRC-PDX mouse model while maintaining acceptable levels of safety (100). Generally, self-assembled drugs have unique anti-tumor effects and are low in toxicity. Through blocking the supply of tumor nutrients, improving drug targeting, and even recruiting multiple immune cells, they can achieve tumor therapy. Therefore, development and research into self-assembled drugs is warranted. Anti-tumor potential of self-assembled drugs creates new hope for tumor treatment, and the PDX and PDO models facilitate clinical transformation as well.

5 Perspective and conclusion

The rapid development of immunotherapy drugs brings hope to clinical patients with cancer (100, 106–108). However, the preclinical evaluation of drugs still restricts the development of drug research. Although the drug evaluation system has advanced from a 2D cell line evaluation system to PDX/PDO system and even developed a PDX model with human immune cells to more accurately simulate the immune environment *in vivo* (109, 110), there are still limitations. The establishing cycle of PDX/humanized PDX is long, the technology is challenging, and it cannot completely simulate the TME. Although the modeling cycle of PDOs is short, but it is still necessary to investigate whether the medium possesses antigenicity because the composition of the medium is unknown. In addition, despite the extensive genetic heterogeneity of tumors *in vivo*, it is unknown whether tumor organoids can capture the entire range of heterogeneity that originates from the primary tumor (111). Despite the complexity of cancer, there are still several unresolved issues, including those related to its pathogenesis, mechanism of metastasis, patient response to treatment, or mechanism of drug resistance. Further studies are required to constantly improve the simulation of TME to create PDX/PDO that is more similar to the primary tumor characteristics, to better serve drug development.

Author contributions

WZ wrote the manuscript. XZ reviewed and edited the manuscript. All authors contributed to the article and approved the submitted version.

Conflict of interest

The authors declare that the research was conducted in the absence of any commercial or financial relationships that could be construed as a potential conflict of interest.

Publisher's note

References

1. Van Dyke T, Jacks T. Cancer modeling in the modern era: progress and challenges. *Cell* (2002) 108(2):135–44. doi: 10.1016/s0092-8674(02)00621-9

2. He W, Wang S, Yan J, Qu Y, Jin L, Sui F, et al. Self-assembly of therapeutic peptide into stimuli-responsive clustered nanohybrids for cancer-targeted therapy. *Advanced Funct Mater* (2019) 29(10):1807736. doi: 10.1002/adfm.201807736

3. Martinez-Jimenez F, Muinos F, Sentis I, Deu-Pons J, Reyes-Salazar I, Arnedo-Pac C, et al. A compendium of mutational cancer driver genes. *Nat Rev Cancer* (2020) 20 (10):555–72. doi: 10.1038/s41568-020-0290-x

4. Quail DF, Joyce JA. Microenvironmental regulation of tumor progression and metastasis. *Nat Med* (2013) 19(11):1423–37. doi: 10.1038/nm.3394

5. Yan S, Yan J, Liu D, Li X, Kang Q, You W, et al. A nano-predator of pathological MDMX construct by clearable supramolecular gold(I)-thiol-peptide complexes achieves safe and potent anti-tumor activity. *Theranostics* (2021) 11(14):6833–46. doi: 10.7150/thno.59020

6. Bilotta MT, Antignani A, Fitzgerald DJ. Managing the TME to improve the efficacy of cancer therapy. *Front Immunol* (2022) 13:954992. doi: 10.3389/fimmu.2022.954992

7. Ioannides CG, Whiteside TL. T Cell recognition of human tumors: implications for molecular immunotherapy of cancer. *Clin Immunol Immunopathol* (1993) 66 (2):91–106. doi: 10.1006/clin.1993.1012

8. Xiao Y, Yu D. Tumor microenvironment as a therapeutic target in cancer. *Pharmacol Ther* (2021) 221:107753. doi: 10.1016/j.pharmthera.2020.107753

9. Biswas SK. Metabolic reprogramming of immune cells in cancer progression. *Immunity* (2015) 43(3):435–49. doi: 10.1016/j.immuni.2015.09.001

10. Domblides C, Lartigue L, Faustin B. Control of the antitumor immune response by cancer metabolism. *Cells* (2019) 8(2):104. doi: 10.3390/cells8020104

11. Ren M, Zheng X, Gao H, Jiang A, Yao Y, He W. Nanomedicines targeting metabolism in the tumor microenvironment. *Front Bioeng Biotechnol* (2022) 10:943906. doi: 10.3389/fbioe.2022.943906

12. Oiseth S, Aziz M. Cancer immunotherapy: a brief review of the history, possibilities, and challenges ahead. *J Cancer Metastasis Treat* (2017) 3:250–61. doi: 10.20517/2394-4722.2017.41

13. Ishida Y, Agata Y, Shibahara K, Honjo T. Induced expression of PD-1, a novel member of the immunoglobulin gene superfamily, upon programmed cell death. *EMBO J* (1992) 11(11):3887–95. doi: 10.1002/j.1460-2075.1992.tb05481.x

14. Leach DR, Krummel MF, Allison JP. Enhancement of antitumor immunity by CTLA-4 blockade. *Science* (1996) 271(5256):1734–6. doi: 10.1126/science.271.5256.1734

15. Ai L, Xu A, Xu J. Roles of PD-1/PD-L1 pathway: Signaling, cancer, and beyond. *Adv Exp Med Biol* (2020) 1248:33–59. doi: 10.1007/978-981-15-3266-5_3

16. Hausser HJ, Brenner RE. Phenotypic instability of saos-2 cells in long-term culture. *Biochem Biophys Res Commun* (2005) 333(1):216–22. doi: 10.1016/j.bbrc.2005.05.097

17. Abaan OD, Polley EC, Davis SR, Zhu YJ, Bilke S, Walker RL, et al. The exomes of the NCI-60 panel: a genomic resource for cancer biology and systems pharmacology. *Cancer Res* (2013) 73(14):4372–82. doi: 10.1158/0008-5472.CAN-12-3342

18. Tsai S, McOlash L, Palen K, Johnson B, Duris C, Yang Q, et al. Development of primary human pancreatic cancer organoids, matched stromal and immune cells and

3D tumor microenvironment models. *BMC Cancer* (2018) 18(1):335. doi: 10.1186/s12885-018-4238-4

19. Ho T, Msallam R. Tissues and tumor microenvironment (TME) in 3D: Models to shed light on immunosuppression in cancer. *Cells* (2021) 10(4):831. doi: 10.3390/cells10040831

20. Xie G, Dong H, Liang Y, Ham JD, Rizwan R, Chen J. CAR-NK cells: A promising cellular immunotherapy for cancer. *EBioMedicine* (2020) 59:102975. doi: 10.1016/j.ebiom.2020.102975

21. Hemminki O, Dos Santos JM, Hemminki A. Oncolytic viruses for cancer immunotherapy. *J Hematol Oncol* (2020) 13(1):84. doi: 10.1186/s13045-020-00922-1

22. Song Q, Zhang CD, Wu XH. Therapeutic cancer vaccines: From initial findings to prospects. *Immunol Lett* (2018) 196:11–21. doi: 10.1016/j.imlet.2018.01.011

23. Shi J, Kantoff PW, Wooster R, Farokhzad OC. Cancer nanomedicine: progress, challenges and opportunities. *Nat Rev Cancer* (2017) 17(1):20–37. doi: 10.1038/nrc.2016.108

24. Muntimadugu E, Kommineni N, Khan W. Exploring the potential of nanotherapeutics in targeting tumor microenvironment for cancer therapy. *Pharmacol Res* (2017) 126:109–22. doi: 10.1016/j.phrs.2017.05.010

25. Tentler JJ, Tan AC, Weekes CD, Jimeno A, Leong S, Pitts TM, et al. Patient-derived tumour xenografts as models for oncology drug development. *Nat Rev Clin Oncol* (2012) 9(6):338–50. doi: 10.1038/nrclinonc.2012.61

26. Qu J, Kalyani FS, Liu L, Cheng T, Chen L. Tumor organoids: synergistic applications, current challenges, and future prospects in cancer therapy. *Cancer Commun (Lond)* (2021) 41(12):1331–53. doi: 10.1002/cac2.12224

27. Yan J, Zheng X, You W, He W, Xu GK. A bionic-homodimerization strategy for optimizing modulators of protein-protein interactions: From statistical mechanics theory to potential clinical translation. *Adv Sci (Weinh)* (2022) 9(11):e2105179. doi: 10.1002/advs.202105179

28. Rygaard J, Povlsen CO. Heterotransplantation of a human malignant tumour to "Nude" mice. *Acta Pathol Microbiol Scand* (1969) 77(4):758–60. doi: 10.1111/j.1699-0463.1969.tb04520.x

29. Hidalgo M, Amant F, Biankin AV, Budinská E, Byrne AT, Caldas C, et al. Patient-derived xenograft models: an emerging platform for translational cancer research. *Cancer Discovery* (2014) 4(9):998–1013. doi: 10.1158/2159-8290.Cd-14-0001

30. Woo XY, Giordano J, Srivastava A, Zhao ZM, Lloyd MW, de Bruijn R, et al. Conservation of copy number profiles during engraftment and passaging of patient-derived cancer xenografts. *Nat Genet* (2021) 53(1):86–99. doi: 10.1038/s41588-020-00750-6

31. Chuprin J, Buettner H, Seedhom MO, Greiner DL, Keck JG, Ishikawa F, et al. Humanized mouse models for immuno-oncology research. *Nat Rev Clin Oncol* (2023) 20(3):192–206. doi: 10.1038/s41571-022-00721-2

32. Sato T, Vries RG, Snippert HJ, van de Wetering M, Barker N, Stange DE, et al. Single Lgr5 stem cells build crypt-villus structures *in vitro* without a mesenchymal niche. *Nature* (2009) 459(7244):262–5. doi: 10.1038/nature07935

33. Russell L, Peng KW, Russell SJ, Diaz RM. Oncolytic viruses: Priming time for cancer immunotherapy. *BioDrugs* (2019) 33(5):485–501. doi: 10.1007/s40259-019-00367-0

34. Tuveson D, Clevers H. Cancer modeling meets human organoid technology. *Science* (2019) 364(6444):952–5. doi: 10.1126/science.aaw6985

35. Zhou Z, Cong L, Cong X. Patient-derived organoids in precision medicine: Drug screening, organoid-on-a-Chip and living organoid biobank. *Front Oncol* (2021) 11:762184. doi: 10.3389/fonc.2021.762184

36. Nanki K, Toshimitsu K, Takano A, Fujii M, Shimokawa M, Ohta Y, et al. Divergent routes toward wnt and r-spondin niche independency during human gastric carcinogenesis. *Cell* (2018) 174(4):856–869.e817. doi: 10.1016/j.cell.2018.07.027

37. Sachs N, de Ligt J, Kopper O, Gogola E, Bounova G, Weeber F, et al. A living biobank of breast cancer organoids captures disease heterogeneity. *Cell* (2018) 172(1-2):373–386.e310. doi: 10.1016/j.cell.2017.11.010

38. Lee SH, Hu W, Matulay JT, Silva MV, Owczarek TB, Kim K, et al. Tumor evolution and drug response in patient-derived organoid models of bladder cancer. *Cell* (2018) 173(2):515–528.e517. doi: 10.1016/j.cell.2018.03.017

39. Hill SJ, Decker B, Roberts EA, Horowitz NS, Muto MG, Worley MJJr., et al. Prediction of DNA repair inhibitor response in short-term patient-derived ovarian cancer organoids. *Cancer Discovery* (2018) 8(11):1404–21. doi: 10.1158/2159-8290.CD-18-0474

40. Boucherit N, Gorvel L, Olive D. 3D tumor models and their use for the testing of immunotherapies. *Front Immunol* (2020) 11:603640. doi: 10.3389/fimmu.2020.603640

41. Weeber F, Ooft SN, Dijkstra KK, Voest EE. Tumor organoids as a pre-clinical cancer model for drug discovery. *Cell Chem Biol* (2017) 24(9):1092–100. doi: 10.1016/j.chembiol.2017.06.012

42. Guillen KP, Fujita M, Butterfield AJ, Scherer SD, Bailey MH, Chu Z, et al. A human breast cancer-derived xenograft and organoid platform for drug discovery and precision oncology. *Nat Cancer* (2022) 3(2):232–50. doi: 10.1038/s43018-022-00337-6

43. Bar-Ephraim YE, Kretzschmar K, Clevers H. Organoids in immunological research. *Nat Rev Immunol* (2020) 20(5):279–93. doi: 10.1038/s41577-019-0248-y

44. Wu W, Li X, Yu S. Patient-derived tumour organoids: A bridge between cancer biology and personalised therapy. *Acta Biomater* (2022) 146:23–36. doi: 10.1016/j.actbio.2022.04.050

45. Khan E, Shrestha AK, Elkhooly M, Wilson H, Ebbert M, Srivastava S, et al. CNS and PNS manifestation in immune checkpoint inhibitors: A systematic review. *J Neurol Sci* (2022) 432:120089. doi: 10.1016/j.jns.2021.120089

46. Hodi FS, O'Day SJ, McDermott DF, Weber RW, Sosman JA, Haanen JB, et al. Improved survival with ipilimumab in patients with metastatic melanoma. *N Engl J Med* (2010) 363(8):711–23. doi: 10.1056/NEJMoa1003466

47. Dyck L, Mills KHG. Immune checkpoints and their inhibition in cancer and infectious diseases. *Eur J Immunol* (2017) 47(5):765–79. doi: 10.1002/eji.201646875

48. Liu WN, Fong SY, Tan WWS, Tan SY, Liu M, Cheng JY, et al. Establishment and characterization of humanized mouse NPC-PDX model for testing immunotherapy. *Cancers (Basel)* (2020) 12(4):1025. doi: 10.3390/cancers12041025

49. Capasso A, Lang J, Pitts TM, Jordan KR, Lieu CH, Davis SL, et al. Characterization of immune responses to anti-PD-1 mono and combination immunotherapy in hematopoietic humanized mice implanted with tumor xenografts. *J Immunother Cancer* (2019) 7(1):37. doi: 10.1186/s40425-019-0518-z

50. Kleinmanns K, Gullaksen SE, Bredholt G, Davidson B, Torkildsen CF, Grindheim S, et al. Humanized ovarian cancer patient-derived xenografts for improved preclinical evaluation of immunotherapies. *Cancers (Basel)* (2022) 14(13):3092. doi: 10.3390/cancers14133092

51. Rosato RR, Davila-Gonzalez D, Choi DS, Qian W, Chen W, Kozielski AJ, et al. Evaluation of anti-PD-1-based therapy against triple-negative breast cancer patient-derived xenograft tumors engrafted in humanized mouse models. *Breast Cancer Res* (2018) 20(1):108. doi: 10.1186/s13058-018-1037-4

52. Meraz IM, Majidi M, Meng F, Shao R, Ha MJ, Neri S, et al. An improved patient-derived xenograft humanized mouse model for evaluation of lung cancer immune responses. *Cancer Immunol Res* (2019) 7(8):1267–79. doi: 10.1158/2326-6066.CIR-18-0874

53. Lin S, Huang G, Cheng L, Li Z, Xiao Y, Deng Q, et al. Establishment of peripheral blood mononuclear cell-derived humanized lung cancer mouse models for studying efficacy of PD-L1/PD-1 targeted immunotherapy. *MAbs* (2018) 10(8):1301–11. doi: 10.1080/19420862.2018.1518948

54. Zhao Y, Wang J, Liu WN, Fong SY, Shuen TWH, Liu M, et al. Analysis and validation of human targets and treatments using a hepatocellular carcinoma-immune humanized mouse model. *Hepatology* (2021) 74(3):1395–410. doi: 10.1002/hep.31812

55. Martin-Ruiz A, Fiuza-Luces C, Rincon-Castanedo C, Fernandez-Moreno D, Galvez BG, Martinez-Martinez E, et al. Benefits of exercise and immunotherapy in a murine model of human non-small-cell lung carcinoma. *Exerc Immunol Rev* (2020) 26:100–15.

56. Kang Y, Armstrong AJ, Hsu DS. An autologous humanized patient-derived xenograft (PDX) model for evaluation of nivolumab immunotherapy in renal cell cancer: a case report. *Stem Cell Investig* (2022) 9:8. doi: 10.21037/sci-2022-029

57. Vargas R, Gopal P, Kuzmishin GB, DeBernardo R, Koyfman SA, Jha BK, et al. Case study: patient-derived clear cell adenocarcinoma xenograft model longitudinally predicts treatment response. *NPJ Precis Oncol* (2018) 2:14. doi: 10.1038/s41698-018-0060-3

58. Choi B, Lee JS, Kim SJ, Hong D, Park JB, Lee KY. Anti-tumor effects of anti-PD-1 antibody, pembrolizumab, in humanized NSG PDX mice xenografted with dedifferentiated liposarcoma. *Cancer Lett* (2020) 478:56–69. doi: 10.1016/j.canlet.2020.02.042

59. Chen X, Shen C, Wei Z, Zhang R, Wang Y, Jiang L, et al. Patient-derived non-small cell lung cancer xenograft mirrors complex tumor heterogeneity. *Cancer Biol Med* (2021) 18(1):184–98. doi: 10.20892/j.issn.2095-3941.2020.0012

60. Blinova E, Samishina E, Deryabina O, Blinov D, Roshchin D, Shich E, et al. Expression of p53 protein associates with anti-PD-L1 treatment response on human-derived xenograft model of GATA3/CR5/6-negative recurrent nonmuscular invasive bladder urothelial carcinoma. *Int J Mol Sci* (2021) 22(18):9856. doi: 10.3390/ijms22189856

61. Neal JT, Li X, Zhu J, Giangarra V, Grzeskowiak CL, Ju J, et al. Organoid modeling of the tumor immune microenvironment. *Cell* (2018) 175(7):1972–1988.e1916. doi: 10.1016/j.cell.2018.11.021

62. Küçükköse E, Heesters BA, Villaudy J, Verheem A, Cercel M, van Hal S, et al. Modeling resistance of colorectal peritoneal metastases to immune checkpoint blockade in humanized mice. *J Immunother Cancer* (2022) 10(12):e005345. doi: 10.1136/jitc-2022-005345

63. Sun Y, Revach OY, Anderson S, Kessler EA, Wolfe CH, Jenney A, et al. Targeting TBK1 to overcome resistance to cancer immunotherapy. *Nature* (2023) 615:158–67. doi: 10.1038/s41586-023-05704-6

64. Jenkins RW, Aref AR, Lizotte PH, Ivanova E, Stinson S, Zhou CW, et al. Ex vivo profiling of PD-1 blockade using organotypic tumor spheroids. *Cancer Discovery* (2018) 8(2):196–215. doi: 10.1158/2159-8290.Cd-17-0833

65. Chakrabarti J, Koh V, Steele N, Hawkins J, Ito Y, Merchant JL, et al. Disruption of Her2-induced PD-L1 inhibits tumor cell immune evasion in patient-derived gastric cancer organoids. *Cancers (Basel)* (2021) 13(24):6158. doi: 10.3390/cancers13246158

66. Takahashi N, Hoshi H, Higa A, Hiyama G, Tamura H, Ogawa M, et al. An *In vitro* system for evaluating molecular targeted drugs using lung patient-derived tumor organoids. *Cells* (2019) 8(5):481. doi: 10.3390/cells8050481

67. Scognamiglio G, De Chiara A, Parafioriti A, Armiraglio E, Fazioli F, Gallo M, et al. Patient-derived organoids as a potential model to predict response to PD-1/PD-L1 checkpoint inhibitors. *Br J Cancer* (2019) 121(11):979–82. doi: 10.1038/s41416-019-0616-1

68. Esser LK, Branchi V, Leonardelli S, Pelusi N, Simon AG, Klümper N, et al. Cultivation of clear cell renal cell carcinoma patient-derived organoids in an air-liquid interface system as a tool for studying individualized therapy. *Front Oncol* (2020) 10:1775. doi: 10.3389/fonc.2020.01775

69. Ao Z, Wu Z, Cai H, Hu L, Li X, Kaurich C, et al. Rapid profiling of tumor-immune interaction using acoustically assembled patient-derived cell clusters. *Adv Sci (Weinh)* (2022) 9(22):e2201478. doi: 10.1002/advs.202201478

70. Hamdan F, Ylösmäki E, Chiaro J, Giannoula Y, Long M, Fusciello M, et al. Novel oncolytic adenovirus expressing enhanced cross-hybrid IgGA fc PD-L1 inhibitor activates multiple immune effector populations leading to enhanced tumor killing *in vitro*, *in vivo* and with patient-derived tumor organoids. *J Immunother Cancer* (2021) 9 (8):e003000. doi: 10.1136/jitc-2021-003000

71. Klener PJr., Otahal P, Lateckova L, Klener P. Immunotherapy approaches in cancer treatment. *Curr Pharm Biotechnol* (2015) 16(9):771–81. doi: 10.2174/1389201016666150619114554

72. Mitchell MS. Immunotherapy as part of combinations for the treatment of cancer. *Int Immunopharmacol* (2003) 3(8):1051–9. doi: 10.1016/s1567-5769(03)00019-5

73. Wrangle JM, Patterson A, Johnson CB, Neitzke DJ, Mehrotra S, Denlinger CE, et al. IL-2 and beyond in cancer immunotherapy. *J Interferon Cytokine Res* (2018) 38 (2):45–68. doi: 10.1089/jir.2017.0101

74. Monestime S, Lazaridis D. Pexidartinib (TURALIO): The first FDA-indicated systemic treatment for tenosynovial giant cell tumor. *Drugs R D* (2020) 20(3):189–95. doi: 10.1007/s40268-020-00314-3

75. Smeester BA, Slipek NJ, Pomeroy EJ, Laoharawee K, Osum SH, Larsson AT, et al. PLX3397 treatment inhibits constitutive CSF1R-induced oncogenic ERK signaling, reduces tumor growth, and metastatic burden in osteosarcoma. *Bone* (2020) 136:115353. doi: 10.1016/j.bone.2020.115353

76. Furman WL, McCarville B, Shulkin BL, Davidoff A, Krasin M, Hsu CW, et al. Improved outcome in children with newly diagnosed high-risk neuroblastoma treated with chemoimmunotherapy: Updated results of a phase II study using hu14.18K322A. *J Clin Oncol* (2022) 40(4):335–44. doi: 10.1200/jco.21.01375

77. Nguyen R, Moustaki A, Norrie JL, Brown S, Akers WJ, Shirinifard A, et al. Interleukin-15 enhances anti-GD2 antibody-mediated cytotoxicity in an orthotopic PDX model of neuroblastoma. *Clin Cancer Res* (2019) 25(24):7554–64. doi: 10.1158/1078-0432.Ccr-19-1045

78. Zhang B, Li H, Liu W, Tian H, Li L, Gao C, et al. Adoptive cell therapy of patient-derived renal cell carcinoma xenograft model with IL-15-induced γδT cells. *Med Oncol* (2021) 38(3):30. doi: 10.1007/s12032-021-01474-1

79. Depil S, Duchateau P, Grupp SA, Mufti G, Poirot L. 'Off-the-shelf' allogeneic CAR T cells: development and challenges. *Nat Rev Drug Discovery* (2020) 19(3):185–99. doi: 10.1038/s41573-019-0051-2

80. Fournier C, Martin F, Zitvogel L, Kroemer G, Galluzzi L, Apetoh L. Trial watch: Adoptively transferred cells for anticancer immunotherapy. *Oncoimmunology* (2017) 6 (11):e1363139. doi: 10.1080/2162402X.2017.1363139

81. Goto S, Sakoda Y, Adachi K, Sekido Y, Yano S, Eto M, et al. Enhanced anti-tumor efficacy of IL-7/CCL19-producing human CAR-T cells in orthotopic and patient-derived xenograft tumor models. *Cancer Immunol Immunother* (2021) 70 (9):2503–15. doi: 10.1007/s00262-021-02853-3

82. Ye X, Deng X, Wen J, Li Y, Zhang M, Cai Z, et al. Folate receptor-alpha targeted 7x19 CAR-γδT suppressed triple-negative breast cancer xenograft model in mice. *J Oncol* (2022) 2022:2112898. doi: 10.1155/2022/2112898

83. Pang N, Shi J, Qin L, Chen A, Tang Y, Yang H, et al. IL-7 and CCL19-secreting CAR-T cell therapy for tumors with positive glypican-3 or mesothelin. *J Hematol Oncol* (2021) 14(1):118. doi: 10.1186/s13045-021-01128-9

84. Zhao Y, Moon E, Carpenito C, Paulos CM, Liu X, Brennan AL, et al. Multiple injections of electroporated autologous T cells expressing a chimeric antigen receptor mediate regression of human disseminated tumor. *Cancer Res* (2010) 70(22):9053–61. doi: 10.1158/0008-5472.CAN-10-2880

85. Jiang Z, Jiang X, Chen S, Lai Y, Wei X, Li B, et al. Anti-GPC3-CAR T cells suppress the growth of tumor cells in patient-derived xenografts of hepatocellular carcinoma. *Front Immunol* (2016) 7:690. doi: 10.3389/fimmu.2016.00690

86. Choe JH, Watchmaker PB, Simic MS, Gilbert RD, Li AW, Krasnow NA, et al. SynNotch-CAR T cells overcome challenges of specificity, heterogeneity, and persistence in treating glioblastoma. *Sci Transl Med* (2021) 13(591):eabe7378. doi: 10.1126/scitranslmed.abe7378

87. Cao B, Liu M, Huang J, Zhou J, Li J, Lian H, et al. Development of mesothelin-specific CAR NK-92 cells for the treatment of gastric cancer. *Int J Biol Sci* (2021) 17 (14):3850–61. doi: 10.7150/ijbs.64630

88. Ding S, Hsu C, Wang Z, Natesh NR, Millen R, Negrete M, et al. Patient-derived micro-organospheres enable clinical precision oncology. *Cell Stem Cell* (2022) 29 (6):905–917.e906. doi: 10.1016/j.stem.2022.04.006

89. Jacob F, Salinas RD, Zhang DY, Nguyen PTT, Schnoll JG, Wong SZH, et al. A patient-derived glioblastoma organoid model and biobank recapitulates inter- and intra-tumoral heterogeneity. *Cell* (2020) 180(1):188–204.e122. doi: 10.1016/j.cell.2019.11.036

90. Dekkers JF, Alieva M, Cleven A, Keramati F, Wezenaar AKL, van Vliet EJ, et al. Uncovering the mode of action of engineered T cells in patient cancer organoids. *Nat Biotechnol* (2023) 41(1):60–9. doi: 10.1038/s41587-022-01397-w

91. Driehuis E, Kolders S, Spelier S, Lõhmussaar K, Willems SM, Devriese LA, et al. Oral mucosal organoids as a potential platform for personalized cancer therapy. *Cancer Discovery* (2019) 9(7):852–71. doi: 10.1158/2159-8290.Cd-18-1522

92. Mondal M, Guo J, He P, Zhou D. Recent advances of oncolytic virus in cancer therapy. *Hum Vaccin Immunother* (2020) 16(10):2389–402. doi: 10.1080/21645515.2020.1723363

93. Wang Q, Ma X, Wu H, Zhao C, Chen J, Li R, et al. Oncolytic adenovirus with MUC16-BiTE shows enhanced antitumor immune response by reversing the tumor microenvironment in PDX model of ovarian cancer. *Oncoimmunology* (2022) 11 (1):2096362. doi: 10.1080/2162402x.2022.2096362

94. Ding J, Murad YM, Sun Y, Lee IF, Samudio I, Liu X, et al. Pre-existing HSV-1 immunity enhances anticancer efficacy of a novel immune-stimulating oncolytic virus. *Viruses* (2022) 14(11):2327. doi: 10.3390/v14112327

95. Quinn CH, Beierle AM, Hutchins SC, Marayati R, Bownes LV, Stewart JE, et al. Targeting high-risk neuroblastoma patient-derived xenografts with oncolytic virotherapy. *Cancers (Basel)* (2022) 14(3):762. doi: 10.3390/cancers14030762

96. Raimondi G, Mato-Berciano A, Pascual-Sabater S, Rovira-Rigau M, Cuatrecasas M, Fondevila C, et al. Patient-derived pancreatic tumour organoids identify therapeutic responses to oncolytic adenoviruses. *EBioMedicine* (2020) 56:102786. doi: 10.1016/j.ebiom.2020.102786

97. Li L-L, Qiao S-L, Liu W-J, Ma Y, Wan D, Pan J, et al. Intracellular construction of topology-controlled polypeptide nanostructures with diverse biological functions. *Nat Commun* (2017) 8(1):1276. doi: 10.1038/s41467-017-01296-8

98. Nasser TA, Adel R, Badr A, Teleb M, Bekhit AA, Elkhodairy KA, et al. Combined cancer immunotheranostic nanomedicines: Delivery technologies and therapeutic outcomes. *ACS Omega* (2023) 8(5):4491–507. doi: 10.1021/acsomega.2c05986

99. Fisher E, Pavlenko K, Vlasov A, Ramenskaya G. Peptide-based therapeutics for oncology. *Pharm Med* (2019) 33(1):9–20. doi: 10.1007/s40290-018-0261-7

100. Ma F, Liu T, Yang W, You W, He W, Yan J, et al. Turning fluvastatin into a supramolecular immuno-sensitizer towards augmented tumor immunotherapy. *Chem Eng J* (2022) 437:135310. doi: 10.1016/j.cej.2022.135310

101. Xiao YF, Jie MM, Li BS, Hu CJ, Xie R, Tang B, et al. Peptide-based treatment: A promising cancer therapy. *J Immunol Res* (2015) 2015:761820. doi: 10.1155/2015/761820

102. Qiu F, Becker KW, Knight FC, Baljon JJ, Sevimli S, Shae D, et al. Poly (propylacrylic acid)-peptide nanoplexes as a platform for enhancing the immunogenicity of neoantigen cancer vaccines. *Biomaterials* (2018) 182:82–91. doi: 10.1016/j.biomaterials.2018.07.052

103. Wang F, Xu D, Su H, Zhang W, Sun X, Monroe MK, et al. Supramolecular prodrug hydrogelator as an immune booster for checkpoint blocker-based immunotherapy. *Sci Adv* (2020) 6(18):eaaz8985. doi: 10.1126/sciadv.aaz8985

104. Zhou X, Singh M, Sanz Santos G, Guerlavais V, Carvajal LA, Aivado M, et al. Pharmacologic activation of p53 triggers viral mimicry response thereby abolishing tumor immune evasion and promoting antitumor immunity. *Cancer Discovery* (2021) 11(12):3090–105. doi: 10.1158/2159-8290.Cd-20-1741

105. Zhang L, Jiang Z, Yang X, Qian Y, Wang M, Wu S, et al. A totipotent "All-In-One" peptide sequentially blocks immune checkpoint and reverses the immunosuppressive tumor microenvironment. *Adv Mater* (2023) 35(2):e2207330. doi: 10.1002/adma.202207330

106. She J, Li Y, Yan S, Yan Y, Liu D, Li S, et al. *De novo* supraparticle construction by a self-assembled janus cyclopeptide to tame hydrophilic microRNA and hydrophobic molecule for anti-tumor cocktail therapy and augmented immunity. *Chem Eng J* (2020) 401:126080. doi: 10.1016/j.cej.2020.126080

107. Shields C, Wang LL, Evans MA, Mitragotri S. Materials for immunotherapy. *Adv Mater* (2020) 32(13):e1901633. doi: 10.1002/adma.201901633

108. Yan J, He W, Li X, You W, Liu X, Lin S, et al. Carnosic acid-induced co-self-assembly of metal-peptide complexes into a nanocluster-based framework with tumor-specific accumulation for augmented immunotherapy. *Chem Eng J* (2021) 416:129141. doi: 10.1016/j.cej.2021.129141

109. Olson B, Li Y, Lin Y, Liu ET, Patnaik A. Mouse models for cancer immunotherapy research. *Cancer Discovery* (2018) 8(11):1358–65. doi: 10.1158/2159-8290.Cd-18-0044

110. Yan J, Yao Y, Yan S, Gao R, Lu W, He W. Chiral protein supraparticles for tumor suppression and synergistic immunotherapy: An enabling strategy for bioactive supramolecular chirality construction. *Nano Lett* (2020) 20(8):5844–52. doi: 10.1021/acs.nanolett.0c01757

111. Dutta D, Heo I, Clevers H. Disease modeling in stem cell-derived 3D organoid systems. *Trends Mol Med* (2017) 23(5):393–410. doi: 10.1016/j.molmed.2017.02.007

Frontiers in
Bioengineering and Biotechnology

Accelerates the development of therapies, devices, and technologies to improve our lives

A multidisciplinary journal that accelerates the development of biological therapies, devices, processes and technologies to improve our lives by bridging the gap between discoveries and their application.

Discover the latest Research Topics

See more →

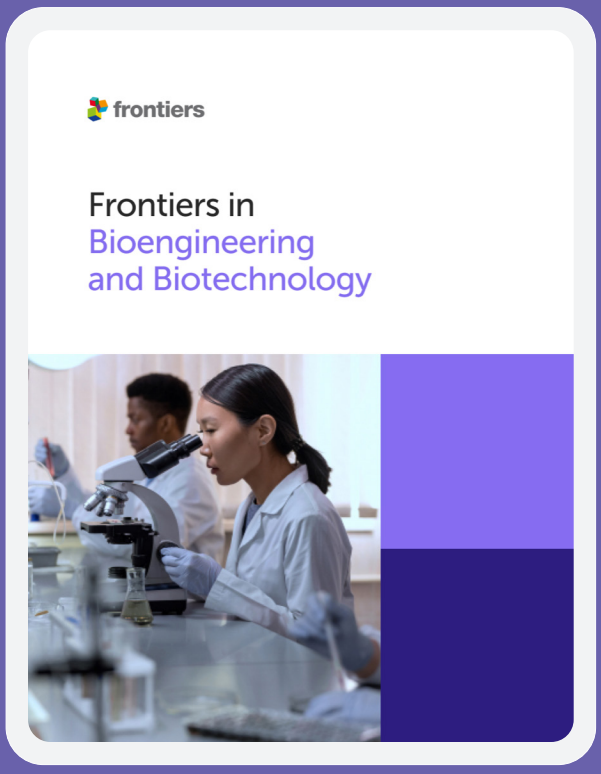

Frontiers

Avenue du Tribunal-Fédéral 34
1005 Lausanne, Switzerland
frontiersin.org

Contact us

+41 (0)21 510 17 00
frontiersin.org/about/contact